TEAM tAO

Table of Contents

28 October 2005

Volume 310

Number 5748

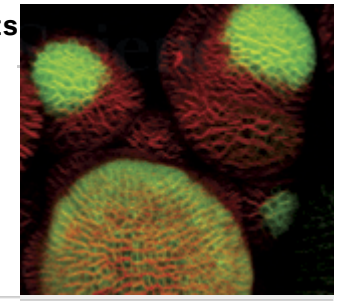

Science



NEW THIS WEEK:

**Gene Fusion and Prostate Cancer**

**Quantum Gas Correlations**

**More Neurons, Less Weight?**

**Bats Linked to SARS**



## RESEARCH

## Counting Statistics and Quantum Gases

Nearly 50 years ago, Hanbury Brown and Twiss showed that photons emitted from a classical thermal light source are correlated, but when the light source was replaced with a coherent one, the correlations disappeared. Their experiment stimulated the birth of modern quantum optics. **Schellekens *et al.*** (p. 648, published online 15 September; see the Perspective by **Knight**) have now observed analogous behavior for ultracold quantum gases and show that atomic correlations vary with the nature of the atom source. For a nondegenerate quantum gas, akin to the thermal optical source, the correlations exist, but when the gas is cooled further to form a coherent ensemble (a Bose-Einstein condensate), the correlations disappear.

## Opto-Optical Modulation

Continued progress in fiber optic communications will rely on the ability to increase the modulation frequency of the optical signal. Present electro-optic modulators typically operate below 100 gigahertz. **Carter *et al.*** (p. 651) describe quantum optical effects in a semiconductor quantum-well structure with an optical response at several terahertz. The effects are analogous to those seen in atomic and molecular three-level systems where a pump beam induces coherent oscillations between the two lower levels and creates electromagnetic-induced transparency for a probe beam when it is resonant with one of the lower-level to upper-level transitions. Full optical control over the modulation process should allow communications to operate at much higher frequencies.

## Demystifying Prostate Cancer Genetics

Many human leukemias display characteristic gene rearrangements, the analysis of which has provided valuable insights into disease mechanisms and stimulated the development of promising therapies such as Gleevec. Gene arrangements also occur in the more common solid tumors, but they are bewilderingly complex and thought to be nonspecific. **Tomlins *et al.*** (p. 644; see the news story by **Marx**) have developed a method that allows them to sort through this cytogenetic complexity and find the gene rearrangements that occur reproducibly in a high percentage of tumors. Using this method, called COPA (for cancer outlier profile analysis), the authors show that the majority of human prostate tumors exhibit chromosomal rearrangements that fuse specific transcription factor genes with the promoter sequences of an androgen-regulated gene, which in turn overexpresses the transcription factor genes in the tumors. These results suggest that COPA may be productively applied to other solid tumors of comparable cytogenetic complexity.

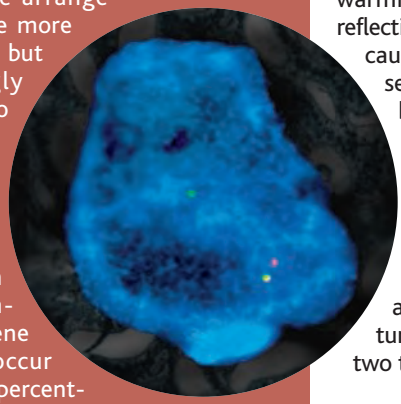

## Ground Truth About Arctic Warming

Although radiative forcing by greenhouse gases will likely have the most significant influence on the amount of surface warming that Earth will experience in the near future, other processes can be just as or even more important in particular regions. **Chapin *et al.*** (p. 657, published online 22 September; see the Perspective by **Foley**) analyzed field data from arctic Alaska that show how changes in summer albedo contribute to warming trends there. These reflectivity effects, now mostly caused by longer snow-free seasons but increasingly by expansion of shrub ranges in the future, are as large in magnitude as those caused by the buildup of greenhouse gases. These changes have the potential to amplify surface temperature increases by factors of two to seven.

## Microscopy of Melting Metal

The nature of the solid-liquid interface is key for understanding processes such as liquid-phase epitaxial growth, wetting, liquid-phase joining, crystal growth, and lubrication. For metals, studying this interface in detail can be difficult because of the elevated temperatures at which melting occurs. Using an advanced high-resolution transmission electron microscope, **Oh *et al.*** (p. 661, published online 6 October) studied the wetting of aluminum sitting on a substrate of alumina and observed crystalline ordering of the liquid atoms adjacent to the ordered solid. The growth of the alumina was facilitated by the interfacial transport of oxygen from the microscope column along the solid-liquid interface.

## Magmatic Activity Maintained

A simple view of oceanic crust formation is that magma rises at spreading ridges and cools as it moves away. During cooling, magnetic minerals preserve the orientation of Earth's magnetic field and create symmetric patterns of magnetic stripes across the ocean floor. Evaluating this simple process has been difficult, however, because most oceanic crust lacks the mineral zircon, which contains sufficient uranium for the most accurate determination of the ages of crystallization of magmas. **Schwartz *et al.*** (p. 654) have now identified and separated zircons from oceanic crust formed along the Southwest India Ridge, a ridge that is spreading slowly. Significant magmatic activity began in each segment of crust long before most of the magmatism and the characteristic magnetic signature were locked in.

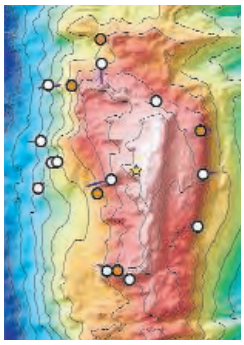

CREDITS (TOP TO BOTTOM): TOMLINS *ET AL.*, SCHWARTZ *ET AL.*

## Inhibiting Bacterial Virulence and Cholera Susceptibility

Bacterial virulence gene products have been neglected as targets for drug discovery because inactivation of virulence has not produced bactericidal or growth inhibitory effects. **Hung *et al.*** (p. 670, published online 13 October) screened a chemical library for molecules that block expression of the cholera toxin gene (*ctxA*) and identified an inhibitor of virulence gene regulation in *Vibrio cholera*. The compound, termed virstatin, affects

CONTINUED ON PAGE 587


Published by AAAS

the activity of a transcription factor, ToxT, the ctxA activator. ToxT activity is inhibited by virstatin in both *V. cholera* and *Escherichia coli*. As expected, virstatin did not affect growth of the bacteria, but nevertheless had a dramatic effect on the intestinal colonization of *V. cholera* in mice.

## Just the Right Size

Two parameters control the eventual size of insects: their growth rate and the length of their growth period. Ecdysone, a major steroid hormone, functions as a developmental timer that controls the length of the growth period. **Colombani *et al.*** (p. 667; see the Perspective by **King-Jones and Thummel**) now show that ecdysone from the prothoracic gland of *Drosophila* also regulates the speed at which the animals grow by inhibiting insulin/insulin-like growth factor signaling. This work provides a conceptual framework for understanding how the final size of an organism is determined and establishes a link between steroid hormone and insulin signaling.

## The Tip of the Needle

The type III secretion apparatus helps transfer proteins from the bacterial cytoplasm into that of a target eukaryotic host cell and includes a well-characterized needle-like structure. The needle tip has not been characterized and represents a critical player in bacteria-cell interaction. **Mueller *et al.*** (p. 674) now present evidence that the needle of the *Yersinia* type III secretion apparatus is topped with a distinct structure, made of a critical protective antigenic protein, LcrV, one of the "translocators" involved in protein transfer.

## Appetite and the Adaptive Brain

Appetite and energy balance are regulated by the hypothalamic region of the brain, and considerable progress has been made in defining the underlying neural circuitry. Two studies underscore the emerging idea that these feeding circuits are not firmly "hardwired" but rather exhibit remarkable plasticity, even in adults. **Luquet *et al.*** (p. 683) show that specific neurons that are strictly required for the regulation of food intake in adult mice can be removed without detriment in newborn mice, which suggests that the feeding circuitry can readily adapt to change early in life. **Kokoeva *et al.*** (p. 679; see the news story by **Vogel**) make the surprising observation that a neurotrophic factor that induces sustained weight loss in adult mice does so by stimulating the proliferation of hypothalamic neurons. Pharmacological inhibition of this neurogenesis compromised the capacity of the neurotrophic factor to induce long-term weight loss. Hypothalamic plasticity thus adds another potentially important layer of complexity to the regulation of body weight.

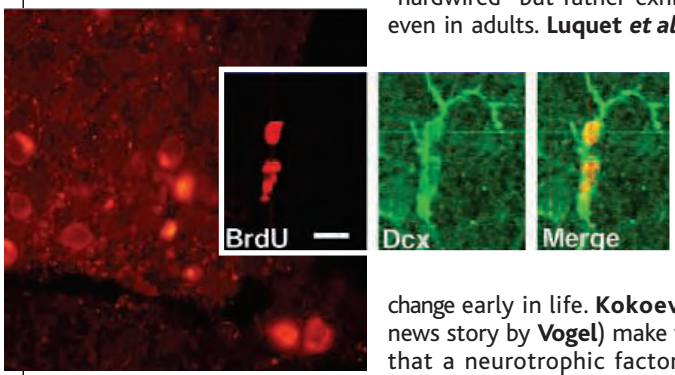


CREDIT: (LEFT) LUQUET *ET AL.*; (INSET) KOKOEVA *ET AL.*

## Bats Again

Attempts to identify the wildlife hosts of emerging diseases have relied on analysis of fecal material from wildlife, trade, and domesticated animals that reveal recent infections circulating in the markets. **Li *et al.*** (p. 676, published online 29 September; see the 30 September news story by **Normile** and the Perspective by **Dobson**) have targeted their investigations on wild bats in China and discovered several genetically diverse coronaviruses, one of which closely resembles the severe acute respiratory syndrome (SARS) coronavirus. These findings implicate bats as the wild reservoir of this virus.


*Published by AAAS*

# Chess Game at the FDA

I am seriously tempted to offer my help to the president in selecting someone to become the next commissioner of the U.S. Food and Drug Administration (FDA). Things have gotten so desperate that the Bush administration might even welcome help from me. After all, I had the job once—even worked for a president who was somewhat evangelical. And after the soap opera they've just put on, it's hard to believe that the new incumbent will last any longer than the last one, or the one before that. So they might turn to me for help—it's really that bad!

Before we plod through the painful recent history of this agency, I remind readers that it was once in respectable shape. A trusted, highly professional agency responsible for regulating about 25 cents of every consumer dollar spent in America, it was also a model for developing new drug approval processes in other countries. Of course, it was no stranger to controversy. Some critics thought that meeting its regulatory requirements added costs and slowed the progress of medical innovation. Others thought it played softball with the pharmaceutical industry, risking the lives of Americans by approving inadequately tested drugs. I've been asked whether the FDA doesn't actually slow the rate of medical innovation. Of course it does! The question is whether the risk of delaying therapies is fairly well balanced against the risk of adverse drug reactions. There is no agreed standard for finding that point of perfect social utility, and the FDA has usually done reasonably well, annoying equally its passionate critics on both right and left.

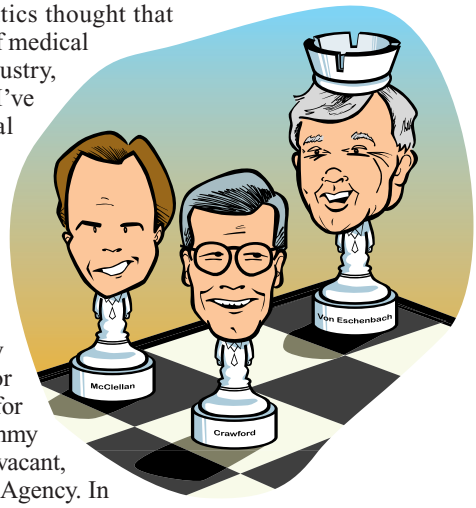


Now, to recent history: Late in his first term, President Bush made a promising move by appointing Mark McClellan, a Stanford economics professor and physician, as the FDA commissioner. The applause had barely died down when McClellan was moved to Baltimore to run the Centers for Medicare and Medicaid Services. Many thought this exile was preparation for his appointment as secretary of Health and Human Services (HHS) when Tommy Thompson left. But Thompson hung in there, and by the time his post was vacant, Michael Leavitt was moved in to HHS from the Environmental Protection Agency. In chess, this move—maneuvering powerful back-row pieces to change their locations—is called "castling." It is becoming increasingly familiar to followers of this administration's personnel policies.

The vacancy at the FDA remained under the acting leadership of Lester Crawford for months until President Bush finally nominated him for commissioner. In my time, Les was a good head of the Bureau of Veterinary Medicine at the agency. But "acting" is never a great job, and his Senate confirmation as commissioner was put on hold by several senators. They wanted his promise to make the "Plan B" morning-after contraceptive easier for consumers to get by moving it from prescription-only to over-the-counter access, as an FDA Advisory Committee had recommended. Eventually, Crawford promised to do so and was confirmed. Meanwhile, a new deputy commissioner was added at the FDA: Scott Gottlieb, a Wall Street drug stock analyst and former American Enterprise Institute scholar. Who picked him isn't clear.

Crawford resigned a scant 2 months after his Senate confirmation, citing age as a reason (at 67?), leaving Plan B still in limbo and of course leaving the FDA slot open once again. You remember castling? Well, the president castled an old Texas friend, National Cancer Institute (NCI) Director Andrew von Eschenbach, right into the interim FDA job. It wasn't quite castling, however, because castling requires the castled piece to move, and von Eschenbach was initially slated to hold both posts! Many insiders were shocked because the NCI develops drugs and sends clinical trials to the FDA, affording an endless opportunity for conflicts of interest.

But hold on. After 2 days, the job-sharing idea disappeared, and it was announced that the NCI would be left in the hands of Deputy Director John Niederhuber, a highly respected surgeon. From this act of the soap opera, two conclusions can be drawn. First, from the reversal, we can gain reassurance that the administration is subject to occasional attacks of embarrassment. Second, the quality of the NCI's new leadership reminds us of baseball Hall of Famer Casey Stengel's mangled version of the old saying: It's an ill wind that blows nobody no good.

Oops! I should have mentioned earlier that the main use of castling in chess is to protect the king.

**Donald Kennedy**
*Editor-in-Chief*

10.1126/science.1121473

CREDIT: TIM SMITH/*SCIENCE*



*Published by AAAS*

# EDITORS' CHOICE

edited by Stella Hurtley

Muraroa atoll.

ECOLOGY/EVOLUTION

## After the Catastrophe

The study of recolonization and succession after catastrophic disturbance can offer insights into the rules governing the assembly of ecological communities and how species interact during colonization and invasion, as well as the speed and trajectory of recovery. Catastrophes—and responses thereto—come in many forms.

Planes *et al.* followed the recovery of coral reef fish assemblages after a thoroughly unnatural catastrophe: the underground nuclear tests carried out at Mururoa atoll in the Pacific between 1976 and 1995. Typically, the pressure wave from each test caused the instant death of all fish within 2000 m of the test site, while leaving the reef structure unchanged. Even so, the fish diversity and abundance that are characteristic of undamaged reef were restored within 1 to 5 years by immigration and recruitment from neighboring areas, suggesting that reef structure is a vital factor in community assembly. In contrast, Pitman *et al.* document a very slow recovery after a catastrophic flood that probably took place in an Ecuadorian tropical rain forest five centuries ago; tree species number has yet to recover to half that of neighboring unaffected areas, and there is a greater abundance of light-demanding early-successional species. — AMS

*Ecology* **86**, 2578 (2005); *J. Trop. Ecol.* **21**, 559 (2005).

VIROLOGY

## Keeping Your Enemies Close

The immune system's battle with the human immunodeficiency virus is now a familiar one, yet an equally important struggle takes place between host and virus within the cell. In particular, the cellular antiviral factors belonging to the APOBEC3 family of cytidine deaminases impair provirus function by peppering the viral genome with unwanted mutations through the replacement of guanine with adenine (G→A). To protect itself, HIV-1 has evolved a protein (Vif) that binds to and directs the degradation of APOBEC3G and APOBEC3F.

By scrutinizing viral sequences derived from patients and short-term viral isolates, Simon *et al.* identified naturally arising variants of the HIV *vif* gene at significant frequency. Some of these mutations caused loss of Vif activity, whereas others modified its function. Correspondingly, provirus sequences from certain individuals with Vif variation carried patterns of G→A replacement that were consistent with activity of APOBEC3G. In other cases, APOBEC3F or both enzymes appeared to be active in generating HIV mutations, suggesting that Vif variants were mediating partial and distinct inhibitory effects on APOBEC3 activity. Thus, rather than simply silencing the APOBEC3 proteins altogether, variation in Vif may allow it to employ the assistance of host factors in increasing viral sequence diversity within an infected individual. — SJS

*PLoS Pathog.* **1**, 20 (2005).

CELL BIOLOGY

## Long-Lived Cells

Long-term storage of cells at very low temperatures can be very costly.

Therefore, simple and reliable methods to maintain stable cells at ambient temperature would be desirable. Prior methods have used trehalose or glycan as additives for relatively short-term cell storage of air-dried cells from monolayers. Jack *et al.* now demonstrate storage of mammalian tissue culture cells at room temperature for up to 6 weeks. In this method, cells are grown in such a way that they cannot attach to the culture vessel surface and form three-dimensional multicellular aggregates. The surface cells of these "spheroids" become quiescent. The spheroids can then be stored on agarose under partial vacuum with antistatic control in the dark at room temperature. After rehydration, cells were able to recover and grow when cultured further. Cell survival and recovery after rehydration depend on endogenous cytokine production and the subsequent activation of JNK and NF–kappa B signaling. Hopefully, the ability to induce metabolic arrest in human cells without chemical intervention will be useful to study cell cycle control and aging as well as other metabolic processes and disease. — BAP

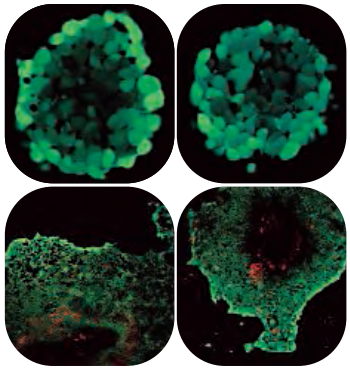

**Outgrowth of cells from spheroids before (left) and after (right) storage. Dead cells are stained red.**

*J. Cell Physiol.* 10.1002/jcp.20499 (2005).

APPLIED PHYSICS

## Carrier Dynamics Under the Microscope

The performance of electronic devices such as thin-film transistors or semiconductor-based light-emitting diodes depends crucially on the dynamics and spatial distribution of the carriers throughout the device. In the case of light-emitting diodes, carriers can be lost because of both radiative and nonradiative recombination. Although imaging the radiative losses is fairly straightforward, imaging the nonradiative recombination centers presents more of a challenge. Okamoto *et al.* have developed a pump-probe technique based on scanning near-field optical microscopy and use it to image, on the submicrometer scale, the radiative and nonradiative recombination centers throughout the active layer of an indium-gallium-nitride quantum-well–based light-emitting diode. Knowledge of the relative contributions

CONTINUED ON PAGE 593





Published by AAAS

from these radiative and nonradiative recombination centers can be expected to lead to improvements in device performance as that information is fed back into the materials preparation and device design. — ISO

*Appl. Phys. Lett.* **87**, 161104 (2005).

EARTH SCIENCE

## Salt and Sustainability

Agriculture in many semi-arid areas of the world requires irrigation—from either stored snowmelt or groundwater. High evaporation rates in turn lead to the accumulation of salts in the soil that hinder productivity and can degrade water quality downstream and, over time, potentially in groundwater. Salination of soils is affecting critical agricultural areas such as the Nile Delta and central California. Schoups *et al*. present a model of the hydrologic history of the San Joaquin Valley, California, that accounts for the salt deposition in soil, the salinity of surface- and groundwater, and the history of water use during the past 60 years. By including information about the shifts in irrigation sources and about extreme droughts, the model accurately predicts the local distribution of salt in the San Joaquin soils. Although the amount of salt in the soils has held steady recently, the model suggests that recharge waters moving through these deposits are increasing the salinity even of deep aquifers, and will likely continue to do so, posing a major problem for the sustainability of agriculture in this region. — BH

*Proc. Natl. Acad. Sci. U.S.A.* 10.1073/pnas.0507723102 (2005).

NEUROSCIENCE

## Adenosine and Sleep

Slow-wave sleep is intricately linked to sleep depth, sleep consolidation, and sleep quality. Slow-wave sleep is also a good measure of the need for sleep, and it is tightly regulated during development. There is accumulating evidence that the neuromodulator adenosine plays an important role in sleep and sleep regulation. Retey *et al*. analyzed the sleep phases and associated EEG patterns of study participants with different genetic variants of the adenosine-metabolizing enzyme adenosine deaminase and of the adenosine $A_{2A}$ receptor. A frequent functional polymorphism in the gene encoding adenosine deaminase contributes to the high inter-individual variability in sleep intensity. Slow-wave sleep was longer and sleep was more intense in participants with the 22G/A genotype than in those with the G/G genotype. Investigation of the $A_{2A}$ receptor polymorphism revealed that the EEG power in the 7.5- to10-Hz frequency range was higher in individuals with the 1976C/C genotype than in others expressing the T/T genotype. However, this difference was observed during the different sleep phases as well as during the waking state. Thus, several aspects of the well-known inter-individual variability in human sleep and the need for sleep are associated with polymorphisms in the adenosinergic system. — PRS

*Proc. Natl. Acad. Sci. U.S.A.* **102**, 15676 (2005).

CHEMISTRY

## Oxidizing Organic Cyanides

Copper monooxygenases can use $O_2$ to hydroxylate a wide variety of substrates; for example, dopamine $\alpha$-monooxygenase can convert benzylcyanide to benzaldehyde and cyanide. Li *et al*. have synthesized a dicopper complex that can hydroxylate nitriles. A binucleating ligand was used that binds two Cu(I) ions through three N atoms and thus allows each Cu(I) to also coordinate a nitrile; an OH on the bridging portion of the ligand is noncoordinating. Addition of $O_2$ at –80°C in nitrile solvent produced a hydroperoxide-bridged Cu(II) species in which the alkylamino N atoms no longer bind the Cu atoms. Warming to room temperature forms the aldehyde from one solvent nitrile, apparently by first eliminating water to form an $\alpha$-hydroxynitrile that rearranges to leave one Cu(II) with a cyanide ligand. This species then dimerizes to form a tetranuclear Cu(II) complex. — PDS

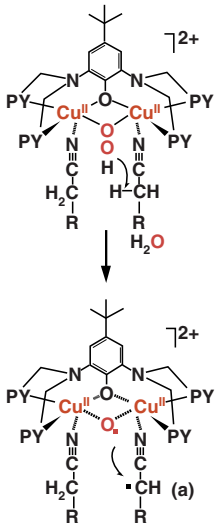


**Reaction scheme.**

*J. Am. Chem. Soc.* 10.1021/ja054948a (2005).

CREDITS: LI *ET AL.*, *J. AM. CHEM. SOC.* 10.1021/JA054948A (2005)



*Published by AAAS*

# NetWatch

edited by Mitch Leslie

IMAGES

## Starring The Cell

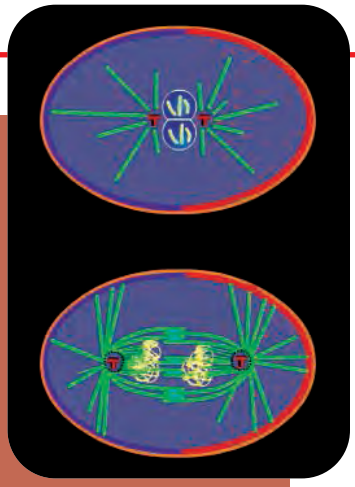

Chromosomes caress, tangle, then get wrenched apart as a French torch song plays in "Twisted Sisters," probably the most touching movie ever made about the first division of meiosis. It's also one of the standouts at the Web site of the Bioclips project, sponsored by the French government. The virtual multiplex displays entrants from the last four rounds of the Cinema of the Cell festival. Held annually at the European Life Scientist Organization meeting, the contest lets researchers and students present their educational Web films, which use techniques from traditional animation to stop-motion with Lego blocks. The more than 30 shorts range from "A Day in the Life of a Social Amoeba" to a work about the establishment of cell polarity in nematodes from auteurs at the University of Wisconsin, Madison (above).

www.bioclips.com

RESOURCES

## Where Birds Count

The careful observations of birdwatchers are invaluable to scientists studying avian distribution and abundance. eBird, a recently revamped site from Cornell University's Lab of Ornithology and the National Audubon Society, helps researchers access and analyze birders' tallies. One of the lab's collaborations with birdwatchers (*Science*, 3 June, p. 1402), eBird lets visitors submit their sightings to a database that already has entries from 15,000 people. Researchers can then parse the records, plotting counts for a particular area or species. For instance, you can chart the number of ospreys seen in each week of the year and map the fish-eaters' favorite haunts.

www.ebird.org

COMMUNITY SITE

## Schizophrenia Symposium

Find out the conclusions of the latest study comparing different antipsychotic drugs, track down a potential collaborator in Italy, or discover what leading schizophrenia researchers have on their minds. You can do all this and more at the Schizophrenia Research Forum, which officially opened this week. Sponsored by the nonprofit National Alliance for Research on Schizophrenia and Depression and the U.S. National Institute of Mental Health, the diverse site is modeled on a meeting place for Alzheimer's researchers (www.alzforum.org). Features include a news section and interviews with scientists such as Robin Murray of the Institute of Psychiatry in London, who helped show that "obstetric events" such as premature birth boost the risk of schizophrenia. Visitors to the Idea Lab can bat around novel notions. Live chats with experts start next month, and a gene database is in the works.

www.schizophreniaforum.org

DATABASE

## Free the Crystals!

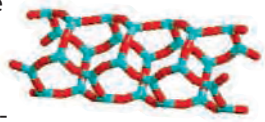

This site is some crystallographers' answer to open-source software, providing an alternative for chemists and other researchers who can't afford the fees charged by suppliers of crystallographic data. Supervised by an international team of scientists, The Crystallography Open Database houses measurements for some 18,000 molecules, from superconducting materials to antibiotics. Visitors can scan the data, which were contributed by site users, for molecules sporting a specific combination of elements. The results appear as a standard "Crystallographic Information File" that includes atomic coordinates and the source of the measurements. A linked site furnishes predicted structures for more than 1500 compounds, such as boron-containing nanotubes (top image) and fluoroaluminate crystals.

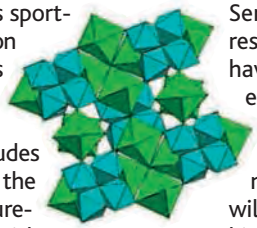

www.crystallography.net

DATABASE

## Dinosaur Name Game

Like the ancient beasts themselves, most of the names scientists have coined for dinosaurs over the last 2 centuries are defunct. At the new database TaxonSearch from paleontologist Paul Sereno of the University of Chicago, researchers can uncover which handles have survived and which have gone extinct as experts have refined taxonomies. Unlike other narrower references, the site focuses on taxonomic levels above the genus, and it will cover all archosaurs—the group that comprises dinosaurs and their kin—except for birds and crocodiles. Dig into the listings to find out who first named a group, its official definition, and its chronological range. For example, the name of the clade Ankylosauridae, to which the herbivore *Ankylosaurus* (above) belongs, dates back to 1908. And if a name has died out, you can learn why. Sereno has posted the first batch of 50 records and plans to add about 700 more within the next few weeks.

Send site suggestions to netwatch@aaas.org. Archive: www.sciencemag.org/netwatch

CREDITS (TOP TO BOTTOM): FONG-MEI LU, LEANNE OLDS, JOHN WHITE/UNIVERSITY OF WISCONSIN, MADISON; FRANCOIS GOHIER/PHOTO RESEARCHERS INC.; CRYSTALLOGRAPHY OPEN DATABASE



Published by AAAS

This Week

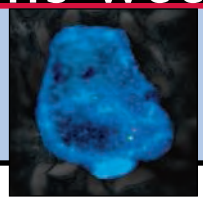

PAGE 603
A cause of prostate cancer?

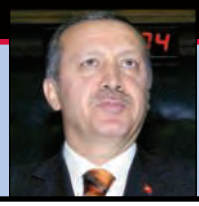

605
Cronyism in Turkish science

SCIENTIFIC COMMUNITY

# 'Security Breach' Leaks NIH Grant Applications Onto Web

When Leemor Joshua-Tor received an e-mail from the National Institutes of Health (NIH) earlier this month regarding her recent grant application, the structural biologist at Cold Spring Harbor Laboratory in New York was hoping for good news. After all, a study section had ranked the proposal highly in June. Instead, the agency informed her that her application—containing a large amount of unpublished data relating to a project she had been working on for 10 years—had been posted on the Internet, freely accessible to the public.

Joshua-Tor was not alone. One hundred and forty grant applications submitted to at least one NIH study section were recently released onto nonsecure Web pages. NIH has been mum about the leaks, citing only a "security breach" and vaguely alluding in a Web-posted open letter to the actions of a peer reviewer. More surprising, the agency has not informed all individuals affiliated with the study section about the incident and has not shared basic information with affected authors regarding exactly when or for how long their supposedly secure proposals were available for public consumption.

"This is the first time I've heard of this happening, and it chills my blood," says Julio Fernandez, a biophysicist at Columbia University, who chairs the Macromolecular Structure and Function C (MSFC) study section that reviewed Joshua-Tor's grant application. "It's an unthinkable attack on the entire system."

NIH spokesperson Don Ralbovsky says the agency can't discuss the specifics of the leak for security reasons. NIH would also not comment on why all affected authors had not been contacted or why individuals affiliated with the MSFC study section, including Fernandez and a number of peer reviewers who served on the section in June and February, had not heard of the incident before *Science* brought it to their attention.

Confused and frustrated by the initial NIH e-mail, Joshua-Tor requested more information. She found the agency's response unsatisfying. Israel Lederhendler, the director of NIH's Office of Electronic Research and Reports Management, directed her to an open letter posted on the agency's grant Web site.* It stated that "a peer reviewer downloaded review materials in a way that allowed Google to capture, index them, and make them accessible via its search engine." The letter added that NIH had addressed the problem and was taking steps to ensure that it didn't happen again. But Joshua-Tor is still left with unanswered questions: "The letter didn't say what exactly had gone up [on the Web] or how long it had been up," she says.

> "It chills my blood. … It's an unthinkable attack on the entire system."
>
> —Julio Fernandez, Columbia University

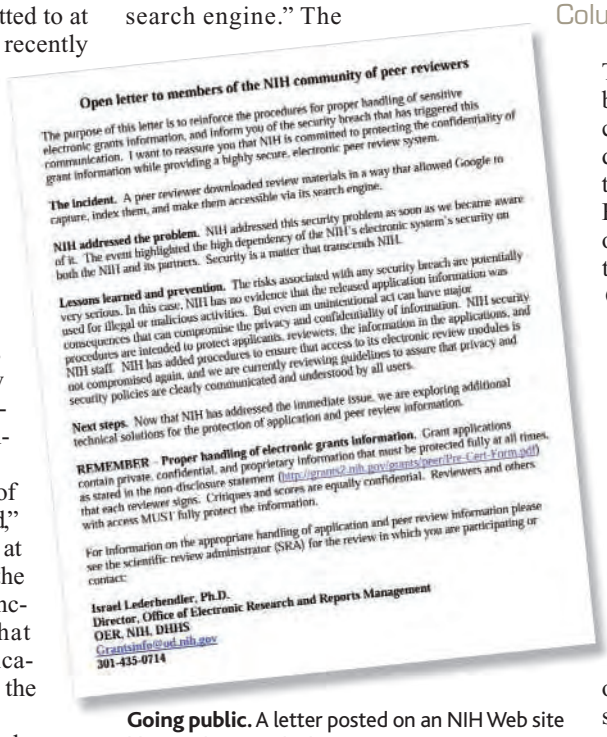

**Open letter to members of the NIH community of peer reviewers**

The purpose of this letter is to reinforce the procedures for proper handling of sensitive electronic grants information, and inform you of the security breach that has triggered this communication. I want to reassure you that NIH is committed to protecting the confidentiality of grant information while providing a highly secure, electronic peer review system.

**The incident.** A peer reviewer downloaded review materials in a way that allowed Google to capture, index them, and make them accessible via its search engine.

**NIH addressed the problem.** NIH addressed this security problem as soon as we became aware of it. The event highlighted the high dependency of the NIH's electronic system's security on both the NIH and its partners. Security is a matter that transcends NIH.

**Lessons learned and prevention.** The risks associated with any security breach are potentially very serious. In this case, NIH has no evidence that the released application information was used for illegal or malicious activities. But even an unintentional act can have major consequences that can compromise the privacy and confidentiality of information. NIH security procedures are intended to protect applicants, reviewers, the information in the applications, and NIH staff. NIH has added procedures to ensure that access to its electronic review modules is not compromised again, and we are currently reviewing guidelines to assure that privacy and security policies are clearly communicated and understood by all users.

**Next steps.** Now that NIH has addressed the immediate issue, we are exploring additional technical solutions for the protection of application and peer review information.

**REMEMBER – Proper handling of electronic grants information.** Grant applications contain private, confidential, and proprietary information that must be protected fully at all times, as stated in the non-disclosure statement (http://grants2.nih.gov/grants/peer/Pre-Cert-Form.pdf) that each reviewer signs. Critiques and scores are equally confidential. Reviewers and others with access MUST fully protect the information.

For information on the appropriate handling of application and peer review information please see the scientific review administrator (SRA) for the review in which you are participating or contact:

**Israel Lederhendler, Ph.D.**
**Director, Office of Electronic Research and Reports Management**
**OER, NIH, DHHS**
Grantsinfo@od.nih.gov
**301-435-0714**

**Going public.** A letter posted on an NIH Web site blames the grant leak on a peer reviewer.

Some affected scientists have yet to hear from NIH. Stephen Sprang, a biochemist at the University of Texas Southwestern Medical Center in Dallas, found out about his grant application going public from a colleague, who discovered Sprang's proposal to the February MSFC study section as well as his own on the Web. "My reaction at the time was, 'This is odd and inappropriate,' " Sprang says. "Grant applications are presumably private, and this felt like an invasion of privacy." Still, he says, it's difficult to assess the consequences of the leak without knowing further details.

One scientist whose grant proposal to the June MSFC study section was also made public believes NIH's eRA Commons site, designed for the electronic exchange of grant information, may have been the source of the leak. The scientist, who declined to be named because his application is still pending, came across his proposal on the Web while doing a Google search for more information on software he uses in his research. He says he was able to access a number of other applications simply by entering the terms "sketch site: era.nih.gov" into Google. When *Science* performed the search, it brought up several grant titles, but the proposals themselves were no longer available.

Some worry that such security lapses could compromise NIH's ambitious plans to make its grant application and review process entirely Web-based. The agency plans to have all grant proposals submitted electronically by May 2007. "I'm sure there will be additional problems," says Vernon Anderson, a biochemist at Case Western Reserve University in Cleveland, Ohio, and a peer reviewer on another MSF study section. Still, he says, "personally, I'm more worried about someone getting my Social Security or credit card number than my grant information." And he notes that even before electronic submissions, there was always the concern that peer reviewers would steal ideas from an applicant's proposal. "But at least then, if someone stole your idea, you could trace it back to the study section," he says. "Now, if something goes up on the Web, there's no way to trace who saw it."

–DAVID GRIMM

CREDIT: NIH

*grants1.nih.gov/grants/letter_to_peer_reviewers.pdf



Published by AAAS





ASTRONOMY

# Science Takes Back Seat as Hubble Shoots the Moon

The Hubble Space Telescope has joined the moon program. For the first time in its 15 years in orbit, NASA researchers late this summer appropriated the observatory for studies not strictly related to science, bypassing the rigorous peer review usually needed to win a slot on Hubble's crowded schedule, NASA revealed just last week. At a press conference on 19 October, the scientists also laid out the observations—although not the detailed data—that they said could help future astronauts learn to live off the land.

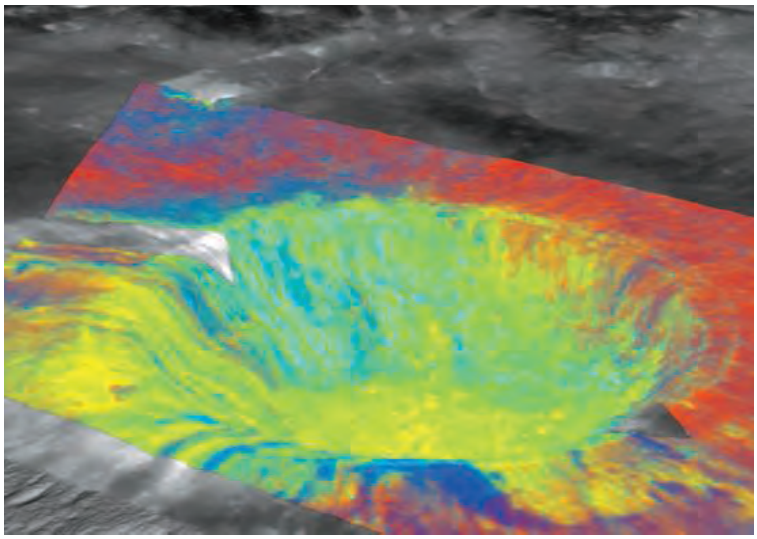

**Hot prospects?** Comparing UV and visible light reflected from Aristarchus impact crater may reveal useful lunar minerals such as ilmenite.

Although NASA's use of the agency's premier scientific facility to push U.S. President George W. Bush's plan to return humans to the moon is unprecedented, researchers aren't complaining—yet. Many say the data are scientifically useful and should herald a flood of new information from two future lunar missions.

As part of the Bush initiative, NASA intends to launch a lunar orbiter in 2008, followed by a robotic lander in the next decade. The instruments aboard the spacecraft will beam back data on potential human landing sites and resources that astronauts could extract, as well as detailed maps and spectroscopic information of value to basic science. Exploration—that is, planning for human visits—rather than pure science is driving the projects, but researchers starved for lunar data are enthusiastic. "Apollo was not driven by science, but it was a quantum leap in our understanding of the solar system," says Carlé Pieters, a geologist at Brown University. "It's high time we got serious about exploring the character of the moon."

The idea of using Hubble to image the moon came from James Garvin, NASA's former chief scientist and now chief scientist at Goddard Space Flight Center in Greenbelt, Maryland, who made a formal study proposal earlier this year. "This is a jump-start for lunar science," he said at the Washington press conference. Hubble spent a dozen orbits in late August imaging three famous sites on the moon: the landing spots for Apollo 15 and Apollo 17 and the Aristarchus plateau, which has never been visited by humans or robots. NASA scientists used soil and rocks astronauts had gathered at the first two sites to calibrate Hubble's ultraviolet sensors for highly accurate analysis of Aristarchus. Because atmospheric interference makes ultraviolet imaging of the moon hard to do from Earth, researchers until now have made do with data from other wavelengths.

The plateau is 200 kilometers across and rises 2 kilometers above the Ocean of Storms. It is punctuated by a massive young crater, 42 kilometers wide and 3 kilometers deep. The crater and the unusual pyroclastic formations in the region, caused by huge plumes of lava, have long drawn scientific interest; the plateau was one of the candidate sites for a follow-on Apollo mission, which was canceled. Geologists are eager to probe the dark basalts disgorged from deep within the lunar interior, which contain volatiles absent from other rocks, for clues to the formation and evolution of the moon.

Garvin also wanted to gather data on a mineral called ilmenite common in Aristarchus's basaltic flows. Made up of oxygen, iron, and titanium, ilmenite could provide a way for astronauts to make water and rocket fuel—and eventually, extract metals—from the lunar surface (*Science*, 12 March 2004, p. 1603). That could significantly lower transportation costs. NASA is funding efforts on Earth to break down ilmenite into its constituent parts. But for such an effort to be feasible, the percentage of ilmenite in the soil would have to be high—and researchers are divided over whether it is. Garvin hinted that the new Hubble data resolve the issue, but he and his team declined to provide details prior to publication.

The Space Telescope Science Institute in Baltimore, Maryland, which operates Hubble and is funded by NASA, agreed to the space agency's unusual request this summer after "extensive interaction," says Bruce Margon, associate director at the institute. Hubble policy written before its launch allows NASA to use the telescope for broader purposes, and Margon adds that "this was a very small project and not an issue of controversy."

Some researchers, however, fear that in a time of tight budgets, science might end up playing second fiddle to exploration. Although remote exploration could provide new opportunities and technologies, "if it is funded by siphoning money away from robotic exploration, the net result will be a … dearth of new discoveries in the cosmos" in the next 1 to 2 decades, warns Jonathan Lunine, a planetary scientist at the University of Arizona in Tucson.

For Pieters, who was not involved in Garvin's project, any lunar data are good news; she notes, for instance, that Hubble's ultraviolet readings will enable researchers to prepare to use similar data when the lunar orbiter is in place. "We don't have good remote-sensing data of the moon," she says. But once NASA's spacecraft arrive there, along with an armada of European, Chinese, and Indian spacecraft, she predicts lunar science will finally come into its own. "At the end of 5 years, it is going to be absolutely fantastic; we'll be close to where we are now with Mars."

–ANDREW LAWLER

CREDIT: NASA/ESA/HST MOON TEAM



Published by AAAS

GENOMICS

# New Haplotype Map May Overhaul Gene Hunting

Three years after it was launched with high hopes of identifying genes behind complex diseases such as diabetes, the first, massive phase of the International HapMap Project is complete. Francis Collins, director of the U.S. National Human Genome Research Institute in Bethesda, Maryland, and a key participant, calls the map "a dream … come true." He and others are concerned, however, that, as with any novel tool, researchers may be reluctant to apply it. And questions about the map's usefulness, which have dogged it from the start, haven't entirely disappeared.

The HapMap denotes haplotypes, stretches of DNA that are inherited together as unbroken blocks and can be identified by just a handful of DNA markers known as SNPs (single-nucleotide polymorphisms), which are variations at the single base level. The map allows gene hunters to get away with less (and thus cheaper) DNA sequencing while still, it's hoped, homing in on disease genes. The current HapMap—a finer-resolution version will come out next year—includes more than 1 million SNPs drawn from the DNA of 269 individuals from four different populations, because haplotype frequencies vary based on evolutionary history. An international consortium announced the draft's completion at the annual meeting of the American Society of Human Genetics in Salt Lake City, Utah, this week; the map was also published in this week's issue of *Nature*. (The U.S. National Institutes of Health contributed more than $60 million toward the map's $138 million price tag; funds also came from the United Kingdom, Japan, China, and Canada.)

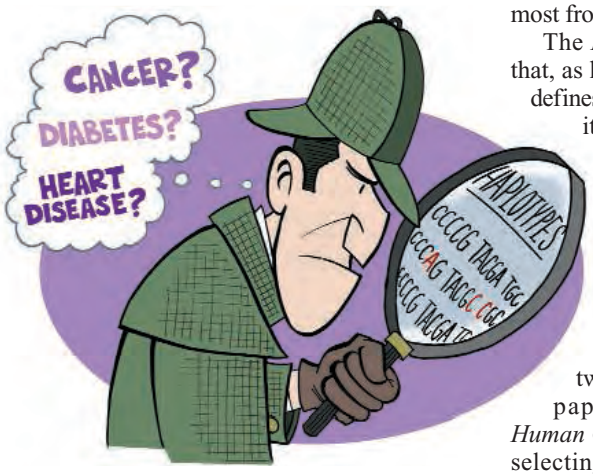


CREDIT: PAT N. LEWIS

Already, data from the map, which are freely available online, are helping pave the way toward finding genes involved in macular degeneration, dyslexia, and hypertension, among other disorders. The HapMap "opens up a really powerful new approach [for finding disease genes], but an unfamiliar one," says Collins. Geneticists aren't necessarily accustomed to a gene-hunting method based on population genetics, Collins explains, so they may need some encouragement to use the HapMap.

David Altshuler of the Broad Institute in Cambridge, Massachusetts, a leader of the HapMap project along with Peter Donnelly of Oxford, agrees. "When you present people with the sort of data they haven't had before, you end up with a lot of foment and confusion and excitement," Altshuler says. More than 500 scientists signed up for a session in Salt Lake City on how to glean the most from the map.

The *Nature* HapMap paper confirmed that, as hoped, a select set of SNPs reliably defines the DNA surrounding them, making it possible to locate relevant genes by comparing haplotype patterns in different groups. It also offers insights, say its more than 200 co-authors, into how evolutionary pressure shaped the genome.

But concern lingers about how the HapMap will perform in the hunt for disease genes. Last week, two German researchers published a paper in the *American Journal of Human Genetics* in which they showed that selecting a different set of SNPs turns up somewhat different haplotypes. The worry is that gene-hunting on different haplotype maps—derived from different sets of SNPs—might lead to divergent results, says co-author Michael Nothnagel, a mathematician at Christian-Albrechts University in Kiel, Germany.

So far, however, there's no evidence to support that contention, say Altshuler and David Cox, chief scientific officer of Perlegen Sciences in Mountain View, California. Cox led a private initiative that published its map in *Science* in February. Although the haplotypes identified in that map, of 71 Americans of Asian, European, and African ancestry, differ somewhat from those in the international consortium map, both should point gene hunters to similar DNA regions, says Cox. Exact haplotype boundaries don't seem to matter much, adds Altshuler, who compares a haplotype block with a mountain: No one agrees precisely on where one begins, but there's no dispute that it's there.

–JENNIFER COUZIN

# ScienceScope

## India Fissions Its Nuclear Research

U.S. and Indian officials gathered in New Delhi last week to start delicate negotiations over how India will separate its vast nuclear establishment into military and civilian components. In July, the allies agreed to share nuclear technology and expertise, an accord that promises to make India, which has refused to sign the Nuclear Nonproliferation Treaty, a full-blown member of the atomic club.

But which Indian facilities and researchers will come in from the cold remains a thorny issue. "There is an internal debate going on within India about where to go with this," says Harvard nonproliferation expert Matthew Bunn. Although some facilities—such as the Bhabha Atomic Research Centre in Mumbai—would likely stay secret, there will be a tug of war over others, including the fast breeder facility in Kalpakkam. Under the new agreement, facilities declared civilian would come under international safeguards and enable scientists to collaborate. U.S. envoy Nicholas Burns, who was in Delhi, warned that the separation plan could take years to implement. Finalizing the much-touted nuclear deal itself will require a series of changes to U.S. law and international rules, which the United States and India hope to see happen by early next year.

–RICHARD STONE

## U.S. Restricts 1918 Flu Virus

As expected, the federal government has declared the resurrected 1918 pandemic influenza virus a select agent and restricted its use. The government is also exploring whether other viruses containing any genes from the 1918 flu should be controlled.

Three weeks ago, researchers at the Centers for Disease Control and Prevention (CDC) in Atlanta, Georgia, and elsewhere reported that they had reconstructed the complete 1918 virus, which killed up to 50 million people (*Science*, 7 October, p. 28). Announced last week by CDC, the new designation requires lab registration with CDC, strict security procedures, and FBI background checks for researchers.

Now the agency must decide whether other viruses containing 1918 flu genes pose similar risks. "Viruses having even one 1918 gene exhibit exceptional lethality," notes microbiologist Richard Ebright of Rutgers University in Piscataway, New Jersey, in submitted comments. Even nucleic acids for 1918 flu genes should be controlled, Ebright argues.

–JOCELYN KAISER


Published by AAAS

NEUROSCIENCE

# Does Brain Cell Growth Drive Weight Loss?

Researchers are proposing that the long-lasting effect of a compound that triggers significant slimming in mice and humans is caused by the growth of new neurons in the brain's appetite-control center. If the find holds up—a company that tried to develop a related compound into a weight-loss drug is skeptical—it would be one of the first demonstrations of a physiological effect of new neurons in the adult mammalian brain.

The compound under debate, ciliary neurotrophic growth factor (CNTF), was originally identified as a protein that helps keep neurons alive and prompts their differentiation. But when researchers tested whether it could keep motor neurons from dying in patients with amyotrophic lateral sclerosis, they found an unexpected side effect: The patients lost their appetites and shed dramatic amounts of weight. Researchers in the late 1990s then found that the compound produced similar results in almost every type of obese mouse—those munching on high-fat diets as well as those with obesity-causing genetic mutations. Initial clinical trials of a related molecule called Axokine showed that it had significant effects in overweight patients as well (*Science*, 7 February 2003, p. 849).

Especially impressive was the long-lasting effect. With most weight-loss drugs, animals and people quickly regain any weight they've lost once they stop treatment. But those receiving CNTF or Axokine don't have the urge to binge that normal dieters do. "Many of us found the effect absolutely stunning," says Jeffrey Flier of Beth Israel Deaconess Medical Center and Harvard Medical School in Boston.

Initial hopes for Axokine dimmed when many patients in larger trials developed antibodies to the drug and stopped responding. But scientists are still trying to figure out why it and CNTF work the way they do. On page 679, Flier and his colleagues Maia Kokoeva and Huali Yin conclude that CNTF prompts the growth of new neurons in the brain region called the hypothalamus, which plays a crucial role in controlling appetite and the body's energy balance.

The researchers gave mice that had been on a 2-month high-fat diet a 7-day treatment of both CNTF and bromodeoxyuridine (BrdU), a compound that marks newly divided cells. The compounds were injected directly into the cerebrospinal fluid via miniature pumps. As expected, compared to a control group, the CNTF-treated mice lost weight during treatment and kept it off for at least 2 weeks after.

At that point, the researchers examined the hypothalamus in both groups of mice.

**More brain, less gain?** Growth of new brain cells may curb appetite.

Those that received CNTF had about six times the number of BrdU-positive cells, especially around areas where the CNTF receptor is expressed. A stain that identifies maturing neurons marked some of the new cells. And some new cells also seemed to respond to an injection of leptin, a hormone made by fat cells that regulates appetite by signaling cells in the hypothalamus and other brain areas.

The team also gave one group of mice CNTF along with AraC, a compound that blocks cell division. The mice that received AraC and CNTF initially lost weight, but after going off both drugs, regained the weight and then surpassed even control mice that had been eating extra calories during the whole experiment. Flier suggests that CNTF has a dual function: During treatment, it suppresses appetite by activating the leptin-responsive pathway in the hypothalamus. And by triggering the growth of new leptin-responsive neurons there, it makes the body more sensitive to leptin even after treatment is stopped.

"It's a very clever set of experiments," says Jeffrey Macklis of Massachusetts General Hospital and Harvard Medical School in Boston, who studies neurogenesis. However, he doubts CNTF is promoting new cell division. More likely, he says, the compound is supporting the survival of immature brain cells that might normally be produced in small numbers in the hypothalamus. Theo Palmer of Stanford University in Palo Alto, California, calls the work "very exciting" but adds that the paper doesn't test whether the leptin-responsive newborn cells are full-fledged neurons or whether newborn cells in other areas contribute to the effects.

Moreover, George Yancopoulos of Regeneron Pharmaceuticals in Tarrytown, New York, the company that developed Axokine, challenges Flier's understanding of how CNTF works. The main effect, he says, can be explained by CNTF's suppression of appetite-increasing molecules such as the signaling factor NPY. Whatever CNTF's mechanism, neuroscientists and metabolism researchers are hungry for a resolution to the mystery.

—GRETCHEN VOGEL

SCIENCE POLICY

## French Agency Cited for Lack of Women

**PARIS**—France's main basic research agency, CNRS, drew sharp criticism this week over the lack of women on its board of directors. The furor erupted when physicist Elisabeth Dubois-Violette, former president of the CNRS scientific council, complained in letters to agency officials and Research Minister François Goulard that a new 21-member board includes only one woman, despite a recent law guaranteeing women parity in the workplace. Goulard added fuel to the fire when he was quoted in the newspaper *Le Monde* as saying that Dubois-Violette was upset because she had not been given a CNRS directorship. Dubois-Violette rejects the accusation: Having served as scientific council chief for 4 years, she told *Science*, "I ... want more time to devote to my research."

The dispute quickly blossomed on the Internet. Cell biologist Alain Trautmann, who led the researcher protest movement against government spending cuts last year, launched a petition calling for more women in science policy positions; early this week it had gathered hundreds of signatures. The fracas is adding to woes of the embattled CNRS, whose top officials—President Bernard Meunier and Director Bernard Larrouturou—have clashed over a plan to reform the agency.

—BARBARA CASASSUS

Barbara Casassus is a writer in Paris.

CREDIT: STEVEN PUETZER/GETTY IMAGES



Published by AAAS

MEDICINE

# Fused Genes May Help Explain the Origins of Prostate Cancer

Although gene fusions are well known to drive the development of blood cancers, such as leukemias and lymphomas, only rarely have they been detected in the common solid cancers, such as breast, prostate, colon, and lung cancer. Now researchers have uncovered the first evidence that such fusions play a widespread role in prostate cancer.

The finding comes from Arul Chinnaiyan of the University of Michigan Medical School in Ann Arbor and his colleagues. On page 644, they report that perhaps as many as 80% of prostate tumors carry fusions of a segment of a gene called *TMPRSS2* with either of two genes encoding related proteins, ERG and ETV1, involved in gene regulation.

Because the two proteins are components of a major cell growth control pathway, the finding may help explain the origins of prostate cancer and provide a new target for therapeutic drugs. "If it holds up, it's the most common somatic [genetic] change in prostate cancer—and it's a fascinating one," says William Isaacs, a prostate cancer expert at Johns Hopkins University School of Medicine in Baltimore, Maryland. "It will invigorate the field in terms of looking for these kinds of fusions in other common cancers."

Although cancer researchers suspected that gene fusions might be lurking in solid cancers, the abnormalities eluded detection partly because the tumors display so many chromosomal abnormalities that it's hard to sort out which are significant. To get around this, Chinnaiyan and his colleagues took a bioinformatics approach to look for "outlier" genes: those that show very high expression in a set of cancers. They first surveyed the Oncomine database, a set of gene-expression data from DNA microarray experiments that was compiled by the Michigan team. "We found that we were picking up known gene rearrangements," Chinnaiyan says. "That told us we were on the right track."

Among the top 10 outlier genes identified were *ERG* and *ETV1*—both overexpressed in prostate cancers. *ERG* was already known to be involved in oncogenic fusions, especially in Ewing sarcoma, a relatively rare bone cancer. And earlier this year, a team led by Gyorgy Petrovics and Shiv Srivastava of the Uniformed Services University in Rockville, Maryland, reported that the gene is overexpressed in prostate cancer. Now, the Chinnaiyan team's work provides a possible explanation for why *ERG* is overactive.

The researchers found that in prostate cancers, each gene was frequently fused to the beginning segments of *TMPRSS2*, which encodes a protein-cutting enzyme that is turned on by the male hormone androgen. The gene fusions occurred both in cultured lines of prostate cells and also in about 80% of the 29 primary prostate cancers examined. They were present, however, only in those cells with high expression of *ERG* or *ETV1*, an indication that the fusions might underlie the excess activity of the genes. The overactivity may be due to the fact that the fused *TMPRSS2* sequences carry so-called androgen response elements needed for androgen stimulation.

Indeed, androgen treatment greatly enhances ERG production in cell lines carrying the fused gene. The finding is intriguing because many prostate cancers are androgen-dependent early on and thus can be treated with drugs that block action of the hormone. Ultimately, though, this dependence is lost and the cancers grow again. The fused *ERG* and *ETV1* genes would be one place to look for the changes leading to that outcome, Isaacs says.

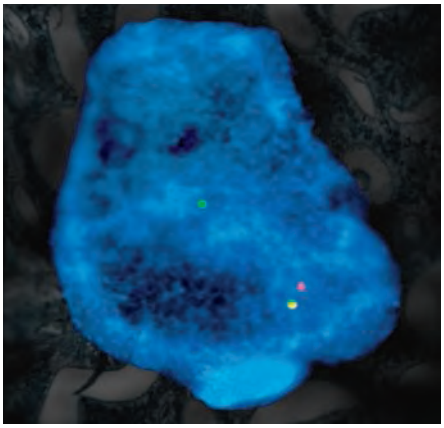

**Getting together.** In this prostate cancer cell, the *ETV1* gene (*red*) and the *TMPRSS2* gene (*green*) are joined (*yellow*) on one chromosome.

CREDIT: S. A. TOMLINS *ET AL.*, *SCIENCE*

Whether identifying these gene fusions will lead to better therapies for prostate cancer remains to be seen. There is precedent, as the leukemia drug Gleevec blocks the product of a fused kinase gene. But ERG and ETV1, which are transcription factors that regulate gene expression, present tougher targets.

Also unknown is whether similar gene fusions, also called translocations, occur in other common solid cancers. Janet Rowley of the University of Chicago, who pioneered the early translocation work, is eager to find out. "This approach cries out for application to all large [gene] expression databases as a remarkable tool for discovery of critical genes and, potentially, new common translocations," she says.

–JEAN MARX

## ScienceScope

### ITER Head Named

The first director-general of the $11 billion International Thermonuclear Experimental Reactor (ITER) is likely to be Kaname Ikeda. A University of Tokyo engineering graduate, Ikeda worked his way up through the ranks at the former Science and Technology Agency before entering Japan's diplomatic corps; he is currently ambassador to Croatia. Barring objections from other ITER partners, Ikeda's appointment will likely be formally announced at an ITER meeting in Vienna in December. European negotiators agreed after an 18-month standoff over the reactor's site to support Japan's director-general nominee; Japan in turn agreed to back the European Union's candidate site of Cadarache, France, where construction could begin by 2007.

–DENNIS NORMILE

### Prize for Cheap Sequencing

The first team to demonstrate a genome sequencing method costing $1000 could win a prize under consideration by the X Prize Foundation in Santa Monica, California. Announced last week at a Hilton Head, South Carolina, meeting and expected to be in the millions of dollars, the award would supplant a $500,000 pledge by the J. Craig Venter Science Foundation in 2003. The X Prize Foundation, which has previously funded spaceflight prizes, will decide next week about the new prize's future. The rules will likely demand that a contestant completely sequence 100 human genomes by the end of the decade—or sooner.

–ELIZABETH PENNISI

### Stem Cell Law Decelerated

Frustrated activists are looking toward next year for a Senate vote to relax restrictions on stem cell research. In July, Senate Majority Leader Bill Frist (R–TN) promised a prompt vote on S. 471, a measure passed by the House in May that would allow federally funded researchers to work with human embryonic stem cell lines now restricted by the White House. Lobbyists say the measure can easily pass the Senate, but hurricanes and Supreme Court nominees have blown stem cells off the calendar. Co-sponsor Arlen Specter (R–PA) said last week that Frist has now committed to bringing it to the floor before next Easter. The House bill passed 238–194 in May; President George W. Bush has threatened a veto.

–CONSTANCE HOLDEN



Published by AAAS

EUROPEAN SCIENCE

# Aggrieved Turkish Scientists Welcome an E.U. Review

Scientists who accuse Turkey's leading politicians of meddling with scientific freedoms and stifling debate are hoping the European Union (E.U.) will take notice. These complaints could have far-reaching consequences: This month, Turkey was invited to apply for E.U. membership, which requires the country to demonstrate that its research establishment meets European standards. Critics say that scientific independence has declined in Turkey, but a Turkish science official dismisses this view as coming from a privileged group that's been displaced by a shakeup.

Several prominent leaders in Turkey's science community—many of them current or former heads of research boards and institutes—have aired grievances about research oversight. They charge, for example, that the government has stacked the board of the country's main research funding body, TÜBITAK, with political supporters. Indeed, critics say that Turkey's Prime Minister Recep Tayyip Erdogan has refused to end political cronyism in spite of several court decisions that declared the disputed appointments illegal. They also say that new rules governing university and research appointments allow politicians to play favorites. If the E.U. investigates, "it's going to be a very uncomfortable problem" for the government, says Sevket Ruacan, a professor emeritus of pathology at Hacettepe University School of Medicine in Ankara and former TÜBITAK board member.

The dispute over TÜBITAK started shortly after Erdogan came to power in May 2003. As the new prime minister and head of the Islamist-leaning Justice and Development Party, he declined to approve the election of six new TÜBITAK board members. According to the body's bylaws, the governing board has the authority to elect new members, although the prime minister appoints them. Erdogan also overruled the board's decision to reelect physicist Namik Kemal Pak as its president. Instead, Erdogan pushed through a new law allowing the prime minister to appoint board members directly. Erdogan then named his own list of six board members and appointed Nüket Yetiş, an engineering professor at Marmara University in Istanbul, acting president.

The critics' second big concern is that a new policy requiring government approval of new university positions will increase political meddling. Until last year, the Turkish board of higher education approved requests for new research positions, from graduate students to assistant professors. But a law passed in May 2004 says the prime minister's office must give the go-ahead before lower-level university posts can be created or filled. "They are taking the universities under their yoke directly," says Istanbul Technical University geologist Celal Sengör, a foreign member of the U.S. National Academy of Sciences and an outspoken government critic. "If they don't like the person, they can take away the position."


**Interference?** Critics say Turkey's Prime Minister Erdogan stacked the nation's main research funding agency, TÜBITAK, with party favorites.

The main opposition party in Turkey has brought both matters to the country's Constitutional Court, which declared the government's moves illegal. But the government's appointees remain in place, and there has been no change in the approval system for new positions. In the meantime, Sengör and others say, the government is funneling more of the country's research budget through TÜBITAK, cutting funds that were previously allocated directly to universities.

But TÜBITAK vice president Ömer Cebeci says that university budgets have increased in the past 2 years, although not as much as TÜBITAK's, which he says has grown from about $8 million in 2003 to more than $60 million this year. He also claims that before the recent shakeup, TÜBITAK had been under the control of insiders who stifled new developments. TÜBITAK stood still for 40 years, he says, "while Turkey and its universities and scientists grew. This was unacceptable. It was a nice toy for a limited number of people." Cebeci says the science community has responded positively to the changes. "In 2003, when the TÜBITAK administration was not getting along with the government, they received 850 funding applications. In 2004, we had proper relations with the government," and the organization received 3800 proposals, he says.

Ruacan, who resigned earlier this year from the TÜBITAK board in part over the legal controversy, says he is torn about the increased budgets. "More money is being given," he acknowledges, but he worries that it may not go to the best science. "It is a sort of a bribe to the scientific community. All of a sudden they have enormous resources, and … universities don't want to speak up" about political influence on funding or appointments, he says.

Aykut Kence, a professor of biology at Middle East Technical University in Ankara and an outspoken proponent of teaching Darwin's theories of evolution (*Science*, 18 May 2001, p. 1286), says that TÜBITAK has rejected all five of his research funding applications since 2003. He says the agency told him the proposals were not original or would not have a significant impact. "I don't want to believe that it is for political reasons," he says, but he adds that he had no trouble getting funding before 2003.

Ruacan says he hopes the E.U. negotiations will encourage the government to abide by the court rulings. "The E.U. talks are going to have a positive effect overall. The E.U. asks so many questions, it sometimes annoys everyone. But in these matters, the E.U. taking notice might encourage the government to pay attention to the law."

–GRETCHEN VOGEL

CREDIT: UMIT BEKTAS/REUTERS

Asian scientists are a major presence in U.S. biomedical research labs. So why do so few hold leadership positions?

# A Glass Ceiling for Asian Scientists?

Virologist Kuan-Teh Jeang always thought it strange that his employer, the National Institutes of Health (NIH), would celebrate Asian Heritage Week each year with a cultural fair. "We're not known for being great cooks or dancers. We're known for being great scientists," says Jeang about an ethnic group that, according to 2000 census data, comprises 14.7% of U.S. life scientists despite being only 4.1% of the nation's overall workforce. So last year, he and the NIH/Food and Drug Administration Chinese American Association launched a new tradition: inviting a distinguished Asian researcher to give a scientific talk.

This May, as Asian Heritage Week approached, Jeang and his colleagues had another idea: Why not use the occasion to examine the status of Asian scientists within NIH's intramural program? Jeang had already collected some disturbing numbers about opportunities for career advancement at NIH, and he was eager to see whether his numbers squared with an official tally by NIH officials.

To his chagrin, they did. Whereas 21.5% of NIH's 280 tenure-track investigators (the equivalent of assistant professors) are Asian, they comprise only 9.2% of the 950 senior investigators (tenured researchers) at NIH. And only 4.7% of the roughly 200 lab or branch chiefs are Asian. (For this story, the term "Asian" includes all scientists with Asian surnames, regardless of their citizenship or immigration status. The group is dominated by scientists of Chinese, Korean, Indian, Pakistani, or Japanese origin.) Within particular institutes, the numbers were even more sobering. As of this spring, just one of 55 lab chiefs at the National Cancer Institute, NIH's largest, was Asian. At the National Institute of Allergy and Infectious Diseases, where Jeang works, none of the 22 lab chiefs was Asian.

To Jeang and others, the numbers point to a glass ceiling for Asian life scientists seeking to move up the career ladder. Asians are welcome in most labs, the numbers seem to say, and those who prove themselves can earn a permanent position. (Taiwan-born Jeang, who holds both an M.D. and Ph.D., came to NIH as a medical staff fellow in 1985 and was tenured in 1993.) But they shouldn't expect to enter senior management. "We feel that the field is not level," says Jeang, who has calculated that, at NIH's three largest institutes, Asians make up roughly 12% of the eligible pool from which lab chiefs are drawn.

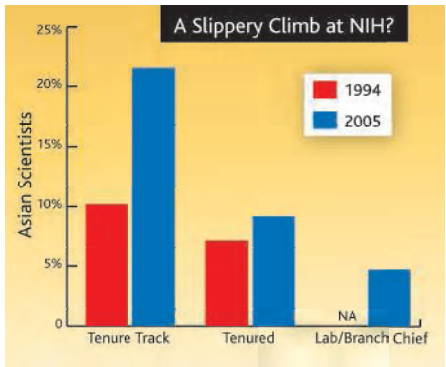


**Pressure from below.** Asian scientists are underrepresented among tenured staff and lab chiefs.

NIH isn't the only place with a glass ceiling, say some Asian life scientists. This summer, neuroscientist Yi Rao of Northwestern University in Evanston, Illinois, took a look at the leadership ranks of the two major professional societies in his field: the Society for Neuroscience (SfN) and the American Society for Biology and Molecular Biology (ASBMB). What he found was even more troubling than the NIH figures.

His snapshot showed that none of the 26 ASBMB council members was Asian, nor were any of the 193 members of the society's 11 standing committees. Asian scientists make up fewer than 4% of the 703-member editorial board at its top-tier *Journal of Biological Chemistry* (*JBC*), and none of the 21 associate editors with decision-making authority. Asians are equally invisible among the leadership ranks of the neuroscience society, Rao found. They hold only two of nearly 300 seats on 18 committees, and none of the 15 elected officer and councilor posts. Looking back, Rao found that only a handful of Asian scientists have ever held such elective positions in the society's 36-year history.

Rao says the message is clear. "However the phenomenon can be described, the underlying problem is discrimination," he wrote in July letters to ASBMB and SfN governing officers. "Chinese Americans tend to be quiet, partly because their voices and concerns are not listened to. But should that mean obedience and subordination forever?"

Senior officials at NIH, SfN, and ASBMB don't dispute the numbers, although some say they were surprised by them. "There's an appearance of a glass ceiling, which is troublesome," says Michael Gottesman, who heads NIH's intramural research program. "It makes you wonder if there's an inherent bias."

Looking for factors that might help explain the gap, he and others tick off the relatively recent arrival on the U.S. scientific scene of Asian scientists, language barriers, and cultural stereotypes that prevent Asians from being more aggressive in seeking pro-

CREDITS (TOP TO BOTTOM): MARTY KATZ; NIH



Published by AAAS

motions and honors. But in the end, they say, their organizations have an obligation to try to improve the situation. "The solution is straightforward. We need to make their accomplishments better known," says Gottesman, who met with Jeang and three other Asian scientists this summer to discuss how NIH could do better.

**The stealth problem**

For Rao, Jeang, and other Asian scientists, the recent data-gathering exercise confirms something they had long felt to be the case. "It's an unspoken truth," says neuroscientist Joseph Tsien of Boston University, who left China in 1986 for graduate school and later became a U.S. citizen. "We don't fall into the typical minority group because we're not underrepresented, especially in science. But you see so many [Asian scientists] at the bottom of the ladder and so few in the top ranks. … It's a funny situation." In a letter this spring to NIH Director Elias Zerhouni that prompted NIH to gather the data, Jeang explains that "we want to disabuse you of the common mythology that Asians don't want to be leaders."

But the issue is also very complicated, says Yu Xie, a sociologist at the University of Michigan, Ann Arbor, who has studied both the behavior of scientists and the growing presence of Asians in U.S. society. "Often people look at statistics, and they jump to the conclusion that there has been discrimination," says Yu, who came to the United States from China in 1982 for graduate school. "I haven't seen any evidence that it is the case. It might be true, but we just don't know enough to reach a conclusion one way or the other." Indeed, several Asian scientists interviewed for this article say they haven't experienced any type of glass ceiling. "I personally don't feel that it applies to me. But I'm not very sensitive," says Liqun Luo of Stanford University in Palo Alto, California, who earlier this year was named a Howard Hughes Medical Institute investigator.

Still, Luo says others have told him that the ceiling exists and that the issue seems to be on people's minds. A Stanford colleague contacted him after receiving Rao's letter, he says, and out of the blue, Luo says he was invited to be on SfN's program committee.

Neuroscientist Eve Marder of Brandeis University in Waltham, Massachusetts, who chairs the society's program committee, says she and the society's other officials believe strongly that all panels should have diverse representation. "It so happens that this year almost none of them do, and I recommended to the committee on committees that they be more proactive." She says she also suggested to Rao a tactic that has helped women rise through the ranks: "Forward us lists of people who are interested, so that nobody can say that they don't know any Asian scientists" who are willing and able to serve the society.

The head of the committee on committees, Irving Levitan of the University of Pennsylvania in Philadelphia, says he was "stunned" when he saw the numbers. "There is great consciousness about gender and underrepresented members," he says. "But frankly, we have not paid attention to Asian Americans because they are so visible in the lab."

**Levelheaded.** NIH's Kuan-Teh Jeang wants a level playing field for Asian scientists.

CREDIT: MARTY KATZ

For some ASBMB officials, the tone of Rao's message was as shocking as the message itself. "It was a very insulting letter," says Linda Pike of Washington University in St. Louis, Missouri. "He was accusing us of doing something that was awful and terrible and mean without bothering to find out why. You can't just look at the numbers."

In her reply to Rao, Pike explored a question often asked when the issue comes up: How many Asian scientists are truly qualified to hold leadership positions? "How many of the Chinese authors of scientific papers are in a position to serve on ASBMB committees?" she asked. "How many choose to return to their country, and how many seriously try to obtain faculty positions in the U.S.?" In addition, she noted that "a lack of language skills could put a faculty member at a severe disadvantage" in obtaining funding and, thus, building the track record needed to move up the career ladder. "While I sympathize with your concerns, there is much more that needs to be examined before diagnosing ASBMB as engaging in discrimination."

Even so, ASBMB is taking the charge very seriously, says president Judith Bond of Hershey Medical Center in Pennsylvania. Last month, Bond says, the society decided to invite "a Chinese-American member" of the *JBC* editorial board to become an associate editor, and the council plans to discuss the issue of a glass ceiling at its December meeting.

For Gottesman, inertia and a limited number of available slots are bigger obstacles to progress than the qualifications of Asian scientists. "The pool is getting bigger," he says. "But the average age of our lab chiefs is about 10 years more than it was 10 years ago. There's a need to turn those positions over more often." He says it's his job to remind the scientific directors to look at a broader spectrum of potential candidates for these jobs.

A glass ceiling doesn't mean that no individuals have risen to great prominence in the profession. Examples abound. In fact, some Asian scientists say that the critics have gone overboard in painting a bleak picture of the United States. "They are fighting for a good cause, but they are going to an extreme," says Mu-Ming Poo, a neuroscientist at the University of California, Berkeley, about those who claim that the data prove a glass ceiling exists. "The United States is the most tolerant society in the world, including China, for foreign scientists. In 10 years, Yi Rao will probably be holding one of these leadership positions, and so will many of his colleagues."

Indeed, many are anticipating a rosier future. It will come, they say, both because of the graying of the current generation of leaders and because Asian scientists will become more adept at learning how to get ahead. "This is America. And you need to embrace those qualities that are appropriate for success," says Victor Dzau, chancellor for health affairs at Duke University in Durham, North Carolina, who was born in Shanghai and educated in Canada and the United States. "It will require a conscious effort. But I would predict that the disparity will narrow as the next generation moves forward."

Jeang also believes that change is coming. Last year, he says, he was on the brink of leaving NIH when a senior colleague convinced him that history was on his side. "When I was growing up at NIH," the colleague confided to Jeang, "every chief of medicine and every director was a WASP. But all their right-hand men were Jewish doctors. Now all our right-hand people are Asian. It just takes time." That pep talk, plus a recent meeting with Gottesman, has persuaded Jeang that NIH means business. So he says he'll stick around and wait for a time when the disparity disappears.

–JEFFREY MERVIS



Published by AAAS

# South Africa's Bone Man: 80 and Still Digging Into the Past

**With a career spanning the days of legends like Dart and the Leakeys and today's systematic practitioners, Phillip Tobias has shaped paleoanthropology, and much else, in southern Africa**

JOHANNESBURG, SOUTH AFRICA— The year before Phillip Vallentine Tobias was born, miners blasting a lime deposit in South Africa found a grapefruit-sized skull that seemed more rock than bone. That fossil, the Taung child, was sent to anatomy professor Raymond Dart, who startled scientists in 1925 by contending that the child's skull represented an intermediate creature between ape and man—igniting a fierce debate about the African origins of humanity that took 2 decades to resolve.

Eighty years later, Tobias—who succeeded Dart as head of the University of the Witwatersrand's anatomy department and surpassed his mentor's expertise in studying ancient human bones—now waits anxiously to join younger colleagues in examining what he believes to be the most important South African fossil since the Taung skull: the complete skeleton of "Little Foot," an *Australopithecus* ape-man who fell to his death 3 million years ago in Sterkfontein cave, about 60 kilometers west of here.

**Among old friends.** Tobias with *Australopithecus* and other skulls from southern Africa.

During the 8 decades between the Taung skull and Little Foot, Tobias—perhaps South Africa's most honored living scientist—pursued his career as an anatomist and emerged as a key figure in paleoanthropology between visionary pioneers such as Dart and today's more systematic practitioners. Digging into Tobias's career, one unearths strata after strata, marking a complex scientific life that has crossed many disciplines—from caves to chromosomes, from studies of human growth to detailed analyses of fossil skulls. Two themes stand out: humankind and Africa.

"I have sometimes been asked, in a derisive tone: 'What has *Africa* given the world?'" says Tobias, enunciating each syllable as he sits in his memento-filled office at the Witwatersrand University medical school. "And I reply: 'Africa has given the world *humanity*.' That's not a bad contribution."

Tobias's own contributions to Africa, to his university (known as Wits), and to science have been considerable. He has authored 1130 publications, including landmark studies of the *Australopithecus* ape-man and the early human *Homo habilis*; conducted groundbreaking research into the growth patterns of the San, or Bushmen, and other indigenous Africans; enthralled students with his legendary lectures; and "inspired a generation of paleoanthropologists and many more by standing firmly against apartheid and pushing forward with science in South Africa," says paleoanthropologist Tim White of the University of California, Berkeley.

When Tobias turned 80 this month, he was overwhelmed by the outpouring of affection and praise. The nation's Royal Society honored him with a special issue of its journal; the new visitor center at Sterkfontein cave was named the Tobias Center; and more than 250 colleagues, officials, and friends gathered for a dinner in his honor—with a skeleton named Yorick presiding next to the podium. The first volume of Tobias's memoirs, *Into the Past*, was published this month, and Wits is holding an international "African Genesis" paleoanthropology conference in his honor.

Tobias's personality looms large at Wits. He is legendary for his punctuality, his long but brilliant lectures, and his incredible memory for detail. Although he retired as an active anatomy professor in 1990, Tobias remains emeritus director of the university's Sterkfontein Research Unit and works in his office at the Wits medical school several times a week.

During a 2-hour interview, Tobias joked about the "rogues' gallery" of 20th century paleoanthropologists and political figures that fills nearly every inch of his office wall. He had anecdotes about every luminary pictured: Dart, "the most unforgettable figure known to me"; Louis and Mary Leakey, pictured at the Olduvai Gorge, where they found hominid bones that Tobias analyzed; and Ralph von Koenigswald, a friend who analyzed the Java Man fossils; as well as two former South African leaders, Jan Smuts, a champion of fossil digs, and Nelson Mandela, who awarded Tobias the Order of the Southern Cross for service to the nation.

As a Wits medical student in the mid-1940s, Tobias entered an anatomy department led by Dart that was "steeped in physical anthropology." But Tobias focused on genetics. He and a fellow Wits student, Sydney Brenner—later to win a Nobel Prize for his work in molecular genetics—both analyzed mammalian chromosomes. Whereas Brenner joined the exodus of South African scientists who left the country during the 1950s, Tobias opted to stay and fight the apartheid system at the university level. He became president of the National Union of South African Students at Wits and later helped lead the effort to force an official inquiry into physicians' mistreatment and neglect of Stephen Biko, a leader of the antiapartheid struggle who died in prison.

While he was working on chromosomes, Tobias also traveled to South African sites to dig up and collect fossils. "I had two strings in my bow: genetics and anthropology," he recalls. In 1955, one of his mentors—Oxford University anatomist Wilfrid LeGros Clark—suggested that Tobias make a choice; he opted to pursue physical anthropology. He began to study the San people of south-central Africa, research that led to groundbreaking publications showing that the Bushmen were getting taller. Later, however, Tobias and colleagues showed that this was not true of other indigenous populations in

CREDIT: GRAEME WILLIAMS



Published by AAAS

South Africa, and other studies confirmed that growth trends in many poorer nations did not match those of the developed world. "To my horror, I found that South African black people of the Bantu language group were not getting taller."

While studying the anatomy of living humans, Tobias retained his fascination with the remains of hominids that had died 2 million or more years earlier. When a Wits group led by Tobias began finding fossils at the Makapansgat lime-works site in 1945, legendary fossil-finder Robert Broom took notice and began his own research there. Broom's competition and the fossil finds at the site enabled Tobias to convince Dart—who had been stung by the negative reaction to his Taung skull paper in 1925—to return to paleoanthropology in the early 1950s. Although Dart was eventually proven correct about the Taung skull, his analysis of an array of sharp bones and other fossils at Makapansgat, which led him to conclude that early man was bloodthirsty and violent, was widely criticized. "Louis Leakey and I felt that the early humans were really rather gentle creatures," says Tobias.

Dart was Tobias's mentor in anatomy, but it was the Leakeys who drew him into the upper echelons of paleoanthropology. "I had avoided encroaching on Dart's domain, handing over fossils to him and confining my studies to living humans, until the Leakeys in 1959 asked me to tackle the analysis of the 'Dear Boy' fossil [then *Zinjanthropus*, but now called *Australopithecus boisei*]," says Tobias. "That launched me onto the pathway of paleoanthropology, which has been my major interest for the last 46 years."

Tobias views himself as a "hybrid" of two types of paleoanthropologist: the visionaries like Dart and Louis Leakey and the more detail-oriented laboratory analysts. White agrees, saying that "Tobias has played a crucial role in bridging paleoanthropology's pioneers with its modern practitioners." According to Tobias, "Louis Leakey tended to jump to conclusions; I was the one who often filled in the details." For example, after the Leakeys found the fossils later classified as *Homo habilis*, "Louis knew by instinct that this was a *Homo* specimen—that is, human, not ape-man. But I would not accept Louis's judgment on *H. habilis* until I had filled in all the details."

Paleoanthropologist Richard Leakey, the son of Louis and Mary, contends that Tobias's two-volume study of the *H. habilis* fossils "set a standard in paleoanthropology that I believe never will be equaled." Leakey, White, and paleoanthropologist Alan Walker of Pennsylvania State University, University Park, agree that Tobias will be remembered not only for that and his *Australopithecus* analysis but also for continuing the Sterkfontein excavation, despite years of backbreaking work during which few significant hominid fossils were found. Says Walker: "His work with various colleagues at Sterkfontein has produced large numbers of very important hominid fossils."

**The bone collector.** Tobias in Paris in 1955 with Neadertal, Cro-Magnon, and other skulls.

CREDIT: PAN MACMILLAN

On the surface, Sterkfontein seems an unlikely place for blockbuster discoveries. The dolomite cave lies under a nondescript landscape in hilly and rocky farmland west of Johannesburg. But the cave, first mined for its lime in the 1890s, preserved thousands of high-quality fossils in its breccia deposits. Broom died in 1951 and others left the dig; by the early 1960s, Sterkfontein lay neglected. "I started planning a new dig and—after consulting with leading people in the field—we decided to take a systematic approach, which has continued since 1966—5 days a week, 48 weeks a year," says Tobias, making it the longest continuous excavation of any cave in the world. "We have taken out about 600 hominid specimens since then."

The most startling find came in the mid-1990s when Ron Clarke of Wits spotted a hominid foot bone in a tray full of animal fossils and returned to the area the fossils came from. Clarke has spent the years since then carefully chiseling rock away from the bones his team discovered, exposing as much as possible of the complete skeleton in situ, dubbed Little Foot. The excavation is now nearly complete, and Clarke plans to make a plastic cast of the skeleton later this year and remove the fossil bones for analysis. "It is the oldest complete skeleton of a hominid ever found," says Tobias. Richard Leakey predicted that Little Foot, once excavation and analysis are completed, will prove to be "probably the most important to have been found in southern Africa."

Even so, south and eastern Africa are no longer the sole sources of early hominid fossils. Recent finds in Chad and Ethiopia have yielded fossils estimated to be much older than the South African and Tanzanian hominids. Over the past dozen years, scientists have discovered new species of fossil hominids at the rate of nearly one per year. Tobias is excited by the finds in Chad and Ethiopia and predicts that—if molecular evolutionists are correct that the chimpanzee-human split occurred more than 7 million years ago—excavations in less well dug sands of northern Africa may yield even older hominid fossils. "I would not be surprised if researchers in, say, Morocco eventually will find evidence of earlier hominids," says Tobias.

To peer even further back into humanity's origins, scientists will need a type of paleoanthropology very different from the pioneering digs in which Tobias began his career. "Today, we must work in teams," he says. "We need geophysicists to examine the paleomagnetism of the Earth's crust; dating experts to develop new techniques; molecular evolutionists; we need 'old-fashioned' anatomists who can read the bones; and our cultural brethren to help describe how the early hominids lived."

"Gone are the days of one strong, usually white male doing all the research," says Tobias. "These days, if you are excavating in areas that are not in your own country, you have a solemn duty to work with local scientists and students. … This is the new approach to paleoanthropology, and it is a good thing."

–ROBERT KOENIG

Robert Koenig is a writer in Pretoria, South Africa.

# The Plan to Unlock Lake Vostok

**After a 6-year pause to consider the risks of environmental contamination, a Russian research team will resume drilling through the Antarctic ice next month**

Beneath an ice sheet 4 kilometers thick lies one of the most isolated bodies of water on Earth, the immense Lake Vostok of East Antarctica. It has been locked up, researchers think, for more than 10 million years. But it may not remain so much longer. A team of Russian researchers is poised to resume drilling through its ice cap next month, restarting a project that has been on hold since 1999 while experts debated how to proceed. Despite an extensive review, some still fear that the team's approach could alter the lake and make it impossible to obtain untainted water samples.

But the Russians, led by Valerii Lukin, an oceanographer who directs the Russian Antarctic Expedition and ice coring at Vostok, have promised they will take it slowly, studying the ice as they inch toward the lake's surface. In late 2007, they plan to poke through and take the first sip of the waters.

Vostok is the largest of more than 100 subglacial lakes in the Antarctic. None has been directly sampled, and scientists in a variety of fields are eager to tap one. What they know at present comes mainly from ice cores and flyover observations, including radar and gravity measurements. Geologists and glaciologists want a peek at isotopes taken from the lake to understand how such lakes form and behave. Climate researchers would like to see if the sediments hold records of Antarctica's past. And biologists want to verify studies that suggest Lake Vostok supports life despite its utter darkness, near-freezing waters, and scant nutrients (*Science*, 2 March 2001, p. 1689).

But Antarctic researchers from several nations are concerned about contamination. The borehole at the Russian site now brims with 60 tons of drilling fluid, a soup of kerosene and Freon that teems with foreign bacteria. The critics worry that a leak could muck up the ecosystem permanently. The Russian team, however, is confident that its extraction technique will prevent this. And because Antarctica has no laws—just international treaties—there is little to hold them back.

### What lies beneath?

Surveys have identified about 145 subglacial lakes dotted around Antarctica, but the figure "is by no means exhaustive," says Martin Siegert, a glaciologist at the University of Bristol, U.K. "It wouldn't surprise me if there are more than 1000." Yet for many scientists, Vostok remains the Holy Grail. The Manhattan-shaped lake is probably the largest—250 kilometers long and 50 kilometers wide—and possibly the oldest. It sits in a deep depression between two tectonic plates, says glaciologist Michael Studinger of Columbia University's Lamont-Doherty Earth Observatory in Palisades, New York. Glaciologists believe it may have formed before Antarctica froze solid, 15 million to 30 million years ago. Climate records don't reveal much about this period, but sediments on the lake floor could give "a record of Antarctica's change from greenhouse to icehouse," Studinger says.

Although researchers have taken no direct samples, cores from ice just above Lake Vostok have given them a glimpse of its chemistry and the potential for life inside. Studies of trapped isotopes and of the ice's crystal structure suggest that the ice melts at the base of the sheet, mixes with the lake, and slowly refreezes, locking some water in this "accreted" ice. "We used to think some heat source below Lake Vostok was necessary to keep it liquid," Studinger says. But isotopes in the accreted ice suggest that the underlying rock "seems to be a rather old and stable piece of crust." The uniform heat rising from Earth's depths, coupled with the immense pressure of the overlying ice, appears to keep the lake liquid.

The primary scientific disagreements center on whether the lake can sustain life. Microbiologist John Priscu of Montana State University in Bozeman says his group has recently cultured about two dozen samples of bacteria from accreted ice; they can tolerate temperatures below 10°C but grow slowly. He estimates there are about 100 bacteria per milliliter in the accreted ice and predicts that the surface waters hold about 10,000 per milliliter, about a hundredth the density in the open ocean—still a lot given the conditions.

Radically different results come from studies led by Sergey Bulat, a molecular biologist at the Petersburg Nuclear Physics Institute in Russia. Using different methods to clean drilling fluid off ice cores and different standards to identify lake inhabitants, his group found little DNA in the accreted ice that they consider to be from bacteria in the lake. And the DNA they did find, surprisingly, matched most closely that of heat-loving bacteria in hot springs. Bulat speculates that the lake bottom could have warm vents, similar to deep-sea vents.

Still others are skeptical about most of the data on life from Lake Vostok's accreted ice. Molecular biologist Eske Willerslev, who studies ancient DNA at Copenhagen University in Denmark, says, "It's a very promising area, but it needs much more controlled experiments." The first step toward resolving differences, scientists

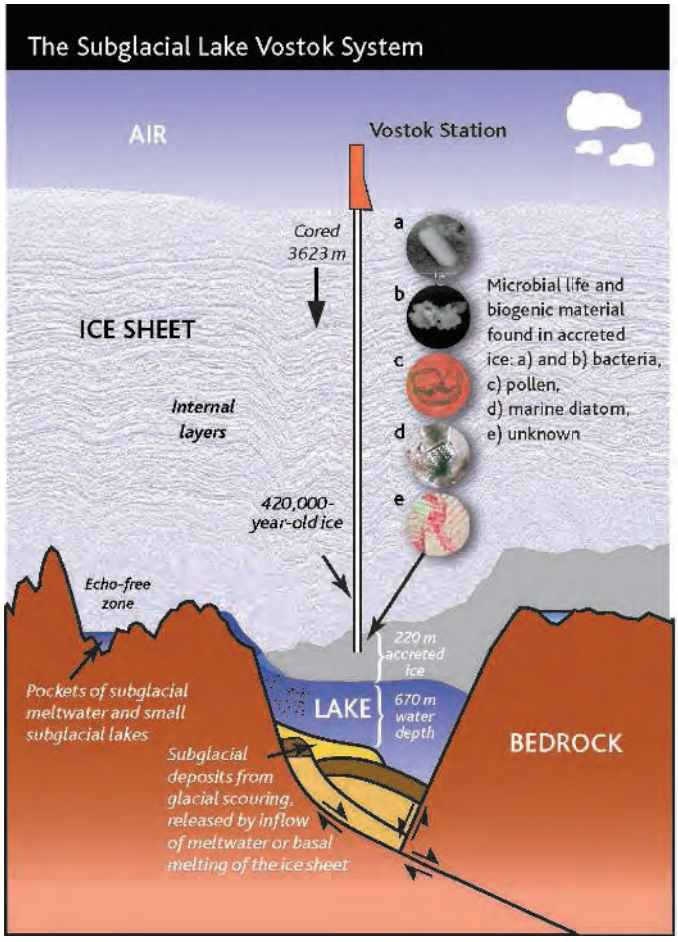


CREDIT: M. STUDINGER AND R. E. BELL/LAMONT-DOHERTY EARTH OBSERVATORY; INSET IMAGES (TOP TO BOTTOM): J. PRISCU; D. KARL; L. BURCKLE AND R. SAMBROTTO (C-E)



Published by AAAS

agree, is to get some lake samples. "We know more about the deepest parts of the oceans than we do about these lakes," Priscu says. "Until we get into these lakes, we'll just sit here and speculate."

### A big surprise

Working on climate studies, the Russian team has already extracted one of the world's longest ice cores above Lake Vostok, drilling 97% of the way through the ice sheet. They stopped to consult other experts around the world in 1999, about 130 meters short of the lake's surface. The Russian government has given the team permission to use a mechanical drill to go 50 meters further in the 2005–'06 season, starting in November. The team plans to drill mechanically another 50 meters in 2006–'07, then switch to a hot, ice-melting probe for the final 30 meters in 2007–'08. After poking through the base, they will allow water to flood up into the borehole and freeze, then take out an ice core. "It's a quite cheap, doable, plausible experiment," Siegert says.

But critics of the plan worry that the pressure may drive lake water into the drilling fluid. Some point to a bad experience with the North Greenland Ice Core Project in 2004. Researchers drilled to the bottom of the island's ice sheet to collect water samples but had a "big surprise," says glaciologist Sigfus Johnsen of Copenhagen University, who worked on the project. Five meters higher than expected, water flooded into the hole and got contaminated with drilling fluid. Perhaps they broke through sooner, Johnsen says, because the base was not flat but ridged with high conduits. Priscu's group found bacteria in the ice core, but he asks: "Are they from the drilling fluid or the bottom of the ice sheet? We don't know." Willerslev, who has also studied the same cores, says, "The samples are completely contaminated and completely useless."

A mishap like this is unlikely at Vostok because the ice ceiling over the water is unlikely to have conduits, Johnsen says. Still, the base might have weak "soggy ice" that will give way, worries microbial ecologist Cynan Ellis-Evans of the British Antarctic Survey in Cambridge. Others contest this: "There are no arguments to say the quality of the ice is poor," says glaciologist Jean-Robert Petit of the Laboratory of Glaciology and Geophysiology of the Environment in Grenoble, France. And the Russians are "very good drillers and have great engineers," Priscu says. "They seem genuinely concerned about environmental disasters." Nonetheless, Petit, Priscu, and others are concerned.

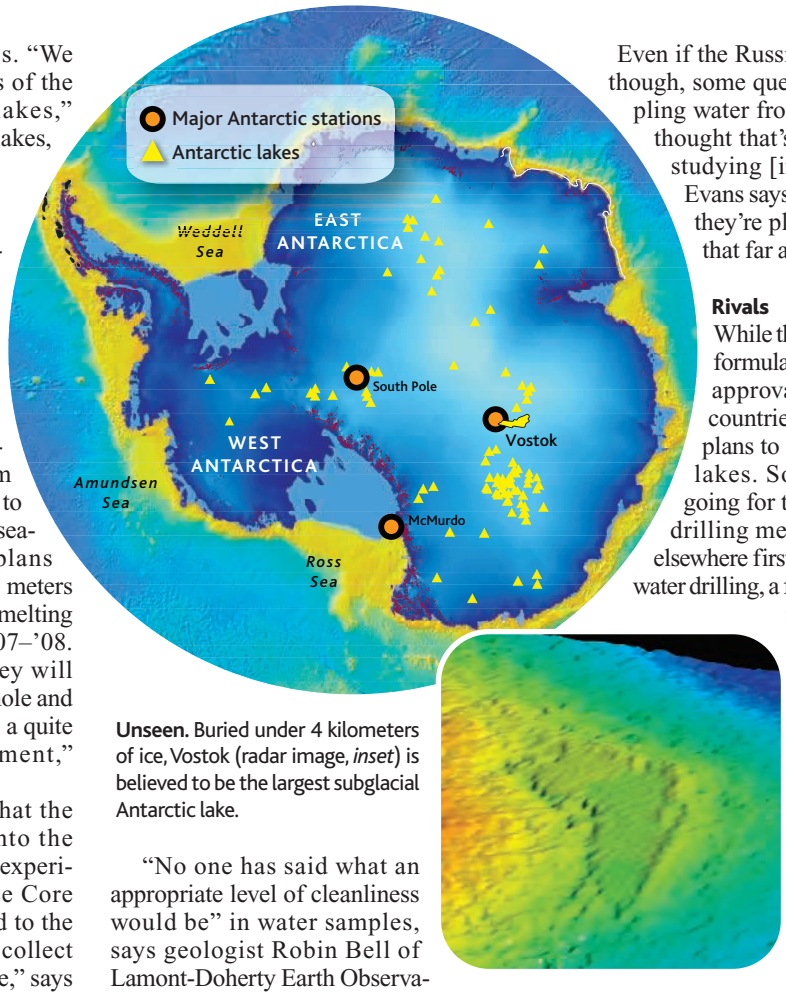


**Unseen.** Buried under 4 kilometers of ice, Vostok (radar image, *inset*) is believed to be the largest subglacial Antarctic lake.

"No one has said what an appropriate level of cleanliness would be" in water samples, says geologist Robin Bell of Lamont-Doherty Earth Observatory. Many are also skeptical of the Russian team's plans because their drilling equipment has not been field-tested. (Project chief Lukin says tests are not necessary.) "There's a lot of discomfort with the Russian plan," Bell says.

Even a little bacteria from the drilling fluid could swamp life in the lake or swap DNA and viruses with indigenous microbes. If the lake gets exposed to outside bacteria, says microbial ecologist Cynan Ellis-Evans of the British Antarctic Survey, "you've opened Pandora's box." The Russians' plan has also drawn the ire of the Antarctic and Southern Ocean Coalition (ASOC), a nongovernmental watchdog organization. "Russia's using technology that was never designed to be ultraclean. It's not up to the task," says Ricardo Roura of ASOC.

But Lukin thinks the critics are exaggerating. He agrees that the lake is under pressure: He estimates about 375 times atmospheric pressure at its surface, comparable to the deep ocean. But he says the weight of the drilling fluid in the borehole should roughly balance it, holding the drilling apparatus in place and keeping the lake's water put. Besides, Lukin says, the apparatus is designed to prevent leakage: "I am convinced the concerns about possible contamination of the lake's water with the drilling fluid do not have any physical grounds."

Even if the Russian plan goes smoothly, though, some question the value of sampling water from the lake's surface. "I thought that's what we were already studying [in accreted ice]," Ellis-Evans says. "I cannot see that what they're planning would put us all that far ahead."

### Rivals

While the Russian team has been formulating its plan and seeking approval, researchers in other countries have been cooking up plans to explore other subglacial lakes. Some argue that before going for the crown jewel, Vostok, drilling methods should be tested elsewhere first. A leading option is hot-water drilling, a fast and clean but energy-intensive method that many think impractical for Vostok, which boasts Earth's coldest recorded temperature, –89°C. U.K. researchers are focused on Lake Ellsworth, a relatively small subglacial lake in West Antarctica, and Italian researchers are targeting Lake Concordia, a neighbor of Vostok in East Antarctica about half the size. These plans are in their infancy, however, and researchers are unlikely to get in and take water samples before 2007, when Russia plans to enter Vostok. Should Russia decide to go ahead without waiting for data from other sites, there is little other countries could do.

The main forum for vetting research proposals is the annual Antarctic Treaty Consultative Meeting, where researchers submit environmental assessments and get back advice. The Russian team has already submitted preliminary assessments for the next 2 years. This satisfies the requirements for now, but the treaty requires Russia to submit a more comprehensive assessment 60 days before drilling to the water's surface. After they see the details, researchers worldwide will weigh in.

Countries are not obliged to follow such advice, but normally they do. If Russia were to go forward in the face of international opposition, "it would absolutely be a big break from tradition," Ellis-Evans says. Lake Vostok could become a test of how well the treaty actually protects the continent. "It's a showcase for the Antarctic Treaty," Priscu says. But ultimately the decision on whether and how to go into Lake Vostok rests with Lukin's team and the Russian government.

**–MASON INMAN**

Mason Inman is a writer in San Francisco, California.

CREDITS: MAP ADAPTED FROM MICHAEL STUDINGER/LAMONT-DOHERTY EARTH OBSERVATORY; SOURCE: MARTIN SIEGERT; INSET: M. STUDINGER



Published by AAAS

# 'Deviant' Burials Reveal Death on The Fringe in Ancient Societies

**Bodies buried in unusual ways—decapitated, stuffed into caves, or set aside in special cemeteries—offer clues to how the ancients treated their misfits**

**CORK, IRELAND**—From the numerous deep blade cuts on the back of the young man's skull, it seemed likely that the executioner had made a bad job of it. "It took at least four blows to get his head off," said Jo Buckberry, an osteologist at the University of Bradford, U.K. She added that the angles of the cuts suggest that the man had been kneeling with his head down when the blade fell.

Back in the 1960s, the excavators of this site of Walkington Wold in East Yorkshire had concluded that the skeletons they unearthed—nearly all decapitated males—were victims of a massacre during the late Roman occupation of Britain, around the 4th century C.E. But Buckberry's study of 11 of the skeletons, presented at a meeting* here last month, suggests that these were executions rather than war casualties. And recent radiocarbon dates on three skeletons show that they were buried at different times between 640 and 1030 C.E., during the Anglo-Saxon period and long after the Roman occupation. Thus Buckberry concludes that Walkington Wold was a special burial ground for criminals only.

Buckberry's talk was part of a daylong session devoted to "deviant" burials. Archaeologists have long analyzed elite burials, marked by opulent grave goods and dramatic monuments. But researchers recognize that in many societies, special burials were also given to outcasts and certain classes of people, including criminals, women who died during childbirth, people with disabilities, and unbaptized children. Investigating such burials can give insights into the "broader social and religious beliefs" of a society, says session organizer Eileen Murphy, an archaeologist at Queen's University in Belfast, Northern Ireland.

The session covered burials from 5000 years ago in Britain to 19th century Vienna and demonstrated some of the imaginative ways that humans have disposed of the corpses of people deemed to be different: Their bodies have been stuffed into crevasses in remote caves, tossed into peat bogs, and sliced into pieces, among other practices. Sometimes the motive behind such burials is clear. For example, in Catholic Ireland stillborn and unbaptized children were buried in isolated, unconsecrated burial grounds called *cillini*, beginning sometime after the 13th century C.E. and continuing as late as the early 20th century, says Murphy. But the reasons remain obscure for the relatively rare "charcoal burials" found across Europe between about 700 and 1250 C.E., in which the deceased was laid on top of or below a layer of charcoal.

**Cast out.** Decapitation cut marks suggest the headless bodies at Walkington Wold were executed criminals.

CREDIT: J. BUCKBERRY/UNIVERSITY OF BRADFORD

Moreover, because burial practices change over time, they can be used to track changes in societal values. Archaeologist Andrew Reynolds of the Institute of Archaeology in London described a survey of some 30 sites that suggests that Anglo-Saxons began to bury executed criminals separately only after they converted from paganism to Christianity beginning in the 7th century C.E. Previously, criminals and other outcasts were buried along with the rest of the community, although their bodies were often treated differently. For example, they were often buried face-down, their limbs were sometimes amputated, and their bodies were weighed down with stones; contemporary writings suggest these practices arose out of fear that the bodies might run around at night.

The switch to burying outcasts separately probably reflects new Christian ideas about "cleanliness and uncleanliness," as well as a continuing fear of the dead from pagan times, says Reynolds. "It is the geographical separation of 'bad' people rather than the individual burial rites that marks the major change in behavior between the two periods," Reynolds concludes.

Yet isolated burial is not always an indication of outcast status, argued biological anthropologist Stephany Leach of University College Winchester in the U.K. Leach reported on her studies of human remains from five caves in a 16-kilometer radius in a hilly region north of Manchester. Her work is the first systematic study of the bones, most of which were recovered in the early 20th century. New radiocarbon dates revealed that the burials clustered tightly between 4800 and 5000 years ago during the Early Neolithic period in Britain, when most burials were in scattered graves or in artificial earthen mounds called barrows, a treatment possibly reserved for the elite.

Leach found that the cave burials were all either children or adults suffering from severe arthritis or serious injuries. The early excavation records showed that some of the skeletons had been deliberately packed into cave alcoves and crevasses with a mixture of limestone and plant material known as tufa. Where the burial conditions were poorly recorded, Leach nevertheless often found traces of tufa on the bones. She considered several hypotheses to explain these burials, including that the people were spiritually excluded from the community or that they were simply left behind when the group moved on. But in her view the tufa packing shows special care, and she suggests that the suffering of these people was acknowledged by their burials in a "special" place.

Other researchers find Leach's ideas intriguing but say more data are needed. "Her findings do suggest that these were special members of society, but we need to know more," says Murphy. New excavations of nearby caves may help establish whether the burials really were special or just "a normal part of the repertory of Neolithic burials," she says. One thing seems certain: Burials at the margins of a culture have much to say about the core values of the society that interred them.

—MICHAEL BALTER

* 11th Annual Meeting of the European Association of Archaeologists, Cork, Ireland, 5–11 September 2005.



Published by AAAS

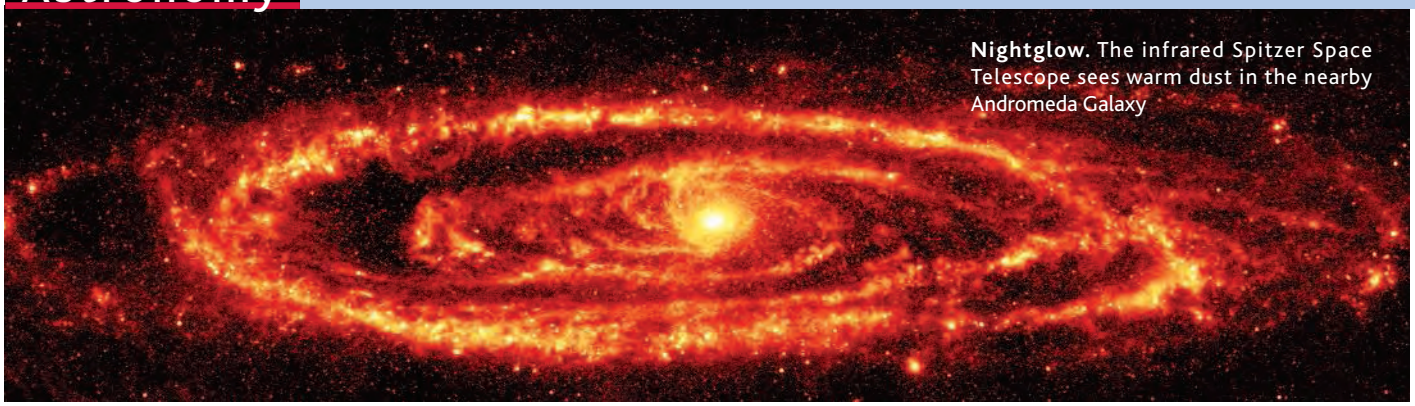

**Nightglow.** The infrared Spitzer Space Telescope sees warm dust in the nearby Andromeda Galaxy

# Astronomers Sweep Space for The Sources of Cosmic Dust

**Tiny interstellar grains dim the brilliance of many stars and galaxies, but the origins of the universe's ubiquitous dust remain hazy**

Long before the love song "Smoke Gets in Your Eyes" made its debut in 1933, astronomers had to contend with a smoky pall that dulled their view of the universe. Dark, sooty particles and fine, sandlike grains drift among the stars, obscuring attractions such as the cores of galaxies and the nurseries where new stars emerge. "Dust was a thing that just got in the way," says astronomer Angela Speck of the University of Missouri, Columbia.

Today, that dirty reputation has faded. Astronomers know that interstellar dust illuminates the erratic deaths of stars, and it traces a direct link from stars to the birth of our solar system—and ultimately, to Earth. Researchers can deduce the histories of ancient stellar grains, embedded for billions of years in meteorites and cometary debris. Yet astronomers still have a poor grasp of where these flakes of the cosmos puff into existence.

New observing tools are making inroads. Most notably, NASA's Spitzer Space Telescope is sensing the infrared warmth of dust motes near and far, within our Milky Way and in galaxies from the early universe. Much of the dust has an organic component, showing that old stars and ultraviolet light can combine to create a pervasive prebiotic haze.

But Spitzer and other telescopes have not yet resolved a key puzzle: Does most dust condense in gentle breezes of gas emitted in the dying gasps of stars like our sun, or as a result of the much rarer concussive blasts of supernova explosions? Models predict that vast volumes of dust, roughly equal in mass to our sun, should form in the aftermath of a supernova. However, observers have spotted less than 1% of that amount in the debris from these detonations. "This is a real conundrum," says astronomer Robert Gehrz of the University of Minnesota, Twin Cities.

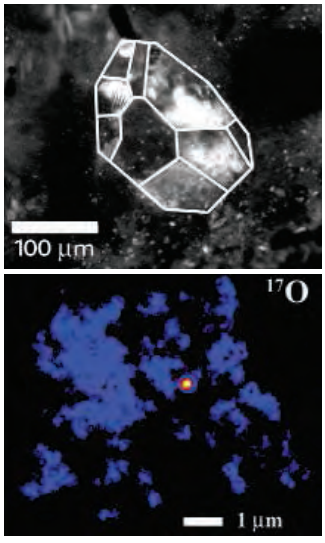


**Alien dust.** Isotope analysis singles out silicate grains from a supernova (*top*) and an old star.

### Stellar Grape-Nuts

No matter its source, interstellar dust rarely lasts long in its pristine state. Just a few hundredths of a micrometer across when they condense, dust grains easily disintegrate if they encounter shock waves or harsh radiation. Survival is a group effort: Grains clump like lint, often with help from icy rinds of water or carbon mon-oxide. This buildup is most fruitful in the reservoirs of gas called giant molecular clouds, which span dozens of light-years. As grains stick, they morph into micrometer-sized blobs that look like fractal clusters of Grape-Nuts cereal. Many such conglomerates settle into the whorls of nascent planetary systems around protostars, where they catalyze the growth of ever-larger pebbles.

By examining individual grains within primitive meteorites, researchers can unlock what astronomer Donald Clayton of Clemson University in South Carolina calls the "cosmic chemical memory" of interstellar dust. "It's a beautiful thing," says one of Clayton's former students, Eli Dwek of NASA's Goddard Space Flight Center in Greenbelt, Maryland. "Each dust particle locks in the composition of the source where it formed."

For example, one of the first extrasolar grains identified in meteorites was silicon carbide. The isotopic makeup of this cinderlike material did not resemble the blended ingredients of our solar system. Rather, cosmochemists found, the distinctive dust came from the smoky winds of old stars that sloughed off their outer layers in languorous waves.

Our sun will reach this brief phase of evolution in several billion years, as will all stars with about 0.8 to 8 times the sun's mass. When such stars run out of hydrogen at their cores, they start to fuse helium. That reaction releases more energy, bloating the stars into red giants. Later still, the helium begins to run dry. The stars then contract and expand in on-again, off-again pulses of helium burning, creating unstable orbs that would envelop the orbit of Mars in our solar system. For hundreds of thousands of years, stars in these rhythmic last gasps of fusion reside on what astronomers call the "asymptotic giant branch" (AGB) of a diagram that plots stellar evolution.

Gravity at the surfaces of distended AGB stars is so low that the outer layers escape with each expansive throb. When this liberated gas cools below 2000 kelvin, it starts to form tiny grains of dust. Their nature depends on the proportions of two elements forged by the stars' nuclear fires: carbon and oxygen, which quickly combine to make stable carbon monoxide gas. If there's carbon left over, a fraction of the gas will condense into sooty compounds such as graphite, silicon carbide, and complex organic molecules called polycyclic aromatic hydrocarbons. Oxygen-rich atmospheres spawn aluminum and titanium oxides as well as silicates with

CREDITS (TOP TO BOTTOM): NASA/JPL-CALTECH/K. GORDON, UNIVERSITY OF ARIZONA; S. MESSENGER *ET AL./SCIENCE*



*Published by AAAS*

calcium, magnesium, and iron—the stuff of sand and rocks.

As more dust forms, radiation from the luminous stars—thousands of times brighter than our sun—pushes on the grains. The dust accelerates away and drags more gas with it, making the stars shed mass copiously. Late-stage AGB stars may vanish in optical light as the new dust screens our view, but they shine with a dazzling infrared glow. A new Spitzer image of the nearby Andromeda galaxy features thousands of false-color red dots that astronomers believe are shrouded AGB stars.

Each low-mass AGB star is a modest dust factory, but there are so many of them that they may be the predominant sources of cosmic dust. Indeed, most of the presolar isotopes in dust grains embedded in meteorites appear to have arisen by capturing neutrons inside AGB stars. The stars then ejected the isotopes in gentle stellar winds, says cosmochemist Ernst Zinner of Washington University in St. Louis, Missouri. "Supernovae get a lot of the glory," Speck observes. "But the isotopes we see indicate that most of these grains formed at a much slower rate, not explosively."


CREDIT: SIDNEY HARRIS/SCIENCECARTOONSPLUS.COM

**Hot blasts, cold clumps?**

Galaxies today may teem with AGB stars, but that was not the case in the early universe. It takes billions of years for stars like our sun to reach the AGB phase. So if those stars churn out most cosmic dust, then galaxies in the young universe should have been much cleaner than today's polluted systems.

That's not what telescopes see. In the mid-1990s, a submillimeter instrument on the U.K.–operated James Clerk Maxwell Telescope at Mauna Kea, Hawaii, spotted extremely dusty galaxies that existed when the universe was just one-quarter of its current age. And in the past year, the Spitzer Space Telescope has found primordial galaxies choked with warm dust—in some cases, less than a billion years after the big bang.

Supernovae are the most logical sources, many astronomers maintain. A star more hefty than eight times the mass of our sun keeps fusing progressively heavier elements at the end of its life. It forms nested layers of carbon, oxygen, magnesium, silicon, sulfur, and ultimately iron at the core. When the thermonuclear chain stops at iron, the core implodes. The star then detonates its rich broth of heavy elements—the prime ingredients of new dust—into space.

Turbulent eddies within the debris concentrate the gas. For a while, any solid material that tries to form is instantly rended by the hot environment. "It takes at least a year for temperatures to get low enough to condense the seeds of dust grains," says postdoctoral researcher Ben Sugerman of the Space Telescope Science Institute in Baltimore, Maryland. "Around 1.5 to 2 years is when we really start to see unambiguous evidence."

The best evidence for dust freshly created by a stellar bomb is Supernova 1987A, which burst into view in the neighboring Large Magellanic Cloud in February 1987. Astronomers saw three convincing signs: an extra infrared glow from cooling grains, a simultaneous dimming of optical light, and spectral lines showing dust in front of receding gas on the far side of the expanding cloud. "The gold standard is to see all three, and that's only been done for 1987A," says Sugerman. "It's the only one people don't argue about."

Sugerman and co-workers are using Spitzer and the 8.1-meter Gemini North Telescope at Mauna Kea to survey supernovae that popped off in other galaxies within the past several years. The team has found solid markers of newly manufactured dust in one of those remnants, Sugerman told *Science*.

But there's a serious problem. Data for both the new supernova and 1987A point to a smidgen of dust: about 1/1000 the mass of our sun. That's a factor of 100 to 1000 less than models predict. Rich supplies of fresh dust could hide in two ways, Sugerman notes. The dust may cool off faster than expected, below the sensitivity of infrared surveys to date. It also may clump in knots, shielding the interior dust from detection. Other astronomers claim to see a bit more dust made by different supernovae, but some emission could come from preexisting shells of dust ejected by the stars before their doom.

Another recent analysis also came up short. Gehrz and his colleagues at the University of Minnesota, including Charles Woodward and graduate student Tea Temim, used Spitzer to study the iconic Crab Nebula. There, dust has spread out for nearly a millennium since the supernova was recorded in 1054 C.E. Spitzer measured some coarse dust particles but saw no fine dust suffusing the remnant. Blazing energy from the Crab's active pulsar may have eradicated the small grains. "This adds credence to the theory that supernovae may destroy their own dust," Gehrz says.

Shock waves from a supernova's interaction with nearby matter are a real hazard for new dust, says astronomer Peter Meikle of Imperial College London, U.K. "I am confident that a lot of grains form in supernovae, but they may get destroyed when they go whacking into the interstellar medium," he says. Even so, Meikle suspects that supernovae did pump waves of dust into the earliest galaxies. In that era, the explosions would have expanded more smoothly into relatively uncluttered space.

Although they seem rare, supernova-spawned dust grains do survive today. Zinner and collaborators have identified several hundred silicon carbide and graphite grains from supernovae. Researchers also found a fleck of the common mineral olivine in a particle collected in Earth's atmosphere by a NASA aircraft. A team led by cosmochemist Scott Messenger of NASA's Johnson Space Center in Houston, Texas, described the tiny crystal in *Science* (29 July, p. 737). "This grain had a unique isotopic composition," says Messenger, including a "whopping enhancement" in oxygen-18. The signatures suggest that the grain's parent gases arose in the helium-burning shell of a massive star, with doses of the heavier elements deeper within.

Messenger and Zinner expect that concerted searches will unveil more supernova grains. If all goes well, such detective work will become easier after 15 January 2006. On that date, NASA's Stardust mission will drop a capsule softly onto the Utah desert with a precious payload: particles collected from a close flyby of comet Wild 2 (*Science*, 9 January 2004, p. 151). Frozen into the comet's body, researchers believe, are the constituents of the solar nebula—including bits of dirt that drifted toward our gestating sun 4.6 billion years ago. Scrutiny of those grains will take years, but it may settle the question of whether our primal seeds had calm or cataclysmic origins.

–ROBERT IRION

# Random Samples

Edited by Constance Holden

## Big Fish

A new study of tropical fish shows that when given an opportunity for social advancement, a meek male can quickly turn into a macho one—and this transformation is triggered by a dramatic burst of gene expression in the brain.

The study, by researchers at Stanford University in Palo Alto, California, and Duke University in Durham, North Carolina, was published in the November issue of *PLoS Biology* and focused on

**Two dominant cichlids in a territorial confrontation.**

mating behavior in the cichlid *Astatotilapia burtoni*. Dominant males, the only ones that reproduce, are marked by bright coloring, larger testes, and aggressive behavior. Subordinate males can "ascend" to dominant status, but it's not clear under what circumstances, says lead author Sabrina Burmeister, now at the University of North Carolina, Chapel Hill.

To find out more, the team allowed small groups of male and female fish to interact over 2 weeks, then removed the dominant male. It took only minutes for some of the subordinates to change color and develop dominant behavior. Upon killing the fish, the team found that expression of *egr-1*, a brain gene related to reproductive maturation, more than doubled in the newly dominant males.

Gregory Ball, a neuroscientist at Johns Hopkins University in Baltimore, Maryland, says the study shows that social cues alone can have "powerful" effects on gene expression in the brain. "It is quite reasonable to speculate that other species, including humans, who regularly encounter complex social situations, ... also exhibit such expression," he says.

## New Guinea Back in Time

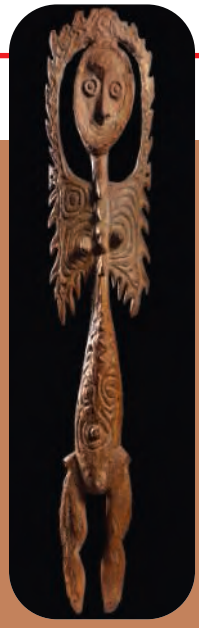

This wooden female figure was carved by people in Papua New Guinea around the 16th century. Carbon-14 dating has revealed the vintages of this and other New Guinea carvings, surprising scientists who assumed that no wooden objects could survive that long in the tropical climate.

The sculptures are part of a large collection donated by New York entrepreneur John Friede to the de Young Museum in San Francisco, California. When Friede asked scientists to date 145 artifacts—most collected around the turn of the last century—"nobody expected these things to be older than a few generations," says Gregory W. L. Hodgins, an archaeologist and biochemist at the University of Arizona, Tucson. But dating at the National Science Foundation–Arizona Accelerator Mass Spectrometer Lab revealed 33 to have been created before 1670, and a mask was dated back to the 7th century C.E.

The Neolithic revolution—when farming took hold, enabling society to diversify—did not occur in New Guinea until the 16th century, says Hodgins. "That is such a huge event. ... To have artifacts from before that is breathtaking."

## Stem Cell Slide?

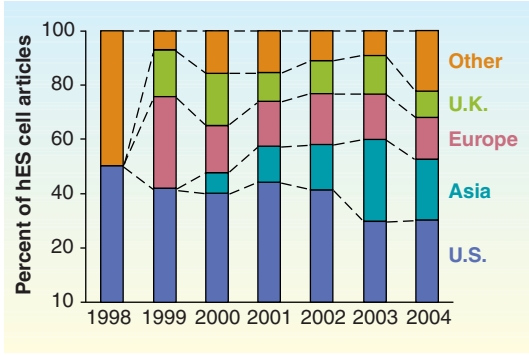


Although many believe human embryonic stem (hES) cell research in the United States is suffering because of government restrictions, it's hard to come by data on the issue. But Aaron Levine, a Princeton University doctoral student in science and public policy, has given it a try. He compared the number of hES cell–related publications since such cells were first derived in 1998 with numbers of papers appearing in five other hot fields of biotech during the 6 years following their introduction. The proportion of papers from U.S. authors fell from 41% (of a total of 41 papers) in 1998 to 30% (of 193) in 2003.

The U.S. combined percentages of papers in the other five fields, including DNA microarrays and RNA interference, were consistently higher, going from 74% in the first year to 51% in the sixth. Levine offers some possible explanations, including that more research may be conducted in the U.S. private sector, where there is "less incentive to publish." However, his own conclusion is that for hES cell research, the U.S. "is indeed falling uncharacteristically behind." The paper appeared in the 14 September issue of *Politics and the Life Sciences*.

## Acid Sketch

Is it art? No, it's phenyl threonine, one of the amino acid building blocks of protein, magnified 20 times. It won sixth prize in Nikon's 2005 Small World exhibit unveiled this month.

CREDITS (TOP TO BOTTOM): THE FRIEDE COLLECTION; SABRINA BURMEISTER; MARGARET N. OECHSLI



Published by AAAS

Edited by Yudhijit Bhattacharjee

## JOBS

**Back to academe.** John Graham, the Bush Administration's controversial regulatory czar, is leaving in February to become dean of the Pardee RAND Graduate School, a public policy institution in Santa Monica, California.

Graham, 49, came to the White House's Office of Information and Regulatory Affairs (OIRA) in 2001 from Harvard, where he founded a risk-analysis think tank whose studies were often criticized as pro-industry (*Science*, 14 December 2001, p. 2277). Graham's efforts to bolster the role of OIRA in shaping agency regulations have drawn fire from public interest groups. And his new standards for peer review of agency documents drew criticism from many scientific groups before they were scaled back (*Science*, 23 April 2004, p. 496).

But environmental policy expert Jonathan Wiener of Duke University School of Law in Durham, North Carolina, praises Graham for requiring agencies to review regulations more rigorously early in the process, resulting, for example, in a strong Environmental Protection Agency diesel-emissions rule. As for the peer-review standards, "it's too soon to tell what the impact will be," Wiener says.

**Global solutions.** Organic chemist Goverdhan Mehta is the new president of the International Council for Science (ICSU), an independent organization comprising national societies such as the United States's National Academy of Sciences, as well as international scientific unions.

Mehta, a professor at the Indian Institute of Science in Bangalore, began his 3-year term last week as ICSU rolled out plans for increasing the role of scientists in mitigating the effects of natural disasters such as the Kashmir earthquake and Hurricane Katrina. The organization also launched a polar research initiative that, among other goals, aims to increase understanding of climate change.

"These are really mega-issues of international dimension," says Mehta, 62, who succeeds zoologist Jane Lubchenco. "They require the involvement of a body which can access talent and expertise and cut across countries and disciplines."

**Medicine monitor.** A Food and Drug Administration (FDA) insider has been named the new director of the agency's Office of Drug Safety. Gerald J. Dal Pan, who currently oversees the Division of Surveillance, Research, and Communication Support in FDA's Center for Drug Evaluation and Research, will take on the high-profile post that's been vacant for 3 years.

The drug safety office keeps an eye on approved medications and ensures that companies complete promised post-marketing studies. After Vioxx was pulled from the market by its maker last year and questions arose about the pediatric safety of antidepressants, FDA officials came under fire for giving insufficient funding and independence to the office. Although the appointment of a new director is welcome, "this doesn't change the fact that the FDA needs to be restructured so that the drug safety office is truly independent from the office that reviews new drugs," Senator Charles Grassley (R–IA), who has led FDA hearings, said in a statement.

## AWARDS

**Genomics pioneer.** Robert H. Waterston received the $200,000 Peter Gruber Foundation Genetics Award last week at the American Society of Human Genetics meeting in Salt Lake City, Utah.

Image not approved for online use

Waterston, a geneticist at the University of Washington, Seattle, and his colleagues helped bring the human genome within reach by sequencing a nematode, showing that whole-genome projects were possible. While at Washington University in St. Louis, Missouri, his team helped complete the human genome as well as the chimp and mouse genomes. Waterston led the push to have sequence data released immediately on the Internet, helping usher in high-throughput biology while maintaining small-lab values.

"He is genuinely a role model for how you can do big science in a very personal way," says Jeffrey Murray, a geneticist at the University of Iowa, Iowa City. The prize has been awarded since 2001. Past winners include Nobel laureate Robert Horvitz.

## NONPROFIT WORLD

**Sharing a treatment.** An experiment that uses stem cells from bone marrow to treat heart failure worked so well on Ian Rosenberg that the 70-year-old retired U.K. fashion businessman has launched a charity to test it on others. In the last year, his Heart Cells Foundation has raised more than $1.5 million and this fall is backing the first large-scale U.K. clinical trial at the Barts and The London NHS Trust hospital.

As part of the trial, researchers aim to treat 700 cardiomyopathy patients over 4 years by taking stem cells from their hips and injecting them into the coronary arteries or heart—or by injecting growth factor drugs in an attempt to cause stem cells to spill out of the bone marrow and into the bloodstream. In smaller trials conducted over the past 5 years, the therapy has produced mixed results. But it worked for Rosenberg, who received the treatment 2 years ago at the Johann Wolfgang Goethe University Hospital in Frankfurt, Germany. It "has given me years I never thought I would have," he says.

Got any tips for this page?
E-mail people@aaas.org

CREDITS (TOP TO BOTTOM): SUSIE FITZHUGH; OMB; ICSU; HEART CELLS FOUNDATION



Published by AAAS

## A Plea to Save the Voyager Mission

YOUR SPECIAL COVERAGE OF THE VOYAGER 1 spacecraft's journey out of the solar system was most welcome (Special Section: Voyager 1 crosses the termination shock, 23 Sept., pp. 2015–2029). The data now being received from the interstellar medium are, as the various articles show, valuable space science as well as testimony to a remarkable era of exploration.

How ironic and shortsighted it is that just as this happens, NASA has scheduled operation of the mission to cease. In order to save a couple of tenths of a percent of the cost, NASA would shut off the first interstellar spacecraft.

The Planetary Society just sent a petition signed by 10,000 people protesting this action to the Senate and House authorizing committees with jurisdiction over NASA, asking them to direct NASA to operate this mission. Those who read and enjoyed the special section on Voyager might want to add their names by writing to Senator Kay Bailey Hutchison and Representative Ken Calvert about Voyager.

LOUIS FRIEDMAN
Executive Director, The Planetary Society, Pasadena, CA 91106, USA.

## Revisiting the Grand Canyon

IT WAS WITH WISTFULNESS THAT I READ JOHN Schmidt's review of James Powell's book *Grand Canyon* ("The grand question," 16 Sept., p. 1818). I was a teenager in the late 1960s when my family took an epic car trip around the United States, visiting the Grand Canyon and many other national parks. As a budding naturalist, I was eager to hear the words of park rangers and avidly read interpretive material. I made lists of plants and animals and soaked up information about habitats, succession, geological change, and evolution. In a fit of nostalgia, I recently repeated the epic with my wife and two children, driving from Washington State to Florida, hitting as many of the parks as we could. The only place I could find scientific content was in the less visited parks that had not been remodeled in a while. The Grand Canyon was the most chilling. The modern visitor center was architecturally magnificent but intellectually vacuous. With open spaces and giant images, it emphasized only

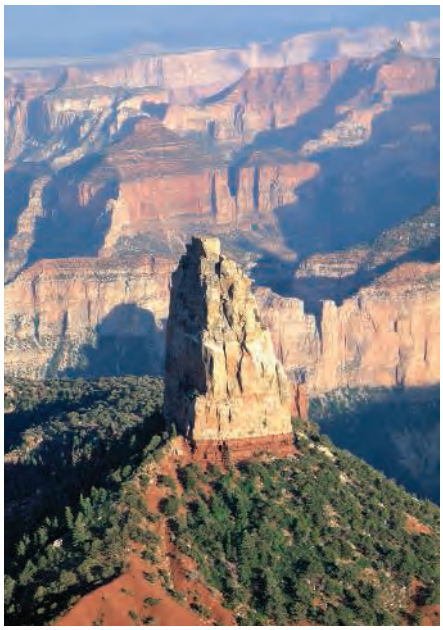

Point Imperial, North Rim, Grand Canyon.

CREDIT: H. SPICHTINGER/ZEFA/CORBIS

the aesthetic experience. There was homage to John Wesley Powell, the man who carried out early explorations of the canyon and helped found the U.S. Geological Survey and the National Geographic Society. Yet the principles he so strongly promoted—rationalism and scientific curiosity as a means of appreciating the world and improving human welfare—were being relegated to obscurity. Schmidt notes that on viewing the canyon we ask, "How did this happen?" The current displays and signage at the Grand Canyon do their best to avoid any such question. As we left the park, we stopped to watch the sunrise at Desert View, a popular site. The most prominent sign at the overlook addressed only the visual beauty of the canyon and the religious significance of a distant mountain to Native Americans. One paragraph began, "The landscape seems consciously designed."

JOHN T. LONGINO
The Evergreen State College, Olympia, WA 98505, USA.

## Déjà Vu All Over Again for Nuclear Power?

RECENT HEADLINES IN MANY NEWS SOURCES have proclaimed a revival for nuclear power. Eliot Marshall's article "Is the friendly atom poised for a comeback?" (News Focus, 19 Aug., p. 1168) poses the issue as a question rather than a conclusion, but nevertheless falls into step with the other sources by not mentioning the role of public acceptance in the fate of this technology. Three decades ago, Alvin Weinberg, then a leading spokesman for the technology, sagely observed: "The public perception and acceptance of nuclear power appears to be the question we missed rather badly in the very early days. This issue has emerged as the most critical question concerning the future of nuclear energy" [(*1*), p. 19].

A review of all available national surveys, not just general questions about the idea of nuclear electricity or about its future, indicates an American public who, although somewhat less opposed than in the past, is still not eager to build more nuclear power plants and is strongly opposed to having one sited in their community if they don't already have one. Even when asked whether they would favor nuclear power as a way of dealing with climate change, a majority remains opposed (*2*). Continued inattention to public acceptability has the very real potential of converting Weinberg's retrospection to a prescient forecast.

EUGENE A. ROSA
Department of Sociology and Thomas F. Foley Institute for Public Policy and Public Service, Washington State University, Pullman, WA 99164–4020, USA. E-mail: rosa@wsu.edu

**References**
1. A. Weinberg, *Am. Sci.* **64,** 16 (1976).
2. E. Rosa, *The Future of Social Acceptability of Nuclear Power in the United States* (Institute Français des Relations Internationales, Paris, 2004).

## Issues Surrounding Nuclear Power

YOUR SERIES OF ARTICLES ON "RETHINKING nuclear power" (News Focus, 19 Aug., pp. 1168–1179) are a useful coverage of much of the reemerging nuclear debate, but they fall short with respect to two aspects.

Their emphasis, like the nuclear debate itself, is on a technical solution to greenhouse emissions. But climate change is only one symptom among many of excessive demands by humans on the natural environment. There are too many of us demanding too much from a finite planet. Emphasis on technical solutions to particular threats to the exclusion of an attack on the underlying causes ensures that these solutions are, at best, temporary, and, at worst, may lead to even more serious threats.

Although the misuse of nuclear knowledge and materials for war or terrorism is mentioned, the world context in which this might occur, and have to be countered, is envisaged as being much like today: reasonable economic buoyancy and inter-


Published by AAAS

national relationships. The advent of the oil peak threatens to change this context dramatically. A progressive rise in oil prices will leave the poor within rich countries, and poor countries as a whole, behind. It is likely to increase tensions at all levels well within the time horizon in which the articles contemplate a possible large increase in the use of nuclear power. The increased risk of deliberate nuclear misuse when the oil starts to run out is the context in which any expanded use of nuclear energy needs to be considered.

JOHN R. COULTER
Adelaide, Australia. E-mail: jrpfc@netspace.net.au

## The Benefits of Solar Thermal Energy

THE ARTICLE "IS IT TIME TO SHOOT FOR THE sun?" (R. F. Service, News Focus, 22 July, p. 548) on solar energy overlooked a proven and affordable energy source that is already available, solar thermal energy with storage via heat transfer fluid. A recent National Research Council report (*1*) put the cost of a large plant at $0.08/kWh, not competitive with conventional coal ($0.04/kWh), but cheaper than electricity from clean coal power plants equipped for $CO_2$ sequestration [$0.07/kWh plus the cost of $CO_2$ sequestration (*2*)].

Solar thermal energy has an unacknowledged, unique feature (*3*). A solar-concentrating collector and its associated heat storage can be regarded as a fuel plant, which feeds a conventional steam power plant. As the investment for the power plant is less than 14% of the total, it can be overdesigned by a factor of three. This gives the system control capabilities not affordable or available in any clean power plant technology. For intermediate loads (8:00 AM to 9:00 PM), 50% of our electricity requirements, the cost remains $0.08/kWh, cheaper than nuclear energy or clean coal ($0.11/kWh and $0.10/kWh, respectively).

All solar thermal power plants need to be competitive is a government subsidy for a few large demonstration plants, as were available for the development of nuclear and clean coal plants. The cost of generating power with solar cells is now three to six times more expensive than with a solar thermal plant. Should solar cells ever become really cheap, instantaneously dispatchable solar thermal energy could compensate for their lack of storage capacity and they could become attractive for large-scale use and merit a large research effort.

REUEL SHINNAR
The Clean Fuels Institute, The City College of New York, 140th Street at Convent Avenue, New York, NY 10031, USA.

**References**
1. National Research Council, "Critique of the Sargent and Lundy Assessment of Cost and Performance. Forecasts for Concentrating Solar Power" (National Academies Press, Washington, DC, Dec. 2002).
2. N. Holt, paper presented at the Gasification Technologies Conference, Washington, DC, 4 to 6 Oct. 2004.
3. R. Shinnar, F. Citro, in preparation (available at http://csauth.ccny.cuny.edu/ci/cleanfuels/upload/Solar%20Thermal%20Energy-06-30-05.pdf).

## A "Chick-a-dee" or a "Co-qui"?

I READ WITH GREAT INTEREST THE REPORT "Allometry of alarm calls: black-capped chickadees encode information about predator size" by C. N. Templeton *et al.* (24 June, p. 1934), who show that black-capped chickadees utilize a graded-response alarm call to warn against predators with differences in risk as measured by predator size. I was struck by the similarity between the findings of this work and the graded-response aggressive calls of Eleutherodactylus frogs. Similar to the chickadees' "chick-a-dee" calls, where increasing repetition of the "dee" note denotes increased threat, the two-note "co-qui" call of the Puerto Rican coqui, *Eleutherodactylus coqui*, is used with increasing repetition of the second "qui" note during increasingly aggressive interactions with conspecific nest predators (*1*). Other Eleutherodactylus species also use a similar aggressive call system when confronted with conspecific or other predators (*2*, *3*). A possible difference between these signaling systems may be in the interpretation of the calls by the receiver (in the case of the chickadees, this would include other birds at risk of predation, and in the case of the coquis, this would include the predator itself). In either case, this type of sophisticated, graded-response acoustic communication that implies knowledge of the level of threat posed by a predator and conveys this information to a receiver is not limited to birds and mammals, but is also used by lower vertebrates.

**An Eleutherodactylus frog and a black-capped chickadee.**

CREDITS: RAFAEL L. MARQUEZ/CALPHOTOS; DONNA DEWHURST/USFWS

SCOTT F. MICHAEL


*Published by AAAS*

Department of Biotechnology, Florida Gulf Coast University, 260 Whittaker Hall, 10501 FGCU Boulevard, South, Fort Myers, FL 33965, USA.

**References**

1. M. M. Stewart, S. A. Rand, *Copeia* **1991**, 1013 (1991).
2. K. E. Ovaska, J. Caldbeck, *Anim. Behav.* **54**, 181 (1997).
3. S. F. Michael, *J. Herpetol.* **31**, 453 (1997).

### Response

**WE THANK MICHAEL FOR POINTING OUT** graded alarm signaling by some Eleutherodactylus frogs. We suspect that many other species, from a wide variety of taxonomic groups, may employ similar graded signaling systems. However, one exciting aspect of the chickadee alarm call communication system is that it incorporates not only a graded signaling system, where subtle variations in the "chick-a-dee" call reflect the degree of threat a perched predator represents, but also aspects of a functionally referential signaling system, where different types of vocalizations, "chick-a-dee" or "seet," refer to the type of predator encounter. Careful examination of other species that are faced with challenging selection pressures from multiple predators may even reveal more complex communication systems.

**CHRISTOPHER N. TEMPLETON[1] AND ERICK GREENE[2]**

[1]Department of Biology, University of Washington, Box 351800, Seattle, WA 98195, USA. [2]Division of Biological Sciences, University of Montana, Missoula, MT 59812, USA.

## Regulating Commercial Cloning of Animals

**AS G. VOGEL REPORTED IN "THE PERFECT** pedigree" (News of the Week, 5 Aug., p. 862), the South Korean lab that recently produced the world's first cloned dog did so purely for the sake of biomedical research. Although the commercial pet-cloning industry may indirectly contribute to this laudable effort by honing techniques for cloning cats and dogs, we are concerned that these private companies lack effective oversight.

The U.S. Department of Agriculture (USDA) recently turned down a petition from the American Anti-Vivisection Society, which had urged the USDA to regulate pet-cloning companies like other animal research facilities under the Animal Welfare Act. The Agriculture Secretary has ruled that, because pet-cloning companies sell companion animals directly to consumers and not to wholesalers, they are simply retail pet breeders, which are exempt from federal regulation (*1*). We believe that this interpretation of the Animal Welfare Act is too narrow and ignores the spirit of the law. Pet cloning is clearly an experimental type of animal breeding that was not envisioned when the law was written in 1985.

To fill this regulatory vacuum, we urge pet-cloning companies to register with the Association for Assessment and Accreditation of Laboratory Animal Care (AAALAC). Esteemed by researchers worldwide, AAALAC is "a private, nonprofit organization that promotes the humane treatment of animals in science" through a voluntary inspections program.

**DUANE C. KRAEMER[1] AND DAVID LONGTIN[2]**

[1]Department of Veterinary Physiology and Pharmacology, College of Veterinary Medicine, Texas A&M University, College Station, TX 77840, USA. E-mail: Dkraemer@cvm.tamu.edu. [2]Potomac, MD. E-mail: davelongtin@yahoo.com

**Reference**

1. I. Oransky, *The Scientist* online news, 19 July 2005 (available at www.the-scientist.com/news/20050719/02).

## Density Is Only Relative

**AS A LONG-TIME READER OF *SCIENCE*, I'M** continually struck by the many parallels and cross-connects among articles from diverse disciplines. The 9 Sept. issue was no exception. A few News Focus articles ("Dissecting a hidden breast cancer risk," J. Couzin, p. 1664; "Deep Impact finds a flying snowbank of a comet," R. A. Kerr, p. 1667; "Coming into focus: a universe shaped by violent galaxies," R. Irion, p. 1668) with illustrations read almost like a sequence of Rorschach ink blots with the interpretations left to your humble readers.

Amongst our *Science* authors, there's propensity
To dissect hidden patterns of relative density
For many things. Some are small,
While others, large. They do enthrall,
And then are pursued with great intensity.

First, mammalian tissue is shown sequentially;
Next, comments on comets hit tangentially;
The impacts there upon a snowball,
As we view the cosmic fireball.
Our Rorschach universe is strange, immensely.

**STACY DANIELS**

Quality Air of Midland, Inc., 3600 Centennial Drive, Midland, MI 48642, USA.

### Letters to the Editor

Letters (~300 words) discuss material published in *Science* in the previous 6 months or issues of general interest. They can be submitted through the Web (www.submit2science.org) or by regular mail (1200 New York Ave., NW, Washington, DC 20005, USA). Letters are not acknowledged upon receipt, nor are authors generally consulted before publication. Whether published in full or in part, letters are subject to editing for clarity and space.

ECOLOGY

# Learning from the Aliens

Michael J. Crawley

A grant application lands with a thump on your desk. You skip straight to the summary section: "This proposal involves the release of an alien disease onto a tropical archipelago with a view to measuring the impact of introduced pathogens on extinction rates of endemic island birds." As my Scottish uncle would have said: "Aye. Right." But this is exactly what happened when colorful but disease-ridden cage birds escaped in Hawaii. *Species Invasions* is a fascinating book that interprets the results of literally hundreds of intentional and unintentional introductions. Representing an extraordinary range of "natural experiments," such invasions by alien species provide unique insights into large-scale and long-term processes in ecology, evolution, and biogeography. We nevertheless need to be circumspect. As unplanned experiments, they lack randomization and there is seldom any data on initial conditions. On the other hand, the introductions were often very well replicated, both within and between different geographic regions. Most major alien pest species were introduced to new environments hundreds or even thousands of times.

**Species Invasions**
**Insights into Ecology, Evolution, and Biogeography**
*Dov F. Sax, John J. Stachowicz, and Steven D. Gaines, Eds.*
Sinauer, Sunderland, MA, 2005. 509 pp. $74.95, £48.99. ISBN 0-87893-821-4. Paper, $49.95, £31.99. ISBN 0-87893-811-7.

The advantages of studying species invasions are several. Ecological and genetic processes can be observed in real time, rather than inferred from the patterns they generate. Rates of spatial spread and genetic change can be estimated from known places and dates of introduction. Although the first paper on species invasions (*1*) appeared in 1919, study of the phenomenon is often traced back to Darwin's *Beagle* voyage, when he documented many European plants thriving as aliens in South America. He pointed out that escape from the parasites and diseases that attack them in their native range may contribute to the rapid spread of invading plants and animals. An influential 1964 Asilomar conference (*2*) and a SCOPE program (*3*) in the 1980s boosted interest in the topic. *Species Invasions* brings readers up to date. The contributors' informative mix of data and theory offers a distinctive perspective on invasion biology.

The reviewer is in the Division of Biology, Imperial College London, Silwood Park, Ascot, Berkshire SL5 7PY, UK. E-mail: m.crawley@imperial.ac.uk

Species invasions can be used to address questions of community assembly and species packing. For instance, how does the establishment of an abundant alien species affect the number and relative abundance of native species that persist? Bruno *et al.* argue that competition is only one of several important factors that structure communities. I believe that, at least for plants, interspecific competition from established native species is the dominant force restricting invasion by aliens; other processes (like herbivory by native animals) typically become important only in places (or at times) where competition from the native vegetation has been reduced by some other means (e.g., increased soil disturbance by feral pigs in Hawaii). However, I agree completely that there is little evidence that competition from alien invasives has caused substantial (or even measurable) extinction of native species. As Sax *et al.* point out for vascular plants, rather than causing catastrophic loss of biodiversity, alien invasions almost always lead to increased total species richness. The majority of established alien plant species never become sufficiently abundant to have important negative impacts on ecosystem functioning or species interactions.

The effects of alien animals such as feral goats and pigs on oceanic islands are well known, but less is understood about the ways the presence of alien plants might alter the disturbance regime and hence influence ecosystem structure and function. D'Antonio and Hobbie address these questions in the context of alien plants that affect fire regimes or increase the rate of nitrogen supply.

Much of what we know about alien diseases concerns catastrophic infections like HIV, chestnut blight, or Dutch elm disease, but Lafferty *et al.* explore several more subtle, community-level effects of disease introductions. The case of the native Hawaiian avifauna is intriguing: there was no vector for the avian pox introduced by the cage birds until 1926, when an alien mosquito was introduced in the discarded bilge water of a visiting ship. From that point, the lowland native birds were rapidly eradicated. In other cases, introduced diseases can be agents of apparent competition, as in the United Kingdom where an alien nematode spread by introduced pheasants induces morbidity in the native gray partridge but not in the pheasants. Globally, however, most recent extinctions of bird species can be attributed to alien predators (e.g., rats and cats on oceanic islands) or habitat destruction by people. Blackburn and Gaston make the point that the particular set of native species that are lost depends on the set of introduced predators, so the attributes of the extinct bird species generally show no clear patterns (large-bodied ground-nesters on islands excepted).

Genetic bottlenecks occur when small numbers of colonists import only a tiny fraction of the allelic variation present in the parent population. However, as various contributors explain, serious reduction in genetic variability as a result of bottlenecks is observed in alien species much less often than was expected by the earliest workers in the field. For inbreeding species, the presence of high genetic variability in the invaded range is generally attributed to multiple introductions (e.g., the thousands of independent introductions for many of the weed species that arrived in the New World as contaminants in seeds from all over Europe and the Middle East). In the native range of inbreeding species, most of the genetic variation arises among populations, whereas variation within populations is typically very low. For outbreeding species, the genotypes of individuals are often sufficiently different that bottleneck effects are unlikely if hundreds (let alone tens of thousands) of individuals are introduced.

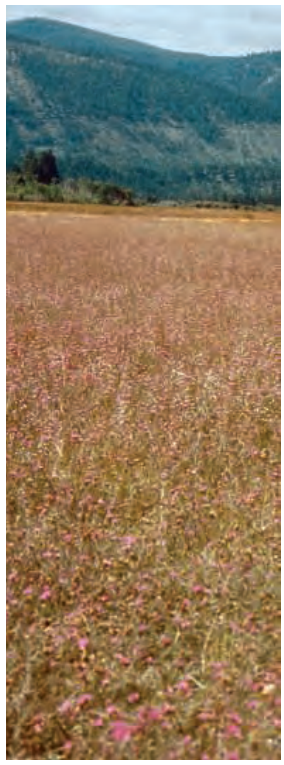

**Weed with a biochemical weapon** (spotted knapweed).

CREDIT: NORMAN E. REES/USDA AGRICULTURAL RESEARCH SERVICE, WWW.FORESTRYIMAGES.ORG

Alien species spreading through new environments encounter novel selection pressures; thus, they offer rich opportunities for studying the rate and predictability of

evolution in the wild. Huey *et al.* discuss some wonderful examples of rapid evolution in the alien range. The classic example is provided by the fruit fly *Drosophila subobscura*, which was introduced repeatedly (and usually unintentionally) into both North and South America. It subsequently exhibited extraordinarily rapid evolution in such traits as wing size and chromosome inversions.

Rice and Sax consider the use of species invasions to test fundamental evolutionary questions, such as the benefits of sexual reproduction. For example, they discuss differences in the spread of introduced sexual and asexual species in two genera of grasses: terrestrial *Cortaderia* in California and marsh *Spartina* in New Zealand. In both cases, the sexual member of the alien pairs became more abundant, spread over a wider area, and occupied a greater range of habitats.

Invasion biology has helped reinvigorate entire subdisciplines within ecology. Allelopathy, the negative effect of one species on another mediated by the release of secondary chemical compounds into the environment, offers an excellent example. This topic had been left stone dead by John Harper's coruscating review (*4*) of a book by E. L. Rice (*5*), in which Harper argued that most if not all of the examples of allelopathy cited by Rice could equally plausibly be attributed to resource competition or to herbivory. As a result, a generation of ecologists steered clear of the difficult and intricately controlled experiments that were necessary to tease apart genuine allelopathy from the plethora of other possible plant-plant interactions. As Callaway *et al.* note, studies of exotic plants—especially the spotted and diffuse knapweeds, *Centaurea maculosa* and *C. diffusa*—have provided the most convincing demonstrations of the importance of allelopathy. In the Rocky Mountain states, these pernicious invaders exclude whole suites of native species to produce extensive monospecific stands. Their root exudates cause 100% mortality in native test plants but are not toxic to the *Centaurea* themselves. They are also much less toxic to coevolved plant species from the knapweeds' original European habitats, which suggests that long-term coexisting species evolve to tolerate each other's biochemistry. Adaptations to live with the allelopathic chemicals of all one's neighbors offer perhaps the best case of coevolutionary relationships within plant communities, relationships that are disrupted by the introduction of alien species.

Discussing the rates and spatial patterns of the spread of alien species, Kinlan and Hastings draw attention to the importance of the mode by which rare long-distance dispersal occurs. They also note the role played by life history traits that affect rates of population growth at low densities (Allee effects); after all, dispersal is only important if the dispersing organisms survive to reproduce in their new surroundings. And the authors' exploration of models and empirical data from various marine and terrestrial taxa reveals that feedback among migration, adaptation, and environmental structure is critical in determining the dynamics of range expansion by alien species.

The volume is more than a collection of case studies; it contains interesting new theory as well. Stachowicz and Tilman provide a lucid introduction to a stochastic model of community assembly, and they address the vexing question of whether the relationship between species richness and invasibility is positive, negative, or contingent. Holt *et al.* investigate evolution and niche conservatism in the context of theoretical models of source and sink populations in temporally variable environments. They point out that evolution can rescue an isolated but initially maladapted invading population from extinction, so long as evolution occurs rapidly enough. This "evolution outside the niche" defines the potential domain into which an alien species can expand. Their discussion also draws attention to the often-contrasting effects of migration on the potential for niche evolution in alien species: Migration provides opportunities for evolution by sustaining local populations in sites outside the initial niche (i.e., in sink habitats where population growth is negative); it increases local abundances, enhancing the opportunity for local mutational input; it alters density-dependent demographic processes; it introduces genetic variation from the source population; but it dilutes locally adapted gene pools, hampering adaptation.

My one serious reservation about the volume is its parochial focus. Virtually all of the authors and most of the examples are American. The editors claim that they "did not attempt to bring together the leaders in the field of invasion biology…but tried instead to draw together leaders and emerging leaders in the fields of ecology, evolution, and biogeography." Although that is fair enough, much of the best work on invasions has been carried out in South Africa, Australia, and continental Europe. Examples from these places, and the insights of the biologists who work there, do not get the coverage they deserve. It is instructive to recall that the major breakthrough in controlling the invasion of species-rich fynbos habitat in the Cape floristic region of South Africa (one of Africa's hottest biodiversity hotspots) did not come until it was pointed out that the invasive trees were wasting vast quantities of Cape Town's precious water supplies through excessive transpiration (*6*). As soon as serious financial resources were committed to the elimination of the alien species (using a combination of mechanical and biological control), large areas of species-rich fynbos were rapidly restored.

*Species Invasions* shows how far we have come since Elton's classic *The Ecology of Invasions by Animals and Plants* (*7*). The volume offers a fine compendium of ideas and examples that will be valuable to students for the number of doors it opens to scores of subdisciplines within ecology. For professionals, it represents a state-of-the-art overview of the issues involved in invasion biology.

**References and Notes**

1. J. Grinnell, *Am. Nat.* **53**, 468 (1919).
2. H. G. Baker, G. L. Stebbins, *The Genetics of Colonizing Species* (Academic Press, New York, 1965).
3. The "Ecology of Biological Invasions" program of the Scientific Committee on Problems of the Environment (SCOPE) produced over 15 edited volumes.
4. J. Harper, *Q. Rev. Biol.* **50**, 493 (1975).
5. E. L. Rice, *Allelopathy* (Academic Press, New York, 1974).
6. V. C. Moran, J. H. Hoffmann, H. G. Zimmermann, *Front. Ecol. Environ.* **3**, 77 (2005).
7. C. S. Elton, *The Ecology of Invasions by Animals and Plants* (Methuen, London, 1958).

10.1126/science.1118216

## BROWSINGS

**What the Dormouse Said.** How the Sixties Counterculture Shaped the Personal Computing Industry. *John Markoff.* Viking, New York, 2005. 336 pp. $25.95. ISBN 0-670-03382-0.

LSD trips, Ken Kesey's Merry Pranksters, Stewart Brand and the *Whole Earth Catalog*, musicians who became the Grateful Dead, communal living, antiwar protests, and Pentagon-funded research all appear in this exploration of the origins of personal computing. Markoff covers events between 1960 and 1975 in the area that would become known as Silicon Valley. He highlights the philosophical clash between two innovative, unconventional labs that shared a hacker culture and antiauthoritarian outlook: While John McCarthy and his Stanford Artificial Intelligence Laboratory sought ways to replace humans with machines, Douglas Engelbart recruited a "lunatic fringe" to the Stanford Research Institute to develop human-centered computing. (In a legendary December 1968 talk, Engelbert unveiled a system that included on-screen text editing, hypertext links among documents, and windows that allowed one to mix text, graphics, and video.) Another narrative thread concerns the conflict between open and proprietary software. The social, political, and cultural connections revealed in Markoff's captivating stories demonstrate the surprising importance of sixties counterculture to the development of today's computing world.

POLICY

# OPV Cessation—the Final Step To a "Polio-Free" World

R. Bruce Aylward,* Roland W. Sutter, David L. Heymann

The World Health Assembly voted in 1988 to eradicate poliomyelitis, on the basis of a large body of evidence indicating the efficacy of a combination of routine immunization, supplementary polio immunization campaigns, and highly sensitive surveillance (*1*). By early 2003, indigenous wild polioviruses were limited to discrete areas of just 6 of the more than 125 countries that were considered infected in 1988. Disease burden declined from an estimated 350,000 cases in 1988 to 784 reported cases in 2003. In that year, however, the initiative faced two potentially fatal challenges. The 12-month suspension of all immunization with oral polio vaccine (OPV) in a number of northern states of Nigeria (*2*) led to reinfection, by mid-2005, in 18 previously polio-free countries, from Mali to Indonesia. The second, and more threatening, development was the failure of very high coverage with trivalent OPV to interrupt polio in some densely populated areas in India and Egypt (*3*). By mid-2005, however, political advocacy had led to the restart of OPV immunization in Nigeria and the "reinterruption" of polio in many reinfected countries, while technical advances [monovalent oral poliovirus type 1 vaccine (mOPV1)] (*4*) had already eliminated some of the polio reservoirs in India and Egypt.

With the interruption of wild polioviruses globally increasingly on track, attention has returned to the challenges posed by the "post-eradication" era. Planning for that era is now driven by the recognition that even with eventual interruption of all wild-type poliovirus, paralytic polio will continue until routine use of live vaccines is stopped (*3*, *5*, *6*).

## The Rationale for Stopping OPV

OPV has been one of the most effective tools for disease prevention in public health. Soon after licensure, however, it was recognized that OPV use resulted in rare cases of vaccine-associated paralytic poliomyelitis (VAPP) (*7*). Consequently, after eliminating indigenous wild poliovirus and because of the progress toward global eradication, some countries with very high immunization coverage have moved to inactivated poliovirus vaccine (IPV) for routine childhood immunization (*8*). Although the public health benefits of OPV continue to outweigh the VAPP risk (*9*), this balance can be expected to change with the interruption of wild-poliovirus transmission in all countries. An estimated 250 to 500 VAPP cases would continue to occur each year in OPV-using countries on the basis of current vaccine utilization patterns. (*10*).

Of even greater significance is the recent documentation that OPV viruses under some circumstances regain both neurovirulence and the capacity to circulate and cause outbreaks (*11*). By mid-2005, such circulating vaccine-derived polioviruses (cVDPVs) had been established as the source of polio outbreaks that paralyzed more than 50 people total in Hispaniola (2000–2001) (*12*), the Philippines (2001) (*13*), Madagascar [2002 (*14*), 2005], China (2004) (*15*), and Indonesia (2005). A seventh such outbreak, in Egypt, has been described retrospectively (*16*). All recent cVDPVs have been rapidly interrupted with an OPV campaign. After global eradication of wild-type polioviruses, however, the continued use of OPV would continually generate cVDPVs. The spread of just a limited number of these cVDPVs would eventually negate the elimination of wild-type polioviruses from human populations.

Finally, the use of OPV in individuals with some primary immunodeficiency syndromes has been shown to result, rarely, in prolonged excretion (>6 months) of vaccine-derived polioviruses; these individuals are called iVDPVs (*17*). Although none of the 28 iVDPVs detected to date are known to have generated secondary cases, and 25 spontaneously stopped excreting or died, "chronic" excretion (>36 months) did occur from four iVDPVs (*18*), all of whom lived in high-income countries that plan to continue IPV use. Acquired immunodeficiency syndromes, such as that associated with HIV infection, have not been associated with prolonged poliovirus excretion (*19, 20*).

## Risks Associated with Stopping OPV

Mathematical modeling suggests that there is a 65 to 90% chance of at least one outbreak of cVDPV occurring somewhere in the world during the 12 months immediately after cessation of OPV use globally, with that risk declining to 1 to 5% at 36 months (*21*). Countries with low routine immunization coverage at the time of OPV cessation are expected to be at greatest risk. The overall probability of substantial international spread of such a virus is remote, especially as monovalent OPVs are available for rapid response.

There is a longer-term risk of reintroducing a wild, vaccine-derived or Sabin poliovirus strain from a vaccine production site, a laboratory, or an iVDPV. The magnitude of the facility-associated risks is largely contingent on the extent of poliovirus destruction before OPV cessation and largely contingent on the quality of high-level biocontainment (*22*). Before OPV cessation, the magnitude of the iVDPV risk must be more accurately defined, and

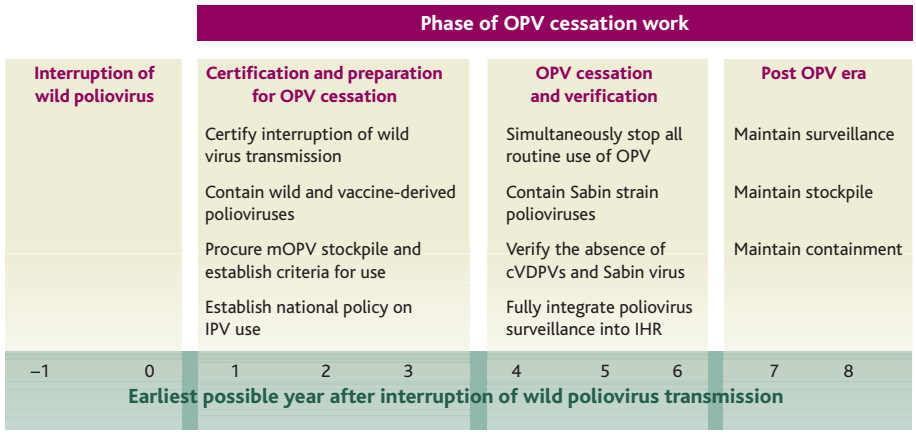


**Major phases for OPV cessation.**

The authors are with the Global Polio Eradication Initiative, World Health Organization, Geneva 27 Switzerland.

*Author for correspondence. E-mail: aylwardb@who.int



Published by AAAS

strategies for clearing chronic iVDPVs must be pursued, including evaluation of potential antiviral drugs.

The final risks derive from intentional use of polioviruses. The risk of an effective bioterrorist incident using poliovirus is remote (*23*), because of high population immunity at OPV cessation, continued access to a polio vaccine stockpile thereafter, and the inherent difficulties in targeting polioviruses. The decision by several countries, including those generally thought to be at highest risk for intentional use of biologic agents, to maintain high population immunity through continued IPV use should further deter intentional use of polioviruses.

### Managing Cessation of Routine OPV Use

In a polio-free world, no vaccination strategy is without risk (*24*). Six major "prerequisites" have been defined to reduce and to manage the risks of paralytic poliomyelitis that would be associated with OPV cessation (for additional details, see table S1).

First, there must be confirmation of interruption of wild-poliovirus transmission globally. In 1995, mainly on the basis of the experience in the Americas (*25, 26*), 3 years was established as the minimum period between the last circulating wild poliovirus in a geographic block of countries and its certification as polio-free (*27*). Quantifiable performance targets were set for polio surveillance based primarily on identification and investigation of children less than 15 years of age with acute flaccid paralysis (AFP) (*28–30*).

Second, biocontainment of all polioviruses must be ensured (*31*). To date, 158 countries have initiated a survey for wild poliovirus materials, covering over 210,000 facilities. As of May 2005, ~800 facilities had been identified with relevant materials, which will either be destroyed or placed under biocontainment. OPV cessation will also require international consensus on, and verification of, biosafety measures for Sabin viruses. The World Health Organization (WHO) is promoting development of IPV from Sabin strains to reduce the risks associated with large-scale wild-poliovirus amplification in the post-OPV era, while facilitating maintenance of a "warm base" for restart of OPV production should that ever prove necessary (*4*).

Third, an international stockpile of monovalent OPV vaccines (mOPV) is being established so that type-specific immunity could be rapidly established if poliovirus were reintroduced (*32*). Bulk vaccine could also be used to resume routine immunization quickly in the "post-OPV" era, while production from seed virus is restarted if required. Criteria for the use of mOPVs must be internationally agreed upon given the implications of reintroducing attenuated poliovirus strains in a post-OPV era. The enhanced efficacy of mOPV and elimination of unnecessary serotypes will further reduce the risk of inadvertently generating a cVDPV during an outbreak response. Strategies for minimizing the risk of a cVDPV after an mOPV response must also be further elaborated, including the potential use of antivirals or a combination of mOPV and IPV in the initial response (*33*).

Fourth, sensitive surveillance for polioviruses must be sustained, particularly during the 3 years immediately after OPV cessation. The existing global AFP surveillance capacity will require continued financial support, with supplementary activities such as systematic screening for iVDPVs. Poliovirus surveillance is being incorporated into the *International Health Regulations* (IHR) to sustain detection and response activities (*34*). Rapid diagnostic tools, particularly Immunoglobulin M (IgM) assays and direct molecular detection techniques, are being evaluated for integration into the global polio laboratory network.

Fifth, extensive work (such as international agreements on timelines) is needed to prepare for simultaneous OPV cessation worldwide. Eliminating the risk of a Sabin strain reintroduction will require rapidly collecting and destroying OPV stocks everywhere.

Finally, each country must decide whether to maintain immunity against polio in the post-OPV era. The risks of intentional or inadvertent poliovirus reintroduction into increasingly naïve populations must be measured against the financial, opportunity, and programmatic costs associated with IPV use (*35*). Such decisions are particularly important in resource-poor settings (*36*). IPV currently costs at least 4 or 5 times the estimated "break-even" price for replacing OPV in routine immunization programmes (*37*), and existing IPV producers have predicted there will not be substantial volume discounts because of high fixed production costs. WHO will continue to review the role of IPV as additional data are collected on both the vaccine and the risks associated with OPV cessation.

The most important lesson for long-term polio immunization policy comes from the smallpox eradication effort—the capacity to conduct research on polio vaccines and control strategies must be maintained to ensure that appropriate tools are always available.

#### References and Notes


1. R. B. Aylward, R. Tangermann, R. Sutter, S. Cochi, in *New Generation Vaccines*, M. M. Levine, J. B. Kaper, R. Rappuoli, M. A. Liu, M. F. Good, Eds. (Marcel Dekker, New York, 3rd ed., 2004), chap. 13, p. 145.
2. E. Samba, F. Nkrumah, R. Leke, *N. Engl. J. Med.* **350**, 645 (2004).
3. World Health Organization (WHO), *Wkly. Epidemiol. Rec.* **79**, 401 (2004).
4. D. L. Heymann, R. W. Sutter, R. B. Aylward, *Nature* **434**, 699 (2005).
5. Immunizations, Vaccines, and Biologicals, "Report of an informal consultation on the identification and management of vaccine-derived polioviruses (VDPVs)" (WHO, Geneva, 2004).
6. Technical Consultative Group to WHO on the Global Eradication of Poliomyelitis, *Clin. Infect. Dis.* **34**, 72 (2001).
7. R. W. Sutter, O. M. Kew, S. L. Cochi, in *Vaccines*, S. A. Plotkin, W. A. Orenstein Eds. (Saunders, Philadelphia, 4th ed., 2003), chap. 25, pp. 651–705.
8. Centers for Disease Control and Prevention (CDC), *Morb. Mort. Wkly Rep.* **49**, (RR5), 1 (2000).
9. WHO position paper, *Wkly. Epidemiol. Rec.* **78**, 241 (2003).
10. Vaccines and Biologicals, "Report of the interim meeting of the Technical Consultative Group (TCG) on the global eradication of poliomyelitis," Geneva, 13 and 14 November 2002 (WHO/V&B/03.04, WHO, Geneva, 2003).
11. O. M. Kew, *Bull. World Health Organ.* **82**, 16 (2004).
12. O. Kew *et al.*, *Science* **296**, 356 (2002).
13. H. Shimizu *et al.*, *J. Virol.* **78**, 13512 (2004).
14. D. Rousset *et al.*, *Emerg. Infect. Dis.* **9**, 885 (2003).
15. CDC, *Morb. Mortal. Wkly. Rep.* **53**, 1113 (2004).
16. C. Yang *et al.*, *J. Virol.* **77**, 8366 (2003).
17. N. A. Halsey *et al.*, *Bull. World Health Organ.* **82**, 3 (2004).
18. C. MacLennan *et al.*, *Lancet* **363**, 1509 (2004).
19. K. A. Hennessey *et al.*, in preparation.
20. E. J. Asturias *et al.*, in preparation.
21. R. J. Duintjer Tebbens *et al.*, Risks of paralytic disease due to wild or vaccine-derived poliovirus after eradication (in preparation).
22. World Health Assembly, Poliomyelitis eradication (WHO, Geneva, 1999), resolution 52.22.
23. L. D. Rotz, A. S. Khan, S. R. Lillibridge, S. M. Ostroff, J. M. Hughes, *Emerg. Infect. Dis.* **8**, 225 (2002).
24. D. A. Henderson, *Clin. Infect. Dis.* **33**, 79 (2001).
25. Pan American Health Organization (PAHO), "Final report of the International Commission for the Certification of Polio Eradication (ICCPE)," (PAHO, Washington, DC, 1994).
26. S. M. Debanne, D. Y. Rowland, *Math. Biosci.* **150**, 83 (1998).
27. "Report of the 2nd Meeting of the Global Commission for the Certification of Poliomyelitis Eradication (WHO, Geneva, 1 May 1997).
28. Acute flaccid paralysis (AFP) surveillance: The surveillance strategy for poliomyelitis eradication, *Wkly. Epidemiol. Rec.* **73**, 113 (1998).
29. J. Smith, R. Leke, A. Adams, R. H. Tangermann, *Bull. World Health Organ.* **82**, 24 (2004).
30. WHO, Polio case counts (www.who.int/vaccines/casecount/case_count.cfm) (accessed 1 May 2005); see (www.polioeradication.org/casecount.asp).
31. Department of Vaccines and Biologicals, "WHO *global action plan for the laboratory containment of wild polioviruses* (WHO/V&B/03.11, WHO, Geneva, 2nd ed., 2002).
32. P. E. M. Fine, R. W. Sutter, W. A. Orenstein, in *Progress in Polio Eradication: Vaccine Strategies for the End Game*, F. Brown, Ed. (Developments in Biologicals Series, Karger, Basel, 2001), vol. 105.
33. P. E. M. Fine, G. Oblapenko, R. W. Sutter, *Bull. World Health Organ.* **82**, 47 (2004).
34. WHO, "Decision instrument for the assessment and notification of events that may constitute a public health emergency of international concern Reports of the Ad Hoc Expert Group on Annex 2" [WHO (www.who.int/gb/ghs/pdf/IHR_IGWG2_ID4-en.pdf). Geneva, 2005].
35. Immunizations, Vaccines and Biologicals, "Vaccine introduction guidelines: Adding a vaccine to the national immunization programme—decision and implementation." (WHO, Geneva, 2004).
36. R. J. Duntjer Tebbens, *Am. J. Epidemiol.* **162**, 358 (2005).
37. N. Sangrujee, V. M. Cáceres, S. L. Cochi, *Bull. World Health Organ.* **82**, 9 (2004).


#### Supporting Online Material

www.sciencemag.org/cgi/content/full/310/5748/625/DC1

10.1126/science.1115813

ATMOSPHERIC SCIENCE

# Tipping Points in the Tundra

Jonathan A. Foley

The recent news from the Arctic is troubling. A new report (*1*) from NASA and the National Snow and Ice Data Center (NSIDC) indicates that the extent of sea ice cover in the Arctic Ocean is now at its lowest level in more than a century. The NASA-NSIDC team has observed four straight years of substantially below-average sea ice, with earlier spring melting and sharp declines in winter ice cover. This comes on the heels of another report by Overpeck *et al.* (*2*), supported by the NSF Arctic System Science program, which suggests that the Arctic is heading toward a new, seasonally ice-free state—a condition not seen for at least a million years. The authors are blunt: "The Arctic system is moving toward a new state that falls outside the envelope…of recent Earth history. This future Arctic is likely to have dramatically less permanent ice than exists at present…a summer ice-free Arctic Ocean within a century is a real possibility…." Overpeck *et al.* conclude that "The change appears to be driven largely by feedback-enhanced global warming, and there seem to be few, if any, processes or feedbacks within the Arctic system that are capable of altering the trajectory…."

Now, turning to the continents surrounding the Arctic Ocean, Chapin *et al.* report new findings on page 657 of this issue (*3*) that confirm that substantial warming over the landmasses of the Arctic is also happening, and is accelerating. In fact, from the 1960s to the 1980s, the Arctic landscapes warmed by roughly 0.15°C per decade, and then the region warmed by nearly 0.3° to 0.4°C per decade since the 1990s.

According to Chapin *et al.*, the accelerated warming over the high-latitude continents appears to be the result of strong positive feedbacks from the land surface on a warming atmosphere. In particular, they suggest that greenhouse warming is now reducing the duration of seasonal snow cover in the Arctic, shortening the snow-covered season by roughly 2.5 days per decade, thereby shifting the albedo (the reflectivity of the surface to sunlight) of the landscape away from bright snow toward darker vegetation and soil. This decrease in albedo allows the ground to absorb more solar radiation, warm the surface, and then provide additional heat to the atmosphere (see the figure, top and middle panels). Chapin *et al.* estimate that this reduction in snow cover, and associated decrease in albedo, resulting from global warming adds another ~3 W $m^{-2}$ of local heating to the atmosphere—an amount that is roughly comparable to what a doubling of $CO_2$ levels would do the global atmosphere.

But changes in snow cover may not be the only feedback process at work in Arctic landscapes. Global warming may also encourage more shrubs to grow in the tundra, and boreal forest to grow farther northward, replacing the tundra ecosystems that exist there today. These changes in the land surface (to a landscape with more shrubs and trees) also profoundly affect the heat transfer between the surface and the atmosphere (see the figure, bottom panel). Although the extent of vegetation expansion in the Arctic has been relatively small so far, it is likely to continue in response to global warming and be a major factor in shaping the climate of the region. From their observations, Chapin *et al.* conclude that widespread shrub and tree expansion could further magnify atmospheric heating over Arctic landmasses by another factor of 2 to 7.

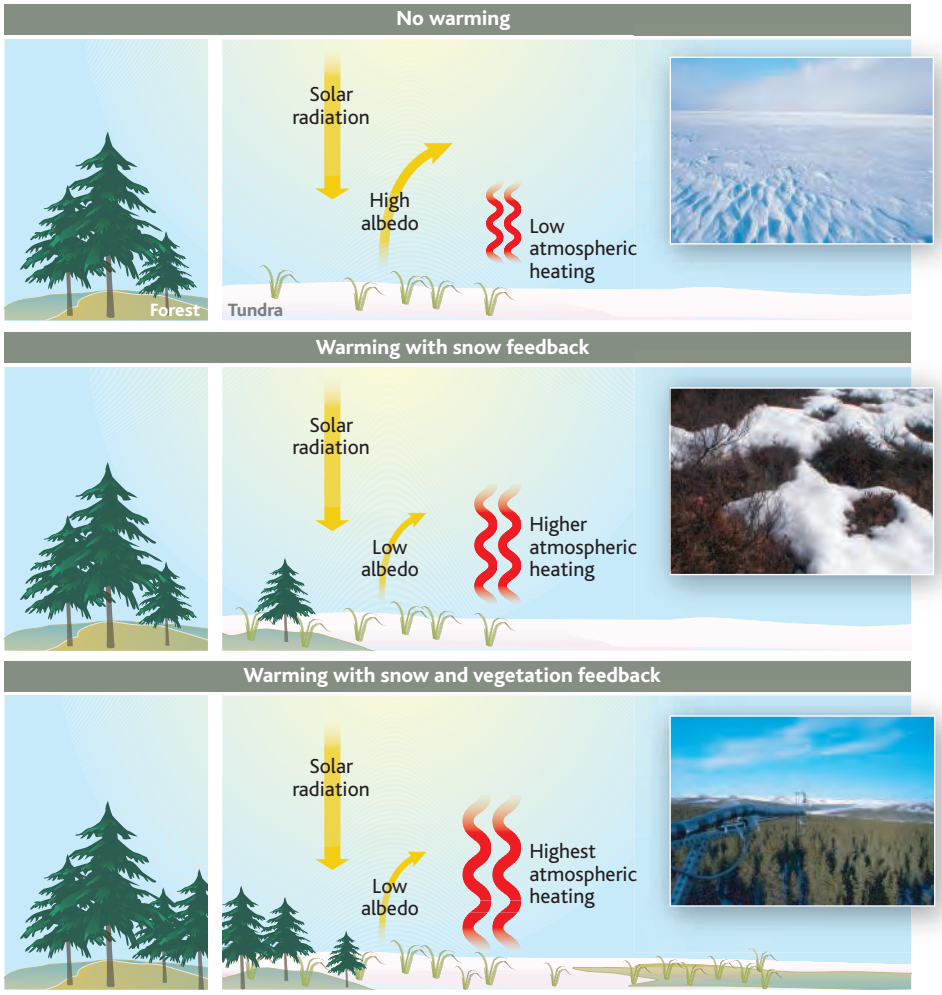


**Vicious cycle.** Chapin *et al.* describe positive-feedback mechanisms from changing snow and vegetation cover on the climate of the Arctic. These mechanisms work to amplify global warming in the Arctic by reducing the highly reflective snow cover (**top** and **middle**) and expanding the cover of shrubs and trees (**top** and **bottom**).

The author is at the Center for Sustainability and the Global Environment (SAGE), Nelson Institute for Environmental Studies, University of Wisconsin, Madison, WI 53726, USA. E-mail: jfoley@wisc.edu

But how well do these new observations fit with the predictions of global climate models (GCMs)? The positive feedbacks on global warming stemming from the reduction in snow cover are already included within GCMs. Nearly all of the models include representations of the physics of land-surface processes, including the energy, moisture, and momentum balance among vegetation, soil, snow, and the atmosphere. As a result, GCMs show strong warming in the polar region; in these areas, the simulated warming is amplified through albedo feedbacks from reduced snow and ice.

Unfortunately, few GCMs represent the possible feedbacks from changing vegetation cover and the associated changes in land-surface properties. As Chapin *et al.* suggest, increases in shrub and forest cover in the Arctic could dramatically amplify global warming in the Arctic, but nearly all GCMs used today do not consider such changes in vegetation cover. However, a study by Levis *et al.* (*4*) used one of the few fully coupled global climate–vegetation models to estimate the potential for vegetation feedbacks on Arctic climate. They concluded that the northward shift of trees and shrubs induced by global warming would raise seasonal temperatures by an additional 1.1° to 1.6°C in spring. Naturally, further investigations with alternative models of climate-vegetation interactions are needed to corroborate this kind of result. But Chapin *et al.* have now provided us with strong empirical evidence to support this hypothesis.

In a way, the Arctic may be the "canary in the coal mine" of our global climate system. Climate theory and models have both suggested that the Arctic region will experience some of the strongest effects of global warming, mainly because of the large magnifying effects of snow, ice, and (possibly) vegetation feedbacks. And now several sources of evidence are showing that not only is the Arctic warming, but also that the feedback mechanisms seem to be kicking into high gear.

Ultimately, this research leads one to wonder whether the Arctic is headed toward a fundamentally different climatic regime—one with much less snow, much less sea ice, and possibly more shrubs and forest. Furthermore, scientists and decision-makers must ask what this radically different climate future means for the species and peoples that call the Arctic home today, including polar bears, seals, and Inuit communities. And given the massive inertia of the global climate system—with the significant degree of additional warming already "in the pipeline," even if $CO_2$ levels were to stabilize today (*5*)—combined with the difficulty of achieving drastic decreases in greenhouse emissions anytime in the near future, one also has to ask: Is the Arctic we know today already lost? To answer these questions, studies like that of Chapin *et al*. demand more attention.

**References**

1. See http://nsidc.org/news/press/20050928_trendscontinue.html.
2. J. Overpeck *et al.*, *Eos Trans. AGU* **86**, 309 (2005).
3. F. S. Chapin III *et al.*, *Science* **310**, 657 (2005); published online 22 September 2005 (10.1126/science.1117368).
4. S. Levis, J. A. Foley, D. Pollard, *J. Geophys. Res.* **26**, 747 (1999).
5. J. Hansen *et al.*, *Science* **308**, 1431 (2005).

10.1126/science.1120104

VIROLOGY

# What Links Bats to Emerging Infectious Diseases?

**Andrew P. Dobson**

Three species of horseshoe bats (*Rhinolophus* spp.) have now been officially recorded as the natural reservoir host of the coronavirus that causes severe acute respiratory syndrome (SARS) [see the report by Li *et al*. on page 676 of this issue (*1*) and the report by Lau *et al*. (*2*)]. The emergence of this pathogen (SARS-CoV) in southern China in 2002–2003 almost brought the burgeoning economy of Southeast Asia to its knees (*3, 4*). Bats are now known to be natural reservoir hosts to several other new emergent disease pathogens: Nipah and Hendra viruses (*5*) and potentially Ebola and Marburg viruses. They are also reservoirs to "older" and more well-known pathogens, such as rabies virus, which frequently resurge into human populations or domestic livestock. Fieldwork on SARS illustrates not only the crucial role that conservation organizations play in frontline research on emergent diseases, but also the shortcomings in our understanding of the etiology of these diseases.

The author is in the Department of Ecology and Evolutionary Biology, Princeton University, Princeton, NJ 08544–1003, USA. E-mail: dobber@princeton.edu

A key step in determining the threat imposed by new pathogens is identifying the route along which they are transmitted from their reservoir to new hosts such as domestic livestock or humans. In the case of pathogens that use bats as reservoirs, a common route seems likely. Bats' feeding habits are constrained by the aerodynamics of flight, so they can't ingest huge amounts of food. Yet many bats are frugivorous—that is, they meet their energy requirements by ingesting fruits. But instead of swallowing them, they chew them to extract the sugars and higher energy components, and then spit out the partially digested fruits, which drop to the ground. Other animal species can ingest these fruit remnants and may consequently become infected with virus particles in residual bat saliva. A small variant on this is required in the case of the insectivorous *Rhinolophus* bat species, but they also discard the heavier body parts of the insects they eat, which are then ingested by terrestrial foraging species. This provides a route for SARS-CoV to be infrequently transmitted to masked palm civets (*Paguma larvata*), the animals that were initially considered to be the potential virus reservoirs in the SARS epidemics. It would also explain how gorillas, chimpanzees, and duikers acquire Ebola virus during seasonal fruiting events when bats and primates feed in or below fruit-bearing trees. The animal pens of the pig farms where the Nipah virus outbreak in Malaysia was first reported were littered with partially digested fruits that were regurgitated from bats. Similar observations were reported at the site of the Hendra virus outbreak in Queensland, Australia. In Bangladesh, the Nipah virus has been shown to be transmitted directly from bats to humans. There, during the fruiting season, young boys climb trees to pick fruit. They frequently add fruit that is partially chewed by bats to their collections, which they then sell to the local salesmen. The fruit is pulped to produce a drink that is sold in neighboring villages. The Nipah outbreaks there often follow the trails of these bicycle-borne salesmen (*6*).

The transmission dynamics of these emerging viruses can be readily modeled in a framework originally developed to examine the rate of spread of HIV-AIDS in populations with heterogeneous mixing of people with different levels of sexual activity (*7*). The key difference with using this approach to examine emergent diseases is that transmission of emergent pathogens between populations tends to be unidirectional (*8*). Thus, bats transmit SARS-CoV to palm civets, but not *vice versa*. This means that control of the disease has to

focus on either controlling its abundance in its reservoir, preventing its spillover between hosts, or rapidly reducing its spread once it has infected humans or domestic livestock. This creates a dilemma for both public health and conservation biology: Should we attempt to control potentially emergent pathogens by focusing on their reservoir hosts, or should we try and prevent the spillover events that allow the pathogen to spread in a new population? A third option is to develop a vaccine to protect hosts in the spillover population. Unfortunately, because spillover is likely to be a random event, effective protection requires that all individuals in the spillover population become protected. We have never achieved this level of coverage for well-known pathogens that have fairly safe and effective vaccines (*9*).

**Bats, the great natural reservoir for viruses.** Knowing more about bat ecology and immunology is crucial to controlling spillover of viruses and related diseases to humans.

The two viable alternatives are either to reduce the prevalence of the pathogen in the reservoir host, or to identify the conditions that lead to spillover and attempt to minimize these. The latter will involve surveying a diversity of wild species for potential pathogens and unraveling the changes in ecological conditions that lead to spillover events. In both these areas, conservation organizations seem to be playing almost as important a role as medical schools. This is both ironic and tragic given that conservation nongovernmental organizations have much smaller budgets and broader agendas than medical schools.

Is it unusual that so many emergent diseases use bats as reservoirs? What's special about bats? We often forget that bats form a sizable proportion of mammalian diversity; the 916 extant species constitute about 20% of this diversity (*10*). Thus, if all potential reservoirs were created equal, we would expect almost as many emergent pathogens from bats as from small mammals. This is not the case; less than 2% of human pathogens have bats as natural reservoirs [bats may be persistently infected, yet never display any pathologies (*11*)]. These data suggest that bats are not overrepresented in the numbers of pathogens that emerge from them. What is more conspicuous is the pronounced pathology of pathogens that spill over from bats and that most of these spillovers have occurred in the last 20 years. What might cause this?

One obvious difference between bats and other mammals is that bats fly. This means that they have hollow bones, as do birds. But bone marrow is where most mammals produce the B cells of the immune system. Where do bats produce B cells? Unfortunately, we don't know enough about bat immunity to address this question. They may compensate by increasing B cell production in the marrow of their pelvis and legs, but we have little data on this. Bats are long-lived, highly gregarious, and can enter torpor. We do not know whether these traits allow these ancient mammals to differ from other mammals in the way they combat potential viral infections. Are there differences in the functionality or type of receptors required for infection? Are there bat antiviral proteins (interferons) that can stop viral replication as in other mammals, or do bats possess a mechanism to prevent their inactivation? Alternatively, we could ask if bats possess a novel innate immunity that allows them to cope with certain classes of viruses in ways that other mammals cannot. If the latter is the case, then what would studies of bat immunity tell us about new ways to attack and treat viral diseases? The literature is silent on this. Very few medical schools have experimental bat colonies, and work in this area may be a little "outside the box" for conservative funding agencies.

Knowing more about bats, and particularly more about bat ecology and immunology, is crucial if we are to develop new treatments and ways to control the viral diseases that are an increasing threat to humans. Assuming we can control these diseases by simply controlling bats is both naïve and short-sighted. Instead, we must recognize that increased rates of spillover-mediated pathogen transmission from bats to humans may simply reflect an increase in their contact through anthropogenic modification of the bat's natural environment. The emergence of Nipah virus and SARS-CoV epitomizes this situation. In regions where large areas of bat habitat have been converted to agricultural land or oil palm plantations, the surviving bat populations will be concentrated in the remaining patches of forest that provide the resources they need. When these patches of fruit trees are used as shade for intensive animal husbandry, then it is highly likely that the fruits and insects chewed by bats will find their way into the human food chain.

The scientists who revealed the bat reservoir of SARS-CoV operate within a new intellectual paradigm. They call their discipline "conservation medicine" (*12*). It brings together the two areas of natural science that will be crucial to the future welfare of humans: health sciences (human, veterinary, and plant pathology) and the ecological sciences that monitor the health of populations, communities, and ecosystems. The Millenium Ecosystem Assessment has emphasized the dependence of human health and economic well-being on goods and services provided by the natural environment (*13*). This dependence can only be actively capitalized upon if we increase our understanding of the population dynamics and ecology of new and old infectious diseases. Conservation medicine is an idea whose time has come none too soon.



**References and Notes**


1. W. Li *et al.*, *Science* **310**, 676 (2005); published online 29 September 2005 (10.1126/science.1118391).
2. S. K. P. Lau *et al. Proc. Natl. Acad. Sci. U.S.A.* **102**, 14040 (2005).
3. A. R. McLean, R. M. May, J. Pattison, R. A. Weiss, in *SARS. A Case Study in Emerging Infections* (Oxford Univ. Press, Oxford, 2005).
4. U. D. Parashar, L. J. Anderson, *Int. J. Epidemiol.* **33**, 628 (2004).
5. A. D. Hyatt, P. Daszak, A. A. Cunningham, H. Field, A. R. Gould, *EcoHealth* **1**, 25 (2004).
6. V. P. Hsu *et al. Emerg. Infect. Dis.* **10**, 2082 (2004).
7. O. Diekmann, J. A. P. Heesterbeek, J. A. J. Metz, *J. Math. Biol.* **28**, 365 (1990).
8. A. P. Dobson, *Am. Nat.* **164**, S64 (2004).
9. D. J. Nokes, R. M. Anderson, *Lancet* **2**, 1374 (1988).
10. K. E. Jones, A. Purvis, A. MacLarnon, O. R. Bininda-Emonds, N. Simmons, *Biol. Rev.* **77**, 223 (2002).
11. M. E. J. Woolhouse, S. Gowtage-Sequeria, *Emerg. Infect. Dis.*, in press.
12. A. A. Aguirre, R. S. Ostfeld, G. M. Tabor, C. House, M. C. Pearl, in *Conservation Medicine. Ecological Health in Practice* (Oxford Univ. Press, Oxford, 2002).
13. Millenium Ecosystem Assessment. *Ecosystems and Human Well-Being: A Framework for Assessment* (Island Press, Washington, DC, 2003).


14. I am grateful to J. Childs, P. Daszak, A. Hyatt, S. Kutz, J. Rowenthal, and S. Luby for comments on an earlier draft of this essay. My research is funded by the NIH/NSF Ecology of Infectious Disease Program.

10.1126/science.1120872

DEVELOPMENTAL BIOLOGY

# Less Steroids Make Bigger Flies

Kirst King-Jones and Carl S. Thummel

The simple observation that higher organisms achieve a final body size that is characteristic of their species raises the profound biological question of how that final size is achieved. Detailed studies over the past decade have provided part of the answer, demonstrating that insulin signaling plays a central role in directing animal growth. However, it remains unclear why growth is largely restricted to juvenile stages and how it is terminated upon sexual maturation. A report by Colombani *et al.* (*1*) on page 667 of this issue provides important new insights into the coordination of growth and maturation, using the fly *Drosophila melanogaster* as a model. The study shows that the steroid hormone ecdysone, which directs insect maturation, suppresses growth by antagonizing insulin activity.

Enhanced online at www.sciencemag.org/cgi/content/full/310/5748/630

Insulin-like peptides and the insulin receptor drive organismal growth, acting through a cellular signaling cascade that includes phosphatidylinositol 3-kinase (PI3K). Superimposed on insulin-mediated growth is temporal control by hormones that direct the juvenile-to-adult transition. In insects, this temporal control is provided by pulses of the steroid hormone ecdysone that are released from the prothoracic gland in response to neuropeptide signaling. Ecdysone pulses trigger two larval molts to accommodate the ~200-fold increase in mass that occurs as the larva feeds. Increases in ecdysone at the end of the last larval stage terminate feeding and initiate maturation via metamorphosis. The rate of larval growth and the duration of feeding both contribute to final body size, with no further growth occurring after puparium formation.

Colombani *et al.* exploited earlier studies showing that ectopic expression of PI3K accelerates cell growth, whereas expression of a dominant negative form ($PI3K^{DN}$, which inhibits PI3K) retards cell growth (*2*). Expressing these insulin regulators specifically in the prothoracic gland affected the size of the gland as expected but, remarkably, had the opposite effect on overall body size. Activated insulin signaling in the prothoracic gland created smaller animals, whereas insulin inhibition created larger animals. Enlarging the prothoracic gland by expressing insulin-independent growth regulators had no effect on body size, indicating that gland size per se is not the culprit. Rather, changes in insulin signaling within the prothoracic gland affect overall body size (see the figure). Given that the primary function of this organ is to produce ecdysone, the authors used various strategies to measure ecdysone levels in animals that express either PI3K or $PI3K^{DN}$ in their prothoracic glands. They found that larvae with smaller glands produced less ecdysone, whereas those with enlarged glands produced more. This suggests that the effects of prothoracic gland insulin activity on body size are mediated by changes in ecdysone levels (see the figure). This proposal is reminiscent of the effects of insulin on insect ovaries, where it promotes ecdysone production (*3*, *4*). Feeding ecdysone throughout larval stages or inactivating the ecdysone receptor resulted in reduced or increased body weight, respectively, further defining a role for ecdysone in insect growth.

How do changes in ecdysone levels affect final body size? One possibility arises from the role of the hormone in determining the duration of larval feeding. Changes in ecdysone levels could direct shorter or longer feeding periods. Alternatively, ecdysone could affect larval growth rates, allowing animals to achieve different sizes over the same time interval. Colombani *et al.* favor the latter model and show that the growth rate is enhanced in larvae that express $PI3K^{DN}$ in their prothoracic gland, but is reduced in larvae that express PI3K, with little or no effect on the timing of

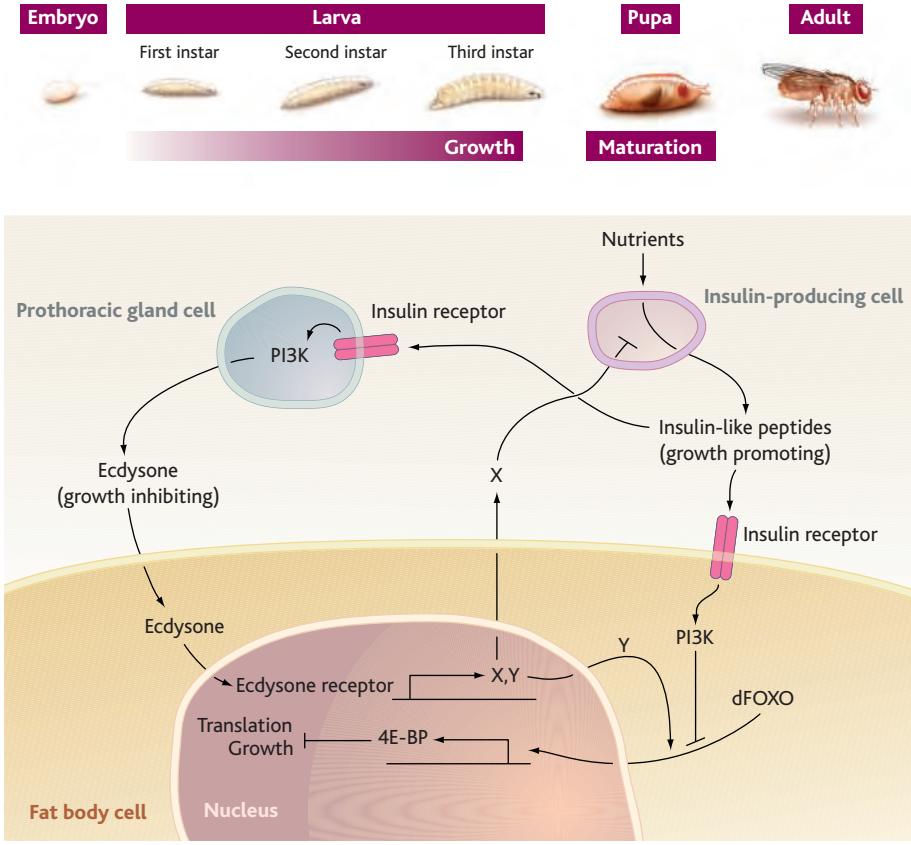


**Coordination of organism growth through insulin and ecdysone signaling.** (**Top**) The four major stages of the *Drosophila* life cycle are depicted: embryonic, larval, pupal, and adult. Growth occurs during larval stages in response to insulin signaling and basal levels of the steroid hormone ecdysone. This is followed by sexual maturation during metamorphosis. (**Bottom**) The prothoracic gland releases ecdysone that activates the ecdysone receptor in fat body cells, producing an unknown factor X. This factor may suppress growth by inhibiting the release of insulin-like peptides from insulin-producing cells. Insulin-like peptides activate the insulin receptor and PI3K signaling pathway that blocks nuclear translocation of the transcription factor dFOXO. The ecdysone receptor may also induce expression of a factor Y that directs nuclear translocation of dFOXO, activating genes that inhibit growth, including that which encodes the 4E-BP protein translation inhibitor.

The authors are in the Howard Hughes Medical Institute, Department of Human Genetics, University of Utah School of Medicine, Salt Lake City, UT 84112, USA. E-mail: kirst@genetics.utah.edu; carl.thummel@genetics.utah.edu

larval molts or puparium formation. In addition, they found that feeding ecdysone to larvae that express $PI3K^{DN}$ in their prothoracic gland slowed the enhanced growth of these animals, suggesting that the increased growth rate is indeed due to reduced ecdysone titers.

Finally, the authors show that expression of PI3K in the prothoracic gland and changes in ecdysone signaling affect components of the insulin signaling pathway in other tissues in a manner that is consistent with the effects on growth. Expression of PI3K in the prothoracic gland resulted in increased translocation of the transcription factor dFOXO into nuclei of fat body cells. This consequently increased expression of a direct target of dFOXO, the 4E-BP protein synthesis inhibitor. These are all indicators of decreased insulin signaling and reduced growth (see the figure). A similar effect was seen by feeding ecdysone to normal (wild-type) larvae. Conversely, inactivating the ecdysone receptor in the fat body decreased nuclear levels of dFOXO and reduced 4E-BP expression, further suggesting that ecdysone regulates organismal growth through effects on the insulin signaling pathway. The observation that a mutant fly lacking functional dFOXO does not exhibit the growth defect caused by expressing PI3K in the prothoracic gland also supports this model. Moreover, Colombani *et al.* show that reducing ecdysone receptor activity exclusively in the fat body is sufficient to produce larger animals, indicating that this tissue (the insect equivalent of mammalian liver and adipose tissue) plays a central role in relaying systemic information regarding final overall body size, albeit through an unknown signal (see the figure).

Several important questions remain. First, is insulin signaling in the prothoracic gland a natural means of regulating ecdysone titers? It will be interesting to determine whether tissue-specific loss-of-function mutations in insulin signaling components in the prothoracic gland have the predicted effects on ecdysone titers and body size. A second related question is whether changes in insulin signaling in the prothoracic gland affect body size solely through changes in ecdysone levels. Partial reduction in the activity of key enzymes in the ecdysone biosynthetic pathway would address the question of whether the corresponding changes in ecdysone levels are sufficient to alter body size. Further studies will also have to examine how insulin balances its normal growth-promoting effects with its proposed growth-inhibitory effects through ecdysone synthesis (see the figure).

Another critical question is whether changes in larval growth rates alone explain the observed effects on body size. This question is highlighted by two recent studies (*5*, *6*) that use similar strategies to modulate prothoracic gland insulin activity and report comparable effects on body size and larval growth rates. In contrast to the work of Colombani *et al*., however, these studies find that the larval stages are shorter for small animals and prolonged for larger animals, indicating that the duration of the larval growth phase contributes to final body size. The fact that each study uses different transgenic tools to modulate prothoracic gland insulin activity may provide one reason for the observed differences in developmental timing. In addition, small differences in the duration of larval development can have a significant effect on overall body size, given that *Drosophila* larvae gain on average 7% of their weight per hour. Moreover, as shown by Mirth *et al.* (*5*), nutrition and photoperiod can affect the degree of overall growth directed by insulin signaling in the prothoracic gland. Clearly, more work is required to resolve this discrepancy.

Our current understanding of ecdysone action is derived largely from studies of high-titer ecdysone pulses in directing developmental transitions during the insect life cycle. However, these three new reports draw our attention back to basal ecdysone levels and their roles in insect physiology. Although relatively few studies have addressed this issue, basal ecdysone levels maintain cell proliferation in the eye primordium of the moth *Manduca sexta*, with higher hormone titers arresting proliferation and promoting eye maturation (*7*). In addition, studies of the wing imaginal discs of the butterfly *Precis coenia* demonstrate a requirement for both ecdysone and bombyxin (a lepidopteran insulin-like peptide) for growth (*8*). The molecular basis of these effects, however, remains unclear. The results reported by Colombani *et al*., along with the related studies by Mirth *et al.* (*5*) and Caldwell *et al*. (*6*), provide insights into how steroid and insulin signaling are integrated to coordinate growth and maturation, and establish new directions for future studies of growth regulation in higher organisms.

**References**


1. J. Colombani *et al*., *Science* **310**, 667 (2005); published online 22 September 2005 (10.1126/science.1119432).
2. J. S. Britton, W. K. Lockwood, L. Li, S. M. Cohen, B. A. Edgar, *Dev. Cell* **2**, 239 (2002).
3. M. A. Riehle, M. R. Brown, *Insect Biochem. Mol. Biol.* **29**, 855 (1999).
4. M. P. Tu, C. M. Yin, M. Tatar, *Aging Cell* **1**, 158 (December, 2002).
5. C. Mirth, J. W. Truman, L. M. Riddiford, *Curr. Biol.* 10.1016/j.cub.2005.09.017.
6. P. E. Caldwell, M. Walkiewicz, M. Stern, *Curr. Biol.* 10.1016/j.cub.2005.09.011.
7. D. T. Champlin, J. W. Truman, *Development* **125**, 2009 (1998).
8. H. F. Nijhout, L. W. Grunert, *Proc. Natl. Acad. Sci. U.S.A.* **99**, 15446 (2002).


10.1126/science.1120410

PHYSICS

# The Observation of Matter Wave Fluctuations

**Peter L. Knight**

This month's Nobel Prize in Physics recognizes Roy Glauber for his work in quantum optics, and especially for his role in distinguishing the different kinds of fluctuations or correlations that exist in natural light from thermal sources such as the Sun, which are quite different from those of the unnatural radiation from a laser. On page 648 of this issue, we see a further chapter opening in this story, in which Schellekens *et al.* (*1*) report on observations of analogous fluctuations in matter waves, those formed from cold atoms. Using a clever microchannel plate detection scheme, they have been able to demonstrate the transition from the fluctuations in a thermal cloud of atoms to the lack of fluctuations in a coherent Bose condensate as their atom cloud cooled.

The author is at the Blackett Laboratory, Imperial College London, London SW7 2AZ, UK. E-mail: p.knight@imperial.ac.uk

The study of fluctuations in thermal light was initiated in the 1950s by the British astronomers R. Hanbury Brown and R. Q. Twiss (*2*), who were eager to develop a new method to determine the size of stars that improved on Michelson's stellar interferometer (see the figure). Hanbury Brown had a curious initiation into the study of fluctuating signals: Almost kidnapped from the student labs by the then-rector of Imperial College, Henry Tizard, he was press-ganged into joining the nascent British radar project at Bawdsey, and after the war joined Lovell's group setting up the Jodrell Bank Observatory in Cheshire. He and Twiss were determined to show that an intensity interferometer would generate the improvements they sought over the Michelson interferometer, and started by demonstrating the effect in a laboratory experiment with thermal light from a spectral lamp (this later led to the successful

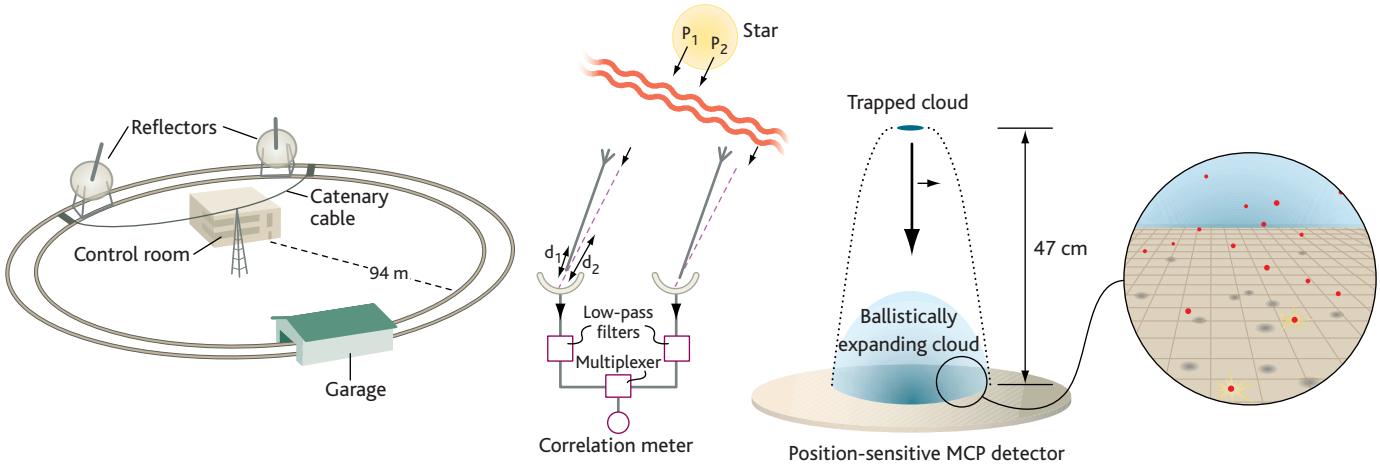


**Coherence in light and matter.** (**Left**) Sketch of the intensity interferometer used by Hanbury Brown and Twiss to measure the fluctuations in light from stars to deduce stellar sizes (*2*). (**Middle**) Schematic of the Hanbury Brown and Twiss measurement of the correlations observed at two points from an extended optical source such as a star (*2*). (**Right**) Schematic of the matter wave interferometry experiment performed by Schellekens *et al*. (*1*) where an extended source of cold atoms is dropped onto a position-sensitive multichannel plate (MCP) detector.

Narrabri telescope). They were able to demonstrate the existence of the excess fluctuations from this thermal source, later to be called "photon bunching." This initially caused much consternation and confusion, as doubters misunderstood a dictum from Dirac that photons should only interfere with themselves and not each other (*3*). Clarification came from the work of Purcell and from Mandel, Wolf, and others (*4*) on the counting statistics of light, and this phase really marked the beginning of the development of quantum optics as a subject.

With the advent of the laser, these questions were revisited. Lasers are stable, lack the Gaussian fluctuations of thermal light, and would show no such correlations. Glauber developed a sophisticated quantum theory of coherence that showed how bunching, laser light, and even anticorrelation could be accommodated within a consistent theoretical framework [(*5*); for an overview, see (*6*)].

Underpinning this framework of coherence theory was the role of quantum statistics and indistinguishability: Integer-spin boson particles show two-body interferences that are quite different from those of fermionic half-integer particles. Much attention has been paid to this, but this has only been accessible to study when cold atoms became available by means of laser cooling. A pioneering experiment to investigate atomic correlations was performed in 1996 at the University of Tokyo, by Yasuda and Shimizu, using a continuous beam of neon atoms (*7*). Now Schellekens *et al.* (*1*) have investigated the correlations from a cloud of cold atoms, much closer in spirit to the original Hanbury Brown and Twiss (HBT) experiment, which sought spatial information. They investigated the size over which the cloud remained correlated—a kind of speckle experiment familiar from light scattering. Such effects can be seen with the eye: If you look at sunlight scattered in the open air from a rough surface (technically a "rugous" surface) such as a fingernail, you can observe the twinkling of the scattered light. Schellekens *et al.* studied these fluctuations in a cold cloud of atoms released to fall on a microchannel plate detector where the pairwise correlations can be investigated as a function of the separation of the two chosen detection points (see the figure). Their correlation length $l$ is exactly as predicted by elementary optics: $l = L\lambda/2\pi s$, where $L$ is the distance from the cloud to the detector (this translates into a drop time), $s$ is the size of the cloud, and $\lambda$ is the de Broglie wavelength of the atomic matter wave. Analysis of the analog of the HBT intensity correlations leads to a deviation from unity given by a Gaussian with a characteristic length scale that is precisely this correlation length.

This is exactly what Schellekens *et al.* observed. As the temperature of the atom cloud changed, the size $s$ changed, as the cloud was formed in a harmonic well whose filling (and thus size) depends on temperature. In these experiments, the size $s$ was really small, crucial in leading to a large enough outcome. But once the temperature was lowered sufficiently to allow the atoms to Bose-condense, the correlation length increased to such an extent that the fluctuations disappeared, just as their optical counterparts did when light from a laser was studied [by the pioneers of photon statistics Arecchi, Pike, and Mandel (*4*) among others] from below threshold (when they are essentially thermal) to way above threshold when they are coherent.

So this experiment [and the earlier Tokyo University beam experiment (*7*), together with a related experiment from Öttl *et al.* (*8*)] marks the beginning of a new era in atom optics. It would be interesting to see (as Schellekens *et al.* state) what would result if a fermionic cloud were used and whether the statistics would indeed show the antibunching effect. Another quantum gas to investigate would be the Mott insulator state formed in optical lattices. Studies of these have been pioneered in the laboratory by another of this year's Physics Nobelists, Theodor Hänsch. The localized Fock nature of the Mott state should reveal dramatically different statistics. Another would be the nature of fluctuations in clouds formed from the dissociation of a molecular condensate where there is considerable analogy with two-mode squeezing, and where one might expect to see bunching within each subspecies component of the dissociation but correlations across species (*9*), a little like the statistics seen in jets formed from high-energy hadronic collisions. Much remains to be done in this exciting field.

**References**

1. M. Schellekens *et al.*, *Science* **310**, 648 (2005); published online 15 September 2005 (10.1126/science.1118024).
2. R. Hanbury Brown, R. Q. Twiss, *Nature* **178**, 1046 (1956).
3. P. A. M. Dirac, *The Principles of Quantum Mechanics* (Oxford Univ. Press, Oxford, 1982).
4. L. Mandel, E. Wolf, *Selected Papers on Coherence and Fluctuations of Light* (Dover, New York, 1970).
5. R. J. Glauber, in *Quantum Optics and Electronics*, C. Dewitt, A. Blandin, C. Cohen-Tannoudji, Eds. (Gordon and Breach, New York, 1965).
6. C. C. Gerry, P. L. Knight, *Introductory Quantum Optics* (Cambridge Univ. Press, Cambridge, 2005).
7. M. Yasuda, F. Shimizu, *Phys. Rev. Lett.* **77**, 3090 (1996).
8. A. Öttl, S. Ritter, M. Köhl, T. Esslinger, *Phys. Rev. Lett.* **95**, 090404 (2005).
9. S. M. Barnett, P. L. Knight, *J. Opt. Soc. Am. B* **2**, 467 (1985).

10.1126/science.1120023

RETROSPECTIVE

# Joseph Rotblat (1908–2005)

John P. Holdren

Sir Joseph Rotblat, who died on 31 August in London at the age of 96, was a participant in the Manhattan Project, a pioneer in medical physics, and one of the towering figures of the 20th century in the domain of the social responsibilities of scientists. He was the only scientist to leave the American-British atomic-bomb project on moral grounds once it became clear that the Germans would not succeed in developing the bomb. Thereafter, he devoted the rest of a long career in science to clarifying the health impacts of ionizing radiation. His parallel career in public affairs focused on building international communication and cooperation to reduce the dangers posed by nuclear weapons.

Rotblat was the youngest of the 11 signers of the 1955 Russell-Einstein Manifesto, which called upon scientists to "assemble in conference to appraise the perils that have arisen as a result of the development of weapons of mass destruction." (Most of the other signers, including Albert Einstein, Bertrand Russell, Max Born, Frederic Joliot-Curie, Linus Pauling, and Hideki Yukawa, already had Nobel Prizes.) He was instrumental in planning the resulting 1957 conference in Pugwash, Nova Scotia, which spawned a new international organization—the Pugwash Conferences on Science and World Affairs. It has since held some 300 conferences, symposia, and workshops on arms control and peace-building.

Even at the height of the Cold War, the Pugwash Conferences were able to assemble scientists and public figures from both sides of the Iron Curtain for private discussions of the thorniest science-and-security issues of the time. These meetings are widely credited with laying the technical foundations for the Nuclear Non-Proliferation Treaty, the Partial Test Ban Treaty, the Anti–Ballistic Missile Treaty, the Biological Weapons Convention, and the Chemical Weapons Convention, among others. Joseph Rotblat was the organization's first and longest serving secretary general (1957 to 1973), and later its president (1988 to 1997). For its entire existence until his death this year, he was its animating spirit and the embodiment of its commitment to diminish the dangers from weapons of mass destruction and from war itself.

The author is at the Woods Hole Research Center, Woods Hole, MA 02543, USA and Harvard University, Cambridge, MA 02138, USA. E-mail: john_holdren@harvard.edu

A Polish Jew, Rotblat completed his doctorate in physics at the University of Warsaw. In 1939, he accepted a research fellowship to work under James Chadwick, the discoverer of the neutron, at the University of Liverpool. Later that year, he returned to Warsaw to collect his young Polish wife, but she was too ill to travel, and he had to return to England without her. The next day Hitler invaded Poland, and Rotblat never saw his wife again.

Rotblat's own experiments at the end of the 1930s had shown that the newly discovered fission process emitted neutrons, and he was one of the first to realize that this opened the possibility of a chain reaction that could yield immense explosive power. With Chadwick, he went to the Los Alamos National Laboratory in New Mexico in 1943 as part of the British team assigned to the Manhattan Project (although he did not become a British citizen until after the war).

When it became clear in 1944 that the Germans were losing the war—and clear, as well, through intelligence that was shared with Rotblat, that the German atomic bomb project had gone nowhere—he packed his bags, left Los Alamos, and returned to Liverpool. He later told me and others that he had no wish to work on an atomic weapon destined for use against Japan, known not to be developing such a weapon itself.

Back in England, he switched the focus of his scientific work to medical physics, pioneering the use of linear accelerators for radiation therapy and becoming one of the world's leading authorities on fallout and the effects of ionizing radiation on humans. He also began to work on educating the public and policy-makers on the dangers of nuclear weapons and shortly after the war's end, became one of the founders of the Atomic Scientists Association—the British counterpart to the Federation of American Scientists that was established in the United States at about the same time.

In 1954, Rotblat met the eminent British philosopher and mathematician Bertrand Russell through a British Broadcasting Corporation television program about the hydrogen bomb in which they were both interviewed. He became an adviser to Russell on the details of nuclear-weapon science, and was subsequently recruited by Russell to sign the Russell-Einstein Manifesto and chair the press conference that released the document

Recognizing that the knowledge of how to build nuclear weapons could not be eradicated, the signers of the Russell-Einstein Manifesto emphasized that safety for civilization would come only when war itself was abolished as a means of settling disputes among nations. A prohibition on nuclear weapons, while desirable, would only be a way station on the road to safety. Joseph Rotblat, however, became increasingly preoccupied with the urgency of reaching that way station and he made its pursuit the central aim of his own life's work in the nuclear arena and a major theme within the Pugwash Conferences.

He contributed a number of significant ideas to the multidecade debate about the desirability and feasibility of eliminating nuclear weapons, along with tireless energy, unmatched eloquence, and total commitment to the cause of peace. The Pugwash Conferences served as an invaluable vehicle for pursuing these goals. Knowing full well that this quest would take longer than the span of his own life, he invested tremendous effort in recruiting to the cause, and mentoring students and young scientists. He was instrumental in founding in the 1980s, and nurturing thereafter, an international Student/Young Pugwash counterpart to the "senior" organization.

In 1995, Joseph Rotblat was awarded half of the Nobel Peace Prize with a citation that read "for efforts to diminish the part played by nuclear arms in international affairs and, in the longer run, to eliminate such arms." The other half of the prize went to the Pugwash organization. Rotblat was elected to the United Kingdom's Royal Society in the same year and was knighted in 1998. With his passing, the world has lost a great champion of peace. But the compelling example of his life, which has already inspired and instructed so many about the social responsibilities of science and scientists, will continue to do so.

10.1126/science.1121081

CREDIT: PUGWASH CONFERENCES

edited by Edward W. Lempinen

SCIENCE AND SOCIETY

# AAAS Fighting to Defend the Integrity of Science Education

With evolution on trial in Pennsylvania and under renewed attack by the Kansas State Board of Education, AAAS has stepped up its high-profile campaign to protect the integrity of science education by defending the scientific underpinnings of evolution and making clear that science and religion should not be pitted against each other.

In a series of interviews, press briefings, and op-ed commentaries, AAAS Chief Executive Officer Alan I. Leshner and other AAAS officials have stressed that most religious leaders accept evolution and that many scientists are religious. But, they said, leaders of the intelligent design movement who claim scientific motives are actually trying to undermine science—at significant risk to U.S. students.

The world's religions "bring great value to many people's lives," said AAAS President Gilbert S. Omenn. But "they do not prepare students for a world in which math, science, and empirically tested evidence are essential" for advancing human health, security, and economic progress.

"We have a well-established tradition of separation of church and state," Omenn said. "Forcing creationism or its slightly modernized incarnation as 'intelligent design' into the schools, let alone the science classroom, violates this basic tenet of American society. As many clergy vigorously agree, let's encourage children and adults to practice their religion in their places of worship and their homes, and protect the precious time that children have in school."

The controversy over teaching evolution in public school science classes has been a recurring part of American culture—and a continuing interest of AAAS. In the 1920s, AAAS supported the teaching of evolution and raised money to help defend Tennessee biology teacher John Scopes. Throughout the past decade, AAAS's Dialogue on Science, Ethics, and Religion (DoSER) has produced conferences and books on the issue.

The controversy has been building again in recent years, with anti-evolution efforts in more than 20 states. But two events this year have pushed it into national headlines.

THE YORK DISPATCH

Wednesday, October 5, 2005

It's Not the Scopes Monkey Trial II

Opinion by Alan Leshner
American Association for the Advancement of Science

With intelligent design on trial in Pennsylvania, the *York (Pennsylvania) Dispatch* published a column by AAAS CEO Alan I. Leshner.

A trial began last month in U.S. District Court in Harrisburg, Pennsylvania, featuring eight families who sued the Dover Area School District for requiring 9th-grade biology students to hear a statement that questions evolution and promotes intelligent design (ID).

In the weeks leading up to the trial, Leshner was a guest on ABC's *World News Tonight, NBC Nightly News,* MSNBC-TV and National Public Radio. After a teleconference, Lesher and Eugenie Scott, executive director of the National Center for Science Education, were cited by the *Washington Post,* the *Philadelphia Inquirer*, China's Xinhua news agency, and others.

He also was quoted by *New York Times Magazine* columnist William Safire. "Whether or not there is or was an intelligent designer is not a scientific question," he told Safire. "It's not an alternative to evolution. What they are trying to do is get religion in the science classroom."

As the trial began, a column written by Leshner was published in the *York (Pennsylvania) Dispatch,* a leading daily newspaper in the Dover area. "Despite their professed devotion to science, ID advocates have published nothing in mainstream, peer-reviewed journals," he wrote. "Their allies in the sciences are few, and mostly fringe players…. Finding a few scientists who endorse a belief does not make it science." A similar column was published in three other Pennsylvania newspapers: the *Allentown Morning Call,* the *Scranton Times,* and the *Harrisburg Patriot-News.*

Albert H. Teich, AAAS head of Science and Policy Programs, defended the teaching of evolution in an August appearance on CNN. DoSER Director Connie Bertka told the *Philadelphia Inquirer* that the controversy would not end with the trial. "This will continue to be a problem until, as a society,

AAAS GOVERNANCE

## Council Reminder

The next meeting of the AAAS Council will take place during the Annual Meeting and will begin at 9:00 a.m. on Sunday, 19 February 2006 in the Landmark Ballroom of the Renaissance Grand Hotel in St. Louis, Missouri. Individuals or organizations wishing to present proposals or resolutions for possible consideration by the Council should submit them in written form to AAAS Chief Executive Officer Alan Leshner by 15 November 2005. This will allow time for them to be considered by the Committee on Council Affairs at their fall meeting.

Items should be consistent with AAAS's objectives and be appropriate for consideration by the Council. Resolutions should be in the traditional format, beginning with "Whereas" statements and ending with "Therefore be it resolved."

Late proposals or resolutions delivered to the AAAS Chief Executive Officer in advance of the February 2006 Open Hearing of the Committee on Council Affairs will be considered, provided that they deal with urgent matters and are accompanied by a written explanation of why they were not submitted by the November deadline. The Committee on Council Affairs will hold its open hearing at 2:30 p.m. on 18 February 2006 in the Portland/ Benton Rooms of the Renaissance Grand Hotel.

Summaries of the Council meeting agenda will be available during the annual meeting at both the AAAS Information Desk and in the AAAS Headquarters office. A copy of the full agenda will also be available for inspection in the Headquarters Office.



Published by AAAS

we come to grips with it," she said.

In Kansas, meanwhile, AAAS Fellow John Staver went before the Board of Education on 13 September to complain of "inaccurate" and "misleading" information in the board's proposed new science standards. The standards redefine science, he said, so that science might allow for supernatural explanations of the natural world.

The prevailing definition is "one of the primary reasons that science has been fruitful in producing useful knowledge," said Staver, director of the Center for Science Education at Kansas State University.

"We are pleased that AAAS is being proactive and vocal on important and divisive issues, including the teaching of evolution," said Gerry Wheeler, executive director of the National Science Teachers Association. "AAAS's ability to translate complex scientific concepts for the general public will help ensure that pseudo-science and other nonscientific ideas do not become a part of science instruction."

**2006 ANNUAL MEETING**

## Grand Challenges, Great Opportunities

From sustainability to the future of mathematics, from video games to the frontiers of space, the 2006 AAAS Annual Meeting will deliver more cutting-edge science and technology than any conference of its kind in the world.

Under the banner of "Grand Challenges, Great Opportunities," the meeting is expected to bring thousands of scientists, students, teachers and families to St. Louis, Missouri, from 16 to 20 February, 2006.

Among the highlights:

**A nanotechnology seminar** will examine promising applications, potential health risks, and broad societal implications.

**Family Science Days** will feature hands-on workshops and demonstrations to educate and entertain. Last year, they drew nearly 3,000 children and family members.

**"Physics and Economics of Virtual Worlds"** will examine the video game industry, a cultural and economic force.

**The "AAAS Evolution Event for St. Louis–Area Teachers"** will expand the dialogue on teaching evolution in U.S. public schools.

**"Beyond Pi: Grand Challenges in the Mathematical Sciences"** is a daylong event that should have broad multidisciplinary appeal.

Altogether, there will be more than 200 symposia, lectures, seminars, and other sessions. For more about the program and registration, see www.aaasmeeting.org.

## AAAS Members Elected as Fellows

In September, the AAAS Council elected 376 members as Fellows of AAAS. These individuals will be recognized for their contributions to science at the Fellows Forum to be held on 18 February 2006 during the AAAS Annual Meeting in St. Louis. The new Fellows will receive a certificate and a blue and gold rosette pin as a symbol of their distinguished accomplishments. Presented by section affiliation, they are:

### Agriculture, Food, and Renewable Resources

Jose M. Amador, Texas A&M Research and Extension Center, Weslaco • Alan B. Bennett, Univ. of California, Davis • Peter Bretting, USDA-ARS, Beltsville, MD • Bruce C. Campbell, USDA-ARS Western Regional Research Center, Albany, CA • Kenneth G. Cassman, Univ. of Nebraska, Lincoln • Gebisa Ejeta, Purdue Univ. • Charles A. Francis, Univ. of Nebraska, Lincoln • Scot H. Hulbert, Kansas State Univ. • William K. Lauenroth, Colorado State Univ. • Hei Leung, International Rice Research Institute, Manila • Na-Sheng Lin, Academia Sinica, Taiwan • Richard H. Loeppert, Texas A&M Univ. • Timothy D. Paine, Univ. of California, Riverside • Pedro A. Sanchez, Earth Institute at Columbia Univ. • Lawrence B. Schook, Univ. of Illinois Urbana • Jei-Fu Shaw, Academia Sinica, Taiwan

### Anthropology

Stephen J. Beckerman, Pennsylvania State Univ. • Russell L. Ciochon, Univ. of Iowa • Gary M. Feinman, Field Museum, Chicago • William L. Hylander, Duke Univ. • Clifford J. Jolly, New York Univ. • William H. Kimbel, Arizona State Univ. • Jeffrey T. Laitman, Mount Sinai School of Medicine, New York City • William C. McGrew, Miami Univ. • Thomas C. Patterson, Univ. of California, Riverside • Payson D. Sheets, Univ. of Colorado, Boulder

### Astronomy

Sushil K. Atreya, Univ. of Michigan, Ann Arbor • Henry C. Ferguson, Space Telescope Science Institute, Baltimore • Alan W. Harris, Space Science Institute, Boulder • David C. Jewitt, Univ. of Hawaii, Honolulu • Steven D. Kawaler, Iowa State Univ. • Eugene H. Levy, Rice Univ. • J. Michael Shull, Univ. of Colorado, Boulder • Mark Vincent Sykes, Planetary Science Institute, Tucson • Paul Robert Weissman, Jet Propulsion Lab.

### Atmospheric and Hydrospheric Sciences

Francisco P. Chavez, Monterey Bay Aquarium Research Institute, Moss Landing, CA • Peter Henry Gleick, Pacific Institute for Studies in Development, Environment, and Security, Oakland, CA • Philip B. Russell, NASA Ames Research Center • Graeme L. Stephens, Colorado State Univ. • Susan E. Trumbore, Univ. of California, Irvine • Peter J. Webster, Georgia Institute of Technology • Douglas R. Worsnop, Aerodyne Research, Inc., Billerica, MA • Yuk L. Yung, California Institute of Technology

### Biological Sciences

Jill P. Adler-Moore, California State Polytechnic Univ., Pomona • Michael F. Allen, Univ. of California, Riverside • Todd Alan Anderson, Texas Tech Univ. • Michael L. Arnold, Univ. of Georgia • Julia N. Bailey-Serres, Univ. of California, Riverside • Tania A. Baker, Massachusetts Institute of Technology • Barbara Gail Beckman, Tulane Univ. • Jeffrey Lynn Bennetzen, Univ. of Georgia • Nora J. Besansky, Univ. of Notre Dame • Roger K. Bretthauer, Univ. of Notre Dame • Arturo Casadevall, Albert Einstein College of Medicine • Vicki L. Chandler, Univ. of Arizona • Joanne Chory, Salk Institute for Biological Studies, La Jolla, CA • Keith Clay, Indiana Univ., Bloomington • Gloria M. Coruzzi, New York Univ. • Evan H. DeLucia, Univ. of Illinois, Urbana-Champaign • Daniel R. Gallie, Univ. of California, Riverside • Robert C. Gallo, Univ. of Maryland Biotechnology Institute • James I. Garrels, Garbrook Associates, Beverly, MA • N. Louise Glass, Univ. of California, Berkeley • Takashi Gojobori, National Institute of Genetics, Mishima, Japan • Carla B. Green, Univ. of Virginia • Joel Francis Habener, Massachusetts General Hospital, Boston • James Edward Haber, Brandeis Univ. • Benjamin D. Hall, Univ. of Washington • Joyce Libby Hamlin, Univ. of Virginia • Linda Kay Hanley-Bowdoin, North Carolina State Univ. • Jon Fewell Harrison, Arizona State Univ. • Stephen Coplan Harrison, Harvard Medical School • Alan Hastings, Univ. of California, Davis • John E. Hearst, Cerus Corp., Concord, CA • Tina M. Henkin, Ohio State Univ., Columbus • Joan Herbers, Ohio State Univ., Columbus • Daniel Herschlag, Stanford Univ. • Philip Andrew Hieter, Univ. of British Columbia • Tatsuya Hirano, Cold Spring Harbor Lab. • F. Kay Huebner, Ohio State Univ., Columbus • James H. Hunt, Univ. of Missouri, St. Louis • Richard Timothy Hunt, Clare Hall Labs., South Mimms, England • Robert D. Ivarie, Univ. of Georgia • Richard A. Jorgensen, Univ. of Arizona • Fotis C. Kafatos, EMBL, Heidelberg, Germany • Nancy Pulane Keller, Univ. of Wisconsin, Madison •





Published by AAAS

David Kowalski, Roswell Park Cancer Institute, Buffalo • Adam Kuspa, Baylor College of Medicine • Laura Landweber, Princeton Univ. • Meredith Anne Lane, Global Biodiversity Information Facility, Copenhagen • Linda L. Lasure, Pacific Northwest National Lab. • Walter S. Leal, Univ. of California, Davis • Leslie A. Leinwand, Univ. of Colorado, Boulder • Laura S. Levy, Tulane Univ. • Jim Jung-Ching Lin, Univ. of Iowa • Jonathan B. Losos, Washington Univ. • Dario Maestripieri, Univ. of Chicago • Vivek Malhotra, Univ. of California, San Diego • Richard B. Meagher, Univ. of Georgia • Synthia H. Mellon, Univ. of California, San Francisco • Sabeeha Merchant, Univ. of California, Los Angeles • Aaron P. Mitchell, Columbia Univ. • Edward J. Mullaney, USDA-ARS Southern Regional Research Center, New Orleans • Michael W. Nachman, Univ. of Arizona • Berl R. Oakley, Ohio State Univ., Columbus • Philip Osdoby, Washington Univ. • Stephen W. Pacala, Princeton Univ. • Jeffrey D. Palmer, Indiana Univ., Bloomington • Patricia G. Parker, Univ. of Missouri, St. Louis • Aristides A. N. Patrinos, U.S. Dept. of Energy, Germantown, MD • Thomas D. Petes, Univ. of North Carolina, Chapel Hill • Christoph Plass, Ohio State Univ., Columbus • Louise Prakash, Univ. of Texas Medical Branch • Satya Prakash, Univ. of Texas Medical Branch • Patricia J. Pukkila, Univ. of North Carolina, Chapel Hill • Michael D. Purugganan, North Carolina State Univ. • John Ralph, Univ. of Wisconsin, Madison • Yasuko Rikihisa, Ohio State Univ., Columbus • George D. Rose, Johns Hopkins Univ. • Fred D. Sack, Ohio State Univ., Columbus • Sandra L. Schmid, Scripps Research Institute, La Jolla, CA • Eric Ursell Selker, Univ. of Oregon, Eugene • Fred Sherman, Univ. of Rochester • David J. Sherratt, Univ. of Oxford, England • Arend Sidow, Stanford Univ. • Rama S. Singh, McMaster Univ. • Neelima Roy Sinha, Univ. of California, Davis • D. Peter Snustad, Univ. of Minnesota, St. Paul • David R. Soll, Univ. of Iowa • L. Andrew Staehelin, Univ. of Colorado, Boulder • Bruce William Stillman, Cold Spring Harbor Lab. • Douglas M. Stocco, Texas Tech Univ. • Bernard S. Strauss, Univ. of Chicago • Kevin Struhl, Harvard Medical School • Lloyd W. Sumner, Samuel Roberts Noble Foundation, Ardmore, OK • Michael R. Sussman, Univ. of Wisconsin, Madison • Edward I. Bradbridge Thompson, Univ. of Texas Medical Branch • Donald M. Waller, Univ. of Wisconsin, Madison • Xuemin Wang, Univ. of Missouri, St. Louis • Margaret Werner-Washburne, Univ. of New Mexico • Susan R. Wessler, Univ. of Georgia • James Francis White Jr., Rutgers Univ. • H. Steven Wiley, Pacific Northwest National Lab. • Huntington F. Willard, Duke Univ. • Chun-Fang Wu, Univ. of Iowa • Zhenbiao Yang, Univ. of California, Riverside • Meng-Chao Yao, Fred Hutchinson Cancer Research Center, Seattle • JiuJiang Yu, USDA-ARS Southern Regional Research Center, New Orleans

### Chemistry

Daniel J. Auerbach, Hitachi Global Storage Technologies, San Jose, CA • Carlos F. Barbas III, Scripps Research Institute, La Jolla, CA • Mary W. Baum, Princeton Univ. • Henry N. Blount, III, National Science Foundation • Joel M. Bowman, Emory Univ. • Michael S. Chapman, Florida State Univ. • David L. Clark, Los Alamos National Lab. • Dimitri Coucouvanis, Univ. of Michigan, Ann Arbor • Larry R. Dalton, Univ. of Washington • Paul Davidovits, Boston College • Dana D. Dlott, Univ. of Illinois, Urbana-Champaign • Richard Eisenberg, Univ. of Rochester • Gregory J. Exarhos, Pacific Northwest National Lab. • John T. Fourkas, Boston College • Samuel H. Gellman, Univ. of Wisconsin, Madison • Arun K. Ghosh, Univ. of Illinois, Chicago • James L. Gole, Georgia Institute of Technology • Vicki H. Grassian, Univ. of Iowa • Naomi J. Halas, Rice Univ. • Lawrence Brook Harding, Argonne National Lab. • John F. Hartwig, Yale Univ. • W. Christopher Hollinsed, DuPont Experimental Station, Wilmington, DE • Mark A. Johnson, Yale Univ. • Bruce D. Kay, Pacific Northwest National Lab. • Richard A. Keller, Los Alamos National Lab. • John W. Kozarich, Activx Biosciences Corp., La Jolla, CA • Harold H. Kung, Northwestern Univ. • Deborah E. Leckband, Univ. of Illinois, Urbana-Champaign • Timothy J. Lee, NASA Ames Research Center • James L. Leighton, Columbia Univ. • Hung-wen Liu, Univ. of Texas, Austin • Charles E. McKenna, Univ. of Southern California • Terry A. Miller, Ohio State Univ., Columbus • Tyrone D. Mitchell, National Science Foundation • Martin Moskovits, Univ. of California, Santa Barbara • Milan Mrksich, Univ. of Chicago • Amy Sue Mullin, Boston Univ. • Carlos A. Murillo, Texas A&M Univ. • Donna J. Nelson, Univ. of Oklahoma • Keith A. Nelson, Massachusetts Institute of Technology • Cheuk-Yiu Ng, Univ. of California, Davis • Mitchio Okumura, California Institute of Technology • Thomas L. Poulos, Univ. of California, Irvine • G. K. Surya Prakash, Univ. of Southern California • Peter Pulay, Univ. of Arkansas • Antonio Redondo, Los Alamos National Lab. • Dagmar Ringe, Brandeis Univ. • Celeste M. Rohlfing, National Science Foundation • Dennis R. Salahub, Univ. of Calgary • Joseph B. Schlenoff, Florida State Univ. • Ayusman Sen, Pennsylvania State Univ. • J. Fraser Stoddart, Univ. of California, Los Angeles • Weihong Tan, Univ. of Florida • Michael J. Therien, Univ. of Pennsylvania • Jacopo Tomasi, Univ. of Pisa, Italy • Robert Tycko, National Institutes of Health • David E. Wemmer, Univ. of California, Berkeley • John C. Wright, Univ. of Wisconsin, Madison • Xiaoliang Sunnery Xie, Harvard Univ.

### Dentistry and Oral Health Sciences

Beverly A. Dale-Crunk, Univ. of Washington

### Education

William W. Cobern, Western Michigan Univ. • John C. Kotz, State Univ. of New York, Oneonta • Jay B. Labov, National Research Council • Madeleine J. Long, AAAS • Robert J. Semper, Exploratorium, San Francisco

### Engineering

J. K. Aggarwal, Univ. of Texas, Austin • Cynthia J. Atman, Univ. of Washington • Prith Banerjee, Univ. of Illinois, Chicago • Frank S. Bates, Univ. of Minnesota, Minneapolis • Rafael L. Bras, Massachusetts Institute of Technology • Jeffrey J. Chalmers, Ohio State Univ., Columbus • Mohamed Jamal Deen, McMaster Univ. • Leonard C. Feldman, Vanderbilt Univ. • Morteza Gharib, California Institute of Technology • Hans G. Hornung, California Institute of Technology • John L. Hudson, Univ. of Virginia • Frank P. Incropera, Univ. of Notre Dame • Alex K-Y. Jen, Univ. of Washington • Kannan M. Krishnan, Univ. of Washington • Mary E. Lidstrom, Univ. of Washington • William M. Miller, Northwestern Univ. • José M. F. Moura, Carnegie Mellon Univ. • Wolfgang Porod, Univ. of Notre Dame • Ishwar K. Puri, Virginia Polytechnic Institute and State Univ. • Steven A. Ringel, Ohio State Univ., Columbus • Michael Shur, Rensselaer Polytechnic Institute • Subhash C. Singhal, Pacific Northwest National Lab. • Gregory N. Stephanopoulos, Massachusetts Institute of Technology • Dwight C. Streit, Northrop Grumman Space Technology, Redondo Beach, CA • Rao Y. Surampalli, U.S. Environmental Protection Agency, Kansas City, KS • Elias Towe, Carnegie Mellon Univ. • Charles B. Watkins, City College of New York

### General Interest in Science and Engineering

Adlai J. Amor, Arlington, VA • Marta Cehelsky, InterAmerican Development Bank, Washington, DC • Kathleen M. Donovan, Univ. of Central Oklahoma, Edmond • Kendrick Frazier, Albuquerque, NM • Michael Strigel, Wisconsin Academy of Sciences, Arts and Letters, Madison

**Geology and Geography**
J. David R. Applegate, U.S. Geological Survey, Reston, VA • Bruce A. Bolt, Univ. of California, Berkeley (posthumous award) • William E. Doolittle, Univ. of Texas, Austin • Richard M. Forester, U.S. Geological Survey, Denver • Claude Hillaire-Marcel, Univ. of Quebec • Roger L. Kaesler, Univ. of Kansas • Erle G. Kauffman, Indiana Univ., Bloomington • Richard Marston, Kansas State Univ. • Peter Molnar, Univ. of Colorado, Boulder • Lonnie G. Thompson, Ohio State Univ., Columbus • Youxue Zhang, Univ. of Michigan, Ann Arbor

**History and Philosophy of Science**
William Bechtel, Univ. of California, San Diego • Ronald L. Numbers, Univ. of Wisconsin, Madison • M. Norton Wise, Univ. of California, Los Angeles

**Industrial Science and Technology**
Robert Boily, Inforex, Inc., Laval, Quebec • Charles L. Liotta, Georgia Institute of Technology • Steven W. Popper, RAND, Santa Monica, CA

**Information, Computing, and Communication**
Ashok K. Agrawala, Univ. of Maryland, College Park • Daniel M. Cotter, URS Corp., Gaithersburg, MD • James D. Foley, Georgia Institute of Technology • Eugene C. Freuder, Univ. College Cork, Ireland • Philip Green, Univ. of Washington • Joseph Y. Halpern, Cornell Univ. • Ravishankar K. Iyer, Univ. of Illinois, Urbana-Champaign • Anil K. Jain, Michigan State Univ. • Christopher R. Johnson, Univ. of Utah • Suzanna E. Lewis, Univ. of California, Berkeley • Linda R. Petzold, Univ. of California, Santa Barbara • Eric S. Roberts, Stanford Univ. • Daniel P. Siewiorek, Carnegie Mellon Univ. • Walter L. Warnick, U.S. Dept. of Energy, Germantown, MD

**Linguistics and Language Science**
Sheila E. Blumstein, Brown Univ. • Frederick J. Newmeyer, Univ. of Washington • Keren Rice, Univ. of Toronto

**Mathematics**
Jennifer Tour Chayes, Microsoft Research, Redmond, WA • Robert M. Miura, New Jersey Institute of Technology • T. Christine Stevens, St. Louis Univ. • Robert Williams, Univ. of Texas, Austin

**Medical Sciences**
Peter C. Agre, Johns Hopkins Univ. • Rolf Frederick Barth, Ohio State Univ., Columbus • H. Franklin Bunn, Harvard Medical School • Paul A. Bunn, Univ. of Colorado, Denver • Harvey Cantor, Harvard Medical School • Robert D. Cardiff, Univ. of California, Davis • Valerie P. Castle, Univ. of Michigan, Ann Arbor • E. Antonio Chiocca, Ohio State Univ., Columbus • Dennis W. Choi, Merck & Co., Inc., West Point, PA • Linda C. Cork, Stanford Univ. • Harry C. Dietz, III, Johns Hopkins Univ. • Duane J. Gubler, Univ. of Hawaii, Honolulu • Paul A. Insel, Univ. of California, San Diego • Sissy Meihua Jhiang, Ohio State Univ., Columbus • Michael D. Lairmore, Ohio State Univ., Columbus • Stuart B. Levy, Tufts Univ. • David E. Pleasure, Children's Hospital of Philadelphia • Teresa K. Woodruff, Northwestern Univ.

**Neuroscience**
David F. Clayton, Univ. of Illinois, Urbana • David H. Cohen, Columbia Univ. • Ronald M. Harris-Warrick, Cornell Univ. • Susan Hockfield, Massachusetts Institute of Technology • Mark F. Jacquin, Washington Univ. • Lawrence Kruger, Univ. of California, Los Angeles • Susan E. Leeman, Boston Univ. • Irwin B. Levitan, Univ. of Pennsylvania • Joe L. Martinez Jr., Univ. of Texas, San Antonio • Richard G. M. Morris, Univ. of Edinburgh • Richard T. Robertson, Univ. of California, Irvine • Richard E. Zigmond, Case Western Reserve Univ.

**Pharmaceutical Sciences**
Ian A. Blair, Univ. of Pennsylvania • Edward Chu, Yale Univ. • Steven Grant, Virginia Commonwealth Univ./Medical College of Virginia • Anthony J. Hickey, Univ. of North Carolina, Chapel Hill • C. Anthony Hunt, Univ. of California, San Francisco • Andrej Rotter, Ohio State Univ., Columbus

**Physics**
Samuel H. Aronson, Brookhaven National Lab. • Neil V. Baggett, U.S. Dept. of Energy, Washington, DC • Dawn A. Bonnell, Univ. of Pennsylvania • Swapan Chattopadhyay, Thomas Jefferson National Accelerator Facility, Newport News, VA • Alan W. De Silva, Univ. of Maryland, College Park • J. Thomas Dickinson, Washington State Univ. • Louis F. DiMauro, Ohio State Univ., Columbus • Robert E. Ecke, Los Alamos National Lab. • C. W. Francis Everitt, Stanford Univ. • Roger W. Falcone, Univ. of California, Berkeley • Theodore Alan Fulton, Warren, NJ • P. Chris Hammel, Ohio State Univ., Columbus • Peter Hänggi, Univ. of Augsburg, Germany • Richard D. Hazeltine, Univ. of Texas, Austin • Arthur F. Hebard, Univ. of Florida • Siegfried S. Hecker, Los Alamos National Lab. • Ulrich Walter Heinz, Ohio State Univ., Columbus • John F. Holzrichter, Berkeley, CA • V. M. Kenkre, Univ. of New Mexico • Daniel J. Larson, Pennsylvania State Univ. • Thomas A. Mehlhorn, Sandia National Labs. • Miklos Porkolab, Massachusetts Institute of Technology • Ramamoorthy Ramesh, Univ. of California, Berkeley • Bharat Ratra, Kansas State Univ. • Z. F. Ren, Boston College • William C. Stwalley, Univ. of Connecticut • Michael S. Turner, National Science Foundation and Univ. of Chicago • Chandra M. Varma, Univ. of California, Riverside • Alfons Weber, National Institute of Standards and Technology

**Psychology**
Norman Bruce Anderson, American Psychological Association • David Harrison Barlow, Boston Univ. • John D. Corrigan, Ohio State Univ., Columbus • Richard L. Doty, Univ. of Pennsylvania • James S. Jackson, Univ. of Michigan, Ann Arbor • John F. Marshall, Univ. of California, Irvine • Earl K. Miller, Massachusetts Institute of Technology • Barbara J. Rolls, Pennsylvania State Univ. • Donald Thomas Stuss, Rotman Research Institute, Baycrest Center for Geriatric Care, Toronto • Daniel M. Wegner, Harvard Univ. • David R. Williams, Univ. of Rochester

**Social, Economic, and Political Sciences**
Robert J. Blendon, Harvard School of Public Health • Howard Kunreuther, Univ. of Pennsylvania • Edward L. Miles, Univ. of Washington • James K. Mitchell, Rutgers Univ. • Willie Pearson, Jr., Georgia Institute of Technology • Jeffrey D. Sachs, Columbia Univ. • Paul M. Sniderman, Stanford Univ. • Richard C. Sutch, Univ. of California, Riverside

**Societal Impacts of Science and Engineering**
John P. Boright, National Academy of Sciences • Barry Bozeman, Georgia Institute of Technology • Bruce B. Darling, Univ. of California, Oakland • Rachel E. Levinson, Office of Science and Technology Policy • James D. Wilson, Committee on Science, U.S. House of Representatives

**Statistics**
Jianqing Fan, Princeton Univ. • Sallie Keller-McNulty, Los Alamos National Lab. • Sally C. Morton, RAND Corp., Santa Monica, CA • Carol K. Redmond, Univ. of Pittsburgh




Published by AAAS

# Progress in Modeling of Protein Structures and Interactions

Ora Schueler-Furman,[1,2] Chu Wang,[1] Phil Bradley,[1] Kira Misura,[1] David Baker[1,3]*

The prediction of the structures and interactions of biological macromolecules at the atomic level and the design of new structures and interactions are critical tests of our understanding of the interatomic interactions that underlie molecular biology. Equally important, the capability to accurately predict and design macromolecular structures and interactions would streamline the interpretation of genome sequence information and allow the creation of macromolecules with new and useful functions. This review summarizes recent progress in modeling that suggests that we are entering an era in which high-resolution prediction and design will make increasingly important contributions to biology and medicine.

In 1973, Anfinsen demonstrated that the amino acid sequence of a protein completely specifies its three-dimensional structure and hence that the native structures of proteins are likely to correspond to global free-energy minima (*1*). Since then, the de novo structure prediction problem has been well posed—find the lowest free-energy conformation for an amino acid sequence. Yet at the start of the structural genomics efforts in the late 1990s, computational methods remained far from achieving the high-resolution structures available from x-ray crystallography and nuclear magnetic resonance (NMR), and hence embarking on large-scale experimental structure determination with its associated high cost was well warranted. We suggest that recent progress in high-resolution modeling of biomolecules is such that, although the de novo folding problem is far from solved, computational structural biology is reaching a stage where it can contribute both to determining structures of naturally occurring biomolecules and the creation of new ones.

There have been two distinct areas of development in molecular modeling methodology and software—the first aimed at simulating macromolecular dynamics, the second at prediction and design. We focus on the second area, and for the first we refer to recent reviews (*2*, *3*). Two blind tests provide a gauge of progress in prediction of the structures of proteins and protein-protein complexes, namely CASP [http://predictioncenter.org (*4*)] and CAPRI [Critical Assessment of Protein Interactions; http://capri.ebi.ac.uk/ (*5*, *6*)]. Results obtained in the recent CASP and CAPRI experiments, together with recent design results, highlight progress in modeling. This review describes these recent results and outlines the physical basis for the new generation of computational models, the origins of improvement in modeling, and current challenges and bottlenecks.

## Prediction Versus Design

Prediction and design are inverse problems: The prediction problem is to find the lowest energy structure for a specified sequence, and the design problem, to find the lowest energy sequence for a specified structure (Fig. 1A). Success in both efforts requires development of an accurate potential function—a quantitative model of the energetics of macromolecular interactions. Evaluation and improvement of the model can be spurred by using the same potential for both problems because the scope of the applicable tests is thereby increased considerably. The commonalities extend to the optimization methods (Fig. 1B). We have taken advantage of this in the development of the ROSETTA software package (used in the prediction and design examples from our laboratory described here), which uses essentially the same protein representation, potential function, and optimization methodology for prediction and design (*7*).

## Energy Function

A large collection of experimental data on the effects of point mutations on protein stability (*8*–*11*) has highlighted the critical contribution of tight complementary packing in the core to protein stability. This is likely to derive both from attractive van der Waals interactions among protein atoms and from the dependence of the solvation free energy on the size of the cavity occupied by the protein. Experimental data have also highlighted the contribution of hydrogen bonding and hydrophobic/polar partitioning to protein stability. Alterations in the charge of surface side chains generally have little effect on stability, suggesting that long-range electrostatic interactions are substantially screened by both dynamic and static induced polarization effects.

In light of these data, successful approaches have focused on packing interactions, hydrogen bonding, and solvation effects represented with implicit solvation models (*12*, *13*) that favor burial of nonpolar atoms and exposure of polar atoms. These approaches have borrowed much from the molecular mechanics force fields used to simulate dynamics (*14*–*16*), notably the classical description in which energies are computed as sums over interactions between a relatively small set of different atom types, the use of a Lennard Jones potential to describe van der Waals interactions between atoms, and parameters for ideal bond lengths and angles. There are also important differences. Whereas the parameterization of molecular mechanics force fields relies primarily on experimental data on small molecules, the new force fields also derive parameters from experimental structural and thermodynamic data on proteins. In contrast to most molecular mechanics force fields, which represent hydrogen bonding as a dipole-dipole interaction, the orientation dependence that arises from the partially covalent character of the hydrogen bond is treated explicitly (*17*), both on the basis of geometrical distributions observed in proteins and quantum chemistry calculations on simple model systems (*18*). Longer range electrostatic interactions are generally dampened considerably. Torsional potentials, which are notoriously difficult to determine in molecular mechanics force fields, are obtained by directly inverting probability distributions from protein structures, and the representation of the protein chain is much stiffer—bond lengths and angles are generally kept rigid, and side-chain conformations are restricted to the vicinity of the rotameric states observed in protein structures. The stiffer representation reduces the frequency of false attractors by considerably reducing the size of configurational space. These differences have been driven by the con-

[1]Department of Biochemistry, University of Washington, Seattle, WA 98195, USA. [2]Department of Molecular Genetics and Biotechnology, Hebrew University, Hadassah Medical School, Jerusalem 91120, Israel. [3]Howard Hughes Medical Institute, Seattle, WA 98195, USA.

*To whom correspondence should be addressed. E-mail: dabaker@u.washington.edu

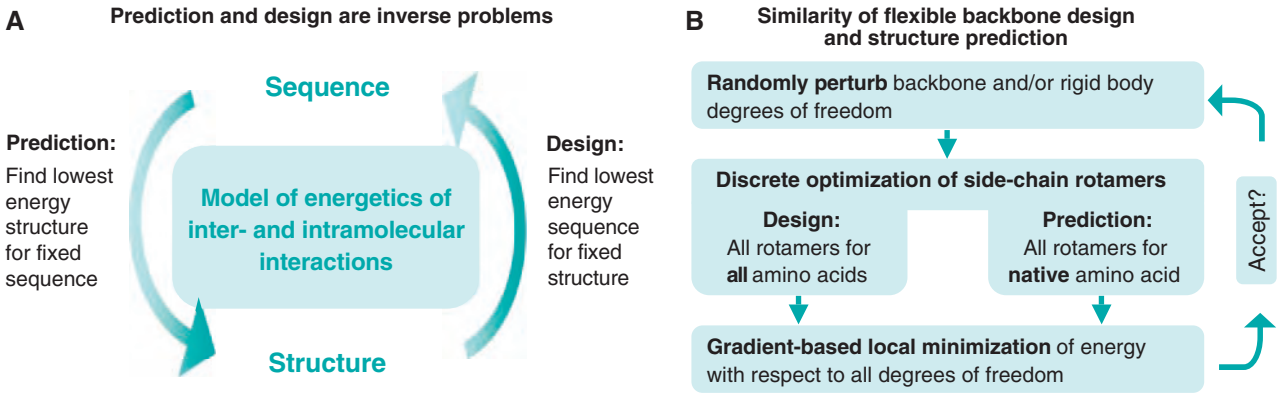


**Fig. 1.** Prediction and design. (**A**) Structure prediction and fixed backbone design are inverse problems. Completing the cycle corresponds to flexible backbone design, which requires optimization of both sequence and structure. (**B**) Algorithmic similarity of structure prediction, protein-protein docking, and flexible backbone design illustrated by the Monte Carlo minimization (MCM) high-resolution refinement protocol.

stant rigorous testing of the force field and representation by prediction and design calculations, which have the advantage that they can fail quite dramatically and highlight shortcomings in the approach.

## Conformational Searching

A good energy function is not enough; a formidable challenge to prediction and design of protein structures and interactions is the very large size of the spaces that must be searched. For protein structure prediction, for example, with as few as three possible states per residue, the number of states of a 100-residue chain is astronomical [this is the often referred to "Levinthal's paradox" (*19*)]. Protein-protein docking requires a search over possible rigid body orientations of the partners, and most current design problems involve a search over protein backbone conformations, as well as amino acid sequences.

An effective approach to conformational sampling is to start with low resolution and go to high resolution. The low-resolution step searches for minima in an energy landscape dominated by hydrophobicity (the burial of nonpolar groups away from solvent), with the sharply varying van der Waals interactions smoothed by spatial averaging. Because sterics (tight complementary packing) is a critical contributor to the specificity of native protein structures and interactions, the native minima cannot be identified reliably with this averaged out representation, and the goal in this step is not to uniquely identify the native state, but to identify a set of energy minima that is almost certain to include the native conformation. Low-resolution approaches to docking, prediction, and design are further described in the next sections.

The second, more computationally intensive step in both the prediction and design of structure and interactions is the search for well-packed low-energy structures in the vicinity of each of the minima of the averaged-out landscape identified in the initial low-resolution step. In this step, all atoms are represented explicitly and steric interactions are not damped or averaged out. In this very rugged landscape, 1 Å deviations of atoms from the native structure can produce overlaps and huge spikes in the energy. This landscape is difficult to explore, but the native minimum is generally substantially deeper than non-native minima (which is not generally the case at the low-resolution stage).

Because the landscape is so rugged, optimization is challenging. A number of methods have been described to address this problem (*20*–*22*). The method used in ROSETTA couples Monte Carlo minimization (MCM) with discrete side-chain optimization (Fig. 1B). For each attempted move, an initial random perturbation of the backbone torsion angles (protein structure prediction) or rigid body degrees of freedom (protein-protein docking) is followed by discrete optimization of side-chain rotamer conformations and then by gradient-based local minimization on all degrees of freedom. MCM, which effectively flattens all barriers to the height of the nearest local minimum, has been found to be a powerful global optimization method for a broad range of problems (*23*, *24*).

## Protein-Protein Docking and CAPRI

Rigid backbone protein docking is less challenging in terms of conformational searching than structure prediction or design because there are fewer degrees of freedom to be sampled. The low-resolution search can be performed using an elegant fast Fourier transformation (FFT)–based approach (*25*) or by real space MC. For high-resolution refinement, it is advantageous to simultaneously optimize both side-chain and rigid body degrees of freedom; MCM-based methods such as that outlined above (Fig. 1B) and that described in (*24*) have proven particularly effective.

Accurate predictions by several groups who entered CAPRI (*5*, *26*) indicate that high-resolution modeling methods are beginning to work for protein docking that does not involve pronounced backbone conformational changes. As an example we show results for two CAPRI targets, for which we carried out the MCM with side-chain flexibility protocol many independent times using different random-number seeds. The resulting energy landscape for target 12 (cohesin-dockerin) is shown in Fig. 2A. Three complexes have considerably lower energies than the others (Fig. 2A, inset), and trajectories starting from these low-energy complexes reveal that they lie at the bottom of a fairly narrow energy funnel (Fig. 2A, main panel).

The lowest energy predicted structures for the cohesin-dockerin complex, as well as for CAPRI target 15: the colicin-immunity protein complex, are shown in Fig. 3, A and B, superimposed on the experimentally determined crystal structures, which were released after the predictions were submitted to CAPRI. Not only the rigid body orientation, but also the conformations of almost all of the side chains, are predicted correctly. Other groups achieved similar successes (*5*, *26*). Current research is directed at incorporating backbone flexibility into protein-protein docking [e.g., (*27*)], which is closely related to the high-resolution protein structure prediction problem.

## Structure Prediction and CASP

Many creative approaches to the de novo prediction of protein structure at low resolution have been described (*28*–*32*). The approach in ROSETTA to de novo structure prediction seeks to recapitulate the trade-off between local and nonlocal interactions during protein folding, by allowing short segments of the chain to flicker between alternative low-energy local conformations while searching for the lowest energy overall conformation of the chain (*33*). The search space is confined to that defined by the local conformational preferences of the protein sequence, and energy minima are identified using MC sampling with the low-resolution representation of the chain described earlier. Plausible candidate structures with primarily

hydrophobic cores and paired β strands can be rapidly generated (~1 min on 1 CPU for a 100-residue protein), but because atomic detail is neglected, the accuracy is generally low and any individual model is likely to be globally incorrect. Conformational sampling at this stage can be improved by generating structures not only for the protein of interest, but also for sequence homologs, which each have somewhat different low-resolution energy landscapes (*34*). High-resolution refinement of the low-resolution models is again carried out using the MCM with side-chain packing protocol described in Fig. 1B.

Progress in de novo structure prediction was highlighted at CASP6, where the first moderately high-resolution de novo structure prediction was made using the two-stage procedure protocol described above, with the initial low-resolution search followed by the flexible side-chain MCM optimization protocol. The root mean square deviation (RMSD) to the native structure after the low-resolution search was 2.2 Å and decreased to 1.6 Å during the flexible side-chain MCM refinement step (Fig. 3C). Although clearly at a lower level of accuracy than the docking predictions shown in Fig. 3, A and B, it is encouraging that some features of the native side-chain packing arrangement are correctly recapitulated. More recently, the same protocol was found to produce accurate predictions for a subset of small protein domains (*34*). The goal of current work on protein structure prediction is to consistently achieve the accuracy of the docking predictions in Fig. 3, A and B.

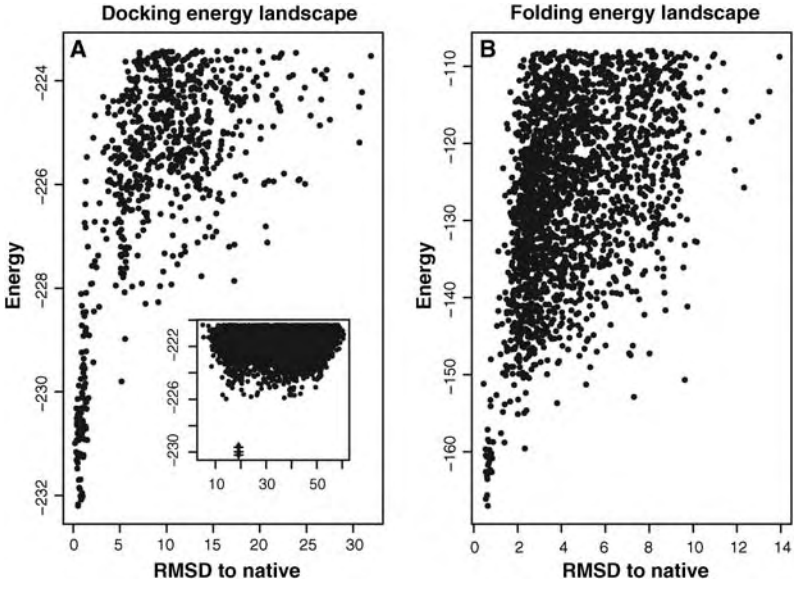


**Fig. 2.** Energy landscapes. Each point represents the lowest energy structure sampled in a single MCM trajectory. **(A)** Docking energy landscape for Capri Target 12 [cohesin-dockerin complex; PDB (Protein Data Bank) ID 1ohz (*66*)]. **(Inset)** In a large collection of trajectories starting from different random orientations that were carried out for the CAPRI experiment, a small number of structures (+) are distinguished from the background population by a significant energy gap. The *x* axis is the RMSD to an arbitrary reference orientation. (Main panel) Trajectories starting from these low-energy structures map out a narrow energy funnel. The *x* axis is the RMSD to the native structure. A deep energy funnel, as in this example, is a strong indicator that a prediction is correct. **(B)** Folding landscape for double-stranded RNA binding protein [PDB ID 1di2 (*67*)]. The backbone RMSD is to the native structure. The energy function (units are in kcal/mol) includes entropic contributions from solvation effects, but not the configurational entropy associated with protein vibrational and side-chain degrees of freedom, and hence is not the true free energy.

## Examples of Protein Design

Protein design has a long history, starting from the realization that side-chain conformations in proteins could to a first approximation be treated as a set of discrete rotameric states and that new sequences and conformations could be derived by combinatorial optimization of this set (*35*). Mayo and co-workers showed that the lowest energy sequence computed for a small naturally occurring structure adopted a structure very close to that of the target starting structure (*36*). Harbury and co-workers (*37*) showed that new helical bundle structures could be created by designing sequences for a set of parametrically generated bundle arrangements. These studies correspond to the right arrow in Fig. 1A. Conceptually similar rotamer search-based design methods have been used to design new protein-protein interfaces, which have been confirmed by x-ray crystallography (*38*–*41*).

More recently, a globular protein fold was designed by alternating between sequence and structure optimization (the complete cycle in Fig. 1A) (*42*). The low-resolution and high-resolution optimization is similar to that used for protein structure prediction; the only notable differences are that in the low-resolution search constraints are added to favor the desired topology, and in the high-resolution search the discrete side-chain optimization is over the conformations of all 20 amino acids (Fig. 1B). The designed protein is exceptionally stable, with a free energy of folding roughly twice that of most naturally occurring proteins in its size range. The high-resolution crystal structure of the designed protein showed that its structure is similar (1.2 Å RMSD) to that of the computer-generated design model (Fig. 3D). The accuracy of the design and the high stability are both likely to stem from the fact that the sequence of the designed protein was optimized entirely for stability; in contrast to most naturally occurring proteins, it contains no regions that are locally suboptimal owing to functional constraints. Consistent with this, prediction of the structure of the designed protein from sequence results in a more accurate prediction than for almost all naturally occurring proteins (*43*).

Recent years have seen important milestones in the design of existing proteins with new functions. A series of small-molecule receptors have been designed that respond to specific ligands—a particularly spectacular achievement is a receptor that causes bacteria to turn green when exposed to TNT (*44*). As in the flexible side-chain docking protocol, these calculations coupled side-chain repacking with rigid body sampling. There has also been exciting progress in the design of new enzymes (*45*–*47*).

## Role of High-Performance Computing

There has been a steady increase in CPU power and decrease in the cost of computing resources over the past 20 years, and this is likely to continue in the near future [Moore's law (*48*)]. It is of considerable sociological interest to identify the stage in this growth of computing power at which different scientific problems become tractable. The coupling of side-chain combinatorial optimization with backbone and/or rigid body optimization as in the protein-protein docking MCM procedure described above, the flexible backbone protein design protocol used to design TOP7, and binding site design for very large numbers of different ligand orientations by Hellinga and co-workers (*47*) were enabled by the increase in computer power; the simultaneous optimization of side-chain and backbone/rigid body degrees of freedom would not have been possible with the computing power available 15 years ago. The example in Fig. 2A shows that in 2005, only three solutions close to the native structure were found in 15 processor (3.2 GHz) days. Carrying out the calculation using a 1995 vintage processor (133 MHz) would have required roughly a year of processor time. Even today, the primary bottleneck to high-resolution structure prediction appears to be conformational sampling, because

the native structure almost always has lower energy than the predicted structures (*34*). The anticipated increase in processor power over the next several years will bring closer in reach the refinement of large protein structures and flexible backbone protein-protein docking, which requires simultaneous optimization of side-chain, backbone, and rigid body degrees of freedom.

## Energy Landscapes

The successful predictions and designs described here suggest that the energy function underlying the calculations may be accurate enough to provide insights into the general properties of the folding and docking free-energy landscapes. Figure 2 shows the energy landscapes for both the docking and structure prediction problems. Notable features include the pronounced minimum in the vicinity of the native structure, and the sharp increase in energy associated with ~2 Å deviations from the native structure. It is important to note that configurational entropy is not accounted for in these landscapes, so the actual free energy landscapes will have somewhat broader minima. The folding and binding "funnels" (*49*) that have been the subject of much discussion are evident, but only in the immediate vicinity of the global minimum. Physically, the short range reflects the critical contribution to the energy from close complementary side-chain packing: Once the backbone coordinates have diverged by more than ~2 Å, the native side-chain packing arrangement is completely disrupted (*50*) and the energy increases substantially. The narrow aperture to the binding and folding funnels may be a characteristic feature of biomolecular recognition and folding.

Is the short-range nature of landscapes compatible with the observation that complexes form and proteins fold in finite time? In the case of complexes, it has been possible to rigorously answer this question in the affirmative by solving the steady-state diffusion equation for interacting partners with "reactive zones" corresponding to the aperture of the binding funnels—the computed rates are on the order of $10^6$ per second (*51*)—consistent with experimentally observed rates for many proteins (faster association rates are likely to reflect long-range electrostatic steering). In the case of monomeric folding, folding can still proceed rapidly if native interactions are on average lower in energy than non-native interactions—the principle of minimal frustration (*49*, *52*)—and indeed for most compact subdomains the native conformation has a lower computed energy than that of essentially all sampled non-native conformations. This is expected given the dominant contribution of short-range packing and hydrogen bonding interactions—a conformation that is very low in energy on a global scale must also be low in energy on a more local scale, just as the optimal solution for a jigsaw puzzle is also optimal (perfectly packed) on a local scale. Indeed, broader energy funnels are observed when the reaction coordinate (*x* axis in Fig. 2) is the fraction of native contacts, rather than the RMSD, consistent with protein folding landscape theory.

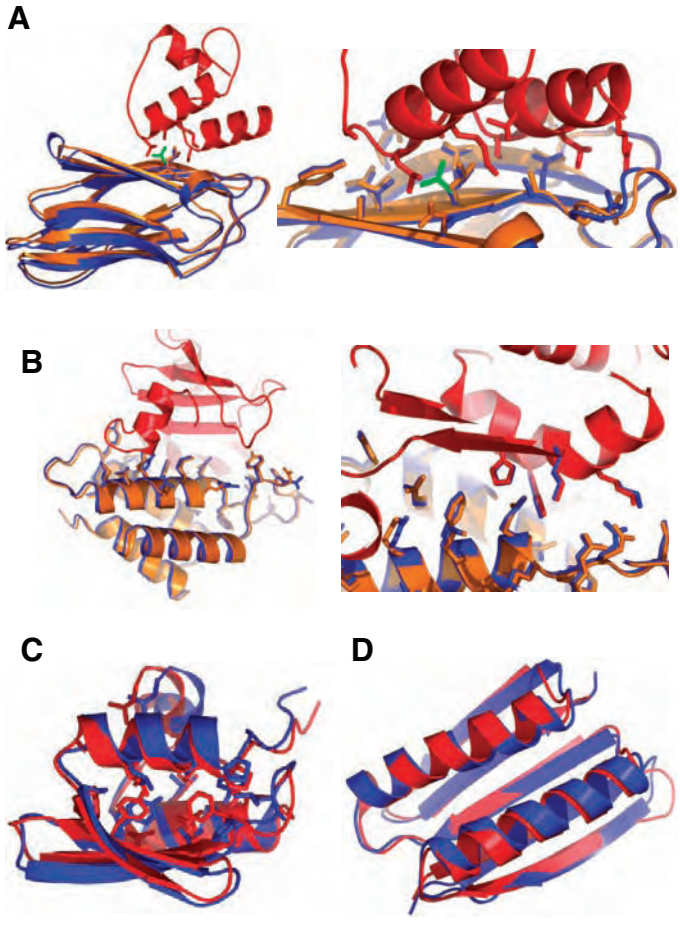


**Fig. 3.** Examples of high-resolution prediction and design. (**A**) CAPRI Target 12 [dockerin–cohesin (*66*); interface residue backbone RMSD = 0.27 Å]. The lowest energy structure in Fig. 2A, main panel, is shown here. The side chain of Leu-83 (green in the free monomer) changes conformation upon binding. Side-chain conformations in red were provided; those in blue were predicted. (**B**) CAPRI Target 15 [ColicinD–Immunity protein D (*68*); interface residue backbone RMSD = 0.23 Å]. No side-chain information was provided for either partner. (**C**) CASP6 de novo structure prediction Target 0281 [hypothetical protein from *Thermus thermophilus* Hb8, PDB ID 1whz (*69*); backbone RMSD = 1.59 Å]. (**D**) TOP7 (RMSD = 1.2 Å) (*42*). (A) and (B) are adapted from figure 1 of (*70*). Blue: models; red and orange: x-ray structures.

The narrow energy funnels around native structures, and the close correspondence of both prediction and designs with experimentally determined structures, have direct bearing on the fundamental question of the range of structures adopted by proteins in solution. Some simulation studies have suggested that in solution, proteins populate a broad range of conformations up to 4 Å RMSD from the crystal structure. In contrast, the short range of the folding and binding funnels suggests that protein cores are confined to within ~1.5 Å of the experimentally determined crystal structures; the substantial increases in energy accompanying larger deviations suggest that such structures are populated at relatively low levels. The coincidence of the energy minima in the prediction and design calculations with the location of the experimentally determined structure further supports this conclusion: If crystal packing interactions randomly selected out a member of a broad ensemble of structures spanning 3 to 4 Å RMSD, one would not expect RMSDs of much less than this between predicted structures and crystal structures or between design models and crystal structures (*53*). Experimental support for this conclusion comes from comparison of protein structures determined in different crystal forms, which suggests backbone variation of less than 1 Å (*54*, *55*), and from recent NMR studies (*56*) that show that agreement between the dipolar couplings and structure is not limited by the intrinsic dynamic behavior of proteins.

## Current Challenges

Considerable challenges remain for high-resolution modeling—this review should not be taken to suggest that the critical problems are by any means solved, but rather that accurate modeling now appears to be an achievable goal. Shortcomings in potential functions include the treatment of buried polar interactions, which are complicated by polarization effects, and the delicate balance between the cost of desolvating a polar or charged group and the favorable hydrogen bonding and electrostatic interactions the group may make upon burial. Consistent prediction and design of polar active sites will require progress in modeling such interactions (*57*). On the sampling side, improvements in methodology and increases in computing capabil-

ities will be necessary for problems with large numbers of degrees of freedom, such as prediction of the structures of large proteins.

To conclude, we list a series of challenges that will spur the next phase of method development. (i) High-resolution refinement of models built by comparative modeling. It is well established that the accuracy of comparative models built by copying a template structure identified using sequence comparison methods decreases steadily with increasing sequence divergence between the sequence being modeled and the protein template owing to structural divergence during protein evolution (*58*, *59*). Recent CASP tests have shown that the best comparative models are currently built by experts such as Ginalski (*60*) who are able to achieve near-perfect alignments of the sequences to proteins of known structure, a critical precondition for further modeling, and go further to improve models using an assortment of protein modeling tools such as MODELLER (*61*), PSIBLAST (*62*), ROSETTA (*7*), PSIPRED (*63*), SQWRL (*64*), and VERIFY3D (*65*) together with visual structural inspection. The challenge is to automatically produce even more accurate structures by high-resolution refinement; the loss of human intuition will have to be compensated by generating starting models for refinement by large-scale sampling of alternative alignments on the basis of alternative homologous structure templates. The methods described in this review are directly applicable to this problem, and it is also a good test of widely used molecular dynamics simulations methods because the starting template can be within 3 Å of the correct structure. (ii) Consistent prediction of the structures of small proteins at atomic-level resolution. (iii) Protein docking with backbone flexibility. This is a formidable challenge because both rigid body and internal backbone degrees of freedom need to be searched. (iv) Prediction and design of the specificity of protein–nucleic acid interactions. (v) Design of new enzymes catalyzing reactions not catalyzed by naturally occurring enzymes. (vi) Prediction of the structures of multidomain and multisubunit protein complexes. We look forward to progress in all of these areas.

**References and Notes**


1. C. B. Anfinsen, *Science* **181**, 223 (1973).
2. R. Schleif, *Methods Enzymol.* **383**, 28 (2004).
3. M. Karplus, J. A. McCammon, *Nat. Struct. Biol.* **9**, 646 (2002).
4. J. Moult, *Curr. Opin. Struct. Biol.* **15**, 285 (2005).
5. J. Janin, *Protein Sci.* **14**, 278 (2005).
6. J. Janin *et al.*, *Proteins* **52**, 2 (2003).
7. C. A. Rohl, C. E. Strauss, K. M. Misura, D. Baker, *Methods Enzymol.* **383**, 66 (2004).
8. K. A. Bava, M. M. Gromiha, H. Uedaira, K. Kitajima, A. Sarai, *Nucleic Acids Res.* **32**, D120 (2004).
9. B. W. Matthews, *Adv. Protein Chem.* **46**, 249 (1995).
10. J. U. Bowie, J. F. Reidhaar-Olson, W. A. Lim, R. T. Sauer, *Science* **247**, 1306 (1990).
11. J. T. Kellis Jr., K. Nyberg, D. Sali, A. R. Fersht, *Nature* **333**, 784 (1988).
12. T. Lazaridis, M. Karplus, *Proteins* **35**, 133 (1999).
13. M. Feig, C. L. Brooks III, *Curr. Opin. Struct. Biol.* **14**, 217 (2004).
14. A. D. Mackerell Jr., *J. Comput. Chem.* **25**, 1584 (2004).
15. B. Brooks *et al.*, *J. Comput. Chem.* **4**, 187 (1983).
16. W. Cornell *et al.*, *J. Am. Chem. Soc.* **117**, 5179 (1995).
17. D. B. Gordon, S. A. Marshall, S. L. Mayo, *Curr. Opin. Struct. Biol.* **9**, 509 (1999).
18. A. V. Morozov, T. Kortemme, K. Tsemekhman, D. Baker, *Proc. Natl. Acad. Sci. U.S.A.* **101**, 6946 (2004).
19. C. Levinthal, in *Mossbauer Spectroscopy in Biological Systems: Proceedings of a Meeting Held at Allerton House, Monticello, Illinois*, J. T. P. DeBrunner, E. Munck, Eds. (Univ. of Illinois Press, Urbana, 1969), pp. 22–24.
20. U. H. Hansmann, Y. Okamoto, *Curr. Opin. Struct. Biol.* **9**, 177 (1999).
21. K. Tai, *Biophys. Chem.* **107**, 213 (2004).
22. M. P. Jacobson *et al.*, *Proteins* **55**, 351 (2004).
23. Z. Li, H. A. Scheraga, *Proc. Natl. Acad. Sci. U.S.A.* **84**, 6611 (1987).
24. R. Abagyan, M. Totrov, *J. Mol. Biol.* **235**, 983 (1994).
25. E. Katchalski-Katzir *et al.*, *Proc. Natl. Acad. Sci. U.S.A.* **89**, 2195 (1992).
26. R. Mendez, R. Leplae, M. F. Lensink, S. J. Wodak, *Proteins* **60**, 150 (2005).
27. C. Dominguez, R. Boelens, A. M. Bonvin, *J. Am. Chem. Soc.* **125**, 1731 (2003).
28. J. U. Bowie, D. Eisenberg, *Proc. Natl. Acad. Sci. U.S.A.* **91**, 4436 (1994).
29. B. Park, M. Levitt, *J. Mol. Biol.* **258**, 367 (1996).
30. D. T. Jones, L. J. McGuffin, *Proteins* **53** (suppl. 6), 480 (2003).
31. J. Skolnick *et al.*, *Proteins* **53** (suppl. 6), 469 (2003).
32. Q. Fang, D. Shortle, *Proteins* **53** (suppl. 6), 486 (2003).
33. K. T. Simons, C. Kooperberg, E. Huang, D. Baker, *J. Mol. Biol.* **268**, 209 (1997).
34. P. Bradley, K. M. Misura, D. Baker, *Science* **309**, 1868 (2005).
35. J. W. Ponder, F. M. Richards, *J. Mol. Biol.* **193**, 775 (1987).
36. B. I. Dahiyat, S. L. Mayo, *Science* **278**, 82 (1997).
37. P. B. Harbury, J. J. Plecs, B. Tidor, T. Alber, P. S. Kim, *Science* **282**, 1462 (1998).
38. T. Kortemme, D. Baker, *Curr. Opin. Chem. Biol.* **8**, 91 (2004).
39. B. S. Chevalier *et al.*, *Mol. Cell* **10**, 895 (2002).
40. T. Kortemme *et al.*, *Nat. Struct. Mol. Biol.* **11**, 371 (2004).
41. J. M. Shifman, S. L. Mayo, *J. Mol. Biol.* **323**, 417 (2002).
42. B. Kuhlman *et al.*, *Science* **302**, 1364 (2003).
43. M. von Grotthuss, L. S. Wyrwicz, J. Pas, L. Rychlewski, *Science* **304**, 1597 (2004).
44. L. L. Looger, M. A. Dwyer, J. J. Smith, H. W. Hellinga, *Nature* **423**, 185 (2003).
45. D. N. Bolon, S. L. Mayo, *Proc. Natl. Acad. Sci. U.S.A.* **98**, 14274 (2001).
46. J. Kaplan, W. F. DeGrado, *Proc. Natl. Acad. Sci. U.S.A.* **101**, 11566 (2004).
47. M. A. Dwyer, L. L. Looger, H. W. Hellinga, *Science* **304**, 1967 (2004).
48. G. E. Moore, *Electronics* **38**, 114 (1965).
49. J. N. Onuchic, P. G. Wolynes, *Curr. Opin. Struct. Biol.* **14**, 70 (2004).
50. S. Y. Chung, S. Subbiah, *Pac. Symp. Biocomput.*, 126 (1996).
51. M. Schlosshauer, D. Baker, *Protein Sci.* **13**, 1660 (2004).
52. J. D. Bryngelson, J. N. Onuchic, N. D. Socci, P. G. Wolynes, *Proteins* **21**, 167 (1995).
53. The similarity of predictions and designs with crystal structures is not likely to be an artifact of the use of force fields in structure determination: X-ray structure determination at high resolution is almost entirely driven by experimental diffraction data, and the force fields typically used in refinement differ from those used in the prediction and design calculations.
54. X. J. Zhang, J. A. Wozniak, B. W. Matthews, *J. Mol. Biol.* **250**, 527 (1995).
55. E. Eyal, S. Gerzon, V. Potapov, M. Edelman, V. Sobolev, *J. Mol. Biol.* **351**, 431 (2005).
56. T. S. Ulmer, B. E. Ramirez, F. Delaglio, A. Bax, *J. Am. Chem. Soc.* **125**, 9179 (2003).
57. J. W. Ponder, D. A. Case, *Adv. Protein Chem.* **66**, 27 (2003).
58. A. Tramontano, V. Morea, *Proteins* **53** (suppl. 6), 352 (2003).
59. G. Wang, R. L. Dunbrack Jr., *Protein Sci.* **13**, 1612 (2004).
60. K. Ginalski, *CASP6 Abstract Book* (http://predictioncenter.org/casp6/abstracts/abstract.html), 64 (2004).
61. A. Fiser, A. Sali, *Methods Enzymol.* **374**, 461 (2003).
62. S. F. Altschul *et al.*, *Nucleic Acids Res.* **25**, 3389 (1997).
63. D. T. Jones, *J. Mol. Biol.* **292**, 195 (1999).
64. A. A. Canutescu, A. A. Shelenkov, R. L. Dunbrack Jr., *Protein Sci.* **12**, 2001 (2003).
65. D. Eisenberg, R. Luthy, J. U. Bowie, *Methods Enzymol.* **277**, 396 (1997).
66. A. L. Carvalho *et al.*, *Proc. Natl. Acad. Sci. U.S.A.* **100**, 13809 (2003).
67. J. M. Ryter, S. C. Schultz, *EMBO J.* **17**, 7505 (1998).
68. M. Graille, L. Mora, R. H. Buckingham, H. Van Tilbeurgh, M. De Zamaroczy, *EMBO J.* **23**, 1474 (2004).
69. M. Kanagawa, S. Yokoyama, S. Kuramitsu, unpublished data.
70. O. Schueler-Furman, C. Wang, D. Baker, *Proteins* **60**, 187 (2005).
71. The software used in the prediction and design examples described above is available free for academic use in the ROSETTA software package (http://depts.washington.edu/ventures/UW_Technology/Express_Licenses/Rosetta/), and personal computers can be enlisted in the conformational sampling essential to the prediction effort at http://boinc.bakerlab.org/rosetta/.


10.1126/science.1112160

# The Asian Tsunami: A Protective Role for Coastal Vegetation

Finn Danielsen,[1]* Mikael K. Sørensen,[2] Mette F. Olwig,[2] Vaithilingam Selvam,[3] Faizal Parish,[4] Neil D. Burgess,[5,6] Tetsuya Hiraishi,[7] Vagarappa M. Karunagaran,[3] Michael S. Rasmussen,[2] Lars B. Hansen,[2] Alfredo Quarto,[8] Nyoman Suryadiputra[9]

The scale of the 26 December 2004 Indian Ocean tsunami was almost unprecedented. In areas with the maximum tsunami intensity, little could have prevented catastrophic coastal destruction. Further away, however, areas with coastal tree vegetation were markedly less damaged than areas without. Mangrove forests are the most important coastal tree vegetation in the area and are one of the world's most threatened tropical ecosystems (*1*).

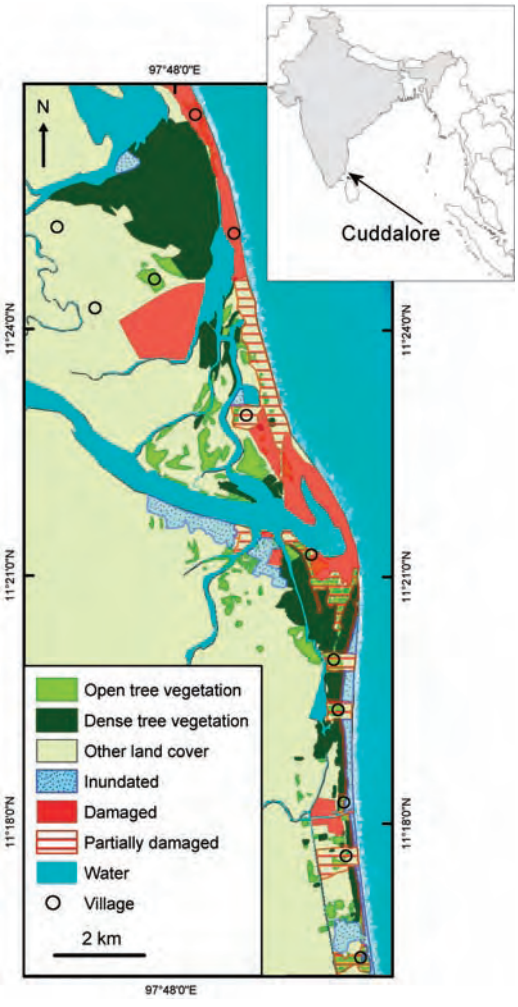


**Fig. 1.** Pre-tsunami tree vegetation cover and post-tsunami damages in Cuddalore District, Tamil Nadu, India.

Measurement of wave forces and modelling of fluid dynamics suggest that tree vegetation may shield coastlines from tsunami damage by reducing wave amplitude and energy (*2*). Analytical models show that 30 trees per 100 $m^2$ in a 100-m wide belt may reduce the maximum tsunami flow pressure by more than 90% (*3*). Empirical and field-based evidence is limited, however.

Cuddalore District in Tamil Nadu, India, provides a unique experimental setting to test the benefits of coastal tree vegetation in reducing coastal destruction by tsunamis (*4*). Cuddalore has a relatively straight shoreline, a fairly uniform beach profile, and a homogenous continental slope. Moreover, the shoreline comprises vegetated as well as non-vegetated areas and was documented by cloudfree pre- and post-tsunami satellite images.

The force of the tsunami impact in Cuddalore is illustrated by the central part of our study area (Fig. 1). At the river mouth, the tsunami completely destroyed parts of a village (fig. S1) and removed a sand spit that formerly blocked the river. However, areas with mangroves (Fig. 1, dark green polygon) and tree shelterbelts were significantly less damaged than other areas (supporting online text). Damage to villages also varied markedly. In the north, stands of mangroves had five associated villages, two on the coast and three behind the mangrove. The villages on the coast were completely destroyed, whereas those behind the mangrove suffered no destruction even though the waves damaged areas unshielded by vegetation north and south of these villages. In the south, the shore is lined with *Casuarina* plantations (Fig. 1). Five villages are located within these plantations and all experienced only partial damage. The plantations were undamaged except for rows of 5 to 10 trees nearest to the shore, which were uprooted (fig. S2).

Our results suggest that mangroves and *Casuarina* plantations attenuated tsunami-induced waves and protected shorelines against damage. Human activities reduced the area of mangroves by 26% in the five countries most affected by the tsunami, from 5.7 to 4.2 million ha, between 1980 and 2000 (*5*). Conserving or replanting coastal mangroves and greenbelts should buffer communities from future tsunami events. Mangroves also enhance fisheries (*6*) and forestry production. These benefits are not found in artificial coastal protection structures. Coastal tree vegetation can be established for investments of U.S.$150 to U.S.$2000 per ha (*7*). Mangroves, however, are suitable for planting only on coastal mudflats and lagoons, which cover ~25% of the continental coastline of the Bay of Bengal (*8*). Elsewhere, the conservation of dune ecosystems or green belts of other tree species, such as *Casuarina*, could fulfil the same protective role.

## References and Notes

1. I. Valiela, J. L. Bowen, J. K. York, *Bioscience* **51**, 807 (2001).
2. S. R. Massel, K. Furukawa, R. M. Brinkman, *Fluid Dyn. Res.* **24**, 219 (1999).
3. T. Hiraishi, K. Harada, *Greenbelt Tsunami Prevention in South-Pacific Region*, available at http://eqtap.edm.bosai.go.jp/useful_outputs/report/hiraishi/data/papers/greenbelt.pdf (2003).
4. Materials and methods are available as supporting material on *Science* Online.
5. Food and Agriculture Organization (FAO), *State of the World's Forests* (FAO, Rome, 2003).
6. P. J. Mumby *et al.*, *Nature* **427**, 533 (2004).
7. F. Parish, *Assessment of Cost of Mangrove Replanting in Tsunami-Impacted Regions* (Global Environment Centre, Selangor, Malaysia, 2005).
8. V. J. Chapman, Ed., *Wet Coastal Ecosystems*, vol. 1 of *Ecosystems of the World* (Elsevier, Amsterdam, 1977), p. 3.
9. We thank T. Y. Chee, D. Lee, T. Nuyim, I. Renshaw, E. Topp-Jørgensen, and E. Wikramanayake for assistance. Supported by the Solstice Foundation.

**Supporting Online Material**

www.sciencemag.org/cgi/content/full/310/5748/643/DC1
Materials and Methods
SOM Text
Figs. S1 and S2
Table S1
References and Notes

10 January 2005; accepted 20 September 2005
10.1126/science.1118387

[1]NORDECO, Skindergade 23, Copenhagen DK-1159, Denmark. [2]Geographic Resource Analysis and Science, University of Copenhagen, Øster Voldgade 10, Copenhagen, Denmark. [3]M. S. Swaminathan Research Foundation, 3rd Cross Street, Taramani, Chennai 600 113, India. [4]Global Environment Centre, 2nd Floor, Wisma Hing, 78, Jalan SS2/72, 47300 Petaling Jaya, Selangor, Malaysia. [5]Conservation Biology Group, Department of Zoology, University of Cambridge, Cambridge, UK. [6]World Wildlife Fund USA, 1250 24th Street NW, Washington, DC 20037–1193, USA. [7]Port and Airport Research Institute, Nagase 3-1-1, Yokosuka, Japan. [8]Mangrove Action Project, Post Office Box 1854, Port Angeles, WA 98362–0279, USA. [9]Wetlands International Indonesia, Post Office Box 254/BOO, Bogor 16002, Indonesia.

*To whom correspondence should be addressed. E-mail: fd@nordeco.dk

# Recurrent Fusion of *TMPRSS2* and ETS Transcription Factor Genes in Prostate Cancer

Scott A. Tomlins,[1] Daniel R. Rhodes,[1,2] Sven Perner,[7,9] Saravana M. Dhanasekaran,[1] Rohit Mehra,[1] Xiao-Wei Sun,[7] Sooryanarayana Varambally,[1,6] Xuhong Cao,[1] Joelle Tchinda,[7] Rainer Kuefer,[10] Charles Lee,[7] James E. Montie,[3,5,6] Rajal B. Shah,[1,3,5,6] Kenneth J. Pienta,[3,4,5,6] Mark A. Rubin,[7,8] Arul M. Chinnaiyan[1,2,3,5,6]*

Recurrent chromosomal rearrangements have not been well characterized in common carcinomas. We used a bioinformatics approach to discover candidate oncogenic chromosomal aberrations on the basis of outlier gene expression. Two ETS transcription factors, *ERG* and *ETV1*, were identified as outliers in prostate cancer. We identified recurrent gene fusions of the 5′ untranslated region of *TMPRSS2* to *ERG* or *ETV1* in prostate cancer tissues with outlier expression. By using fluorescence in situ hybridization, we demonstrated that 23 of 29 prostate cancer samples harbor rearrangements in *ERG* or *ETV1*. Cell line experiments suggest that the androgen-responsive promoter elements of *TMPRSS2* mediate the overexpression of ETS family members in prostate cancer. These results have implications in the development of carcinomas and the molecular diagnosis and treatment of prostate cancer.

A central aim in cancer research is to identify altered genes that play a causal role in cancer development. Many such genes have been identified through the analysis of recurrent chromosomal rearrangements that are characteristic of leukemias, lymphomas, and sarcomas (*1*). These rearrangements are of two general types. In the first, the promoter and/or enhancer elements of one gene are aberrantly juxtaposed to a proto-oncogene, thus causing altered expression of an oncogenic protein. This type of rearrangement is exemplified by the apposition of immunoglobulin (*IG*) and T cell receptor (*TCR*) genes to *MYC*, leading to activation of this oncogene in B and T cell malignancies, respectively (*2*). In the second, the rearrangement fuses two genes, resulting in the production of a fusion protein that may have a new or altered activity. The prototypic example of this translocation is the *BCR-ABL* gene fusion in chronic myelogenous leukemia (CML) (*3*, *4*). Importantly, this finding led to the development of the promising cancer drug imatinib mesylate (Gleevec) (*5*). In contrast to leukemias, epithelial tumors (carcinomas) display many nonspecific but few recurrent chromosomal rearrangements (*6*). This karyotypic complexity is thought to reflect secondary genomic alterations acquired during tumor progression.

We hypothesized that rearrangements and high-level copy number changes that result in marked overexpression of an oncogene should be evident in DNA microarray data but not necessarily by traditional analytical approaches. In the majority of cancer types, heterogeneous patterns of oncogene activation have been observed; thus, traditional analytical methods that search for common activation of genes across a class of cancer samples (e.g., *t* test or signal-to-noise ratio) will fail to find such oncogene expression profiles. Instead, a method that searches for marked overexpression in a subset of cases is needed. Toward this end, we developed a method termed cancer outlier profile analysis (COPA). COPA seeks to accentuate and identify outlier profiles by applying a simple numerical transformation based on the median and median absolute deviation of a gene expression profile (*7*) (fig. S1A).

**Cancer outlier profile analysis.** We applied COPA to the Oncomine database (*8*), a compendium of 132 gene expression data sets representing 10,486 microarray experiments. COPA correctly identified several outlier profiles for genes in specific cancer types in which a recurrent rearrangement or high-level amplification is known to occur (Table 1 and fig. S1, B and C). We focused our analyses on outlier profiles of known causal cancer genes, as defined by the Cancer Gene Census (*9*), that ranked in the top 10 outlier profiles in an Oncomine data set (Table 1 and table S1), because we felt these genes would be the most likely to participate

**Table 1.** Cancer outlier profile analysis (COPA). Genes known to undergo causal mutations in cancer that had strong outlier profiles. "X" indicates literature evidence for the acquired pathognomonic translocation. "XX" indicate that samples in the study were characterized for the indicated translocation. "Y" indicates consistent with known amplification. Double asterisks indicate *ERG* and *ETV1* outlier profiles in prostate cancer. A complete listing of genes known to undergo causal mutations ranking in the top 10 of all studies in Oncomine, along with the relevant references, is included as table S1.

| Rank | % | Score | Gene | Cancer | Study | Evidence |
|---|---|---|---|---|---|---|
| 1 | 95 | 20.056 | *RUNX1T1* | Leukemia | (*23*) | XX |
| 1 | 95 | 15.4462 | *PRO1073* | Renal | (*24*) | X |
| 1 | 90 | 12.9581 | *PBX1* | Leukemia | (*25*) | XX |
| 1 | 95 | 10.03795 | *ETV1* | Prostate | (*15*) | ** |
| 1 | 90 | 7.4557 | *WHSC1* | Myeloma | (*26*) | X |
| 1 | 75 | 5.4071 | *ERG* | Prostate | (*27*) | ** |
| 1 | 75 | 4.3628 | *ERG* | Prostate | (*28*) | ** |
| 1 | 75 | 4.3425 | *CCND1* | Myeloma | (*29*) | X |
| 1 | 75 | 3.4414 | *ERG* | Prostate | (*15*) | ** |
| 1 | 75 | 3.3875 | *ERG* | Prostate | (*30*) | ** |
| 3 | 95 | 13.3478 | *FGFR3* | Myeloma | (*29*) | X |
| 4 | 75 | 2.5728 | *ERBB2* | Breast | (*31*) | Y |
| 6 | 90 | 6.6079 | *ERBB2* | Breast | (*32*) | Y |
| 9 | 95 | 17.1698 | *ETV1* | Prostate | (*16*) | ** |
| 9 | 90 | 6.60865 | *SSX1* | Sarcoma | (*33*) | X |
| 9 | 75 | 2.2218 | *ERG* | Prostate | (*34*) | ** |

[1]Department of Pathology, [2]Bioinformatics Program, [3]Department of Urology, [4]Department of Internal Medicine, [5]Michigan Urology Center, [6]Comprehensive Cancer Center, University of Michigan Medical School, 1301 Catherine Street, Ann Arbor, MI 48109–0602, USA. [7]Department of Pathology, Brigham and Women's Hospital, [8]Dana-Farber Cancer Institute, [9]Department of Pathology, Harvard Medical School, Boston, MA 02115, USA. [10]Department of Urology, Faculty of Medicine, University of Ulm, Ulm 89075, Germany.

*To whom correspondence should be addressed. E-mail: arul@umich.edu

in uncharacterized alterations. The general COPA methodology can be applied to any expression data (*10*).

**Outlier profiles for *ERG* and *ETV1* in prostate cancer.** In several independent data sets, COPA identified strong outlier profiles in prostate cancer for *ERG* (21q22.3) and *ETV1* (7p21.2) (Table 1), two genes that encode ETS family transcription factors and are involved in oncogenic translocations in Ewing's sarcoma and myeloid leukemias (*11*, *12*). In total, COPA ranked *ERG* or *ETV1* within the top 10 outlier genes in six independent prostate cancer profiling studies.

Fusion of the 5′ activation domain of the Ewing sarcoma breakpoint region 1 (*EWSBR1*) gene to the highly conserved 3′ DNA binding domain of an ETS family member, such as *ERG* [t(21;22)] or *ETV1* [t(7;22)], is characteristic of Ewing's sarcoma (*11*, *13*, *14*). Because translocations involving ETS family members are functionally redundant in oncogenic transformation, only one type of translocation is typically observed in each case of Ewing's sarcoma. We hypothesized that, if *ERG* and *ETV1* are similarly involved in the development of prostate cancer, their outlier profiles should be mutually exclusive—that is, each tumor should overexpress only one of the two genes.

Thus, we examined the joint expression profiles of *ERG* and *ETV1* across several prostate cancer data sets and found that they invariably showed mutually exclusive outlier profiles, consistent with our hypothesis. Exclusive outlier expression of *ERG* and *ETV1* was identified in two large-scale transcriptome studies (*15*, *16*), which profiled grossly dissected prostate tissues with the use of different microarray platforms (Fig. 1). Similar results were obtained in prostate tissue samples obtained by laser capture microdissection (LCM) (fig. S2A). In addition to exclusive outlier expression of either *ERG* or *ETV1* in epithelial cells from prostate cancer or metastatic prostate cancer, *ETV1* and *ERG* were not overexpressed in the precursor lesion prostatic intraepithelial neoplasia (PIN) or adjacent benign epithelia (fig. S2A). The observed exclusive outlier pattern is consistent with other translocations where an activating gene can fuse with multiple partners, such as the fusion of the immunoglobulin heavy chain promoter to *CCND1* or *FGFR3*, t(11,14) or t(4,14), respectively, in specific subsets of multiple myeloma (*17*) (fig. S2B).

**Recurrent gene fusion of *TMPRSS2* to *ERG* or *ETV1* in prostate cancer.** To determine the mechanism responsible for *ERG* and *ETV1* overexpression, we identified prostate cancer cell lines and clinical specimens that overexpressed *ERG* or *ETV1* by using quantitative polymerase chain reaction (QPCR) (Fig. 2A). The LNCaP prostate cancer cell line and two specimens obtained from a patient with hormone-refractory metastatic disease (MET26-RP, residual primary carcinoma in the prostate, and MET26-LN, a lymph node metastasis) overexpressed *ETV1*. A lymph node metastasis from a second patient (MET-28LN) and two prostate cancer cell lines, VCaP and DuCaP, overexpressed *ERG*. We did not find consistent amplification of *ERG* or *ETV1* in samples with respective transcript overexpression, so we considered the possibility of DNA rearrangements. We measured the expression of *ETV1* exons by exon-walking QPCR in samples that displayed *ETV1* overexpression. We used five primer pairs spanning *ETV1* exons 2 through 7 and found that although LNCaP cells showed essentially uniform overexpression of all measured *ETV1* exons, both MET26 specimens showed >90% reduction in the expression of *ETV1* exons 2 and 3 compared with exons 4 to 7 (Fig. 2B).

To characterize the complete 5′ *ETV1* transcript, we performed 5′ RNA ligase-mediated rapid amplification of cDNA ends (RLM-

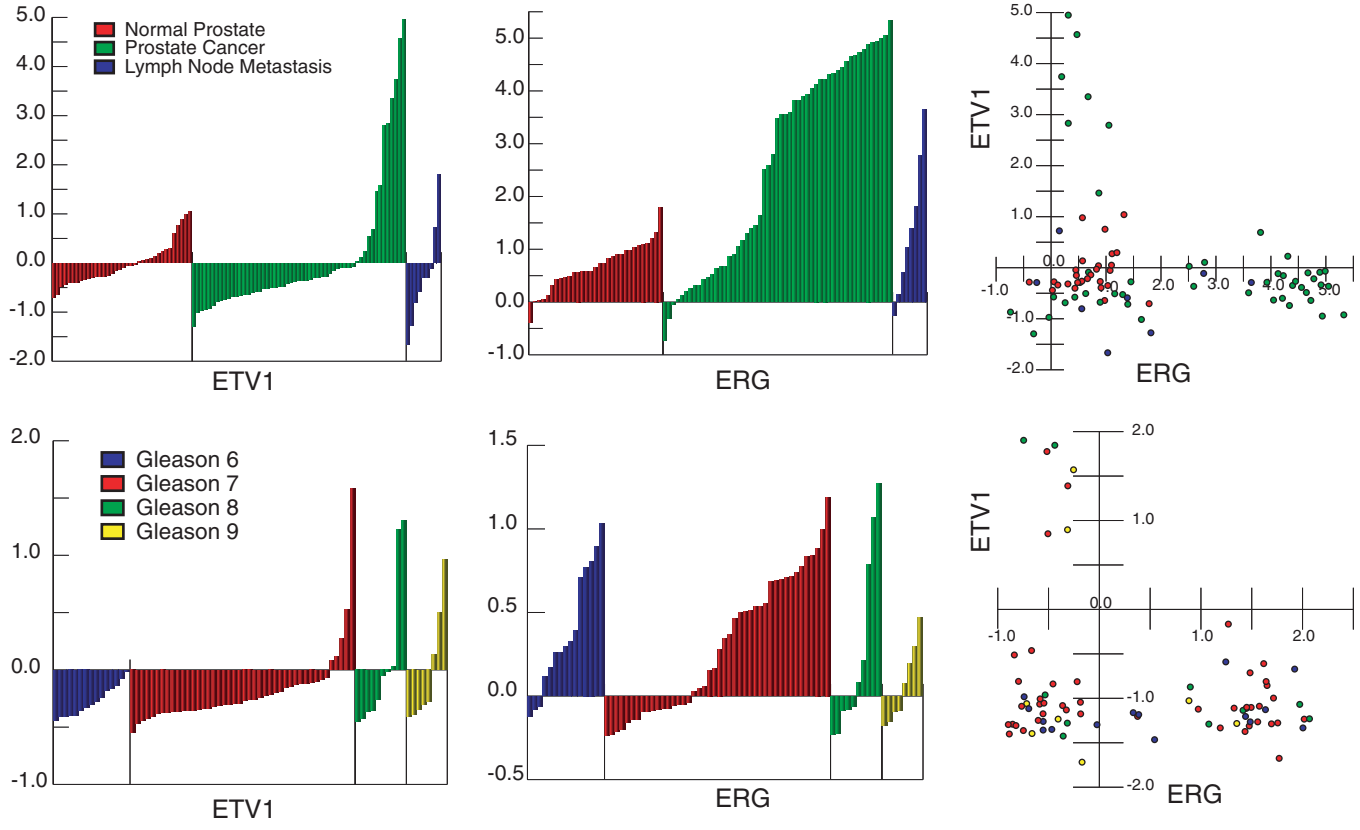


**Fig. 1.** COPA of microarray data revealed *ETV1* and *ERG* as outlier genes across multiple prostate cancer gene expression data sets. *ETV1* and *ERG* expression (normalized expression units) are shown from all profiled samples in two-large scale gene expression studies [top data set from (*15*) and bottom data set from (*16*)]. Visualization tools incorporated in Oncomine (*10*) were used to generate graphical displays. Sample classes are indicated according to the color scale. In the data set from (*16*), prostate cancer samples were classified on the basis of Gleason grade. Scatter plots of *ERG* and *ETV1* expression across all of the profiled samples are shown (**right**).

RACE) on LNCaP cells and MET26-LN. In addition, we also performed RLM-RACE to obtain the complete 5′ transcript of *ERG* in MET28-LN. Sequencing of the cloned products revealed fusions of the prostate-specific gene *TMPRSS2* (*18*) (21q22.2) with *ETV1* in MET26-LN and with *ERG* in MET28-LN (Fig. 2C). In MET26-LN, two RLM-RACE PCR products were identified. The first product, *TMPRSS2:ETV1a*, resulted in a fusion of the complete exon 1 of *TMPRSS2* with the beginning of exon 4 of *ETV1* (Fig. 2C). The second product, *TMPRSS2:ETV1b*, resulted in a fusion of exons 1 and 2 of *TMPRSS2* with the beginning of exon 4 of *ETV1* (fig. S3). Both products are consistent with the exon-walking QPCR described above, where MET26-LN showed loss of overexpression in exons 2 and 3. In MET28-LN, a single RLM-RACE PCR product was identified, and sequencing revealed a fusion of the complete exon 1 of *TMPRSS2* with the beginning of exon 4 of *ERG* (*TMPRSS2:ERGa*) (Fig. 2C).

**Validation of *TMPRSS2:ERG* and *TMPRSS2:ETV1* gene fusions in prostate cancer.** On the basis of these results, we designed QPCR primer pairs with forward primers in *TMPRSS2* and reverse primers in exon 4 of *ERG* or *ETV1*. We performed SYBR Green (Molecular Probes, Eugene, OR) QPCR with the use of both primer pairs across a panel of samples from 42 cases of clinically localized prostate cancer and metastatic prostate cancer and depict representative results (Fig. 2, D and E). These 42 cases were selected on the basis of previous cDNA microarray or QPCR results indicating overexpression of *ERG* or *ETV1*. We were limited to samples with remaining material, and thus this cohort does not represent a random sampling. In addition to QPCR, we also performed standard reverse transcription PCR (RT-PCR) with the same primers used for QPCR, or with a different forward primer in *TMPRSS2* and reverse primers in exon 6 of *ERG* and exon 7 of *ETV1* on a subset of the samples with or without fusions as determined by using QPCR (fig. S4, A and B). Electrophoresis of QPCR products and sequencing of cloned RT-PCR products from MET-26RP and MET-26LN revealed the presence of both *TMPRSS2:ETV1a* and *TMPRSS2:ETV1b*. The molecular evidence for *TMPRSS2:ERG* and *TMPRSS2:ETV1* fusions in cases and cell lines overexpressing the respective ETS family member are summarized (fig. S5). From QPCR melt curve analysis and gel electrophoresis of QPCR and RT-PCR products, PCA4 produced a larger amplicon than *TMPRSS2:ERGa*. Subsequent RLM-RACE analysis and sequencing of the RT-PCR product confirmed a fusion of the complete exon 1 of *TMPRSS2* with the beginning of exon 2 of *ERG* (*TMPRSS2:ERGb*) (fig. S3). Evidence for the *TMPRSS2:ERG* and *TMPRSS2:ETV1* fusions were only found in cases that overexpressed *ERG* or *ETV1*, respectively, by QPCR or DNA microarray. These results are also in agreement with the exclusive expression observed in our outlier analysis.

**Genomic confirmation of *TMPRSS2:ETV1* translocation and *ERG* rearrangement.** We used interphase fluorescence in situ hybridization (FISH) to validate the rearrangements at the chromosomal level on formalin-fixed paraffin-embedded (FFPE) specimens from the two cases initially used for RLM-RACE, MET26 and MET28 (Fig. 3). With the use of probes for *TMPRSS2* and *ETV1*, normal peripheral lymphocytes (NPLs) demonstrated a pair of red and a pair of green signals (Fig.

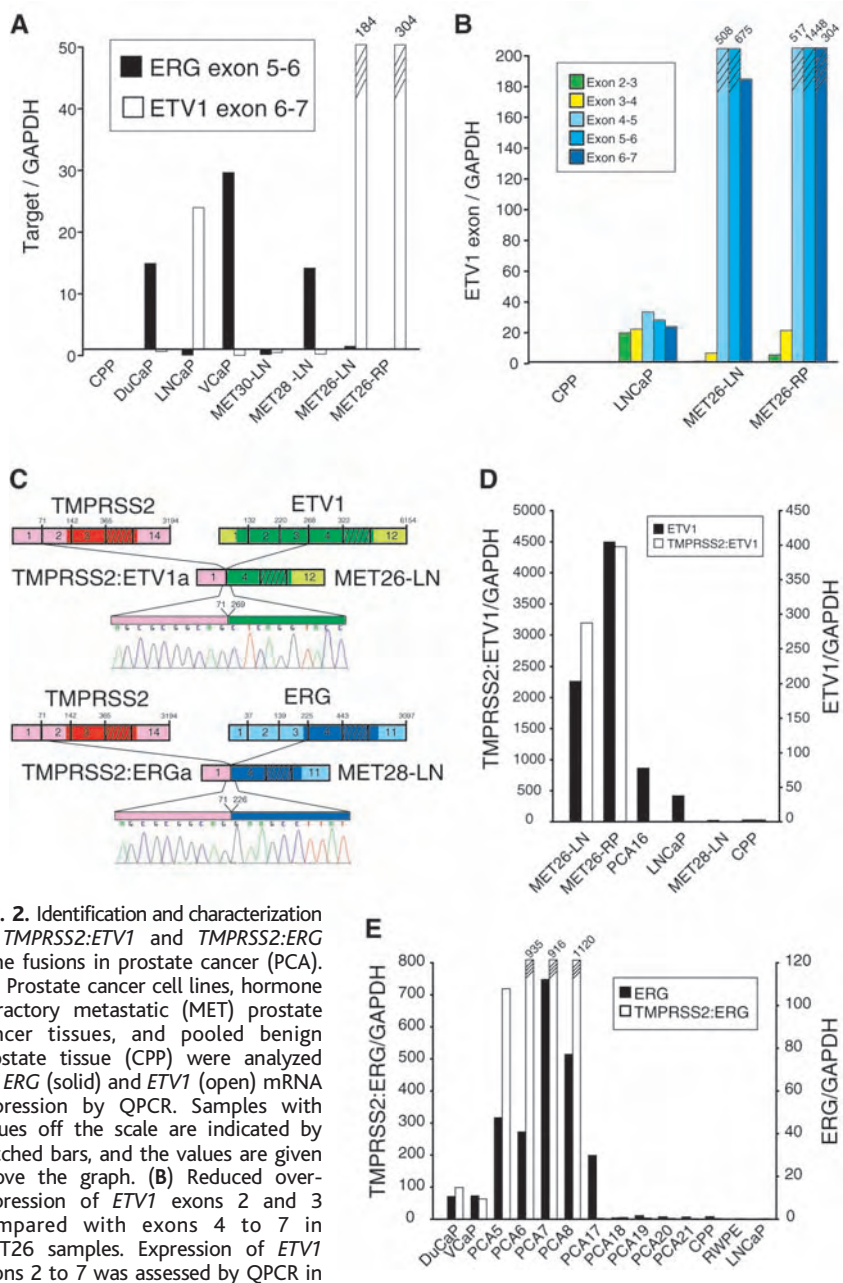


**Fig. 2.** Identification and characterization of *TMPRSS2:ETV1* and *TMPRSS2:ERG* gene fusions in prostate cancer (PCA). (**A**) Prostate cancer cell lines, hormone refractory metastatic (MET) prostate cancer tissues, and pooled benign prostate tissue (CPP) were analyzed for *ERG* (solid) and *ETV1* (open) mRNA expression by QPCR. Samples with values off the scale are indicated by hatched bars, and the values are given above the graph. (**B**) Reduced overexpression of *ETV1* exons 2 and 3 compared with exons 4 to 7 in MET26 samples. Expression of *ETV1* exons 2 to 7 was assessed by QPCR in LNCaP cells and MET26-LN and MET26-RP samples. (**C**) Schematic of 5′ RLM-RACE revealing fusion of *TMPRSS2* with *ETV1* in MET26-LN and *ERG* in MET28-LN. Structures for the *TMPRSS2*, *ERG*, and *ETV1* genes have their basis in the GenBank reference sequences. The numbers above the exons (indicated by boxes) indicate the last base of each exon. Untranslated regions are shown in corresponding lighter shades. Coding exons not depicted are indicated by hatched boxes. Identified *TMPRSS2* fusions are colored and numbered from the original reference sequences. Line graphs show the position and automated DNA sequencing of the fusion points. (**D**) Validation of *TMPRSS2:ETV1* expression using fusion-specific QPCR in MET26-LN and MET26-RP. Expression of *ETV1* (solid, right axis) and *TMPRSS2:ETV1* (open, left axis) was assessed by QPCR. (**E**) Validation of *TMPRSS2:ERG* expression using fusion-specific QPCR in cell lines and PCA specimens. Expression of *ERG* (solid, right axis) and *TMPRSS2:ERG* (open, left axis) was assessed by QPCR.

3A). However, MET26 showed fusion of one pair of signals, indicative of probe overlap (Fig. 3B) and consistent with the expression of the *TMPRSS2:ETV1*. Because of the proximity of *TMPRSS2* to *ERG* on chromosome 21, ~3 megabases (fig. S6A), we used probes spanning the 5′ and 3′ regions of the *ERG* locus to assay for gene rearrangements. By using these probes, we observed a pair of yellow signals in NPLs (Fig. 3C); however, in MET28, one pair of probes split into separate green and red signals, indicative of a rearrangement at the *ERG* locus (Fig. 3D) and consistent with the expression of *TMPRSS2:ERG*. We next performed both individual FISH analyses described above on serial tissue microarrays containing cores from 13 cases of localized prostate cancer and 16 cases of metastatic prostate cancer (Fig. 3E). Of 29 cases, 23 (79.3%) showed evidence of *TMPRSS2:ETV1* fusion (7 cases) or *ERG* rearrangement (16 cases).

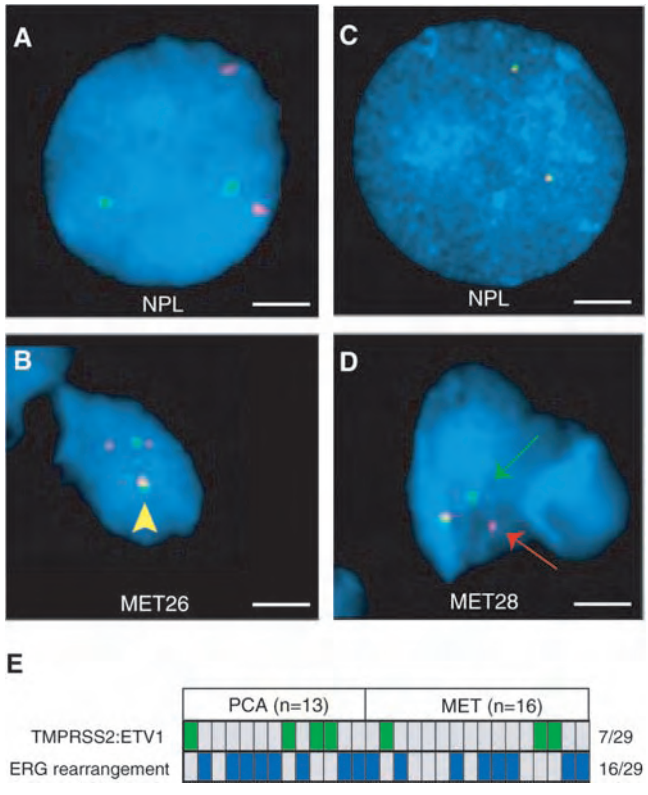


**Fig. 3.** Interphase FISH on FFPE tissue sections confirms *TMPRSS2:ETV1* gene fusion and *ERG* gene rearrangement. (**A** and **B**) NPLs showed two *ETV1* (red) and two *TMPRSS2* (green) signals, whereas MET26 showed fusion of the signals as indicated by the yellow signal (yellow arrowhead). (**C** and **D**) For detection of *ERG* gene rearrangements, we used a split-signal approach, with two probes spanning the *ERG* locus. NPLs showed two yellow signals, indicating overlap of the 5′ (green signal) and 3′ (red signal) regions of *ERG*, whereas MET28 shows a rearrangement of *ERG* as indicated by the split signal of the 5′ and 3′ probes (red and green arrows). Scale bars for all images are 2.5 μm. (**E**) Matrix representation of FISH results using the same probes as (A) to (D) on an independent tissue microarray containing cores from clinically localized (PCA) and metastatic (MET) prostate cancer. Cores positive for *TMPRSS2:ETV1* probe fusion or split-signal *ERG* probes are indicated by colored cells. All negative findings are indicated by gray cells. The number of positive cases for each feature is indicated to the right of the matrix.

As additional confirmation of the *ERG* rearrangement, we performed FISH on metaphase spreads of VCaP cells, which express the *TMPRSS2:ERGa* transcript. This assay revealed co-localization of 5′ *TMPRSS2* and 3′ *ERG* probes with splitting of the 5′ and 3′ *ERG* signals, supporting the molecular results (fig. S6). In addition, Southern blotting using a probe in the intron between exons 1 and 2 of *TMPRSS2* revealed a unique band in VCaP cells, consistent with a rearrangement at this locus (fig. S7).

**Fusion of *TMPRSS2* and *ERG* results in androgen regulation of *ERG*.** *TMPRSS2* is expressed in normal and neoplastic prostate tissue and is strongly induced by androgen in androgen-sensitive prostate cell lines (*18–20*). To investigate whether the *TMPRSS2:ERG* fusion results in the androgen regulation of *ERG*, we assessed the expression of *ERG* by QPCR in androgen-treated VCaP cells, which express *TMPRSS2:ERGa*, and LNCaP cells, which do not express a fusion transcript. Both VCaP and LNCaP respond to androgen stimulation with increased expression of *PSA*, which is expressed at a similar amount in both cells and is sensitive to the androgen receptor antagonists bicalutamide and flutamide (Fig. 4A). However, in addition to expressing ~2000-fold more *ERG* than LnCAP cells, only VCaP cells responded to androgen stimulation with increased *ERG* expression sensitive to bicalutamide and flutamide (Fig. 4B). A similar increase in *ERG* expression upon androgen stimulation was observed in DuCaP cells, which express *TMPRSS2:ERGa*, whereas RWPE, PC3, and PC3 cells expressing the human androgen receptor express low concentrations of *ERG* that are not androgen-responsive (fig. S8). These results suggest that the fusion with *TMPRSS2* may explain the aberrant expression of *ERG* or *ETV1* in specific subsets of prostate cancer.

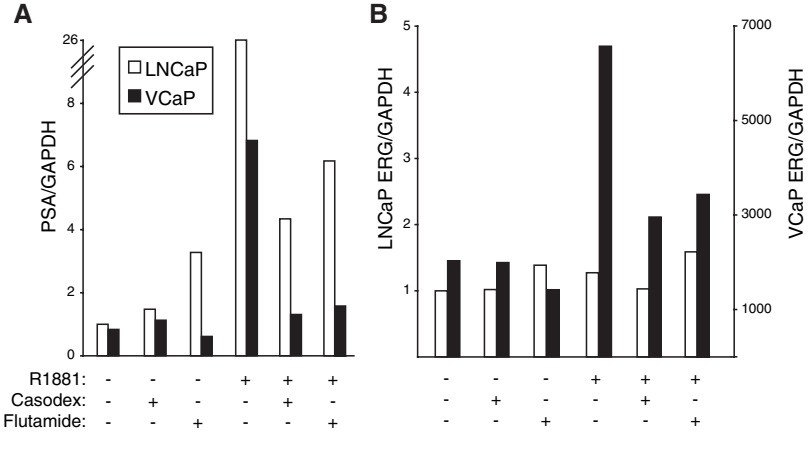


**Fig. 4.** Androgen regulation of *ERG* in VCaP prostate cancer cells carrying the *TMPRSS2:ERG* fusion. (**A**) *PSA* expression relative to *GAPDH* in androgen-sensitive LNCaP (open) and VCaP (solid) cells was assessed by QPCR. (**B**) *ERG* (exon 5 to 6) expression relative to *GAPDH* in LNCaP (open, left axis) and VCaP (solid, right axis) cells. Cell lines were incubated with vehicle or 10 μM of the androgen receptor antagonists bicalutamide or flutamide for 2 hours before treatment for 24 hours with 0.5 nM of the synthetic androgen R1881 or vehicle as indicated. Relative *PSA* or *ERG* for each sample was normalized to the amount in the LNCaP control.

**Conclusions.** The existence of recurring gene fusions of *TMPRSS2* to the oncogenic ETS family members *ERG* and *ETV1* may have important implications for understanding prostate cancer tumorigenesis and developing novel diagnostics and targeted therapeutics. Several lines of evidence suggest that these rearrangements occur in the majority of prostate cancer samples and drive ETS family member expression. Across three independent microarray data sets, *ERG* or *ETV1* was markedly overexpressed in 95 of 167 (57%) prostate cancer cases, whereas overexpression was never observed across 54 benign prostate tissue samples. Furthermore, a recent study reported that *ERG* was the most commonly

overexpressed oncogene by QPCR in prostate cancer, with 72.0% of cases overexpressing *ERG* (*21*). By using a combination of assays, we found evidence of fusion with *TMPRSS2* in 20 of 22 (>90%) cases that overexpressed *ERG* or *ETV1*, suggesting that the fusion is the most likely cause for the overexpression. FISH analysis on a set of 29 prostate cancer cases selected independently of any knowledge of *ERG* or *ETV1* expression indicates that 23 of 29 (79%) had *TMPRSS2:ETV1* fusions or *ERG* rearrangement. It is possible that this cohort is not representative of all prostate cancer samples and that this may be an overestimate of the prevalence of *TMPRSS2* fusions with ETS family members, because our split-signal approach can detect additional rearrangements involving *ERG*. However, the reported frequencies of *ERG* or *ETV1* overexpression in prostate cancer with our fusion transcript and FISH results suggest that *TMPRSS2* fusions with *ETV1* or *ERG* occur in the majority of prostate cancer cases. Coupled with the high incidence of prostate cancer [an estimated 232,090 new cases will be diagnosed in the United States in 2005 (*22*)], the *TMPRSS2* fusion with ETS family members is likely to be the most common rearrangement yet identified in human malignancies and the only rearrangement present in the majority of one of the most prevalent carcinomas.

Future efforts will be directed at characterizing the expressed protein products, including the effects of N-terminal truncation of ERG and ETV1, and identifying downstream targets and the functional role of the fusions in prostate cancer development. Importantly, the existence of *TMPRSS2* fusions with ETS family members in prostate cancer suggests that causal gene rearrangements may exist in common epithelial cancers but may be masked by the multiple nonspecific chromosomal rearrangements that occur during tumor progression.

### References and Notes


1. J. D. Rowley, *Nat. Rev. Cancer* **1**, 245 (2001).
2. T. H. Rabbitts, *Nature* **372**, 143 (1994).
3. J. D. Rowley, *Nature* **243**, 290 (1973).
4. A. de Klein *et al.*, *Nature* **300**, 765 (1982).
5. M. Deininger, E. Buchdunger, B. J. Druker, *Blood* **105**, 2640 (2005).
6. F. Mitelman, *Mutat. Res.* **462**, 247 (2000).
7. Materials and methods are available as supporting material on *Science* Online.
8. D. R. Rhodes *et al.*, *Neoplasia* **6**, 1 (2004).
9. P. A. Futreal *et al.*, *Nat. Rev. Cancer* **4**, 177 (2004).
10. Detailed results from the application of COPA to Oncomine data sets can be explored at www.oncomine.org.
11. T. Oikawa, T. Yamada, *Gene* **303**, 11 (2003).
12. T. Hsu, M. Trojanowska, D. K. Watson, *J. Cell. Biochem.* **91**, 896 (2004).
13. I. S. Jeon *et al.*, *Oncogene* **10**, 1229 (1995).
14. P. H. Sorensen *et al.*, *Nat. Genet.* **6**, 146 (1994).
15. J. Lapointe *et al.*, *Proc. Natl. Acad. Sci. U.S.A.* **101**, 811 (2004).
16. G. V. Glinsky, A. B. Glinskii, A. J. Stephenson, R. M. Hoffman, W. L. Gerald, *J. Clin. Invest.* **113**, 913 (2004).
17. R. Fonseca *et al.*, *Cancer Res.* **64**, 1546 (2004).
18. B. Lin *et al.*, *Cancer Res.* **59**, 4180 (1999).
19. D. E. Afar *et al.*, *Cancer Res.* **61**, 1686 (2001).
20. E. Jacquinet *et al.*, *Eur. J. Biochem.* **268**, 2687 (2001).
21. G. Petrovics *et al.*, *Oncogene* **24**, 3847 (2005).
22. A. Jemal *et al.*, *CA Cancer J. Clin.* **55**, 10 (2005).
23. P. J. Valk *et al.*, *N. Engl. J. Med.* **350**, 1617 (2004).
24. J. R. Vasselli *et al.*, *Proc. Natl. Acad. Sci. U.S.A.* **100**, 6958 (2003).
25. M. E. Ross *et al.*, *Blood* **102**, 2951 (2003).
26. E. Tian *et al.*, *N. Engl. J. Med.* **349**, 2483 (2003).
27. S. M. Dhanasekaran *et al.*, *FASEB J.* **19**, 243 (2005).
28. J. B. Welsh *et al.*, *Cancer Res.* **61**, 5974 (2001).
29. F. Zhan *et al.*, *Blood* **99**, 1745 (2002).
30. S. M. Dhanasekaran *et al.*, *Nature* **412**, 822 (2001).
31. E. Huang *et al.*, *Lancet* **361**, 1590 (2003).
32. C. Sotiriou *et al.*, *Proc. Natl. Acad. Sci. U.S.A.* **100**, 10393 (2003).
33. T. O. Nielsen *et al.*, *Lancet* **359**, 1301 (2002).
34. Y. P. Yu *et al.*, *J. Clin. Oncol.* **22**, 2790 (2004).


35. We thank D. Roulston and E. Fearon for helpful discussions, D. Robins and K. Burnstein for the PC3+AR cells, and R. Desphande and C. Creighton for technical assistance. Supported by the Early Detection Research Network Biomarker Developmental Lab UO1 CA111275-01 (to A.M.C.); NIH Prostate specialized program of research excellence (SPORE) P50CA69568 (to K.J.P), RO1 CA97063 (to A.M.C.), and R01AG21404 (to M.A.R.); American Cancer Society RSG-02-179-MGO (to A.M.C.); Department of Defense (PC040517 to R.M. and PC020322 to A.M.C.); and the Cancer Center Bioinformatics Core (support grant 5P30 CA46592). D.R.R. is supported by the Cancer Biology Training Program. K.J.P. is an American Cancer Society Clinical Research Professor. A.M.C. is a Pew Biomedical Scholar, and S.A.T. and D.R.R. are Fellows of the Medical Scientist Training Program. Nucleotide sequences for the *TMPRSS2:ETS* fusions have been deposited at GenBank with accession numbers DQ204770 to DQ04773.


**Supporting Online Material**

www.sciencemag.org/cgi/content/full/310/5748/644/DC1
Materials and Methods
Figs. S1 to S8
Tables S1 and S2

20 July 2005; accepted 22 September 2005
10.1126/science.1117679

# REPORTS

## Hanbury Brown Twiss Effect for Ultracold Quantum Gases

**M. Schellekens,[1] R. Hoppeler,[1] A. Perrin,[1] J. Viana Gomes,[1,2] D. Boiron,[1] A. Aspect,[1] C. I. Westbrook[1]***

**We have studied two-body correlations of atoms in an expanding cloud above and below the Bose-Einstein condensation threshold. The observed correlation function for a thermal cloud shows a bunching behavior, whereas the correlation is flat for a coherent sample. These quantum correlations are the atomic analog of the Hanbury Brown Twiss effect. We observed the effect in three dimensions and studied its dependence on cloud size.**

Nearly half a century ago, Hanbury Brown and Twiss (HBT) performed a landmark experiment on light from a gaseous discharge (*1*). The experiment demonstrated strong correlations in the intensity fluctuations at two nearby points in space despite the random or chaotic nature of the source. Although the effect was easily understood in the context of classical statistical wave optics, the result was surprising when viewed in terms of the quantum theory. It implied that photons coming from widely separated points in a source such as a star were "bunched." On the other hand, photons in a laser were not bunched (*2*, *3*). The quest to understand the observations stimulated the birth of modern quantum optics (*4*). The HBT effect has since found applications in many other fields from particle physics (*5*) to fluid dynamics (*6*).

Atom or photon bunching can be understood as a two-particle interference effect (*7*). Experimentally, one measures the joint probability for two particles emitted from two separated source points, $A$ and $B$, to be detected at two detection points, $C$ and $D$. One must consider the quantum mechanical amplitude for the process $A \rightarrow C$ and $B \rightarrow D$ as well as that for $A \rightarrow D$ and $B \rightarrow C$. If the two processes are indistinguishable, the amplitudes interfere. For bosons, the interference is constructive, resulting in a joint detection probability that is enhanced compared with that of two statistically independent detection events, whereas for fermions the joint probability is lowered. As the detector separation is increased, the phase difference between the two amplitudes grows large enough that an average over all possible source points $A$ and $B$ washes out the interference, and one recovers the sit-

[1]Laboratoire Charles Fabry de l'Institut d'Optique, UMR 8501 du CNRS, Centre Scientifique d'Orsay, Bâtiment 503, 91403 Orsay CEDEX, France. [2]Departimento de Fisica, Universidade do Minho, 4710-057 Braga, Portugal.

*To whom correspondence should be addressed. E-mail: christoph.westbrook@iota.u-psud.fr

uation for uncorrelated detection events. This fact was used by HBT to measure the angular size of a star (*8*), but another major consequence of the observation was to draw attention to the importance of two-photon amplitudes and how their interference can lead to surprising effects. These quantum amplitudes must not be confused with classical electromagnetic field amplitudes (*3*). Two-photon states subsequently led to many other striking examples of "quantum weirdness" (*9*). In contrast to a chaotic source, all photons in a single mode laser are in the same quantum state. Hence, there is only one physical process and no bunching effect. A similar effect is expected for atoms in a Bose-Einstein condensate (BEC).

Two-particle correlations have been observed both for cold neutral atoms (*10–12*) and for electrons (*13–15*), and three-particle correlations (*16–18*) at zero distance have also been used to study atomic gases. But the full three-dimensional effect and its dependence on the size and degeneracy of a sample has yet to be demonstrated for massive particles. Here, we demonstrate the effect for a trapped cloud of atoms close to the BEC transition temperature released onto a detector capable of individual particle detection. We extract, for varying cloud sizes, a three-dimensional picture of the correlations between identical particles produced by quantum interference. We also show that a BEC shows no such correlations. The results are in agreement with an ideal gas model and show the power of single particle detection techniques applied to the study of degenerate quantum gases.

The calculation of the phase difference of the possible two-particle detection amplitudes given in (*7*) can be adapted to the case of particles of mass $m$ traveling to a detector in a time $t$. One can show that the correlation length observed at the detectors, that is, the typical detector separation for which interference survives, is $l_i = \frac{\hbar t}{m s_i}$, where $s_i$ is the source size along the direction $i$, $\hbar$ is the reduced Planck's constant, and we have assumed that the size of the cloud at the detector is much larger than the initial size. The optical analog of this expression, for a source of size $s$ and wavelength $\lambda$ at a distance $L$ from the observation plane, is $l = L\lambda/2\pi s$. This is the length scale of the associated speckle pattern. The formula can be recovered for the case of atoms traveling at constant velocity $v$ toward a detector at distance $L$ if one identifies $h/mv$ with the deBroglie wavelength corresponding to velocity $v$. The formula we give is also valid for atoms accelerated by gravity, and the interpretation of $l$ as the atomic speckle size remains valid. A pioneering experiment on atom correlations used a continuous beam of atoms (*10*). For a continuous beam, the correlation time, or equivalently, the longitudinal correlation length, depends on the velocity width of the source and not on the source size. Thus, the longitudinal and transverse directions are qualitatively different. By contrast, our measurements are performed on a cloud of atoms released suddenly from a magnetic trap. In this case, the three dimensions can all be treated equivalently, and the relation above applies in all three. Because the trap is anisotropic, the correlation function is as well, with an inverted ellipticity. Our sample is a magnetically trapped cloud of metastable helium atoms evaporatively cooled close to the BEC transition temperature (*19*) (about 0.5 μK for our conditions). Our source is thus very small, and together with a long time of flight (308 ms) and helium's small mass, we achieve a large speckle size or correlation volume (30 μm by 800 μm by 800 μm), which simplifies the detection problem. For example, the observations are much less sensitive to the tilt of the detector than in (*10*).

To detect the atoms, we use an 8-cm-diameter microchannel plate detector (MCP). It is placed 47 cm below the center of the magnetic trap. A delay line anode permits position-sensitive detection of individual particles in the plane of the detector (*20*) (Fig. 1). Atoms are released from the trap by suddenly turning off the magnetic field. About 10% of these atoms are transferred to the magnetic field–insensitive $m = 0$ state by nonadiabatic transitions (*19*) and fall freely to the detector. The remaining atoms are removed by applying additional magnetic field gradients during the time of flight. For each detected atom, we record the in-plane coordinates $x$ and $y$ and the time of detection $t$. The atoms hit the detector at 3 m/s with a velocity spread below 1%, and so we convert $t$ into a vertical position $z$. The observed root mean square (rms) resolution is $d \sim 250$ μm in $x$ and $y$ and 2 nm in $z$. These data allow us to construct a three-dimensional histogram of pair separations ($\Delta x$, $\Delta y$, and $\Delta z$) for all particles detected in a single cloud. The histograms are summed over the entire atomic distribution and over many shots, typically 1000 (*21*).

Because of our good resolution along $z$, we begin by concentrating on the correlation function along this axis. Normalized correlation functions for various experimental conditions are shown in Fig. 2A. To compute the normalized correlation function, we divide the pair separation histogram by the autoconvolution of the average single particle distribution along $z$. We also normalize the correlation function to unity for large separations. This amounts to dividing, for each elementary pixel of our detector, the joint detection probability by the product of the individual detection probabilities at the two pixels. This gives us the usual normalized correlation function $g^{(2)}(\Delta x = 0, \Delta y = 0, \Delta z)$. The HBT bunching effect corresponds to the bump in the top three graphs of Fig. 2A. The fourth graph shows the result for a BEC. No correlation is observed. [A detector saturation effect in the BEC data required a modified analysis procedure (*21*).] We have also recorded data for a cloud with a 2-mm radius and 1-mK temperature for which the correlation length is so small that the bunching effect is washed out by the in-plane detector resolution. Experimentally, the normalized correlation function in this case is indeed flat to within less than 1%.

We plot (Fig. 2B) the normalized correlation functions in the $\Delta x - \Delta y$ plane and for $\Delta z = 0$ for the same three data sets. The data in Fig. 2B show the asymmetry in the correlation function arising from the difference in the two transverse dimensions of the trapped cloud. The long axis of the correlation function is orthogonal to that of the magnetic trap.

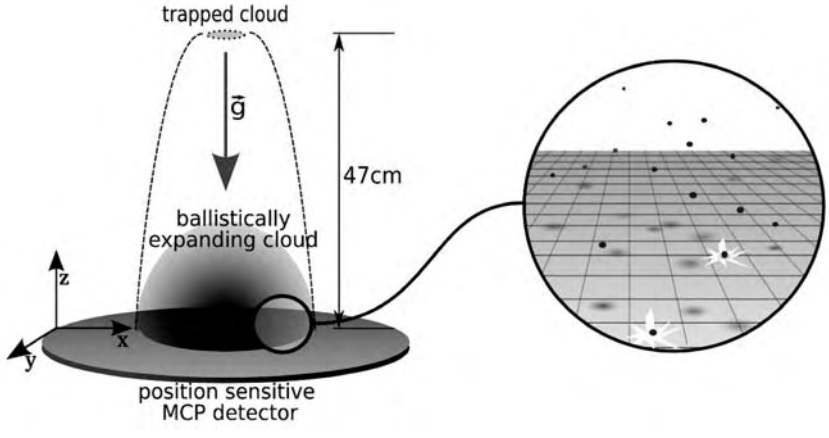


**Fig. 1.** Schematic of the apparatus. The trapped cloud has a cylindrical symmetry with oscillation frequencies of $\omega_x/2\pi = 47$ Hz and $\omega_y/2\pi = \omega_z/2\pi = 1150$ Hz. During its free fall toward the detector, a thermal cloud acquires a spherical shape. A 1-μK temperature yields a cloud with an rms radius of about 3 cm at the detector. Single particle detection of the neutral atoms is possible because of each atom's 20-eV internal energy that is released at contact with the MCP. Position sensitivity is obtained through a delay-line anode at the rear side of the MCP.

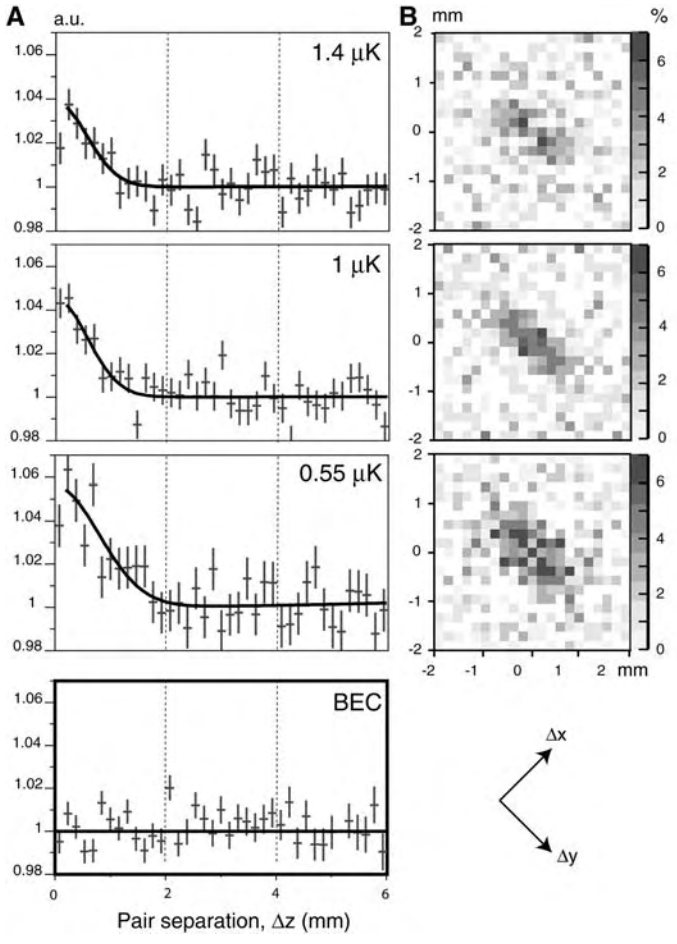


**Fig. 2.** (**A**) Normalized correlation functions along the vertical (*z*) axis for thermal gases at three different temperatures and for a BEC. For the thermal clouds, each plot corresponds to the average of a large number of clouds at the same temperature. Error bars correspond to the square root of the number of pairs. a.u., arbitrary units. (**B**) Normalized correlation functions in the $\Delta x - \Delta y$ plane for the three thermal gas runs. The arrows at the bottom show the 45° rotation of our coordinate system with respect to the axes of the detector. The inverted ellipticity of the correlation function relative to the trapped cloud is visible.

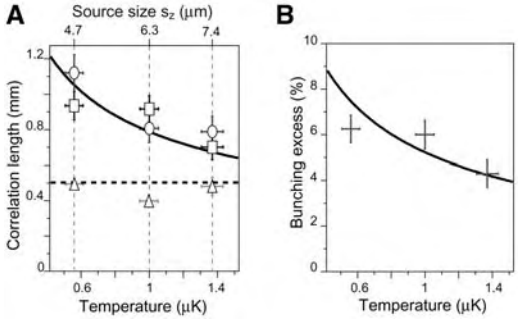


**Fig. 3.** Results of fits to the data in Fig. 2, A and B. (**A**) Fitted correlation lengths $l_x$, $l_y$, and $l_z$ along the three axes (triangles, squares, and circles) as a function of temperature. The upper axis shows the corresponding source size $s_z$. Vertical error bars are from the fits. Horizontal error bars correspond to the standard deviation of the measured temperature. Along the *x* axis, the measurement is entirely limited by the detector resolution. The dotted horizontal line is the result of an independent estimate of the resolution. The result for the *y* axis has been corrected for the finite detector resolution as characterized by the fitted value of $l_x$. The *z* axis suffers from no such resolution limit. The solid curve corresponds to $\hbar t/ms_z$. (**B**) Fitted contrast η of the correlation function for the three temperatures used. The solid line corresponds to the same noninteracting gas model as the line in (A) (*21*) and includes the finite detector resolution.

We expect the experimental normalized correlation function for a thermal bosonic gas to be described by

$$g^{(2)}_{\mathrm{th}}(\Delta x, \Delta y, \Delta z) = 1 + \eta \exp\left(-\left[\left(\frac{\Delta x}{l_x}\right)^2 + \left(\frac{\Delta y}{l_y}\right)^2 + \left(\frac{\Delta z}{l_z}\right)^2\right]\right) \quad (1)$$

We have assumed here that the gas is noninteracting and that the velocity and density distribution remain roughly Gaussian even close to the BEC transition temperature. Numerical simulations indicate that this is a good approximation when the correlation function is averaged over the entire cloud (*22*). As discussed above, the correlation lengths should be inversely proportional to the sizes, $s_i$, of the sample. In a harmonic trap with trapping frequency $\omega_i$ along the *i* direction, one has $s_i = \sqrt{\frac{k_B T}{m\omega_i^2}}$, where $k_B$ is Boltzmann's constant and *T* is the temperature of the atoms. Because *T* is derived directly from the time of flight spectrum, we shall plot our data as a function of *T* rather than of *s*. The parameter η would be unity for a detector whose resolution width *d* is small compared with the correlation length. Our *d* is smaller than $l_y$ but larger than $l_x$, and in this case the convolution by the detector resolution results in an η given roughly by $l_x/2d \sim 5\%$. We use Eq. 1 to fit the data by using η and the $l_i$ as fit parameters and compare the results to the ideal gas model (*21*).

The results for $l_x$, $l_y$, and $l_z$ for our three temperatures are plotted in Fig. 3A. The fitted values of $l_x$ are ~450 μm and are determined by the detector resolution rather than the true coherence length along *x*. The value of $l_y$ has been corrected for the finite spatial resolution of the detector. The fitted value of $l_z$ requires no correction, because in the vertical direction the resolution of the detector is much better. $l_y$ and $l_z$ are consistent and agree with the prediction using the known trap frequencies and temperatures. Figure 3B shows the fitted value of η versus temperature, along with the prediction of the same ideal gas model as in Fig. 3A, using the measured detector resolution. The data are in reasonable agreement with the model, although we may be seeing too little contrast at the lowest temperature. The run at 0.55 μK was above, but very close to, the BEC transition temperature. (We know this because, when taking data at 0.55 μK, about one-third of the shots contained small BECs; these runs were eliminated before plotting Fig. 2.) Future work will include examining whether the effect of the repulsive interactions between atoms or finite atom number must be taken into account.

The results reported here show the power of single particle detection in the study of quantum gases. The correlations we have observed are among the simplest that should be present. Two recent experiments have shown correlations in a Mott insulator (*11*) as well as in atoms produced from the breakup of molecules near a Feshbach resonance (*12*). Improved observations of these effects may be possible with individual particle detection. Other atom pair production mechanisms, such as four-wave mixing (*23*, *24*), can be investigated. A fermionic analog to this experiment using $^3$He would also be (*25*) of great interest.

### References and Notes


1. R. Hanbury Brown, R. Q. Twiss, *Nature* **177**, 27 (1956).
2. F. T. Arecchi, E. Gatti, A. Sona, *Phys. Lett.* **20**, 27 (1966).
3. R. J. Glauber, *Phys. Rev. Lett.* **10**, 84 (1963).
4. R. J. Glauber, *Quantum Optics and Electronics*, C. DeWitt, A. Blandin, C. Cohen-Tannoudji, Eds. (Gordon and Breach, New York, 1965), p. 63.
5. G. Baym, *Acta Phys. Pol. B* **29**, 1839 (1998).
6. B. Berne, R. Pecora, *Dynamic Light Scattering* (Dover, New York, 2000).
7. U. Fano, *Am. J. Phys.* **29**, 539 (1961).
8. R. Hanbury Brown, R. Twiss, *Nature* **178**, 1046 (1956).
9. J. S. Bell, *Speakable and Unspeakable in Quantum Mechanics* (Cambridge Univ. Press, Cambridge, ed. 2, 2004).
10. M. Yasuda, F. Shimizu, *Phys. Rev. Lett.* **77**, 3090 (1996).
11. S. Fölling *et al.*, *Nature* **434**, 481 (2005).

12. M. Greiner, C. A. Regal, J. T. Stewart, D. S. Jin, *Phys. Rev. Lett.* **94**, 110401 (2005).
13. M. Henny *et al.*, *Science* **284**, 296 (1999).
14. W. D. Oliver, J. Kim, R. C. Liu, Y. Yamamoto, *Science* **284**, 299 (1999).
15. H. Kiesel, A. Renz, F. Hasselbach, *Nature* **418**, 392 (2002).
16. Y. Kagan, B. V. Svistunov, G. V. Shlyapnikov, *Sov. Phys. JETP* **42**, 209 (1985).
17. E. A. Burt *et al.*, *Phys. Rev. Lett.* **79**, 337 (1997).
18. B. Laburthe Tolra *et al.*, *Phys. Rev. Lett.* **92**, 190401 (2004).
19. A. Robert *et al.*, *Science* **292**, 461 (2001); published online 22 March 2001 (10.1126/science.1060622).
20. O. Jagutzki *et al.*, *Nucl. Instrum. Methods Phys. Res. A* **477**, 244 (2004).
21. See supporting online materials on *Science* Online for details.
22. M. Naraschewski, R. Glauber, *Phys. Rev. A* **59**, 4595 (1999).
23. L. Deng *et al.*, *Nature* **398**, 218 (1999).
24. J. Vogels, K. Xu, W. Ketterle, *Phys. Rev. Lett.* **89**, 020401 (2002).
25. R. Stas, J. McNamara, W. Hogervorst, W. Vassen, *Phys. Rev. Lett.* **93**, 053001 (2004).
26. A. Öttl, S. Ritter, M. Köhl, T. Esslinger, *Phys. Rev. Lett.* **95**, 090404 (2005).
27. After submission of this manuscript, we became aware of a related experiment concerning atom correlations in an atom laser (*26*). We thank R. Sellem of the Détection Temps, Position Image Technology Division (supported by the Mission Ressources et Compétences Technologiques–CNRS Federation FR2764 and by the Université Paris-Sud) for a decisive role in the development of the time-to-digital converter, and O. Jagutzki for advice on delay lines.

**Supporting Online Material**
www.sciencemag.org/cgi/content/full/1118024/DC1
SOM Text

27 July 2005; accepted 5 September 2005
Published online 15 September 2005;
10.1126/science.1118024
Include this information when citing this paper.

# Quantum Coherence in an Optical Modulator

**S. G. Carter,[1]* V. Birkedal,[1]† C. S. Wang,[2] L. A. Coldren,[2] A. V. Maslov,[3] D. S. Citrin,[4,5] M. S. Sherwin[1]‡**

**Semiconductor quantum well electroabsorption modulators are widely used to modulate near-infrared (NIR) radiation at frequencies below 0.1 terahertz (THz). Here, the NIR absorption of undoped quantum wells was modulated by strong electric fields with frequencies between 1.5 and 3.9 THz. The THz field coupled two excited states (excitons) of the quantum wells, as manifested by a new THz frequency- and power-dependent NIR absorption line. Nonperturbative theory and experiment indicate that the THz field generated a coherent quantum superposition of an absorbing and a nonabsorbing exciton. This quantum coherence may yield new applications for quantum well modulators in optical communications.**

Quantum three-state systems in which two of the states are strongly coupled by an intense laser field have been widely studied in atomic and molecular systems (*1*). The energies of the quantum states are altered as they are "dressed" by the strong light-matter interaction. Such dressed states were first observed by Autler and Townes (AT) in a molecular system driven by a strong radio-frequency field and probed by weak microwaves (*2*). When a radio-frequency resonance occurred, the microwave absorption line split in two. In three-state systems with weak coupling to the environment, AT splitting can evolve into electromagnetically induced transparency (EIT), in which a strong coupling beam induces transparency at a resonance at which the undriven system is opaque (*3*). This transparency is due to quantum interference between the dressed states. EIT is the basis for slow (*4*) and stopped light (*5*, *6*) in atomic systems.

A variety of quantum systems similar to atomic three-state systems can be engineered in semiconductor quantum wells (QWs). A QW is a layer of one semiconductor grown between semiconductors with larger band gaps (*7*). The layer with the smaller gap is sufficiently thin that well-defined sets of quantized states, or subbands, are associated with electron motion parallel to the growth direction. Within each subband, there is a continuum of states associated with different momenta parallel to the plane of the QW (perpendicular to the growth direction). AT-like splitting (*8*), quantum interference (*9*, *10*), and EIT (*11*, *12*) have been reported in QWs, but their observation has been more difficult than in atoms and molecules. This is in part because of much larger absorption linewidths, which result from disorder, from stronger coupling to the environment, or from scattering between subbands.

We have fabricated a particularly simple three-level system in undoped QWs (Fig. 1). The excitation with the lowest frequency occurs at about 350 THz (wavelength 857 nm or energy 1.46 eV) when an electron is promoted from the filled valence subband of highest energy (labeled h1) to the empty conduction subband of lowest energy (labeled e1). The excited electron binds with the hole it left behind to form an exciton with a hydrogen-like wave function in the QW plane. Transitions between different in-plane states (e.g., the 1s and 2p states) are allowed only for in-plane THz polarizations (*13*, *14*), which are not present in the experiments discussed here. The lowest exciton state is labeled h1X. The next exciton state, h2X, consists of an electron from e1 and a hole from the second highest valence subband, h2. NIR transitions between the crystal ground state and h2X are not allowed because of quantum mechanical selection rules. However, intersubband transitions from h1X to h2X are allowed for THz radiation polarized in the growth direction. The three states analogous to those in an AT picture are the crystal ground state, the lowest exciton h1X, and the second exciton h2X (*15*).

This report explores the NIR absorption of undoped QWs at low temperatures (~10 K) when they are driven by strong electric fields polarized in the growth direction with frequencies between 1.5 and 3.9 THz. Because the frequency of the THz laser is about 1% of that required to create an exciton, the strong laser field does not alter the populations of the quantum states of the system. Near 3.4 THz, the drive frequency is resonant with the transition between the two lowest exciton states. The AT splitting of excitons driven by strong intersubband radiation is experimentally observed, and theoretical predictions (*16*, *17*) are confirmed.

The sample consists of 10 $In_{0.06}Ga_{0.94}As$ QWs (each 143 Å) separated by $Al_{0.3}Ga_{0.7}As$ barriers (300 Å). InGaAs QWs were used instead of GaAs QWs so that the GaAs substrate was transparent for NIR light near the exciton energies. A 100-nm layer of aluminum was deposited on the surface of the sample on which the QWs were grown. The metallic boundary condition improved THz coupling and ensured that the THz field at the QWs was polarized almost perfectly in the growth direction (*18*). The interband absorption was probed using broadband, incoherent, NIR light from an 850-nm light-emitting diode focused onto the sample backside to a spot size ~250 μm in diameter. The NIR intensity was less than 0.3 W/cm$^2$. As illustrated in Fig. 1, the NIR beam was transmitted through the transparent substrate, interacted with the QWs, was reflected off of the Al layer, and was then collected and sent to a monochromator with an intensified charge-coupled device detector. The reflected NIR beam was measured during the 1 to 1.5 μs at the peak of the THz

[1]Physics Department and Institute for Quantum and Complex Dynamics (iQCD), Broida Hall Building 572, Room 3410, [2]Electrical and Computer Engineering Department, University of California, Santa Barbara, CA 93106, USA. [3]Center for Nanotechnology, NASA Ames Research Center, MS 229-1, Moffett Field, CA 94035, USA. [4]Electrical and Computer Engineering, Georgia Institute of Technology, Atlanta, GA 30332, USA. [5]Georgia Tech Lorraine, Metz Technopole, 2-3 rue Marconi, 57070 Metz, France.

*Present address: JILA, University of Colorado, 440 UCB, Boulder, CO 80309, USA.
†née Ciulin. Present address: Department of Chemistry, University of Aarhus, Langelandsgade 140, DK-8000 Århus C, Denmark.
‡To whom correspondence should be addressed. E-mail: sherwin@physics.ucsb.edu

pulse (fig. S2). The sample was mounted in a closed-cycle refrigerator and maintained at a temperature near 10 K. The lowest curves in Fig. 1, A to C, display the NIR reflectivity measured without the THz field. (The reflectivity is essentially double-pass transmission in this geometry.) The strong absorption line is from h1X. As expected, no absorption is observed from h2X. The energy of h2X is expected to be ~3.34 THz (13.8 meV) above h1X from calculations (*19*).

The THz radiation, given by the UCSB Free-Electron Lasers, was focused onto the edge of the sample with an off-axis parabolic mirror. The spot size was ~400 μm in diameter for THz frequencies between 2.5 and 3.9 THz, near the h1X-h2X resonance. The THz beam was on for ~4 μs with a repetition rate near 1 Hz. The maximum peak power incident on the sample was ~2 kW, giving a maximum intensity in the sample of ~1 MW/cm$^2$ (~15 kV/cm electric field amplitude). [This estimate of the electric field ignores propagation inside the sample and the Al coating on the surface (*18*)].

The effect of the THz field on the sample reflectivity was quite striking (Fig. 1, A to C). Each graph displays the reflectivity for a series of THz intensities. In Fig. 1A the THz frequency is $f_{THz}$ = 2.52 THz, below the expected h1X-h2X resonance. As the THz intensity increased, the absorption line redshifted and a weaker absorption line appeared above the undriven exciton energy. Near the expected resonance, at $f_{THz}$ = 3.42 THz (Fig. 1B), there was a clear symmetric splitting of the exciton line, which increased as a function of intensity. Just above the resonance, at $f_{THz}$ = 3.90 THz (Fig. 1C), a weaker absorption line appeared below the undriven exciton energy. These measurements were carried out at ~10 K, but the splitting at $f_{THz}$ = 3.42 THz was observed at temperatures up to 78 K.

The calculated reflectivity of a THz-driven QW is shown in Fig. 2 for THz intensities that give spectra comparable to those in Fig. 1. These results were obtained by numerically solving the Schrödinger equation for the dynamics of an optically created electron-hole pair in an infinitely deep QW. The quantization of the electron-hole states, the Coulomb interaction, and the THz field are all treated on an equal footing, without resorting to perturbation theory [see (*20*) for more details]. In essence, the THz field rocks the QW potential, which couples the various confined QW states in a dynamic fashion. All of the QW states are included in the calculations. This approach is equivalent to solving the polarization equation of the semiconductor Bloch equations (SBEs) in the low-density limit (*21*). The reflectivity is defined as the fraction of the incident optical power at a given NIR frequency that is not absorbed.

For these calculations, the absorption strength and energy position of h1X for zero

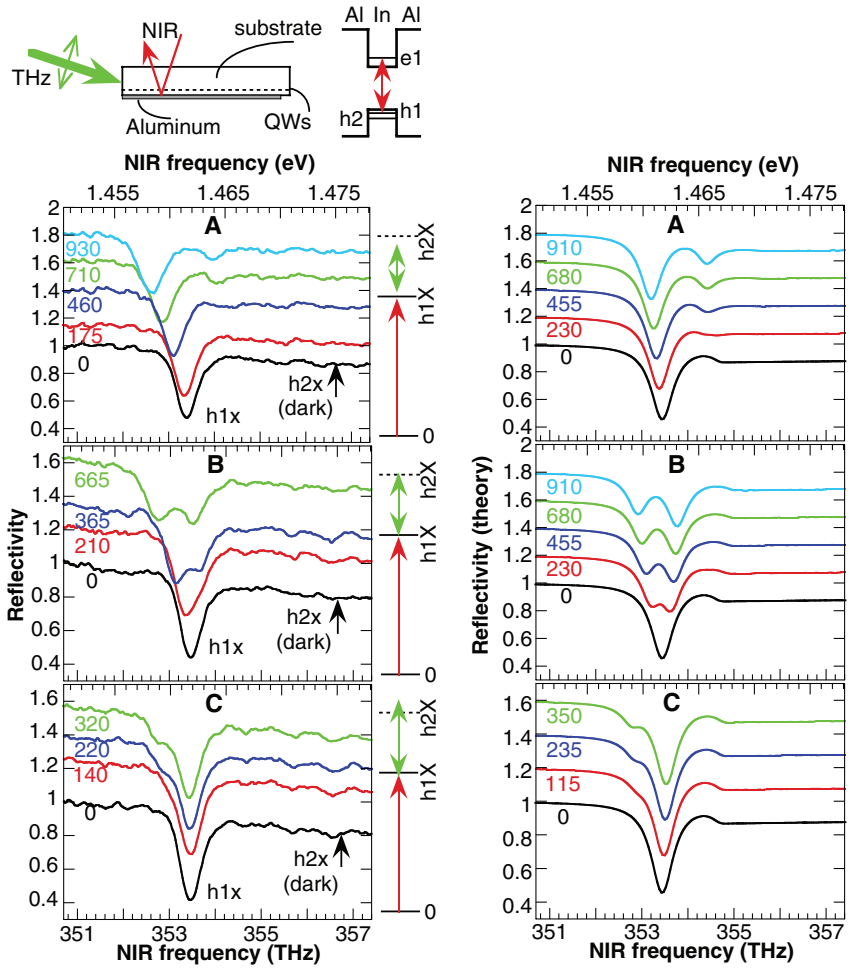


**Fig. 1 (left).** Reflectivity spectra for a series of THz intensities at $f_{THz}$ = (**A**) 2.52 THz, (**B**) 3.42 THz, and (**C**) 3.90 THz. The spectra are offset and labeled according to the THz intensities (in kW/cm$^2$). Level diagrams illustrating the detuning from the expected h1X-h2X resonance are shown to the right of each graph. A schematic of the experimental geometry and the band diagram of a QW along with the relevant subband energies are displayed above. The red arrow represents the lowest excitation of the system, the h1X exciton. The AlGaAs barriers are labeled "Al" and the InGaAs layer is labeled "In." **Fig. 2 (right).** Calculated reflectivity spectra for a series of THz intensities at $f_{THz}$ = (**A**) 2.52 THz, (**B**) 3.42 THz, and (**C**) 3.90 THz. The spectra are offset and labeled according to the THz intensity (in kW/cm$^2$). The absorption strength and energy position of the spectrum for zero THz field were set to best fit the measured reflectivity.

THz field were set to best fit the measured reflectivity. The calculated reflectivity in the presence of the THz field is qualitatively similar to the measured reflectivity, although small differences can be seen. It appears that the calculated splitting at 3.42 THz is more asymmetric than that observed experimentally, indicating that the experimental h1X-h2X resonance is closer to 3.42 THz than 3.34 THz. Also, there is an overall redshift of the measured reflectivity with increasing THz intensity that does not appear in the calculated spectra. This redshift is most likely due to heating by the THz beam and can clearly be seen in fig. S1A, where the absorption line positions are plotted as a function of intensity. The separation between the two absorption lines on resonance at $f_{THz}$ = 3.42 THz is plotted as a function of intensity in fig. S1B. The splitting is discernible over a factor of ~4 in THz intensity (~2 in THz field). Theory and experiment are not far from one another over this limited range, although the dependence of the splitting on THz intensity is closer to a line than the square root function predicted by theory. More work must be done to characterize and understand the dependence of the splitting on THz intensity (*18*).

The reflectivity was measured at many THz frequencies from $f_{THz}$ = 1.53 to 3.90 THz. Absorption spectra for $f_{THz}$ = 2.82 through 3.90 THz (Fig. 3) were obtained by subtracting a linear decrease in reflectivity over the measured NIR frequency span and then calculating the negative natural logarithm of the reflectivity. These absorption spectra were then fit to two Lorentzians. The spectra at $f_{THz}$ = 1.53, 1.98, and 2.52 THz (not shown) were more difficult to fit because the second absorption line was so weak. Differential spectra (spec-

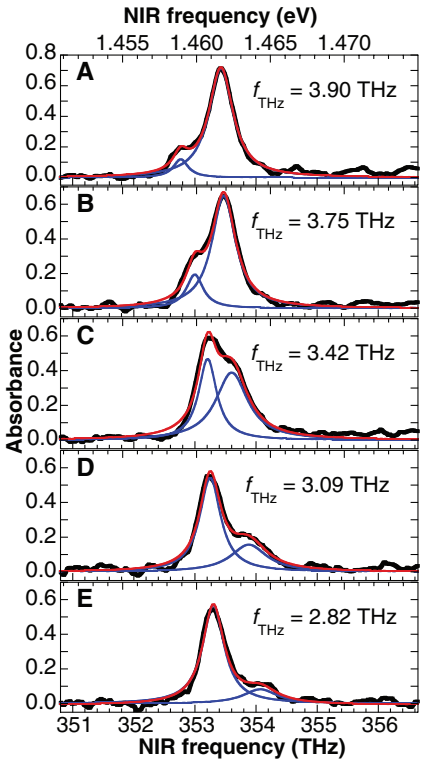


**Fig. 3.** Absorption spectra and fits for $f_{THz}$ = 3.90 THz (**A**) to 2.82 THz (**E**). The black lines represent the absorption obtained from the reflectivity spectra by correcting for the downward slope due to continuum absorption and by taking the negative natural logarithm. The red curves are fits to two Lorentzians; the blue curves are the individual Lorentzians.

trum with THz field minus spectrum without THz field divided by spectrum without THz field) were used to determine the absorption line positions.

Figure 4 displays the absorption line positions as a function of THz frequency. The spectra used were all obtained with a THz intensity near 300 kW/cm$^2$ (within 10%), relatively low because this was the highest available intensity at $f_{THz}$ = 3.75 THz and 3.90 THz. The anticrossing behavior in Fig. 4 near the h1X-h2X resonance is expected for the AT effect. The two absorption lines are associated with the two excitons dressed by the THz field. On resonance, the oscillator strength is shared equally between the two dressed states and the two absorption peaks are equal in magnitude. Off-resonance, the oscillator strength is strongest for the absorption line nearest the undriven exciton line. For low THz frequencies, the weaker peak approaches the h2X energy. The data points connected by solid lines in Fig. 4 are the results of calculations using the model equivalent to the SBE for an intensity of 375 kW/cm$^2$, which agree well with the measurements. The disagreement at 1.53 and 1.98 THz (lower positions) may be due to uncertainty in the THz intensity (*18*).

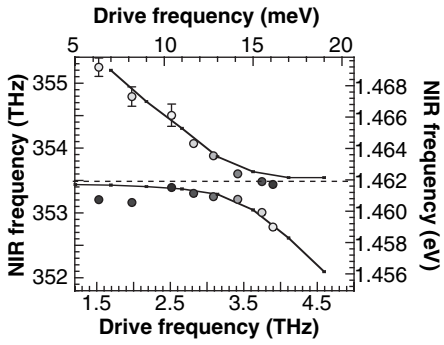


**Fig. 4.** Measured absorption line positions (large circles) versus THz frequency for a THz intensity of ~300 kW/cm$^2$. The absorption strength for each point is represented on a grayscale; darker circles indicate stronger absorption. The standard error of the positions from fitting is indicated by error bars except where smaller than the circle diameter. The data points and solid line represent the calculated absorption positions at a THz intensity of 375 kW/cm$^2$. Near the resonance at $f_{THz}$ = 3.4 THz, the calculated spectra were fit to two Lorentzians to determine absorption positions; away from resonance, the positions were taken at the minimum of the reflectivity for each peak. The horizontal dashed line marks the undriven exciton line position.

Quantum wells driven by growth-direction electric fields are already important as electroabsorption modulators for fiber-optic communications operating with bandwidths <100 GHz (0.1 THz) (*22*). The basis for the QW modulators (QWMs) is the dc quantum-confined Stark effect, wherein a dc electric field polarized in the growth direction causes a redshift of the h1x absorption (*23*). The operating frequencies of QWMs are smaller than the exciton's linewidth. Thus, the response is adiabatic: The NIR absorption spectrum at any instant is determined only by the electric field at that same instant, and not by the modulation frequency. Modulation at higher frequencies is desirable given the 50-THz bandwidth of optical fibers.

Our results show that fascinating quantum effects occur when QWMs are driven in the high-frequency diabatic limit. Most important, AT splitting of excitons due to a strong THz field has been observed. The decrease in absorption at the undriven exciton resonance in the presence of the THz field is certainly suggestive of EIT, although the linewidth of h2X is not expected to be narrow enough for the required quantum interference effects.

The observation of dressed states in this system is noteworthy for several reasons. First, the effects have been observed over a wide range of THz frequencies, where the detuning from the resonance was comparable to the drive frequency. Observation of dressed states at large detunings is possible because the Rabi frequency (half the splitting on resonance) is relatively large, up to 20% of the drive frequency on resonance. Second, the THz driving field does not generate any excited-state population, in part because it is at a much lower frequency than the probe. The driving field is also quasi–continuous wave, which is rare for observations of coherent strong-field effects in semiconductors. Finally, applications to optical communications have been proposed for the THz-driven QW. Two NIR lasers resonant with different dressed states of this system interact strongly (*24*), leading to mutual transparency of the beams depending on their relative phases. This effect could be used for intermodulation of laser beams at arbitrarily low NIR intensities.

## References and Notes


1. M. O. Scully, M. S. Zubairy, *Quantum Optics* (Cambridge Univ. Press, New York, 1997), chap. 7.
2. S. H. Autler, C. H. Townes, *Phys. Rev.* **100**, 703 (1955).
3. S. E. Harris, *Phys. Today* **50**, 36 (July 1997).
4. L. V. Hau, S. E. Harris, Z. Dutton, C. H. Behroozi, *Nature* **397**, 594 (1999).
5. C. Liu, Z. Dutton, C. H. Behroozi, L. V. Hau, *Nature* **409**, 490 (2001).
6. D. F. Phillips, A. Fleischhauer, A. Mair, R. L. Walsworth, M. D. Lukin, *Phys. Rev. Lett.* **86**, 783 (2001).
7. J. H. Davies, *The Physics of Low-Dimensional Semiconductors, an Introduction* (Cambridge Univ. Press, New York, 1998).
8. J. F. Dynes, M. D. Frogley, M. Beck, J. Faist, C. C. Phillips, *Phys. Rev. Lett.* **94**, 157403 (2005).
9. J. Faist *et al.*, *Opt. Lett.* **21**, 985 (1996).
10. H. Schmidt, K. L. Campman, A. C. Gossard, A. Imamoglu, *Appl. Phys. Lett.* **70**, 3455 (1997).
11. G. B. Serapiglia, E. Paspalakis, C. Sirtori, K. L. Vodopyanov, C. C. Phillips, *Phys. Rev. Lett.* **84**, 1019 (2000).
12. M. C. Phillips *et al.*, *Phys. Rev. Lett.* **91**, 183602 (2003).
13. K. B. Nordstrom *et al.*, *Phys. Rev. Lett.* **81**, 457 (1998).
14. S. Hughes, D. S. Citrin, *Phys. Rev. B* **59**, R5288 (1999).
15. The exciton states discussed are those with a 1s in-plane wave function, as these dominate the NIR spectra. The subbands h1 and h2 are "heavy hole" subbands because of their high effective masses. Excitons formed from the valence subbands with a lighter effective mass ("light hole" subbands) are shifted to higher energies as a result of strain and do not appear in the measured spectra. Excitons associated with higher subbands (e2, h3) are sufficiently far away in energy that they should only weakly couple to h1X.
16. A. Liu, C. Z. Ning, *J. Opt. Soc. Am. B* **17**, 433 (2000).
17. A. V. Maslov, D. S. Citrin, *Phys. Rev. B* **62**, 16686 (2000).
18. See supporting data on *Science* Online.
19. All calculations were performed for a 150 Å QW with infinite barriers. The electron and hole effective masses (for the growth direction) were 0.067 $m_0$ and 0.36 $m_0$, respectively.
20. A. V. Maslov, D. S. Citrin, *IEEE J. Sel. Top. Quantum Electron.* **8**, 457 (2002).
21. H. Haug, S. W. Koch, *Quantum Theory of the Optical and Electronic Properties of Semiconductors* (World Scientific, River Edge, NJ, ed. 4, 2004).
22. D. A. B. Miller, *Opt. Photon. News* **1**, 7 (1990).
23. S. Schmitt-Rink, D. Chemla, D. A. B. Miller, *Adv. Phys.* **38**, 89 (1989).
24. A. V. Maslov, D. S. Citrin, *J. Opt. Soc. Am. B* **19**, 1905 (2002).


25. Supported by NSF grants DMR 0244390 (S.G.C., V.B., M.S.S.) and DMR 0305524 (D.S.C.) and by Sun Microsystems. We thank D. Allen, R. Owings, D. Bouwmeester, and A. Wodtke for helpful feedback on the manuscript, and D. Enyeart for skillful operation of the UCSB Free-Electron Lasers.


**Supporting Online Material**

www.sciencemag.org/cgi/content/full/310/5748/651/DC1
SOM Text
Figs. S1 and S2


16 June 2005; accepted 21 September 2005
10.1126/science.1116195

# Dating the Growth of Oceanic Crust at a Slow-Spreading Ridge

Joshua J. Schwartz,[1]* Barbara E. John,[1] Michael J. Cheadle,[1] Elena A. Miranda,[1] Craig B. Grimes,[1] Joseph L. Wooden,[2] Henry J. B. Dick[3]

Nineteen uranium-lead zircon ages of lower crustal gabbros from Atlantis Bank, Southwest Indian Ridge, constrain the growth and construction of oceanic crust at this slow-spreading midocean ridge. Approximately 75% of the gabbros accreted within error of the predicted seafloor magnetic age, whereas ~25% are significantly older. These anomalously old samples suggest either spatially varying stochastic intrusion at the ridge axis or, more likely, crystallization of older gabbros at depths of ~5 to 18 kilometers below the base of crust in the cold, axial lithosphere, which were uplifted and intruded by shallow-level magmas during the creation of Atlantis Bank.

Slow- and ultraslow-spreading ridges with spreading rates of <55 mm/year (*1*) constitute nearly 60% of the total length of midocean ridges. Results from a variety of studies (*2*–*7*) indicate that slow- and ultraslow-spreading oceanic crust is dominantly created by the emplacement of small magma bodies of up to 500 m in thickness (*7*) into zones of partially solidified crystal mush (*2*, *3*). Conventionally, these magma bodies are thought to be emplaced episodically over a short period of time beneath the axial ridge valley; however, there have been few attempts (*5*) to date the timing or rate of their emplacement. Previous U-Pb geochronologic studies of oceanic crust have either focused on dating continental breakup (*8*) or identifying much older, inherited components (*9*). Here, we provide U-Pb age determinations using sensitive high-resolution ion microprobe reverse geometry (SHRIMP-RG) of lower oceanic crust exposed at the tectonically denuded Atlantis Bank oceanic core complex (57°E) on the Southwest Indian Ridge (SWIR).

The SWIR separates the Antarctic and African plates (Fig. 1, inset). Atlantis Bank lies ~100 km south of the SWIR rift valley, where the seafloor spreading half rate is ~8.5 mm/year for the Antarctic plate (*10*, *11*). Our samples are from the footwall of a dissected, long-lived detachment fault system (*12*). Sea-surface magnetic anomalies suggest that oceanic crust at Atlantis Bank formed over a period of ~3.0 million years (My) (table S1). Atlantis Bank consists of variably deformed and denuded lower oceanic crust and upper mantle (*7*, *10*, *12*–*16*). Rocks from Ocean Drilling Program (ODP) Hole 735B and from submersible dives at Atlantis Bank include olivine gabbro, olivine gabbronorite, and oxide gabbro with minor felsic veins (*7*). Fractionated rocks, including oxide gabbro, comprise ~25% of Atlantis Bank and commonly host trace minerals (e.g., zircon) suitable for U-Pb isotopic dating (*17*). Pb/U zircon ages from ODP Hole 735B range from 11.3 million years ago (Ma) (*18*) to 11.93 ± 0.14 Ma (*17*).

We selected 17 zircon-bearing samples of lower oceanic crust (tables S1 and S2) for U-Pb SHRIMP analysis, and these samples yielded 19 Pb/U ages (including one older core age). Samples were collected by both manned submersible and remotely operated vehicles (76%) and dredge (24%). Zircon is concentrated in the more evolved rock types, but was found in olivine to oxide gabbro and in felsic veins. Weighted average $^{206}Pb/^{238}U$ ages of the samples range from 10.6 to 13.9 Ma, with errors of 0.1 to 0.6 My (0.9% to 4%). In general, Pb/U ages young to the north and are consistent with magnetic isochrons over Atlantis Bank (*10*, *11*, *19*). However, four samples (648-20, 467-8, JR31 12-68, and JR31 29-2) record significantly older zircon ages (0.7 to 2.5 My), relative to their predicted magnetic age, and one sample (645-17) has zircons with inherited cores as much as 1.5 My older than their corresponding rims. There is no observed correlation between age and rock type (table S1), and the anomalously old samples are not from any specific part of Atlantis Bank; they appear to be randomly distributed among the nonanomalous age samples and come from different structural depths (Fig. 1). Of the anomalously old samples, JR31 12-68 and 467-8 are two of the northernmost samples, and the differences between the Pb/U and the predicted magnetic ages are dependent on the location of the relatively long-lived C5n magnetic polarity epoch (*19*). Even accounting for errors associated with the location of this chron, samples JR31 12-68 and 647-8 are still significantly older than their predicted magnetic age.

Zircons in sample 645-17 have inheritance in the form of statistically older cores with ages of 12.7 to 13.6 Ma. These cores typically have higher U concentrations and Th/U ratios than their corresponding rims, indicating that crystallization of cores and rims occurred in different chemical environments. The oldest core ages (~13.6 Ma) are interpreted to reflect the true age of the igneous precursor, and the slightly younger core ages (~12.7 to 12.9 Ma) (Fig. 2) are an artifact of the primary ion beam overlapping older and younger components during spot analysis. This overlap was confirmed by detailed backscattered-electron imaging of the zircon pits after ion probe analysis (fig. S2). The inherited zircon cores are 1.5 My older than the predicted magnetic age for this portion of Atlantis Bank (*19*). In contrast, the weighted-average age of the four rims (12.12 ± 0.29 Ma) is consistent with the magnetic age and is interpreted to reflect the timing of crustal accretion at ~12.0 Ma. The observed inheritance likely represents magmatic assimilation during the primary crust-forming event.

To determine whether differences in mineral chemistry exist between the samples with inherited zircon and those without, we made electron microprobe traverses across clinopyroxene and plagioclase crystals (core to rim). The sample with inheritance (645-17) exhibits a wider range in composition for both plagioclase ($An_{26-50}$) and clinopyroxene ($Mg_{54-72}$) than do samples without inheritance (467-8 and 460-15) (table S3). X-ray mapping and microprobe analyses of plagioclase crystals in sample 645-17 (fig. S4) reveal multiple irregularly shaped, rounded, and embayed cores ($An_{42-50}$) surrounded by compositionally uniform mantles ($An_{35-37}$). The transition from core to mantle is marked by a sharp boundary ~30 μm in width. These complex zoning patterns are not observed in plagioclase crystals from samples 467-8 and 460-15. One possible explanation for these zoning patterns is that the cores are relict grains that were resorbed during infiltration of new melt. This interpretation is consistent with the inheritance recognized in this sample.

The Pb/U zircon ages reported here, together with the age reported in (*17*), allow us to place absolute constraints on the time scale for crustal growth at Atlantis Bank. In all, at least 15 (75%) of these 20 ages plot within error of their expected magnetic age (Fig. 3). However, 5 (25%) of our samples are significantly older (up to 2.5 My), indicating that construction of any given piece of slow-spreading oceanic crust may take as long as 2.5 My. This time for the growth of slow-spreading oceanic crust is an order of magnitude greater than expected in conventional

[1]Department of Geology and Geophysics, University of Wyoming, Laramie, WY 82071, USA. [2]U.S. Geological Survey, 345 Middlefield Road, Menlo Park, CA 94025, USA. [3]Woods Hole Oceanographic Institution, Woods Hole, MA 02543, USA.

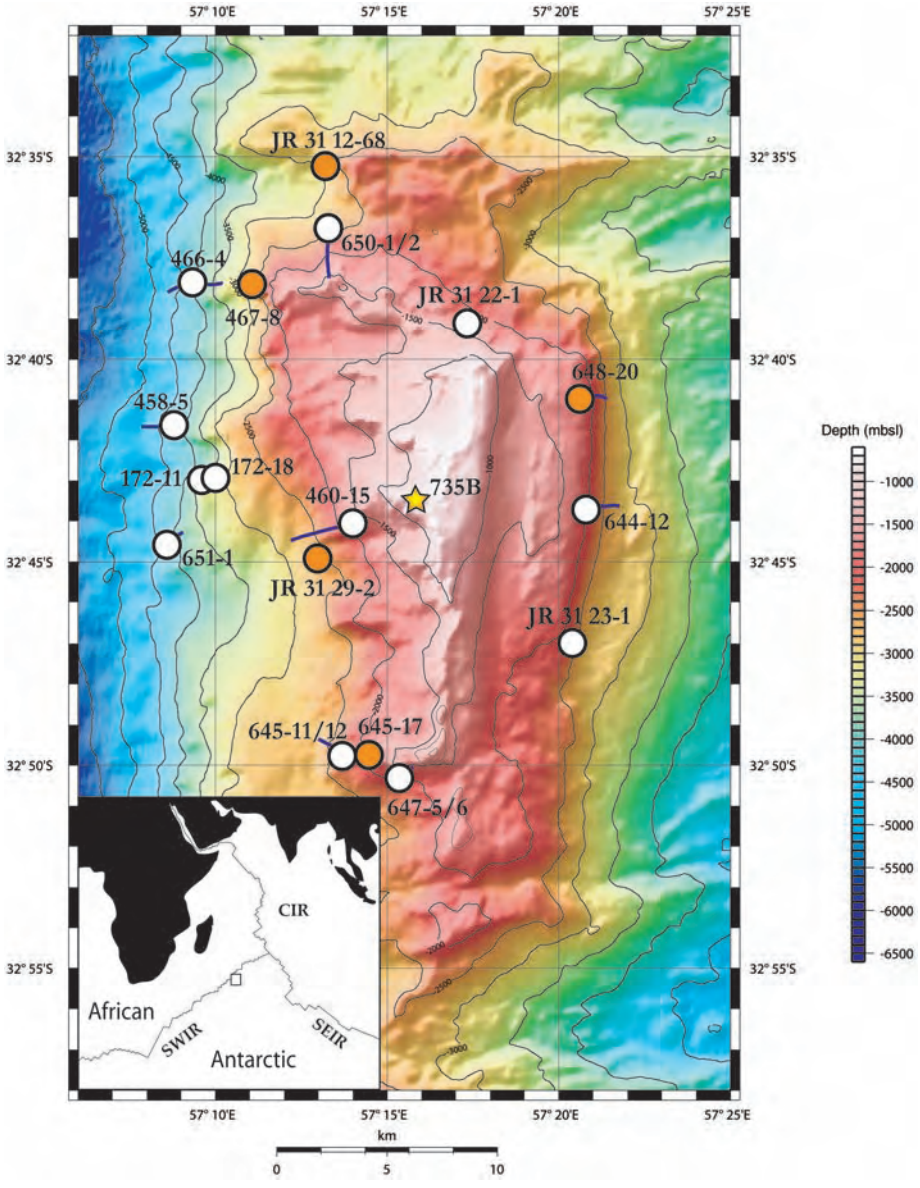


**Fig. 1.** Bathymetric map of Atlantis Bank depicting location of dive tracks (solid blue lines), sample locations (white and orange circles), and ODP Hole 735B (yellow star). Anomalously old Pb/U ages are indicated by orange circles. SWIR, SEIR, and CIR refer to Southwest Indian Ridge, Southeast Indian Ridge and Central Indian Ridge.

models for crustal accretion at midocean ridges (~100,000 to 200,000 years) (*5*).

The existence of both significantly older zircon-bearing rocks and inherited zircon cores as much as 1.5 My older than their corresponding rims (Figs. 2 and 3) requires a mechanism to incorporate older gabbroic material into lower oceanic crust and provides evidence that assimilation of preexisting gabbroic rocks took place during accretion of Atlantis Bank. One possibility is that the locus of magmatism/tectonism shifted (i.e., ridge jump), resulting in the intrusion of new gabbro into preexisting material. Along the Mid-Atlantic Ridge, documented ridge jumps involving migration of the spreading axis are characterized by derelict features including anomalous seafloor bathymetry and fossil rift valleys (*20*), neither of which has been recognized in the vicinity of the Atlantis Bank. It is also difficult to explain the random spatial distribution of anomalously older ages by a ridge-jump model. The observation that ~25% of the material is older further argues that assimilation occurred on a relatively small scale, in contrast to what might be expected from a jump of the spreading ridge beneath older, preexisting crust.

A second possibility is that magmatism varied stochastically in space and time over the full width of the rift valley, resulting in the entrapment of portions of older lower crust by subsequent intrusions. Thus, the older ages that we observe could be from remnants of earlier intrusive bodies, which were temporarily trapped beneath the rift valley before being transported away as part of the heterogeneous crust that forms Atlantis Bank. Although this process may account for some of the younger anomalously old ages, it is difficult to envision portions of the lower crust being trapped for 2.5 My (the oldest anomalous age recorded by our samples).

Uplift and assimilation of previously crystallized gabbroic rocks in the lithospheric upper mantle beneath the axial valley is another mechanism to incorporate older material into a younger crust (Fig. 4). Assuming that the present-day mean, half-spreading rate at the SWIR (7.0 mm/year) roughly corresponds to mantle upwelling rates, a zircon-bearing rock that crystallized at a depth of ~18 km in the mantle beneath the ridge axis would take ~2.5 My to reach the base of the crust. If this rock were assimilated by a shallow-level magma at 11.4 Ma, original zircons would record an age of ~13.9 Ma, corresponding to the oldest age recorded by our samples. Thus, if the spreading rate were constant during the formation of Atlantis Bank, the difference in time between the U-Pb zircon crystallization age and the magnetic age is a proxy for the depth at which zircon crystallized. The age range of our anomalously old samples (0.7 to 2.5 myr) would therefore record crystallization over depths of ~5 to 18 km below the base of the crust. The deduction that crystallization may occur over a range of depths below the ridge axis requires that the proportion of entrapped gabbros increases upward toward the base of the crust as the axial lithospheric mantle is uplifted (Fig. 4).

The above argument assumes that the ambient temperature of the uppermost ~18 km of mantle was less than the nominal zircon closure temperature (*21*, *22*). Although cooling rates for lithospheric mantle below midocean ridges are poorly constrained, calculated and predicted cooling rates for lower oceanic crust close to the Moho are ~$10^4$ °C/My (*23*, *24*). Cooling rates in the lithospheric mantle are likely less than $10^4$ °C/My; nonetheless, a 100-μm zircon with a cooling rate of $10^3$ to $10^4$ °C/My would have a closure temperature in excess of 1000°C, consistent with thermal and rheological models of thick lithosphere at slow- and ultraslow-spreading ridges (*25*). Thus, zircon crystallized at shallow depths in an ascending portion of the lithospheric mantle is likely to record original crystallization ages without substantial Pb loss.

Crystallization of ephemeral melt intrusions may be a common feature within the axial lithosphere of slow- and ultraslow-spreading midocean ridges (*26*). Although there is little data on their size, evolved gabbroic bodies (meters to several hundred meters in thickness) are present in the upper mantle beneath the Mid-Atlantic Ridge at 15°N, having equil-

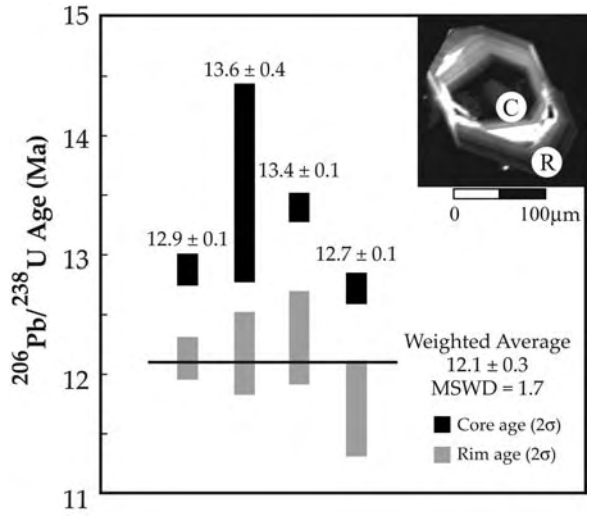


**Fig. 2.** Weighted $^{206}Pb/^{238}U$ ages of four zircon grains from 645-17. Core ages are statistically older than their corresponding rims, indicating a second period of growth at 12.1 Ma. The age of the cores is interpreted to be ~13.6 My, with slightly younger core ages reflecting sampling of older and younger components during spot analysis. A representative cathodoluminescence image is shown with the location of spot analyses. C, core; R, rim.

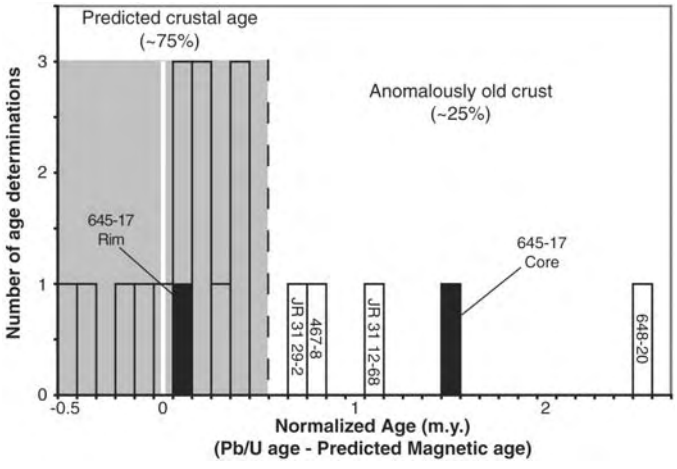


**Fig. 3.** Bar chart showing number of samples versus normalized age, including one data point from John *et al*. (*17*). Gray field encompasses uncertainties (±0.5 My) associated with U-Pb and magnetic age data. About 75% of the analyzed samples plot within error of the predicted crustal age, whereas 25% display anomalously older ages.

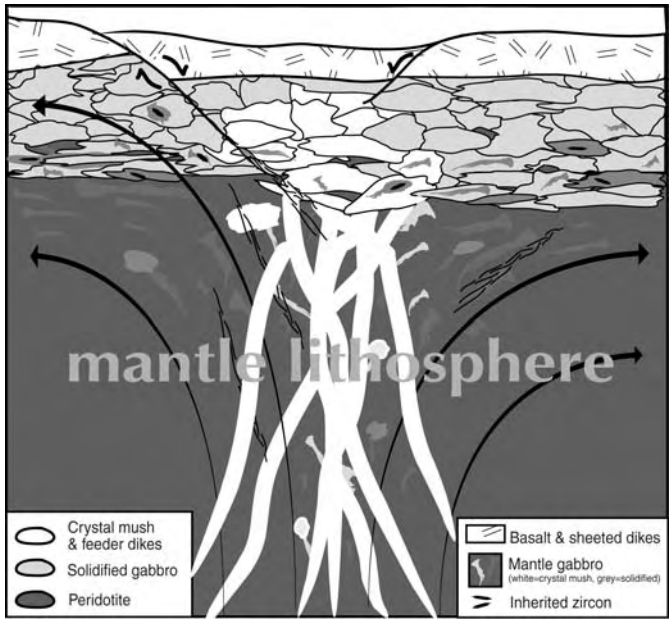


**Fig. 4.** Schematic cross section drawn at ~1:1 scale through axial lithosphere at a slow-spreading midocean ridge. Old gabbroic bodies (white) crystallize in cold lithospheric mantle, are uplifted, and become incorporated/assimilated into the lower crust by shallow-level crust-forming magmas. These older gabbroic bodies constitute up to 25% of lower oceanic crust and likely form a major component of the lithospheric mantle in slow-spreading environments.

ibrated at depths of 15 to 20 km (*27*). Trapped gabbroic bodies have been argued to form a considerable portion of the upper mantle beneath slow-spreading oceanic crust, where melt extraction is inhibited by reduced spreading rates (*28*, *29*).

These observations are corroborated by the absence of primitive lower crustal rocks sampled near the crust-mantle transition along the western flank of Atlantis Bank (e.g., sample 651-1) (*15*, *16*). The presence of disequilibrium plagioclase (sample 645-17) and augite (*30*) in gabbroic rocks from Atlantis Bank is also consistent with early crystallization of preexisting gabbroic rocks within the upper mantle, which subsequently underwent melt-rock interaction and dissolution by later crust-forming magmas. If gabbroic rocks are emplaced within the axial region of upwelling mantle at slow- and ultraslow-spreading ridges, incorporation of these gabbroic bodies is an important process in the growth of oceanic crust.

### References and Notes


1. C. Small, in *Faulting and Magmatism at Mid-Ocean Ridges*, W. R. Buck, P. T. Delaney, J. A. Karson, Y. Lagabrielle, Eds. (American Geophysical Union, Washington, DC, 1998), pp. 1–26.
2. L. S. Magde, A. H. Barclay, D. R. Toomey, R. S. Detrick, J. A. Collins, *Earth Planet. Sci. Lett.* **175**, 55 (2000).
3. M. C. Sinha *et al.*, *Geophys. J. Internat.* **135**, 731 (1998).
4. S. Allerton, J. Escartin, R. C. Searle, *Geology* **28**, 179 (2000).
5. W. P. Meurer, J. Gee, *Earth Planet. Sci. Lett.* **201**, 45 (2002).
6. M. Cannat, J. A. Karson, D. J. Miller, *Proceedings of the Ocean Drilling Program, Initial Reports, Vol. 153* (Ocean Drilling Program, College Station, TX, 1995).
7. J. H. Natland, H. J. B. Dick, in *Proc. Ocean Drill. Program Sci. Results* **176**, 69 (2002).
8. U. Schärer, J. Girardeau, G. Cornen, G. Boillot, *Earth Planet. Sci. Lett.* **181**, 555 (2000).
9. J. Pilot, C.-D. Werner, F. Haubrich, N. Baumann, *Nature* **393**, 676 (1998).
10. H. J. B. Dick *et al.*, *Proc. Ocean Drill. Program Sci. Results* **118**, 359 (1991).
11. A. Hosford *et al.*, *J. Geophys. Res.* **108**, 10.1029/2001JB00064 (2003).
12. H. J. B. Dick, J. H. Natland, D. J. Miller, S. S. Party, *Proceedings of the Ocean Drilling Program, Initial Report, Leg 176* (Ocean Drilling Program, College Station, TX, 1999).
13. H. J. B. Dick *et al.*, *Earth Planet. Sci. Lett.* **179**, 31 (2000).
14. M. Cannat *et al.*, *Proc. Ocean Drill. Program Sci. Results* **118**, 399 (1991).
15. T. Matsumoto, H. J. B. Dick, S. S. Party, *Preliminary Report (ABCDE) Yokosuka/Shinkai 6500 YK01-14 Cruise Results* (Japan Marine Science and Technology Center, Yokosuka-City, Kanagawa, Japan, 2002).
16. H. Kinoshita, H. J. B. Dick, Y. Party, *MODE '98 Leg 4 Cruise Report* ( Japan Marine Science and Technology Center, Yokosuka-City, Kanagawa, Japan, 2001).
17. B. E. John *et al.*, *Earth Planet. Sci. Lett.* **222**, 145 (2004).
18. D. Stakes, C. Mevel, M. Cannat, T. Chaput, *Proc. Ocean Drill. Program Sci. Results* **118**, 153 (1991).
19. A. G. Baines *et al.*, paper presented at American Geophysical Union Fall Meeting, San Francisco, CA, 13 to 17 December 2004.
20. A. M. Freed, J. Lin, P. Shaw, H. J. Melosh, *Geology* **23**, 971 (1995).
21. J. K. W. Lee, I. S. Williams, D. J. Ellis, *Nature* **390**, 159 (1997).
22. D. J. Cherniak, E. B. Watson, *Chem. Geol.* **172**, 5 (2001).
23. L. A. Coogan, G. R. T. Jenkin, R. N. Wilson, *Earth Planet. Sci. Lett.* **199**, 127 (2002).
24. J. Maclennan, T. Hulme, S. C. Singh, *Geology* **33**, 357 (2005).
25. G. Hirth, J. Escartin, J. Lin, *Geophys. Mono.* **106**, 291 (1998).
26. M. Cannat, *J. Geophys. Res.* **101**, 2847 (1996).
27. P. B. Kelemen, S. S. Party, *Proceedings of the Ocean Drilling Program, Initial Report, Leg 209* (Ocean Drilling Program, College Station, TX, 2004).

28. D. Lizarralde, J. B. Gaherty, J. A. Collins, G. Hirth, S. D. Kim, *Nature* **432**, 744 (2004).
29. L. A. Coogan *et al.*, *Chem. Geol.* **178**, 1 (2001).
30. A. Kvassnes, thesis, Woods Hole Oceanographic Institution and Massachusetts Institute of Technology (2004).
31. We thank G. Baines and D. Shillington for discussion; B. Ito for support; F. Mazdab and S. Swapp for sample preparation; JAMSTEC, captain, crew, and science party of MODE '98 and 2000; and F. Oberli, L. Coogan, and an anonymous reviewer for constructive reviews. This work was supported by NSF grant 0352054 to M.J.C. and B.E.J., NASA Space Grant and W.C. Hayes Fellowship to J.J.S., and NASA Space Grant to E.A.M.

**Supporting Online Material**
www.sciencemag.org/cgi/content/full/310/5748/654/DC1
Materials and Methods
Figs. S1 to S4
Tables S1 to S3
References

20 June 2005; accepted 23 September 2005
10.1126/science.1116349

# Role of Land-Surface Changes in Arctic Summer Warming

**F. S. Chapin III,[1]* M. Sturm,[5] M. C. Serreze,[6] J. P. McFadden,[7] J. R. Key,[8] A. H. Lloyd,[9] A. D. McGuire,[2] T. S. Rupp,[3] A. H. Lynch,[10] J. P. Schimel,[11] J. Beringer,[10] W. L. Chapman,[12] H. E. Epstein,[13] E. S. Euskirchen,[1] L. D. Hinzman,[4] G. Jia,[14] C.-L. Ping,[15] K. D. Tape,[1] C. D. C. Thompson,[1] D. A. Walker,[1] J. M. Welker[16]**

**A major challenge in predicting Earth's future climate state is to understand feedbacks that alter greenhouse-gas forcing. Here we synthesize field data from arctic Alaska, showing that terrestrial changes in summer albedo contribute substantially to recent high-latitude warming trends. Pronounced terrestrial summer warming in arctic Alaska correlates with a lengthening of the snow-free season that has increased atmospheric heating locally by about 3 watts per square meter per decade (similar in magnitude to the regional heating expected over multiple decades from a doubling of atmospheric $CO_2$). The continuation of current trends in shrub and tree expansion could further amplify this atmospheric heating by two to seven times.**

The Arctic provides a test bed to understand and evaluate the consequences of threshold changes in regional system dynamics. Over the past several decades, the Arctic has warmed strongly in winter (*1*). However, many Arctic thresholds relate to abrupt physical and ecological changes that occur near the freezing point of water. Paleoclimate evidence, which is mostly indicative of summer conditions, shows that the Arctic in summer is now warmer than at any time in at least the past 400 years (*2*). This warming should have a large impact on the rates of water-dependent processes. We assembled a wide range of independent data sets (surface temperature records, satellite-based estimates of cloud cover and energy exchange, ground-based measurements of albedo and energy exchange, and field observations of changes in snow cover and vegetation) to estimate recent and potential future changes in atmospheric heating in arctic Alaska. We argue that recent changes in the length of the snow-free season have triggered a set of interlinked feedbacks that will amplify future rates of summer warming.

Summer warming in arctic Alaska and western Canada has accelerated from about 0.15° to 0.17°C decade$^{-1}$ (1961–1990 and 1966–1995) (*1*, *3*) to about 0.3° to 0.4°C decade$^{-1}$ (1961–2004; Fig. 1). There has also been a shift from summer cooling to warming in Greenland and Scandinavia, more pronounced warming in Siberia, and continued summer warming in the European Russian Arctic.

The pronounced summer warming in Alaska cannot be readily understood from changes in atmospheric circulation, sea ice, or cloud cover. Changes in the North Atlantic Oscillation and Arctic Oscillation are linked to winter warming over Eurasia. Variations in the Pacific North American Teleconnection,

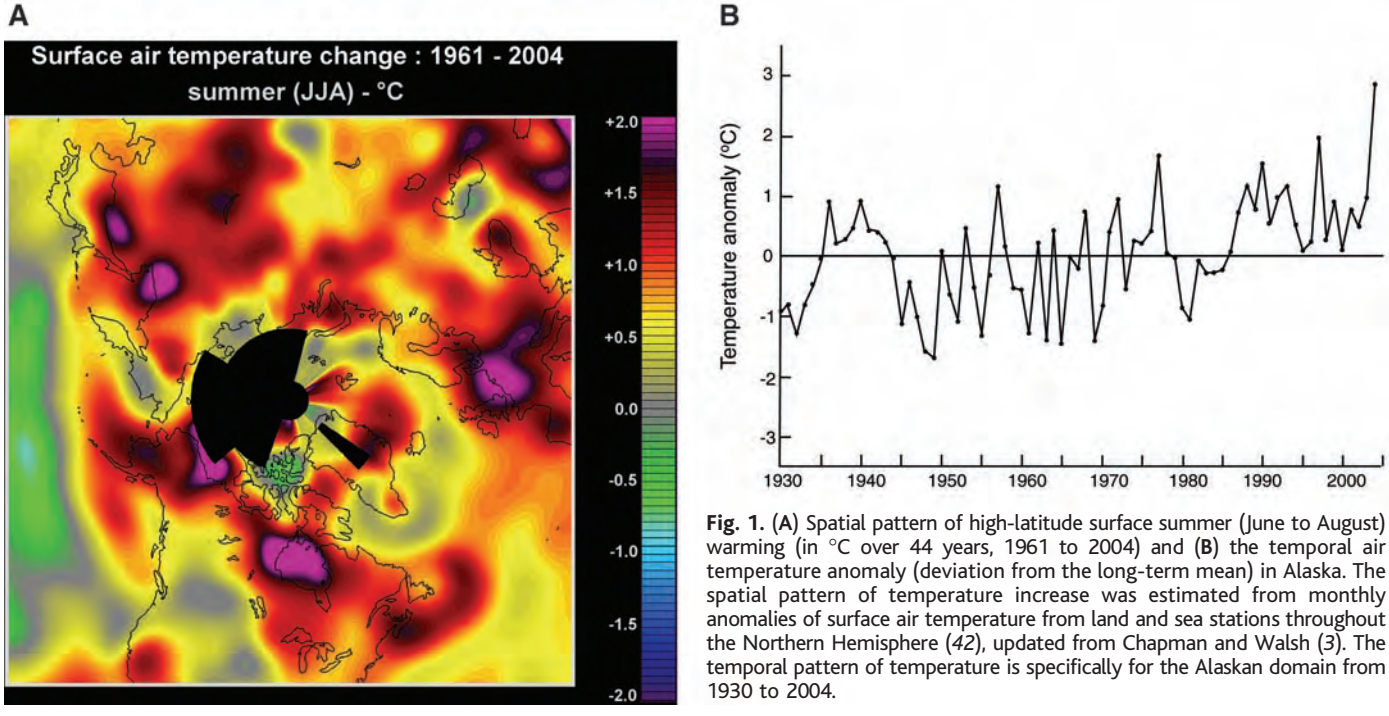


**Fig. 1.** (**A**) Spatial pattern of high-latitude surface summer (June to August) warming (in °C over 44 years, 1961 to 2004) and (**B**) the temporal air temperature anomaly (deviation from the long-term mean) in Alaska. The spatial pattern of temperature increase was estimated from monthly anomalies of surface air temperature from land and sea stations throughout the Northern Hemisphere (*42*), updated from Chapman and Walsh (*3*). The temporal pattern of temperature is specifically for the Alaskan domain from 1930 to 2004.

the Pacific Decadal Oscillation, and El Niño–Southern Oscillation have strong impacts on Alaskan winter temperatures, but their influences on summer temperatures are comparatively weak (*4*–*6*). There has been a pronounced decline in the extent of summer sea ice, especially north of Alaska and Siberia (*1*). This implies that solar energy is increasingly augmenting the sensible heat content of the ocean, some of which can then heat the atmosphere over the ocean and adjacent coast (Fig. 2). However, this mechanism fails to explain strong summer warming over interior Alaska (Fig. 1) (*7*). Further, regional warming trends associated with declining summer sea ice should be more clearly expressed in autumn and winter (*8*), when much of the additional ocean heat gained in summer will be released back to the atmosphere. The satellite record shows increased summer cloud cover in Alaska (Figs. 2 and 3), similar to patterns described for the circumpolar Arctic (*9*). The surface cloud radiative forcing in summer over the low-albedo Alaskan land surface tends to be negative, meaning that the decrease in downwelling shortwave radiation to the surface exceeds the increase in the downwelling longwave flux. The consequent reduction in surface net radiation (Fig. 3) would tend to dampen warming resulting from other causes (*9*).

The summer warming in Alaska is best explained by a lengthening of the snow-free season, causing sensible heating of the lower atmosphere to begin earlier (Fig. 2). Snowmelt has advanced 1.3 days decade$^{-1}$ at Barrow (coastal), Alaska (*10*); 2.3 days decade$^{-1}$ averaged over several (mainly

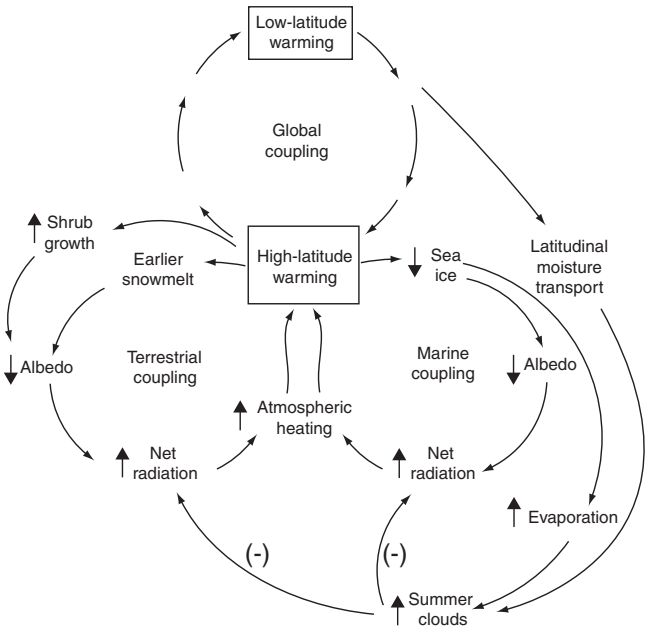


**Fig. 2.** Diagram of feedback loops that couple climatic processes in arctic Alaska. Arrows linking processes indicate a positive effect of one process on another unless otherwise indicated (by minus signs). Quantification of the terrestrial coupling feedback loop is provided in Table 2.

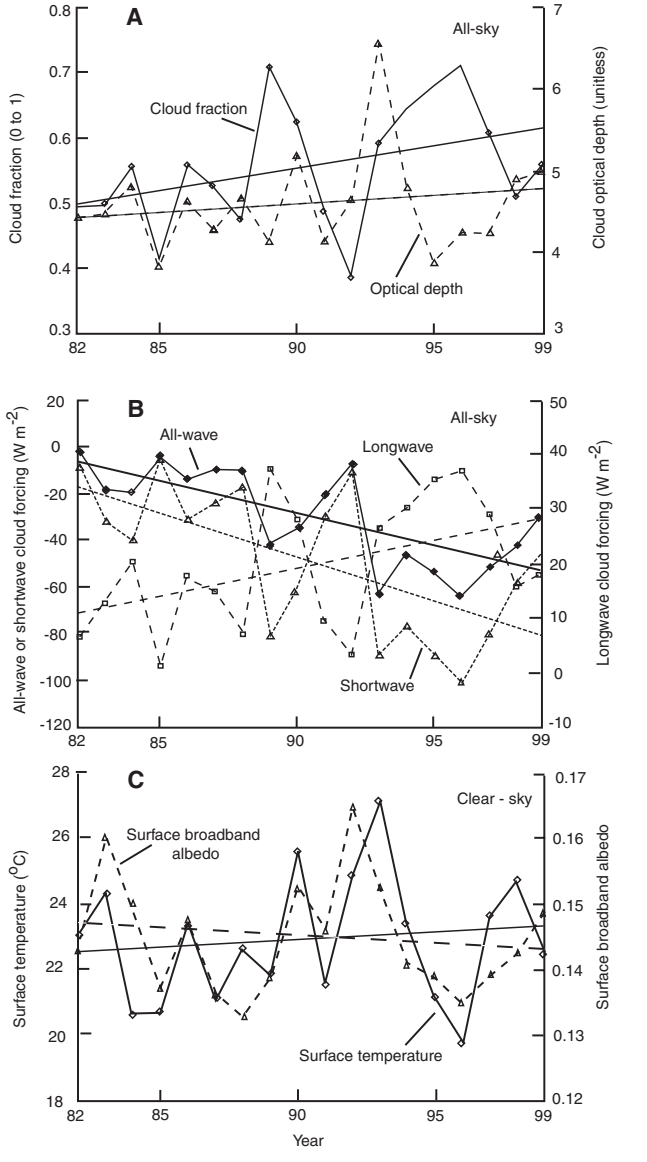


**Fig. 3.** Satellite record of temporal changes in (**A**) mean summer (June to August) cloud fraction [slope ($S$) = 0.0068, $P$ = 0.11] and optical depth ($S$ = 0.0201, $P$ = 0.5); (**B**) mean summer cloud radiative forcing [net ($S$ = –2.71, $P$ = 0.001), longwave ($S$ = 1.02, $P$ = 0.05), and shortwave ($S$ = –3.73, $P$ = 0.004)]; and (**C**) clear-sky summer broadband albedo ($S$ = –0.0002; $P$ = 0.6) and surface temperature ($S$ = 0.050, $P$ = 0.6) in arctic tundra on the North Slope of Alaska. Data for the Alaskan domain are drawn from the panarctic data set of Wang and Key (*9*, *42*).

[1]Institute of Arctic Biology; [2]U.S. Geological Survey, Alaska Cooperative Fish and Wildlife Research Unit; [3]Department of Forest Sciences; [4]Institute of Northern Engineering; University of Alaska Fairbanks, Fairbanks, AK 99775, USA. [5]U.S. Army Cold Regions Research and Engineering Laboratory Alaska, Ft. Wainwright, AK 99703–0170, USA. [6]Cooperative Institute for Research in the Environmental Sciences, University of Colorado, Boulder, CO 80309–0216, USA. [7]Department of Ecology, Evolution, and Behavior, University of Minnesota, Saint Paul, MN 55108, USA. [8]National Oceanic and Atmospheric Administration/National Environmental, Satellite, Data, and Information Service, Madison, WI 53706, USA. [9]Department of Biology, Middlebury College, Middlebury, VT 05443, USA. [10]School of Geography and Environmental Science, Monash University, Clayton, Vic 3800, Australia. [11]Department of Ecology, Evolution and Marine Biology, University of California, Santa Barbara, CA 93106–9610, USA. [12]Department of Atmospheric Sciences, University of Illinois, Urbana, IL 61801, USA. [13]Department of Environmental Sciences, University of Virginia, Charlottesville, VA 22904–4123, USA. [14]Department of Forest, Rangeland, and Watershed Stewardship, Colorado State University, Fort Collins, CO 80523, USA. [15]Palmer Research Station, University of Alaska Fairbanks, Palmer, AK 99645, USA. [16]Environment and Natural Resources Institute, University of Alaska Anchorage, Anchorage, AK 99501, USA.

*To whom correspondence should be addressed. E-mail: terry.chapin@uaf.edu

coastal) stations (*10*); 3.6 days decade$^{-1}$ in the northern foothills of the Brooks Range (*11*); 9.1 days decade$^{-1}$ for the entire Alaskan North Slope [calculated from the satellite data set of Dye *et al*. (*12*)]; and 3 to 5 days decade$^{-1}$ for the region north of 45°N (*12*). Similarly, spring soil thaw has advanced 2.0 to 3.3 days decade$^{-1}$ over North American and Eurasian tundra (microwave satellite) (*13*) and leaf-out date has advanced by 2.7 days decade$^{-1}$ in Alaska (model estimate) (*14*) and by 4.3 days decade$^{-1}$ in North America above 40°N (satellite record) (*15*). We calculate that the observed snowmelt advance of about 2.5 (1.5 to 3.5) days decade$^{-1}$ in the Alaskan Arctic increases the energy absorbed and transferred to the atmosphere per decade by about 26 MJ m$^{-2}$ year$^{-1}$ [3.3 W m$^{-2}$ (Table 1)]. This regional decadal change is comparable (per unit of area) to the global atmospheric heating associated with a doubling of atmospheric $CO_2$, which is projected to occur over multiple decades.

Since 1950, the cover of tall shrubs within Alaska's North Slope tundra has increased 1.2% decade$^{-1}$ (from 14 to 20% cover) (*16*, *17*). The widespread nature of shrub expansion is supported by indigenous observations (*18*) and satellite-derived vegetation indices (*15*, *19*, *20*). A meta-analysis of field warming experiments at 11 arctic sites showed that increasing summer temperature by 1° to 2°C [which is the magnitude observed in Alaska in the past 20 to 30 years (Fig. 1B)] generally triggers increased shrub growth within a decade (*21*), which is consistent with (i) observations of recent shrub expansion (*16*), (ii) the paleorecord of Holocene shrub expansion during warm intervals (*22*), and (iii) greater shrub abundance at the warm end of latitudinal gradients (*23*). Although shrubs increase the amount of absorbed radiation and atmospheric heating, we estimate that they account for only about 2% of the recent warming caused by land-surface change, because of the small area over which documented shrub expansion has occurred to date (Tables 1 and 2).

At the arctic treeline, white spruce (*Picea glauca*) has both expanded into tundra and increased in density within forest tundra regions of western Alaska (*24*). Although the treeline is stable in some areas of Alaska, the majority of studied sites show a treeline advance (*25*). Climate warming promotes forest expansion by creating disturbed sites for seedling establishment in ice-rich permafrost (*26*) and promoting the growth of seedlings (*27*) and (in general) mature trees (*28*). We calculate that 11,600 km$^2$ (2.3% of the treeless area) has been converted from tundra to forest in the past 50 years, based on extrapolation of observed rates of forest expansion [2.55 km in lowlands and 0.1 km at the treeline in the past 50 years] (*25*) to the entire forest-tundra transition zone in Alaska. Although conversion to forest increases absorbed radiation and atmospheric heating 4.7-fold just before snowmelt and by 25% in midsummer, we estimate that this vegetation change accounts for only about 3% of the total warming caused by land-surface change, because of the small areal extent (0.5% decade$^{-1}$) of the vegetation change (Tables 1 and 2). On cloud-free summer days, satellites detect only a weak trend toward reduced broadband albedo and increased surface (skin) temperature over arctic Alaska (Fig. 3), which is consistent with our conclusion that recent vegetation change has caused relatively little regional summer heating.

Although the increased length of the snow-free season is the main cause of summer warming observed to date, the increasing abundance of shrubs and trees is likely to contribute disproportionately to future summer warming. The change in atmospheric heating from before to after snowmelt is much larger in low-statured tundra vegetation than in shrub and forest vegetation that masks the snow surface (Table 1). Our calculations show that if vegetation changes become more widespread, the effects of vegetation would increase substantially, while those of season length would proportionately diminish (Table 1) (*29*). How likely are these vegetation changes to occur? The conversion of arctic tundra to spruce forest never occurred during previous Holocene warm intervals (*22*) and is unlikely to be extensive in the current century because of time lags associated with migration (*30*). Shrub expansion could occur quickly, however, because small shrubs are already present in most tundra areas (*23*).

Shrubs trigger several feedback loops that influence their expansion rate. Shrub growth is stimulated by nitrogen (N) supply (*31*, *32*), so shrub expansion would be accelerated if N cycling rates increased through either increased N concentrations in litter (*33*) or winter soil warming due to snow accumulation beneath shrubs (*34*, *35*). Given observed winter temperature dependence ($Q_{10}$) (*36*), the 3° to 10°C warmer winter temperatures observed beneath shrubs should enhance N mineralization by about 170 mg of N m$^{-2}$ year$^{-1}$, a 25% increase in annual N mineralization, which could support an increase in plant production of about 15 g m$^{-2}$ year$^{-1}$ (*37*). Alternatively, the shrub expansion rate would decline if the increased C:N ratio of the more woody litter (*38*) or soil cooling due to summer shading (*39*) reduced N cycling rates. N addition triggers shrub dominance (*31*) and soil carbon (C) loss (*32*), and shrub dominance correlates with higher winter respiration (*40*) and smaller soil C pools (*41*), suggesting that the positive (stimulatory) biogeochemical feedback loop predominates (*32*).

We have shown that summer warming in the Alaskan sector is occurring primarily on

**Table 1.** Observed changes per decade in summer atmospheric (atmos.) heating (by latent plus sensible heat flux) in Alaskan tundra and potential future changes if arctic tundra were completely converted to shrub tundra or spruce forest. The observed changes are subdivided into changes due to the longer snow-free season and those due to the increased areal extent of shrublands and forest. Also shown is the change in heating associated with a doubling of atmospheric $CO_2$.

| Cause of change | Atmos. heating | | |
|---|---|---|---|
| | (MJ m$^{-2}$ year$^{-1}$)* | (% of total) | (W m$^{-2}$)† |
| Observed change in atmos. heating over tundra (per decade) | | | |
| Due to snowmelt advance‡ | 25.53 | 95 | 3.28 |
| Due to vegetation change | | | |
| Shrub expansion | 0.59 | 2 | 0.08 |
| Forest expansion | 0.88 | 3 | 0.11 |
| Total change | 27.00 | 100 | 3.47 |
| Maximum potential change in atmos. heating over tundra | | | |
| Due to complete conversion to shrubland | | | |
| Effect of snowmelt advance‡ | 19.48 | 28 | 2.51 |
| Effect of shrub expansion | 49.50 | 72 | 6.37 |
| Total change | 68.98 | 100 | 8.88 |
| Due to complete conversion to forest | | | |
| Effect of snowmelt advance‡ | 10.60 | 5 | 1.36 |
| Effect of forest expansion | 190.80 | 95 | 24.54 |
| Total change | 201.40 | 100 | 25.90 |
| Atmos. heating change caused by doubling of atmos. $CO_2$§ | | | 4.4 |

*Data are from Table 2. †Heating averaged over a 90-day snow-free season. ‡Due to an observed advance in the date of snowmelt of 2.5 days decade$^{-1}$. §(*43*).

**Table 2.** Changes from pre-snowmelt to midsummer in the energy budget of tundra, shrubland, and forest in arctic Alaska. Also shown is the observed change in energy budget (per decade) and the potential future change if arctic tundra were completely converted from tundra to shrubland or forest (*42*). $R_s$, incoming shortwave radiation; $R_n$, net radiation.

| Energy budget parameter | Vegetation type | | |
|---|---|---|---|
| | Tundra | Shrub | Forest |
| Pre-snowmelt (June) | | | |
| Albedo | 0.8* | 0.6* | 0.20† |
| $R_n$ (% of $R_s$) | 27* | 39* | 59† |
| Atmos. heating | | | |
| (% of $R_n$)‡ | 38* | 61* | 82† |
| (MJ m$^{-2}$ day$^{-1}$)§ | 2.46 | 5.71 | 11.61 |
| Post-snowmelt (June) | | | |
| Albedo‖ | 0.17 | 0.15 | 0.11 |
| Net radiation (% of $R_s$)‖ | 64.4 | 63.9 | 71.8 |
| Atmos. heating | | | |
| (% of $R_n$)‖ | 82 | 88 | 92 |
| (MJ m$^{-2}$ day$^{-1}$)§ | 12.67 | 13.50 | 15.85 |
| Summer (July) | | | |
| Albedo¶ | 0.17 ± 0.01 (5) | 0.15 ± 0.002 (7) | 0.11 ± 0.004 (10) |
| Net radiation (% of $R_s$)¶ | 64.4 ± 0.6 (8) | 63.9 ± 0.9 (6) | 71.8 ± 4.2 (8) |
| Atmos. heating | | | |
| (% of $R_n$)¶ | 82 ± 3 (11) | 88 ± 2 (7) | 92 ± 2 (18) |
| (MJ m$^{-2}$ day$^{-1}$)# | 8.45 | 9.00 | 10.57 |
| Observed change in atmos. heating over tundra (per decade) | | | |
| Due to snowmelt advance | | | |
| Atmos. heating (MJ m$^{-2}$ year$^{-1}$)** | 25.53 | 19.48 | 10.60 |
| Due to vegetation change | | | |
| Change in area | | | |
| (% of original area)†† | –1.66 | 1.20 | 0.46 |
| Atmos. heating (MJ m$^{-2}$ year$^{-1}$)‡‡ | 0 | 0.59 | 0.88 |
| Potential future change in atmos. heating over tundra due to complete vegetation conversion | | | |
| Due to snowmelt advance | | | |
| Atmos. heating (MJ m$^{-2}$ year$^{-1}$)** | – | 19.48 | 10.60 |
| Due to vegetation change | | | |
| Change in area | | | |
| (% of original area)§§ | – | 100 | 100 |
| Atmos. heating (MJ m$^{-2}$ year$^{-1}$)‡‡ | – | 49.50 | 190.80 |

*(*44*, *45*). †(*46*, *47*). ‡Measured sensible (H) plus latent heat (LE) fluxes (% of $R_n$). §Calculated as $R_s \times (R_n/R_s) \times (H + LE)/R_n$, assuming average $R_s$ at snowmelt at Barrow, Alaska (24 MJ m$^{-2}$ day$^{-1}$) (*44*). ‖Assume values after snowmelt are the same as those measured in midsummer. ¶(*46*–48) (number of sites is shown in parentheses). #Calculated as $R_s \times (R_n/R_s) \times (H + LE)/R_n$, assuming summer average $R_s$ at Toolik Lake, Alaska (16 MJ m$^{-2}$ day$^{-1}$) (*49*). **Change in daily atmospheric heating (MJ m$^{-2}$ day$^{-1}$) (post-snowmelt – pre-snowmelt) × 2.5 days of snowmelt advance per decade. ††Change per decade in observed areal extent of each vegetation type. ‡‡Change in daily heating due to vegetation change (new vegetation – original vegetation) × 90-day season × change in areal extent. §§Assume 100% conversion to the new vegetation type.

land, where a longer snow-free season has contributed more strongly to atmospheric heating than have vegetation changes. This heating more than offsets the cooling caused by increased cloudiness. However, the high temperature sensitivity of several feedback loops, particularly those associated with shrub expansion, suggests that terrestrial amplification of high-latitude warming will likely become more pronounced in the future. Improved understanding of the controls over rates of shrub expansion would reduce the likelihood of unexpected surprises regarding the magnitude of high-latitude amplification of summer warming.

### References and Notes


1. M. C. Serreze *et al.*, *Clim. Change* **46**, 159 (2000).
2. J. Overpeck *et al.*, *Science* **278**, 1251 (1997).
3. W. L. Chapman, J. E. Walsh, *Bull. Am. Meteorol. Soc.* **74**, 33 (1993).
4. S. Corti, F. Molteni, T. N. Palmer, *Nature* **398**, 799 (1999).
5. K. E. Trenberth, J. W. Hurrell, *Clim. Dyn.* **9**, 303 (1994).
6. B. Hartmann, G. Wendler, *J. Clim.*, in press.
7. J. C. Comiso, *J. Clim.* **16**, 3498 (2003).
8. Arctic Climate Impact Assessment, *Impacts of a Warming Arctic* (Cambridge Univ. Press, Cambridge, 2004).
9. X. J. Wang, J. R. Key, *Science* **299**, 1725 (2003).
10. R. S. Stone, E. G. Dutton, J. M. Harris, D. Longnecker, *J. Geophys. Res.* **107**, 4089 (2002).
11. F. S. Chapin III *et al.*, unpublished data.
12. D. G. Dye, *Hydrol. Process.* **16**, 3065 (2002).
13. N. V. Smith, S. S. Saatchi, J. T. Randerson, *J. Geophys. Res.* **109**, D12101 (2004).
14. A. R. Keyser, J. S. Kimball, R. R. Nemani, S. W. Running, *Global Change Biol.* **6** (suppl. 1), 185 (2000).
15. L. Zhou *et al.*, *J. Geophys. Res.* **106**, 20069 (2001).
16. M. Sturm, C. Racine, K. Tape, *Nature* **411**, 546 (2001).
17. K. Tape, thesis, University of Alaska Fairbanks, Fairbanks, AK (2004).
18. N. Thorpe, N. Eyegetok, N. Hakongak, Kitikmeot Elders, in *The Earth is Faster Now: Indigenous Observations of Arctic Environmental Change*, I. Krupnik, D. Jolly, Eds. (Research Consortium of the United States, Fairbanks, AK, 2002), pp. 201–239.
19. C. S. Silapaswan, D. L. Verbyla, A. D. McGuire, *Can. J. Remote Sensing* **27**, 542 (2001).
20. G. J. Jia, H. E. Epstein, D. A. Walker, *Geophys. Res. Lett.* **30**, : 2067 (2003).
21. A. M. Arft *et al.*, *Ecol. Monogr.* **69**, 491 (1999).
22. L. B. Brubaker, P. M. Anderson, F. S. Hu, in *Arctic and Alpine Biodiversity: Patterns, Causes and Ecosystem Consequences*, F. S. Chapin III, Ch. Körner, Eds. (Springer-Verlag, Berlin, 1995), pp. 111–125.
23. H. E. Epstein *et al.*, *J. Biogeogr.* **31**, 1917 (2004).
24. A. H. Lloyd, T. S. Rupp, C. L. Fastie, A. M. Starfield, *J. Geophys. Res.* **107**, 8110 (2003).
25. A. H. Lloyd, *Ecology,* in press.
26. A. H. Lloyd, K. Yoshikawa, C. L. Fastie, L. Hinzman, M. Fraver, *Permafrost Periglacial Processes* **14**, 93 (2003).
27. S. E. Hobbie, F. S. Chapin III, *J. Ecol.* **86**, 449 (1998).
28. J. M. Szeicz, G. M. MacDonald, *J. Ecol.* **83**, 873 (1995).
29. J. A. Foley, J. E. Kutzbach, M. T. Coe, S. Levis, *Nature* **371**, 52 (1994).
30. T. S. Rupp, F. S. Chapin III, A. M. Starfield, *Clim. Change* **48**, 399 (2001).
31. M. S. Bret-Harte, G. R. Shaver, F. S. Chapin III, *J. Ecol.* **90**, 251 (2002).
32. M. C. Mack, E. A. G. Schuur, M. S. Bret-Harte, G. R. Shaver, F. S. Chapin III, *Nature* **431**, 440 (2004).
33. F. S. Chapin III, G. R. Shaver, *Oecologia* **77**, 506 (1988).
34. M. Sturm *et al.*, *J. Clim.* **14**, 336 (2001).
35. M. Sturm *et al.*, *Bioscience* **55**, 17 (2005).
36. C. J. Mikan, J. P. Schimel, A. P. Doyle, *Soil Biol. Biochem.* **34**, 1785 (2002).
37. G. R. Shaver, F. S. Chapin III, *Ecol. Monogr.* **61**, 1 (1991).
38. S. E. Hobbie, *Ecol. Monogr.* **66**, 503 (1996).
39. J. P. McFadden, F. S. Chapin III, D. Y. Hollinger, *J. Geophys. Res.* **103**, 28947 (1998).
40. J. T. Fahnestock, M. H. Jones, P. D. Brooks, D. A. Walker, J. M. Welker, *J. Geophys. Res.* **103**, 29023 (1998).
41. G. L. Michaelson, C.-L. Ping, J. M. Kimble, *Arct. Alp. Res.* **28**, 414 (1996).
42. Materials and methods are available as supporting material on *Science* Online.
43. J. T. Houghton *et al.*, Eds., *Climate Change 2001: The Scientific Basis* (Cambridge Univ. Press, Cambridge, 2001).
44. S. L. Dingman *et al.*, in *An Arctic Ecosystem: The Coastal Tundra at Barrow Alaska*, J. Brown, P. C. Miller, L. L. Tieszen, F. L. Bunnell, Eds. (Dowden, Hutchinson and Ross, Stroudsburg, PA, 1980), pp. 30–65.
45. M. Sturm, T. Douglas, C. Racine, G. E. Liston, *Biogeosciences* **110**, 10.1029/2005JG000013 (2005).
46. H. P. Liu, J. T. Randerson, J. Lindfors, F. S. Chapin III, *J. Geophys. Res. Atmos.* **110**, D13101 (2005).
47. J. Beringer, F. S. Chapin III, C. D. C. Thompson, A. D. McGuire, *Agric. For. Meteorol.* **168**, 10.1016/j.agrformet.2005.05.006 (2005).
48. W. Eugster *et al.*, *Global Change Biol.* **6** (suppl. 1), 84 (2000).
49. F. S. Chapin III, W. Eugster, J. P. McFadden, A. H. Lynch, D. A. Walker, *J. Clim.* **13**, 2002 (2000).



50. This paper is a synthesis product of the Land-Atmosphere-Ice Interactions program of Arctic Systems Science, funded by NSF. The views, opinions, and findings contained in this report are those of the authors and should not be construed as an official National Oceanic and Atmospheric Administration or U.S. government position, policy, or decision.


**Supporting Online Material**
www.sciencemag.org/cgi/content/full/1117368/DC1
Methods
References


13 July 2005; accepted 13 September 2005
Published online 22 September 2005;
10.1126/science.1117368
Include this information when citing this paper.

# Ordered Liquid Aluminum at the Interface with Sapphire

S. H. Oh,[1*] Y. Kauffmann,[2*] C. Scheu,[1,3] W. D. Kaplan,[2†] M. Rühle[1]

**Understanding the nature of solid-liquid interfaces is important for many processes of technological interest, such as solidification, liquid-phase epitaxial growth, wetting, liquid-phase joining, crystal growth, and lubrication. Recent studies have reported on indirect evidence of density fluctuations at solid-liquid interfaces on the basis of x-ray scattering methods that have been complemented by atomistic simulations. We provide evidence for ordering of liquid atoms adjacent to an interface with a crystal, based on real-time high-temperature observations of alumina-aluminum solid-liquid interfaces at the atomic-length scale. In addition, crystal growth of alumina into liquid aluminum, facilitated by interfacial transport of oxygen from the microscope column, was observed in situ with the use of high-resolution transmission electron microscopy.**

Evidence of density fluctuations at solid-liquid interfaces based on x-ray scattering methods (*1*–*5*) and atomistic simulations (*6*–*11*) has promoted interest in fundamental studies of the structure of solid-liquid interfaces. A limited number of studies have been conducted by high-resolution transmission electron microscopy (HRTEM) (*12*–*16*) because of the need for suitable microscopes and material systems that facilitate the study of such experimentally challenging systems. In principle, a liquid metal in contact with a solid ceramic substrate could serve as a model system for in situ HRTEM of solid-liquid interfaces. Earlier work on electron irradiation damage of ceramics has shown that damage processes occurring in alumina ($Al_2O_3$) during transmission electron microscopy (TEM) studies induce the appearance of metallic aluminum (Al) in the form of interstitial dislocation loops, precipitates, or crystallites, as a result of electronic transition and/or ballistic knock-on displacement mechanisms (*17*, *18*). During irradiation with a high-voltage electron microscope (HVEM), the different threshold displacement energies of Al and oxygen mainly account for the selective displacement of Al ions (*19*, *20*). In situ heating in HVEM further accelerates the irradiation damage of alumina, resulting in the formation of liquid Al drops (*21*).

In this study, in situ heating TEM experiments were performed in the Max-Planck-Institut–Stuttgart high-voltage atomic resolution TEM (JEM-ARM 1250, Japanese Electron Optics Laboratory, Inc.) operating at 1.25 MeV. This 0.12-nm-point resolution microscope (*22*) is equipped with a hot-stage and a drift compensator, enabling highly stable working conditions at elevated temperatures up to 1000°C, and an electron energy loss spectroscopy (EELS) detector [Gatan Image Filter (*23*)] for analytical characterization. All experimental work done for this study was conducted between 660° and 800°C (the melting point of Al is ~660°C) and recorded on negatives or on a real-time (25 frames per second) charge-coupled device video camera. Experimental observations were obtained from pure single crystalline alumina ($\alpha$-$Al_2O_3$, sapphire) specimens with different crystalline orientations, prepared by conventional dimpling and Ar ion thinning methods (*24*).

During the examination of the specimens by HVEM and at two temperatures above the melting point of Al, two parallel processes were observed. In some regions, dissociation of the alumina was observed, and in other areas liquid aluminum droplets formed on the alumina specimen (Fig. 1A).

The dissociation of the alumina is probably due to knock-on displacement damage processes that cause oxygen atoms to be knocked out of the alumina into the microscope column, leaving the aluminum atoms behind (*19*, *20*). Above the melting point of Al, the unoxidized Al atoms rapidly diffuse to the free surface and form liquid Al droplets on the alumina specimen.

The liquid drops at the edge of the $Al_2O_3$ crystal can form different interface morphologies, such as those presented schematically in Fig. 1B. All of these interface morphologies were observed. However, only the configuration schematically shown in panel 1 of Fig. 1B provides an interface that can be interpreted by HRTEM, and only data from such interface morphologies are presented here. This was carefully checked during the experiments and subsequently confirmed by HRTEM image simulations.

Electron diffraction patterns of the droplets showed the existence of diffuse scattering rings, typical for short-range order in a liquid phase. Careful analysis of the chemical composition of the liquid droplets in situ, with the use of EELS at 800°C (fig. S1), and ex situ analysis of the solid droplets with a dedicated scanning transmission electron microscope (STEM) (VG HB-501-UX) equipped with an EELS [UHV Enfina (*23*)], confirmed that these droplets are in fact pure aluminum, and no oxygen or other elements were detected within the detection limits (~1.0 atomic %). The chemical state was further probed ex situ by EELS plasmon mapping (fig. S2). The plasmon peaks of Al and $\alpha$-$Al_2O_3$ appear at 15 and 26 eV, respectively, and provide information on the oxidation state of Al. The metallic Al state was detected in the droplets, and only a thin native oxide skin was detected at the surface of the droplets.

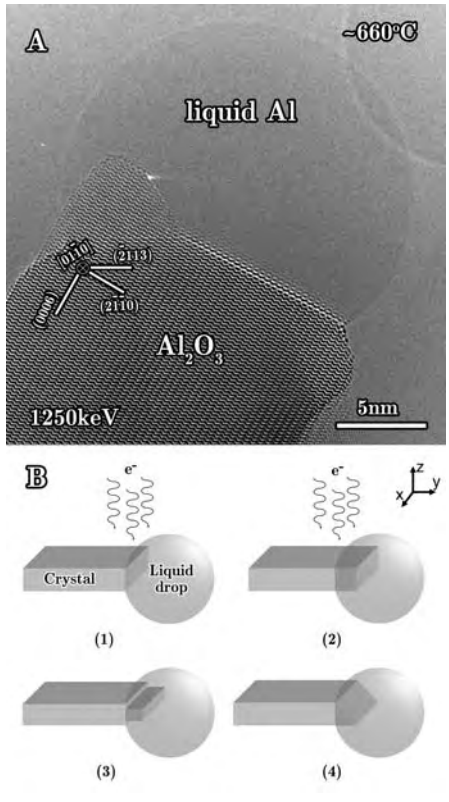


**Fig. 1.** Formation of an aluminum liquid droplet on an alumina TEM specimen. (**A**) Experimental HRTEM image of an aluminum liquid droplet formed on an alumina TEM specimen at ~660°C. The thickness of the crystal is estimated to be ~20 nm (which is approximately the diameter of the droplet). (**B**) Schematic representation of some of the possible interface morphologies formed at the liquid-crystal contact area: (1) Flat edge-on interface. The drop is attached to the substrate at the edge of the crystal, on the facet parallel to the *z* axis. (2) Buried interface inside the liquid. The drop covers the crystal from all directions so the interface of interest is buried inside the drop. (3) Ledge formation. Because of surface roughness and/or different rates of crystal growth, ledges are formed at the interface. (4) An inclined interface.

[1]Max-Planck-Institut für Metallforschung, 70569 Stuttgart, Germany. [2]Department of Materials Engineering, Technion–Israel Institute of Technology, Haifa 32000, Israel. [3]Now Department of Physical Metallurgy and Materials Testing, University of Leoben, A-8700 Leoben, Austria.

*These authors contributed equally to this work.
†To whom correspondence should be addressed. E-mail: kaplan@tx.technion.ac.il

The occurrence of these pure liquid aluminum droplets on the crystalline alumina provides a unique opportunity to probe wetting dynamics at the atomistic level and makes this system suitable for the study of interesting structural phenomena occurring at solid-liquid interfaces. We addressed an intriguing question: What is happening immediately at the interface between the crystal and the liquid at the atomic level? Real-time movies recorded during the in situ heating experiments show a dynamical evolution of the interface. Image analysis of two successive movie images demonstrates layer-by-layer crystal growth into the liquid through ledge migration (Fig. 2). The velocity of the ledge is estimated to be not less than $4 \times 10^{-5}$ cm/s at 750°C (within the time resolution of the video system, 0.04 s).

In addition, along the solid-liquid interface, periodic contrast perturbations are evident (Fig. 3) both perpendicular and parallel to the interface. These contrast perturbations were observed repeatedly (in different specimens and different crystallographic orientations) and under different imaging conditions (objective lens defocus), showing the reproducibility of such observations. The most important question is whether these contrast perturbations are due to ordering in the liquid or caused by imaging artifacts such as delocalization, objective lens defocus, and/or interface inclination.

Delocalization is an imaging artifact that can be notable in high-resolution images, which means that image details are displaced from their true locations in the specimen (*25*). For example, if we look at a line scan across a simulated HRTEM image of an alumina-vacuum interface calculated with the multislice method (*26*) and for the same imaging conditions as the experimental data (the black line in Fig. 4), we observe contrast perturbations in the vacuum which are caused by the delocalization effect. However, inspection of the periodicity of the delocalization fringes and the ones observed in the experimental micrographs (red dots in Fig. 4 and fig. S3, A and B) shows that the periodicities are totally different. To rule out the possibility that this contrast could be generated by delocalization when a "perfect" (completely disordered)

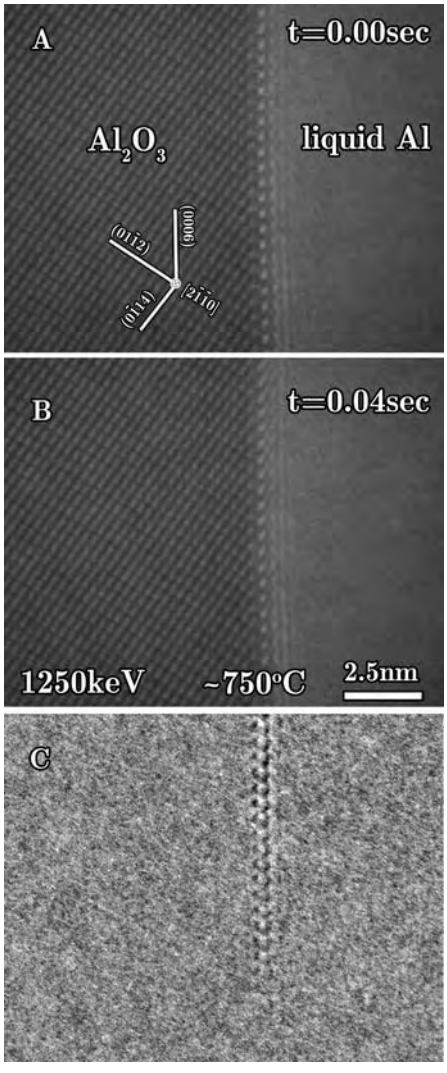


**Fig. 2.** Frame-by-frame HRTEM images of the solid-liquid interface illustrating the ledge migration motion. The frame images (**A**) and (**B**) were captured from the real-time movie (movie S1) recorded at ~750°C in a time sequence of 0.04 s. Any specimen drift contribution to the motion of the image was completely canceled out by the drift compensator device attached to the microscope. (**C**) Difference image obtained by subtracting image (A) from image (B).

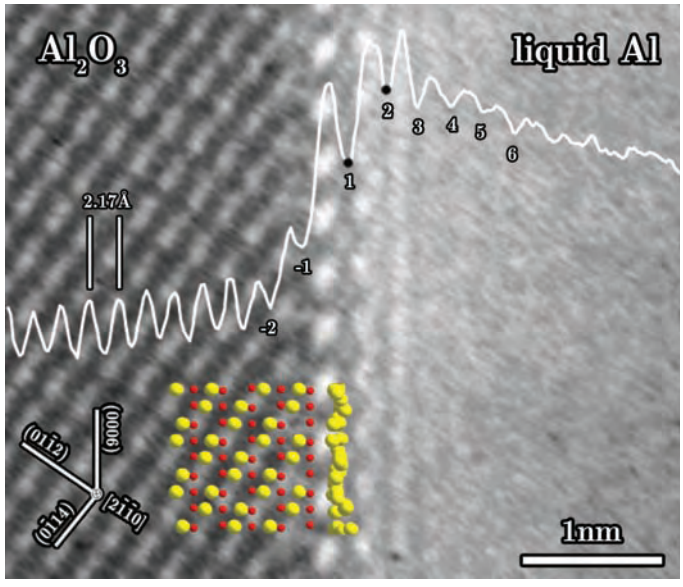


**Fig. 3.** Magnified area from a movie image acquired at ~750°C showing the contrast perturbations in the liquid parallel to the (0006) planes in alumina. The atom positions in the $Al_2O_3$ (red for oxygen and yellow for aluminum) were determined by contrast matching between simulated and experimental images at different objective lens defocus and specimen thickness values. The first layer of liquid atoms is shown schematically. The white line is an average-intensity line scan perpendicular to the interface. The numbers indicate the minima in intensity, which for the negative numbers correlate to the columns of atoms in the sapphire and for the positive numbers correlate to the intensity perturbations in the Al. The two black points at 1 and 2 indicate identified layers of ordered liquid Al.

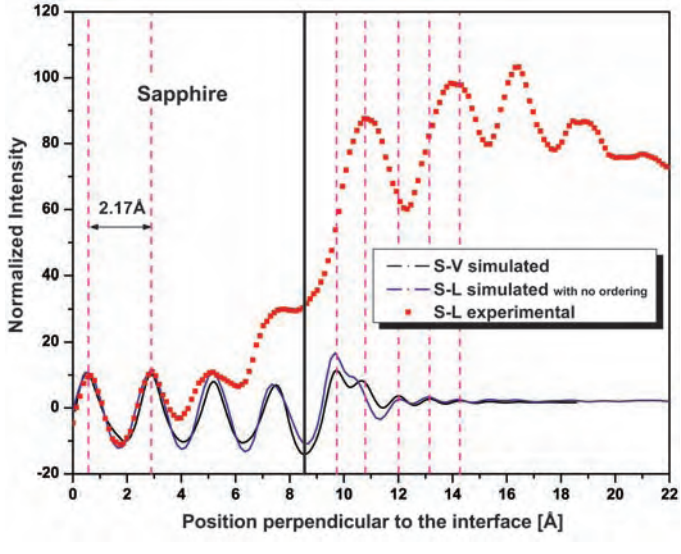


**Fig. 4.** Comparisons between the (normalized) intensity line scans from the solid-liquid experimental image (red squares), a solid-vacuum simulated image (black curve), and an artificial solid-liquid simulated interface which contains no ordering at all (blue curve) (fig. S3, C and D). All images were simulated with imaging parameters matching the experimental conditions (including thermal vibrations due to the high temperature), which were determined by iteratively matching simulated images with the experimental image of alumina (away from the interface). The vertical black line indicates the position of the interface between the crystal and the vapor/liquid.

liquid is present, a HRTEM micrograph of the interface was simulated using atomic coordinates of a perfect alumina crystal adjacent to liquid aluminum generated from molecular dynamics simulations (*27*) at a temperature of 927°C. The line scan across this interface is represented by the blue line in Fig. 4 (see also fig. S3, C and D) and shows a similar periodicity to that of the solid-vacuum interface. These comparisons show that the contrast perturbations observed in the experimental micrographs are not due only to delocalization but rather a convolution of this effect (which is always present) with ordering in the liquid. Another reasonable possibility is that these contrast perturbations are due to interface inclination or ledge growth (as shown schematically in panels 3 and 4 of Fig. 1B). However, detailed image simulations showed that for inclined interfaces or interfaces containing ledges, a gradual decrease in contrast near the interface would be seen, with a contrast very different from that generated by an interface between a crystal and a partially ordered liquid.

Measurements of the spacing between the last layer of the crystal (marked as –1) and the first contrast perturbation in the liquid (marked as 1), from the image shown in Fig. 3, result in a distance (±SD) of ~3.5 ± 0.25 Å. The next spacing between the contrast perturbations (marked as 1 and 2) is 2.85 ± 0.25 Å. Subsequent spacings in the liquid further decrease until they reach the spacing of (0006) planes in alumina (~2.17 Å), within the error range of the measurement (determined by the pixel size). The large change in spacing right at the interface may be caused by delocalization and/or the formation of a transient phase caused by oxygen transport along the interface (*28*, *29*). This can be determined only by deconvoluting the influence of delocalization from the image contrast.

The results presented here provide evidence that crystals can induce ordering in liquids, even in high-temperature metal-ceramic systems. For the specific system in case, oxygen from the microscope column permeates the ordered liquid along the interface, and then is deposited as $Al_2O_3$ by epitaxial growth, facilitated by the motion of interfacial steps. This indicates that crystal-induced ordering of liquids may play an important role in liquid phase epitaxial growth, as well as high temperature wetting. Although ordering in the form of layers of Al atoms parallel to the interface with the crystal was clearly detected, the time-averaged positions of the liquid atoms require further advanced TEM imaging techniques and comparison with computer simulations. Of particular interest is the degree of in-plane order (*11*) and comparison of the local atomistic structure in the liquid with the solidified interface and with Al-$Al_2O_3$ interfaces formed by other processing methods (*30*).


**References and Notes**

1. O. M. Magnussen *et al.*, *Phys. Rev. Lett.* **74**, 4444 (1995).
2. H. Reichert *et al.*, *Nature* **408**, 839 (2000).
3. W. J. Huisman *et al.*, *Nature* **390**, 379 (1997).
4. C. J. Yu, A. G. Richter, A. Datta, M. K. Durbin, P. Dutta, *Phys. Rev. Lett.* **82**, 2326 (1999).
5. A. K. Doerr, M. Tolan, J. P. Schlomka, W. Press, *Europhys. Lett.* **52**, 330 (2000).
6. T. P. Swiler, R. E. Loehman, *Acta Materialia* **48**, 4419 (2000).
7. F. F. Abraham, Y. Singh, *J. Chem. Phys.* **67**, 2384 (1977).
8. J. Q. Broughton, G. H. Gilmer, *J. Chem. Phys.* **84**, 5749 (1986).
9. E. T. Chen, R. N. Barnett, U. Landman, *Phys. Rev. B* **40**, 924 (1989).
10. R. L. Davidchack, B. B. Laird, *Phys. Rev. Lett.* **85**, 4751 (2000).
11. A. Hashibon, J. Adler, M. W. Finnis, W. D. Kaplan, *Interface Sci.* **9**, 175 (2001).
12. J. M. Howe, H. Saka, *MRS Bull.* **29**, 951 (2004).
13. J. M. Howe, *Philos. Mag. A* **74**, 761 (1996).
14. S. E. Donnelly *et al.*, *Science* **296**, 507 (2002).
15. S. Arai, S. Tsukimoto, S. Muto, H. Saka, *Microsc. Microanal.* **6**, 358 (2000).
16. H. Saka, K. Sasaki, S. Tsukimoto, S. Arai, *J. Mater. Res.* **20**, 1629 (2005).
17. J. E. Bonevich, L. D. Marks, *Ultramicroscopy* **35**, 161 (1991).
18. G. Dehm, K. Nadarzinski, F. Ernst, M. Rühle, *Ultramicroscopy* **63**, 49 (1996).
19. G. P. Pells, D. C. Phillips, *J. Nucl. Mater.* **80**, 207 (1979).
20. G. P. Pells, D. C. Phillips, *J. Nucl. Mater.* **80**, 215 (1979).
21. G. P. Pells, *Journal of the American Ceramic Society* **77**, 368 (1994).
22. F. Phillipp, R. Höschen, M. Osaki, G. Möbus, M. Rühle, *Ultramicroscopy* **56**, 1 (1994).
23. Gatan, Inc., Pleasanton, CA.
24. A. Strecker *et al.*, *Zeitschrift Für Metallkunde* **94**, 290 (2003).
25. M. T. Otten, W. M. J. Coene, *Ultramicroscopy* **48**, 77 (1993).
26. P. A. Stadelmann, *Ultramicroscopy* **21**, 131 (1987).
27. F. Ercolessi, J. B. Adams, *Europhys. Lett.* **26**, 583 (1994).
28. G. Levi, W. D. Kaplan, *Acta Materialia* **50**, 75 (2002).
29. M. Hoch, H. L. Johnston, *J. Am. Chem. Soc.* **76**, 2560 (1954).
30. G. Dehm, B. J. Inkson, T. Wagner, *Acta Materialia* **50**, 5021 (2002).



31. We thank F. Phillipp and J. M. Howe for discussions and U. Salzberger, R. Höschen, and J. Thomas for technical assistance. This work was partially funded by the German-Israel Fund (grant I-779-42.10/2003), the German Science Foundation through the Graduiertenkolleg Innere Grenzflächen (GRK 285/3), and the Russell Berrie Nanotechnology Institute at the Technion.


**Supporting Online Material**

www.sciencemag.org/cgi/content/full/1118611/DC1
Materials and Methods
Figs. S1 to S3
References
Movie S1


9 August 2005; accepted 21 September 2005
Published online 6 October 2005;
10.1126/science.1118611
Include this information when citing this paper.


# Stem-Cell Homeostasis and Growth Dynamics Can Be Uncoupled in the *Arabidopsis* Shoot Apex


**G. Venugopala Reddy and Elliot M. Meyerowitz***



**The shoot apical meristem (SAM) is a collection of stem cells that resides at the tip of each shoot and provides the cells of the shoot. It is divided into functional regions. The central zone (CZ) at the tip of the meristem is the domain of expression of the *CLAVATA3* (*CLV3*) gene, encoding a putative ligand for a transmembrane receptor kinase, CLAVATA1, active in cells of the rib meristem (RM), located just below the CZ. We show here that CLV3 restricts its own domain of expression (the CZ) by preventing differentiation of peripheral zone cells (PZ), which surround the CZ, into CZ cells and restricts overall SAM size by a separate, long-range effect on cell division rate.**


Pattern formation in the SAM is a dynamic process that results from active orchestration of spatial and temporal patterns of gene expression and of cellular behavior, by cell-cell communication. In *Arabidopsis thaliana*, the SAM consists of several hundred cells divided into functional domains that are characterized by different cellular behaviors and by different patterns of gene expression (*1*, *2*). Progeny of CZ cells enter into differentiation pathways when they enter the surrounding meristematic regions: the flanking PZ, where leaf and flower primordia are formed, and the RM beneath the CZ, where cells of the stem form. The functional domains of the SAM, CZ, PZ, and RM are established in embryonic development and maintain their relative proportions throughout postembryonic life, even though cells are continually diverted to differentiation pathways. The cells of the CZ signal to the RM by producing the product of the *CLV3* gene, a small extracellular protein thought to be the ligand for the CLAVATA1 receptor kinase, expressed in some RM cells (*3*, *4*). CLV1 acts, at least in part, by down-regulating the activity of the homeodomain protein WUSCHEL (WUS), also expressed in some RM cells (*5*, *6*). WUS acts, in turn, to up-regulate *CLV3* expression in the overlying CZ by means of an unknown diffusible signal (*7*). CLV3 thus


California Institute of Technology, Division of Biology, MC 156-29, 1200 East California Boulevard, Pasadena, CA 91125, USA.

*To whom correspondence should be addressed. E-mail: meyerow@its.caltech.edu

regulates its own expression through a feedback network involving CLV3-expressing cells in the CZ and the cells of the RM (*8*). Loss-of-function *clv3* (or *clv1*) mutants (*9*, *10*) or gain-of-function *wus* mutants (*7*) have a greatly enlarged SAM, which has an enormous CZ and an enlarged RM as well. Nevertheless, how the mutant phenotype results from alteration of the communication between CZ and RM is not known. It has been speculated that the enlarged meristem seen in *clv* loss-of-function mutants results from increased rates of cell division in the meristem, but also that it results from a decreased rate of departure of cells from the meristem to form differentiated tissues (*9*–*11*).

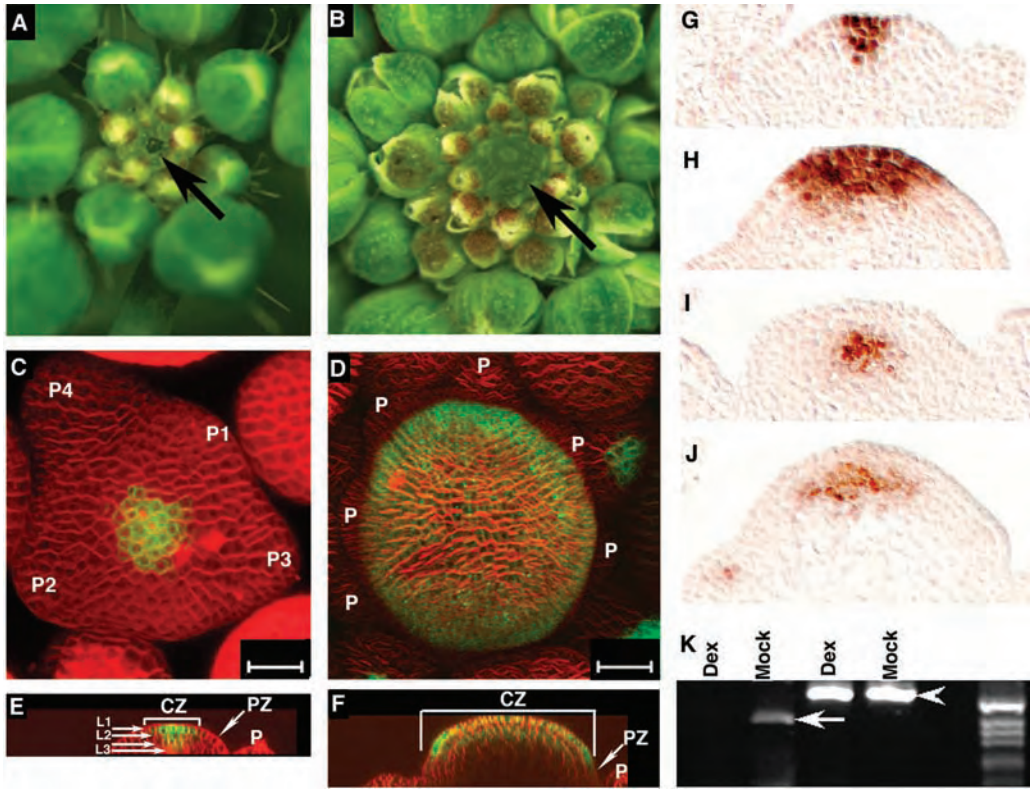


**Fig. 1.** Dex-inducible *clv3* phenotypes. (**A**) SAM of 30-day-old wild-type plant. (**B**) SAM of 30-day-old plant harboring constructs capable of silencing endogenous *CLV3* treated with Dex starting from germination. (**C**) A three-dimensional (3D) reconstructed view of L1 layer of 18-day-old mock-treated SAMs labeled with FM4-64 (red) and p*CLV3*::*mGFP5-ER* (green) marking the CZ. Primordia at different stages of development are marked. (**D**) A 3D reconstructed view of the L1 layer of 18-day-old Dex-treated plant harboring constructs capable of inducing *CLV3* silencing, marked with FM4-64 (red) and p*CLV3*::*mGFP5-ER* (green). Note both the expansion of the CZ and increased SAM size. Primordial outgrowths are marked as P. (**E**) The reconstructed side view of (C), depicting p*CLV3*::*mGFP5-ER* (green) expression in different clonal layers (arrows) and the CZ and the PZ (arrow). (**F**) The reconstructed side view of (D) depicting expanded CZ (green) and the PZ (arrow). (**G**) and (**H**) Longitudinal sections showing the *GFP* RNA expression domain of *pCLV3::mGFP5-ER* in SAMs either mock-treated (G) or treated with Dex (H) for a period of 7 days after bolting. (**I**) and (**J**) Longitudinal sections showing the *WUS* RNA expression domain in SAMs mock-treated or exposed to Dex, respectively, for a period of 7 days after bolting. (**K**) Ethidium bromide–stained agarose gel showing RT-PCR products amplified with *CLV3*-specific (arrow) and *LIPASE*-specific (arrowhead) primers from mock-treated SAMs or those treated with Dex for 6 days. Scale bar in (C) and (D), 20 μM.

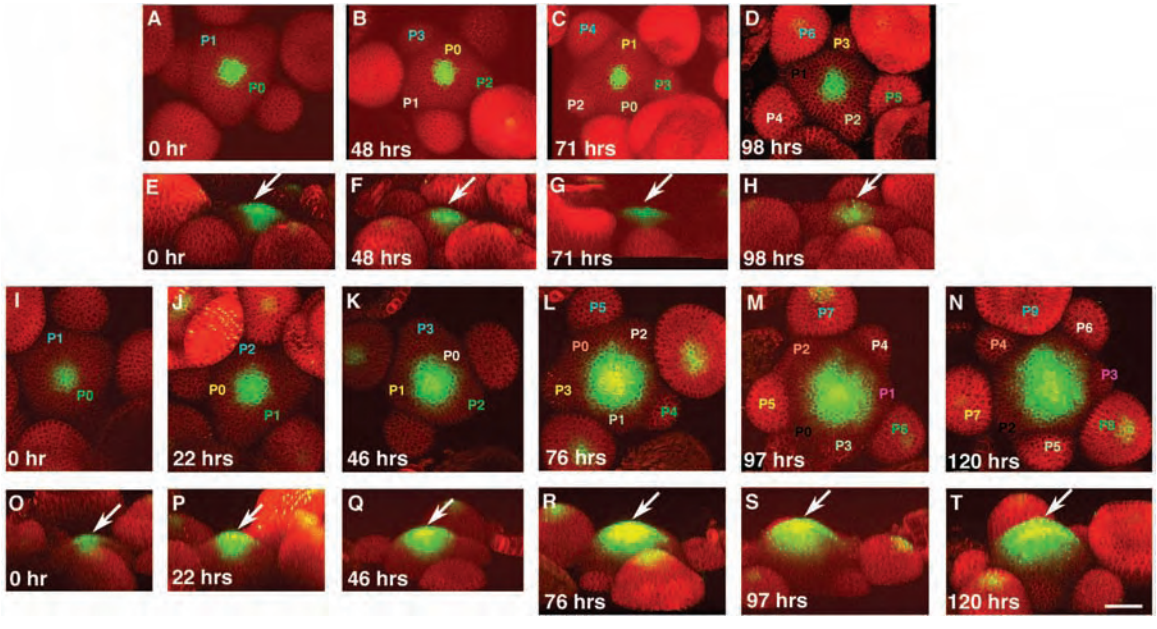


**Fig. 2.** Increase in SAM and the CZ is not due to a reduced rate of differentiation. (**A** to **D**) and (**I** to **N**) are the time series of mock- and Dex-treated SAMs, respectively. Total time elapsed, post treatment, is indicated on individual panels. The 3D views of the L1 layer are labeled with *35S::YFP 29-1* (plasma membrane localized YFP, red) and p*CLV3::mGFP5-ER* (green). Primordia at different stages are marked and the individual primordia are color-coded to track the same primordia over time. (**E** to **H**) The 3D side views of the SAMs in (A to D), respectively. (**O** to **T**) The 3D side views of the SAMs in (I to N), respectively. (I to N) Note gradual expansion of the p*CLV3*::*mGFP5-ER* domain and increase in SAM size upon Dex treatment, while primordial morphogenesis continues unperturbed. Increase in SAM height is evident (O to T). Also note that the radial expansion of the CZ precedes the increase in SAM size (compare I to K with L to N). Arrows point to the CZ. Scale bar, 30 μM.

There are at least three possibilities for the mechanism of enlargement of the CZ in *clv* mutants. The cells of the CZ could divide more rapidly in the mutants, while the transition of CZ daughters into PZ pattern of gene expression proceeds unperturbed; the cells on the boundary of the CZ and PZ could remain CZ cells after division, rather than transitioning to a PZ pattern of gene expression when pushed out of the CZ; or cells of the PZ could be respecified to become CZ cells. Which of these possibilities is correct is not known, nor is the relation between control of CZ size and control of meristem size in *clv* mutants.

Ordinary analysis of the mutants gives clues to the network of interactions but is not adequate to define the function of individual genes in the network of interacting cells. This is because loss or gain of function of one component affects the entire network, so that the ultimate mutant phenotype, assessed long after the initial effects of the mutation, is the result of a series of events that affects the expression of many genes. To understand the function of the *CLV3* gene, we have developed new methods for turning it off in a living, wild-type meristem and then for following in real time the changes in the organization of the SAM and in the rates and patterns of cell division in it. By doing this, we can see the immediate effect of loss of CLV3 function, rather than the eventual effect, and have started to answer the questions of how loss of CLV3 function leads to an enlarged CZ and to an enlarged meristem.

In order to test the immediate effects of perturbation in CLV signaling, transgenic plants capable of conditional *CLV3* silencing were generated. The gene construct introduced has a transcribed region that is capable of silencing *CLV3* by double-stranded RNA interference (dsRNAi); this coding region, which makes a foldback *CLV3* RNA, has already been described (*12*). Conditional induction of the foldback RNA was achieved by use of a two-component transcription activation system with a glucocorticoid-activated artificial transcription factor, GR-LhG4, which is capable of binding to and activating genes adjacent to a multimerized LhG4 binding sequence, *6xOP* (*13*). Plants transgenic for the *GR-LhG4* gene attached to a strong constitutive promoter (the cauliflower mosaic virus 35*S* coat protein gene promoter), p*35S*::*GR-LhG4-N*, were crossed to plants transformed with a p*6xOP*Ω::*CLV3*dsRNAi construct, and doubly transgenic $F_1$ plants were selected. These $F_1$ plants were treated with 10 μM dexamethasone (Dex) from the time of germination until flowering and then were analyzed for SAM defects. Four out of 35 independent RNAi lines examined showed the *clv3* mutant phenotype, massive overgrowth of the SAM (Fig. 1, A and B). Progeny of these lines inherited the ability to suppress CLV3 activity and were used in further analyses. Inducible silencing of the *CLV3* gene was confirmed using reverse transcription polymerase chain reaction (RT-PCR) to show loss of *CLV3* transcripts after Dex treatment (Fig. 1K).

P*35S*::*GR-LhG4-N*; p*6xOP*Ω::*CLV3*dsRNAi plants were crossed to plants transgenic for a CZ reporter construct, p*CLV3*::*mGFP5-ER*, which express a green fluorescent protein (GFP) from the *CLV3* promoter, localized to the endoplasmic reticulum (ER). In untreated or mock-treated plants, GFP-ER fluorescence reflects the expected CZ domain of expression, with fluorescence restricted to the central tip of the SAM, extending from the epidermal to the fourth layer of cells (Fig. 1, C and E). Dex-treated plants, for a period of 16 to 18 days starting from germination, displayed an expanded fluorescence domain (Fig. 1, D and F), concordant with the expanded domain of *CLV3* expression observed by in situ hybridization in *clv* mutants (*3*). RNA in situ hybridization revealed an expanded domain of *GFP* RNA, which ruled out the possibility that the expanded fluorescence domain is due to GFP protein movement or to protein stability, which would cause the GFP to persist through cell divisions (Fig. 1, G and H). Plants that were Dex treated for a period of 7 days also displayed an expanded domain of *WUS* expression (Fig. 1, I and J), and the *WUS* expression domain appeared patchy, as it consisted of cells with variable levels of expression (fig. S2, A to D).

A fourth transgene was added to the lines to enable the detection of all of the plasma membranes in the SAM and, therefore, all of the cell expansions and divisions that occur during observation. This was accomplished by crossing a triply transgenic plant to a plant bearing a p*35S*::*YFP 29-1* transgene, which expresses a plasma membrane–localized yellow fluorescent protein (YFP) in all of the cells of the SAM (*14*). Inflorescence meristems of plants carrying all four constructs were treated with either Dex or a control solution and then imaged at 12- or 24-hour intervals in different experiments. Within 24 hours of Dex treatment, a moderate increase in p*CLV3*

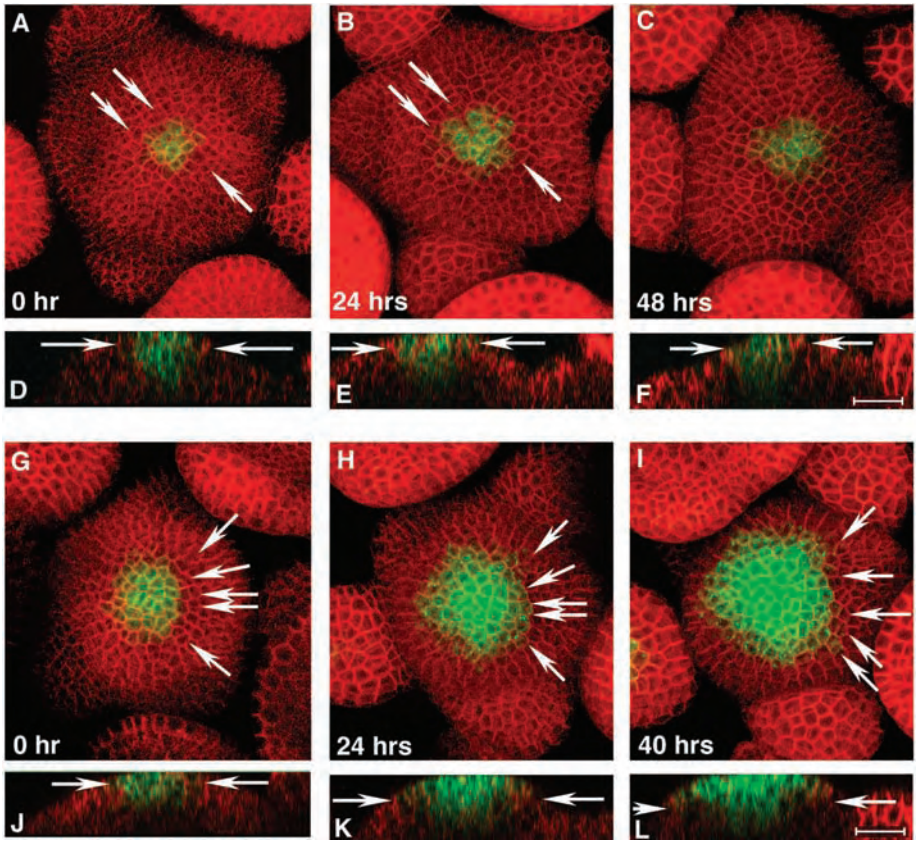


**Fig. 3.** Expansion of the CZ is due to the respecification of PZ cell identity. (**A** to **C**) and (**G** to **I**) Reconstructed views of the L1 layer of SAMs either mock-treated or treated with Dex, respectively, and followed for a period of 48 hours. Total time elapsed, post treatment, is indicated. The CZ behavior (p*CLV3*::*mGFP5-ER*, green) is followed, along with a ubiquitously expressed cell membrane marker (*35S*::*YFP29-1*, red). (A to C) Note only subtle changes to the CZ with time in mock-treated SAM (arrows point to the same cells in images acquired at successive intervals). (G to I) Dex-treated SAM showing both increased expression of p*CLV3* expression within the native domain and also a radial expansion over time (arrows point to the same cells in images acquired at successive intervals). Note the expansion of CZ identity in the first 40 hours without a noticeable effect on the SAM size. (**D** to **F**) and (**J** to **L**) Side views of SAMs represented in (A to C) and (G to I), respectively, and the arrows in each panel indicate outer limits of the CZ. Scale bar, 20 μM.

promoter activity was observed within the native domain, and its expression intensified by 48 hours, coupled with the radial expansion of the p*CLV3*::*mGFP5-ER* expression domain (Fig. 2, I to K). In the following 24-hour window, the expansion of p*CLV3* promoter activity continued, but with a dramatic increase in SAM size, both in height and width ($n$ = 10) (Fig. 2, L and R). Expansion of the CZ and the increase in SAM size continued for the next 2 days, the duration for which live imaging was performed (Fig. 2, M, N, S, and T). Mock-treated plants ($n$ = 10) and Dex-treated plants lacking the *CLV3*dsRNAi construct ($n$ = 8) served as controls and did not show consistent changes in SAM size, or in the *CLV3* expression domain, with time (Fig. 2, A to H; fig. S1, A to D). During the course of the expansion of the *CLV3* expression domain and the increase in SAM size, the process of flower primordium formation continued unperturbed as monitored by the appearance of primordial outgrowths (Fig. 2, I to N), in comparison with mock-treated SAMs (Fig. 2, A to D). Primordial initiation always occurred outside the perimeter of the expanding *CLV3* expression domain (and therefore in the PZ), which demonstrated the functional expansion of the CZ (Fig. 2, L to N). The expansion of the CZ was detected earlier than the increase in overall SAM size, whereas the process of organ primordium initiation continued unchanged, which showed that meristem reorganization precedes excess meristem growth and that increased SAM size is not merely due to a reduction in the rate of PZ cells entering differentiation pathways.

We next tested which of the three hypotheses for the expansion of the CZ after reduction of CLV3 activity is correct—increased rate of cell division in the CZ, decreased transition of CZ cells to PZ cells at the CZ boundary, or switching of PZ cells to a CZ pattern of gene expression—the opposite of the normal differentiation pathway. We did this by monitoring the expansion of the CZ and, meanwhile, using the plasma membrane marker to follow cell division in CZ and PZ cells (Fig. 3, A to C and G to I). Images were acquired about every 12 hours for a 48-hour period after Dex treatment and reconstructed in three dimensions to allow the same sets of cells to be tracked over time. Within 24 hours of Dex treatment, preexisting CZ cells began to express the p*CLV3* marker at an elevated level, and at the same time, some preexisting PZ cells that had not divided after Dex treatment began to show p*CLV3* activity (Fig. 3, G and H, arrows point to the same cells at different times). The radial expansion of the *CLV3* domain was readily visible by 40 hours of treatment, with larger numbers of former PZ cells starting to express p*CLV3* (Fig. 3, G and I). Cell divisions were monitored by the appearance of new cross walls and were not correlated with expansion of the CZ. Similar expansion of the CZ was also noticeable in layers below the epidermal, L1, layer (Fig. 3, J to L). Mock-treated plants showed subtle and slow changes in the p*CLV3* expression levels and domain, with fluctuations in the level of fluorescence in individual CZ cells located at the periphery (fig. S1, A to D, arrows) and with a limited expansion of the p*CLV3* domain (Fig. 3, A and B, arrows). However, they did not show a consistent radial expansion as seen in Dex-treated SAMs. This analysis revealed that the gradual expansion of the CZ after reduction in CLV3 activity results from respecification of PZ cells to CZ fate in a way that is uncoupled from growth, as assayed by *CLV3* expression. The fluctuations of p*CLV3* expression in mock-treated plants may indicate that PZ cell respecification normally occurs at the edge of the CZ and that the size of the CZ in wild type is regulated by maintenance of a dynamic balance between CZ and PZ cells.

To better understand the expansion of the SAM that follows CZ reorganization, we analyzed cell division patterns in the period between 60 and 108 hours after Dex treatment. During this period, maximal SAM growth and continued expansion of the CZ occurs (Fig. 4, F

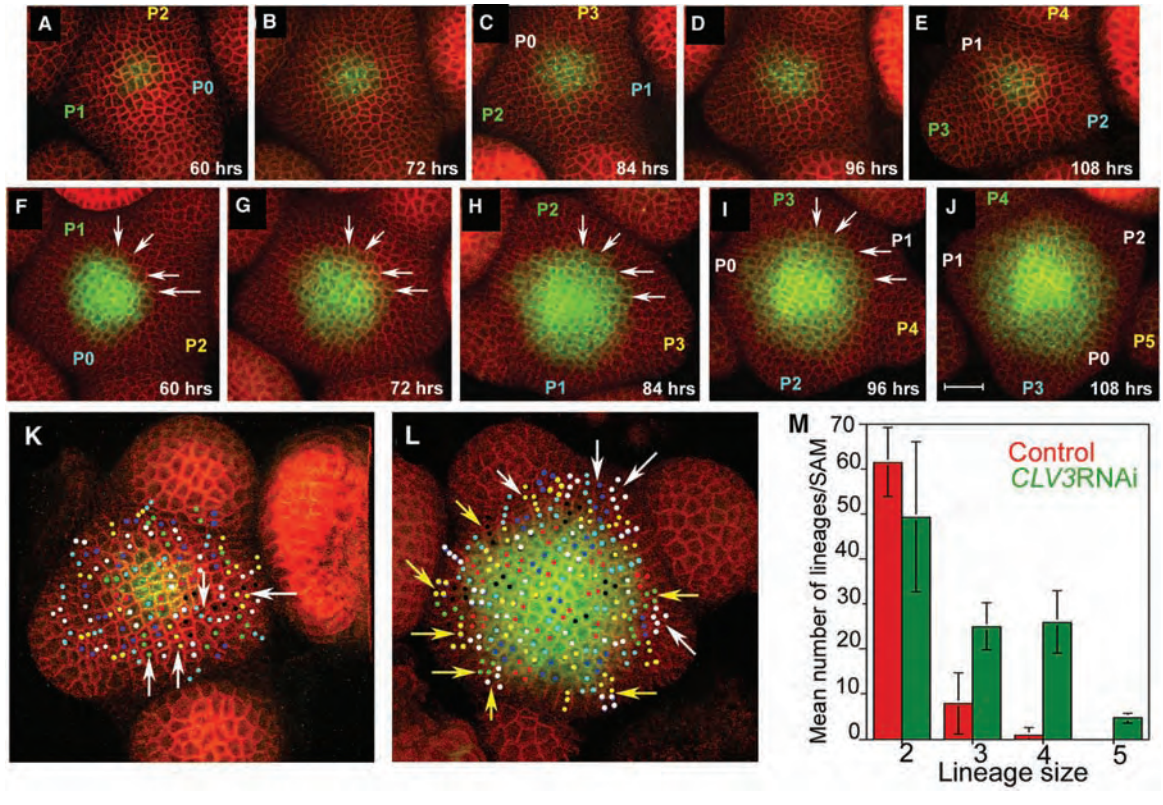


**Fig. 4.** A long-range effect of CLV3 activity on cell division rates. (**A** to **E**) and (**F** to **J**) Reconstructed views of the L1 layer of the SAMs mock-treated or treated with Dex, respectively, starting 60 hours after treatment. Total time elapsed, post treatment, is shown. The CZ behavior (p*CLV3*::*mGFP5-ER*, green) is followed with a cell division marker (*35S*::*YFP29-1*, red). (F to J) Expansion of the CZ continues as more of the PZ cells begin to acquire CZ identity (arrows point to the same cells in images acquired at successive intervals) along with an increase in SAM size. (**M**) The images from the same SAM were used to score for cell division events to reconstruct lineages within the 48-hour period (60 to 108 hours after treatment) and expressed as size of the individual lineages against mean number of lineages per SAM. Error bars represent standard deviation. (**K**) and (**L**) The spatial distribution of lineages represented in (M) in control and Dex-treated SAMs, respectively; CZ size is shown in green. The individual lineages are color-coded. The same color has been assigned to more than one lineage as long as they do not abut each other. White arrows in (K) point to three-celled lineages. White arrows in (L) point to five-celled lineages and the yellow arrows indicate four-celled lineages. Scale bar for (A to J), 20 μM.

to J). Lineage reconstruction was performed for all of the cells of the outermost layer of the SAM, the L1 layer, of Dex-treated plants ($n$ = 3), based on images acquired at 12-hour intervals. Mock-treated plants ($n$ = 3) and Dex-treated plants that did not carry the RNAi construct ($n$ = 2) served as controls. As these two control genotypes showed no significant differences, the control data were pooled. Cell division activity was expressed as the size of individual lineages [the number of progeny cells at 108 hours that descended from a single cell present at 60 hours (Fig. 4M)]. Cells of Dex-treated plants had larger lineages compared with the controls, which demonstrated an increase in cell division after compromise of CLV3 function. The lineage data were represented by superimposing each lineage on a reconstruction of the L1 at the 108-hour time point (Fig. 4, K and L). This revealed that the increase in cell division rate is observed distant from the meristematic center (Fig. 4L) and, therefore, represents a long-distance effect of events that started in the CZ.

This study provides evidence that CLV3 signaling in meristems mediates both cell fate specification and growth control through inhibition of cell division rate, as well as that the processes can be temporally uncoupled. The gradual radial expansion of the CZ that follows reduction in CLV3 activity indicates a process of PZ cell respecification that either spreads from the CZ with time or reflects a gradient of response to a CZ-promoting activity. If the signal does spread with time, it could do so either by diffusion or by stepwise communication between adjoining cells. The presently proposed function of CLV3 is to confine the expression of the transcription factor WUS to a limited set of cells as a result of CLV1 activation, and this is consistent with the WUS in situ hybridization results. A real-time analysis of WUS levels and the *WUS*-expression domain in the reorganizing meristems of *CLV3*-RNAi plants should yield further insights into the relation between cell-cell communication in the SAM and its organization and growth, as should manipulations of WUS activity during live imaging. It is not yet known whether the long-range effect of CLV3 in repressing cell division is mediated through its effect on WUS activity. Earlier studies have proposed that WUS is required for CZ specification and that SHOOTMERISTEMLESS (STM), a homeodomain protein, is required for division of PZ cells (*15*). Such a model would predict that CLV-mediated growth inhibition should impinge on STM and its regulatory cascades. It will be illuminating to test the function of STM and its regulation by the CLV-WUS network in real-time experiments such as those introduced here. However, it is also possible that the increased cell division rates that follow CLV3 removal could be an indirect consequence of the influence exerted by the expanding CZ on adjacent PZ cells. Meristems with alterations in WUS and STM activity, like the experiments related here in which CLV3 activity has been manipulated, should allow the dissection of the influence of signaling between cells on cell-fate specification, organization, and growth in SAMs, despite their being highly coupled in space and in time in wild-type plants.

### References and Notes


1. T. A. Steeves, I. M. Sussex, *Patterns in Plant Development* (Cambridge Univ. Press, New York, 1989).
2. E. M. Meyerowitz, *Cell* **88**, 299 (1997).
3. J. C. Fletcher, U. Brand, M. P. Running, R. Simon, E. M. Meyerowitz, *Science* **283**, 1911 (1999).
4. S. E. Clark, R. W. Williams, E. M. Meyerowitz, *Cell* **89**, 575 (1997).
5. T. Laux, K. F. Mayer, J. Berger, G. Jurgens, *Development* **122**, 87 (1996).
6. K. F. Mayer *et al.*, *Cell* **95**, 805 (1998).
7. H. Schoof *et al.*, *Cell* **100**, 635 (2000).
8. U. Brand, J. C. Fletcher, M. Hobe, E. M. Meyerowitz, R. Simon, *Science* **289**, 617 (2000).
9. S. E. Clark, M. P. Running, E. M. Meyerowitz, *Development* **119**, 397 (1993).
10. S. E. Clark, M. P. Running, E. M. Meyerowitz, *Development* **121**, 2057 (1995).
11. P. Laufs, O. Grandjean, C. Jonak, K. Kieu, J. Traas, *Plant Cell* **10**, 1375 (1998).
12. C. F. Chuang, E. M. Meyerowitz, *Proc. Natl. Acad. Sci. U.S.A.* **97**, 4985 (2000).
13. J. Craft *et al.*, *Plant J.* **41**, 899 (2005).
14. G. V. Reddy, M. G. Heisler, D. W. Ehrhardt, E. M. Meyerowitz, *Development* **131**, 4225 (2004).
15. M. Lenhard, G. Jurgens, T. Laux, *Development* **129**, 3195 (2000).


16. We thank C.-F. Chuang, I. Moore, R. Simon, and D. Ehrhardt for DNA constructs and members of the Meyerowitz laboratory for comments on the manuscript. G.V.R. was a fellow of the Jane Coffin Childs memorial fund for medical research, and this work was supported by U.S. National Science Foundation grant IOB-0211670.


**Supporting Online Material**
www.sciencemag.org/cgi/content/full/1116261/DC1
Materials and Methods
Figs. S1 and S2
References


17 June 2005; accepted 26 September 2005
Published online 6 October 2005;
10.1126/science.1116261
Include this information when citing this paper.


# Antagonistic Actions of Ecdysone and Insulins Determine Final Size in *Drosophila*


**Julien Colombani,[1*†] Laurence Bianchini,[1*] Sophie Layalle,[1*] Emilie Pondeville,[2] Chantal Dauphin-Villemant,[2] Christophe Antoniewski,[3] Clément Carré,[3] Stéphane Noselli,[1] Pierre Léopold[1‡]**



**All animals coordinate growth and maturation to reach their final size and shape. In insects, insulin family molecules control growth and metabolism, whereas pulses of the steroid 20-hydroxyecdysone (20E) initiate major developmental transitions. We show that 20E signaling also negatively controls animal growth rates by impeding general insulin signaling involving localization of the transcription factor dFOXO and transcription of the translation inhibitor *4E-BP*. We also demonstrate that the larval fat body, equivalent to the vertebrate liver, is a key relay element for ecdysone-dependent growth inhibition. Hence, ecdysone counteracts the growth-promoting action of insulins, thus forming a humoral regulatory loop that determines organismal size.**


In metazoans, the insulin/IGF (insulin growth factor) signaling pathway (IIS) plays a key role in regulating growth and metabolism. In *Drosophila*, a family of insulin-like molecules called Dilps activates a unique insulin receptor (InR) and a conserved downstream kinase cascade that includes phosphatidylinositol 3-kinase (PI3K) and the serine-threonine protein kinase Akt [also called protein kinase B (PKB)] (*1*). Recent genetic experiments have established that this pathway integrates extrinsic signals such as nutrition with the control of tissue growth during larval stages (*2*, *3*). The larval period is critical for the control of animal growth, as it establishes the size at which maturation occurs and, consequently, the final adult size. Maturation is itself a complex process that is controlled by the steroid 20-hydroxyecdysone (20E). Peaks of 20E determine the timing of all developmental transitions, from embryo to larva, larva to pupa, and pupa to adult (*4*). Ecdysteroids are mainly produced by the prothoracic gland (PG), part of a composite endocrine tissue called the ring gland (fig. S1A).

Final adult size thus mainly depends on two parameters: the speed of growth (or growth


[1]CNRS/University of Nice–Sophia Antipolis, UMR6543, Parc Valrose, 06108 Nice Cedex 2, France. [2]CNRS FRE2852, Université P. et M. Curie, 7 quai St. Bernard, 75252 Paris, France. [3]Institut Pasteur, 25-28 rue du Docteur Roux, 75724 Paris, France.

*These authors contributed equally to this work.
†Present address: Cancer Research UK, London Institute, 44 Lincoln's Inn Fields, London WC2A 3PX, UK.
‡To whom correspondence should be addressed. E-mail: leopold@unice.fr

rate), which is primarily controlled by IIS, and the overall duration of the growth period, which is limited by the onset of the larval-pupal transition and is timed by peaks of ecdysone secretion (*5*). Little is known about the mechanisms that coordinate these two parameters during larval development (*6*).

To investigate the function of ecdysone in controlling organismal growth, we developed a genetic approach that allowed us to modulate basal levels of ecdysteroids in *Drosophila*. Our initial rationale was to modify the mass of the ring gland in order to change the level of ecdysteroid production. In pursuit of this goal, we manipulated the levels of PI3K activity in the PG by crossing *P0206-Gal4* (*P0206>*), a line with specific Gal4 expression in the PG and corpora allata (CA) (*7*, *8*), with flies carrying UAS constructs that allowed expression of either wild-type PI3K or dominant-negative PI3K ($PI3K^{DN}$). As expected, these crosses produced striking autonomous growth effects in the ring gland, and particularly in the PG: Tissue size was increased upon PI3K activation and decreased upon inhibition (Fig. 1A). Surprisingly, the changes in ring gland growth were accompanied by opposite effects at the organismal level. *P0206>PI3K* animals (with large ring glands) showed reduced growth at all stages of development and produced emerging adults with reduced size and body weight (78% of wild type; Fig. 1, A and B). Conversely, reducing PI3K activity in the ring gland of $P0206>PI3K^{DN}$ animals led to increased growth and produced adults with 17% greater weight on average (Fig. 1, A and B). Adult size increase was attributable to an increase in cell number in the wing and the eye. Adult size reduction was accompanied by a decrease in cell number in the wing and in cell size in the eye (Fig. 1B).

The timing of embryonic and larval development of these animals was comparable to that in controls. Both the L2 to L3 transition and the cessation of feeding (wandering) occurred at identical times (Fig. 1C). Moreover, animals entered pupal development at the same time, except for $P0206>PI3K^{DN}$, which showed a 1- to 2-hour delay intrinsic to the $UAS\text{-}PI3K^{DN}$ line itself. The duration of pupal development was slightly modified, however: Adult emergence was delayed in *P0206>PI3K* and advanced in $P0206>PI3K^{DN}$, albeit by less than 4 hours after 10 days of development (*9*). In contrast, the speed of larval growth was found to be increased in $P0206>PI3K^{DN}$ animals and decreased in the *P0206>PI3K* background at the earliest stage that we could measure (early L2 instar) (Fig. 1D). Because none of these effects were observed when PI3K levels were modified specifically in the CA with the use of the *Aug21-Gal4* driver (fig. S1, B and C), we can conclude that the observed phenotypes are solely due to PI3K modulation in the PG. Together, these results demonstrate that manipulating PI3K levels in the PG induces nonautonomous changes in the speed of larval growth (growth rate effects) without changing the timing of larval development.

To investigate whether these effects could be attributed to changes in 20E levels, we first measured ecdysteroid titers in third-instar larvae of the different genotypes. Early after ecdysis into third instar [74 hours after egg deposition (AED)], ecdysteroids are present at basal level; they accumulate to an intermediate plateau around 90 hours AED and reach peak levels before pupariation (120 hours AED) (*10*). Because early L3 levels are below the detection limit of our enzyme immunoassay, we measured ecdysteroid titers at the intermediate plateau (90 hours AED). In these conditions, we observed a very modest increase of ecdysteroids in *P0206>PI3K* larvae and a small but significant decrease in $P0206>PI3K^{DN}$ animals (Fig. 2A). This was further confirmed by measuring the transcript levels of a direct target of 20E, *E74B*, which responds to low and moderate levels of 20E (*11*) (Fig. 2B). However, in early L3 larvae with basal ecdysteroid levels (74 hours AED), differences in *E74B* transcripts were clearly visible, with a factor of 1.9 increase seen for *P0206>PI3K* and a factor of 1.7 decrease for $P0206>PI3K^{DN}$. These findings establish that basal circulating levels of 20E are modified in response to our manipulation of PI3K levels in the PG, and they also suggest that the observed differences in basal 20E levels equalize with the strong global increase of ecdysteroids in mid- to late L3.

Several related lines of evidence strengthen these results. First, the increase in growth rate and size observed in $P0206>PI3K^{DN}$ animals could be efficiently reversed by adding 20E to their food (Figs. 1D and 2C). Second, feeding wild-type larvae 20E recapitulated the effects observed in *P0206>PI3K* animals (Fig. 2C). Third, ubiquitous silencing of the nuclear receptor EcR by means of an inducible *EcR* RNA interference (RNAi) construct (fig. S2) resulted in a growth increase similar to that observed in $P0206>PI3K^{DN}$ larvae (Fig. 2C). Finally, the *phantom* (*phm*) and *disembodied* (*dib*) genes, which are specifically expressed in the PG and encode hydroxylases required

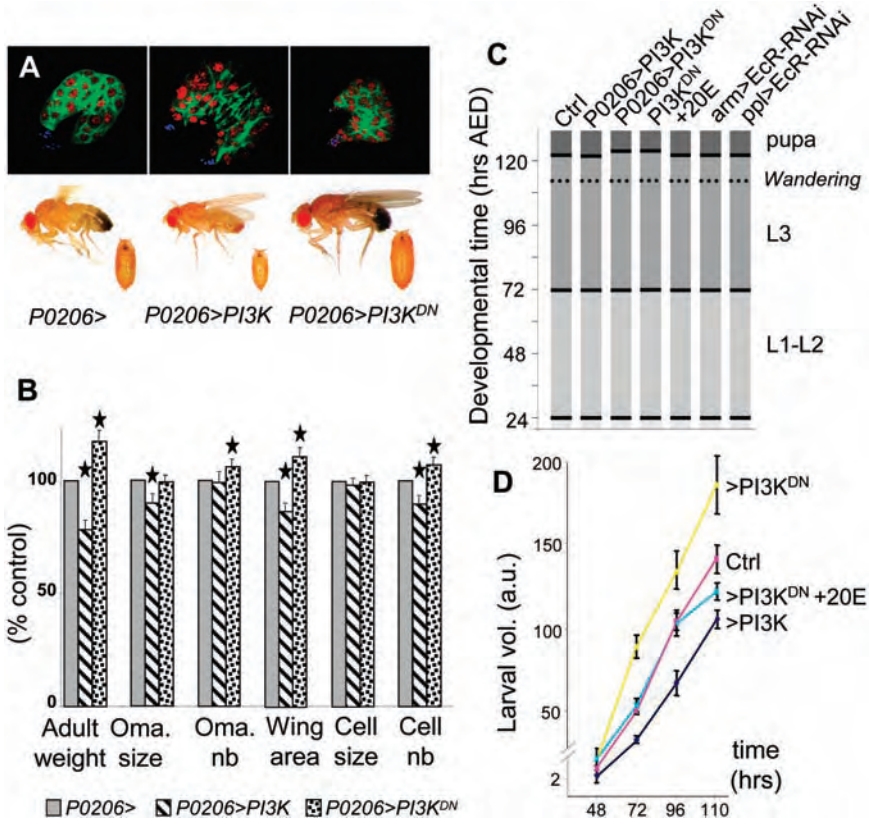


**Fig. 1.** Levels of PI3K signaling in the prothoracic gland control final size by changing the larval growth rate. (**A**) The *P0206-Gal4* line (*P0206>*) expresses Gal4 in the PG and the CA. Varying levels of PI3K in the ring gland produce autonomous growth effects (green, GFP; blue, anti-Elav neuronal marker; red, propidium iodide). Reverse nonautonomous growth effects are observed in pupae and adults. (**B**) Effects on body, tissue, and cell size (for weight measurement, $n = 90$; for ommatidial size, $n = 30$; for wing measurement, $n = 20$; nb, number; $^*P < 0.05$). (**C**) Timing of larval development. Transition timing (horizontal bars) is determined when 50% of the animals have passed a given transition ($n > 40$). (**D**) Measurement of larval growth rates (25°C, $n = 30$; a.u., arbitrary units). Error bars denote SD.

for ecdysteroid biosynthesis (*10*, *12*, *13*), showed increased expression (by factors of 1.65 and 2.2, respectively) upon PI3K activation in the ring gland (Fig. 2D). These results support the notion that 20E biosynthesis is mildly induced in these experimental conditions. In line with our previous results, neither 20E treatment nor EcR silencing had any effect on developmental timing (Fig. 1C). Overall, our results indicate that manipulation of basal levels of 20E signaling in various ways modifies the larval growth rate without affecting the timing of the larval transitions.

Variations in ecdysone levels in animals with different-sized ring glands could be due to changes in the PG tissue mass or, alternatively, to a specific effect of PI3K signaling in the secreting tissue. To distinguish between these two possibilities, we induced extra growth in the PG by treatment with either *Drosophila* Myc (dMyc) or cyclin D/Cdk4, two potent growth inducers in *Drosophila* (*14*, *15*). Although the size of the larval ring gland was markedly increased under these conditions (fig. S1D), no effect on pupal or adult size was observed (*9*), which implies that the size of the ring gland is not the critical factor in control of body size. Instead, it is likely that the InR-PI3K signaling pathway can specifically activate ecdysone production from the PG.

We next examined the possibility that ecdysone signaling could oppose the growth-promoting effects of IIS in the larva. To test this idea, we fed larvae 20E and assessed PI3K activity in vivo with the use of a green fluorescent protein (GFP) fused to a pleckstrin homology (PH) domain (tGPH) as a marker (*2*). Membrane tGPH localization showed a marked decrease in the fat body of 20E-fed animals, and this effect could be reversed by specifically silencing EcR in the fat body (Fig. 3A). This indicates that ecdysone-induced growth inhibition correlates with decreased IIS and is mediated through EcR. Conversely, larvae with *PI3K$^{DN}$* expression in the PG showed a factor of 4.2 increase in the global levels of Akt activity, as measured by phosphorylation levels of Ser$^{505}$ (Fig. 3B). In *Drosophila* cells (as in other metazoan cells), high levels of PI3K and Akt activity cause the transcription factor dFOXO to be retained in the cytoplasm, whereas low levels of PI3K and Akt activity allow dFOXO to enter the nucleus where it promotes *4E-BP* transcription (*16*, *17*). In larvae with ectopic *PI3K* expression in the PG, we observed a strong increase in nuclear dFOXO in fat body cells. Similar results were obtained by feeding larvae with 20E (Fig. 3C). Conversely, inactivation of EcR signaling in fat body cells was accomplished by clonal overexpression of a

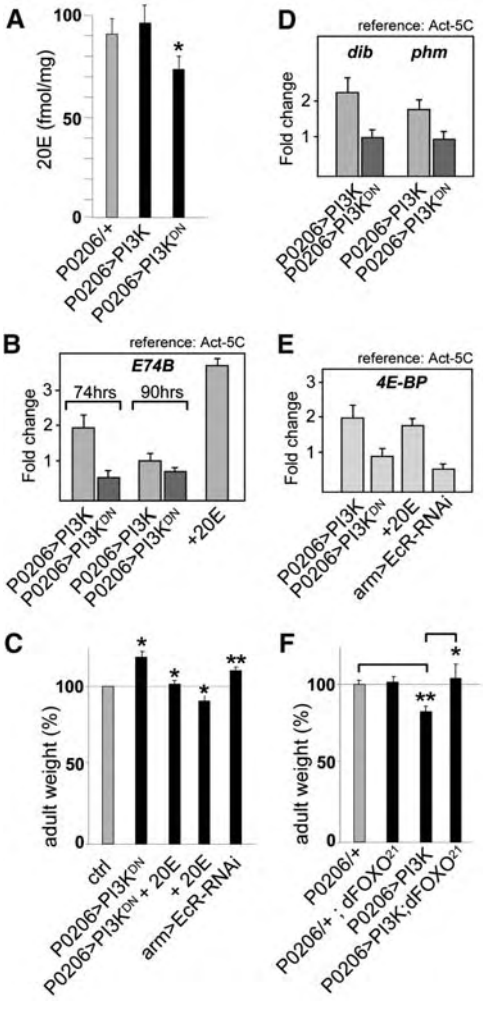


**Fig. 2.** 20E controls larval growth rates and final adult size. (**A**) Ecdysteroid titers in mid-L3 larvae from different genotypes (90 hours AED, $*P < 0.05$). (**B**) Measurement of larval *E74B* transcripts by quantitative reverse transcription polymerase chain reaction (RT-PCR). Fold changes are relative to control (dissection at 74 hours AED or otherwise indicated). (**C**) Effects of feeding 20E and general EcR silencing (*arm>EcR-RNAi*) on larval body weight ($*P < 0.05$, $**P < 0.01$). (**D** and **E**) Measurement of larval *dib*, *phm*, and *4E-BP* transcripts by quantitative RT-PCR. Fold changes are relative to control (dissection at 74 hours AED). (**F**) Growth defects seen in *P0206>PI3K* animals are suppressed in a *dFOXO$^{21}$* homozygous background ($n > 90$, except for *P0206>PI3K; dFOXO$^{21}$*: $n = 60$).

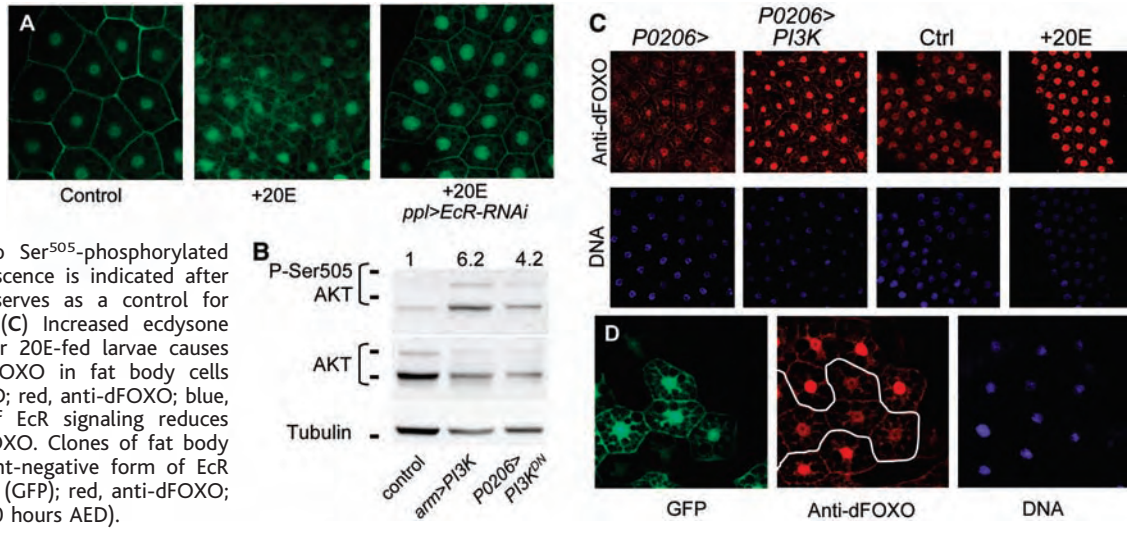


**Fig. 3.** Ecdysone signaling affects growth by modulating IIS. (**A**) Levels of PI3K activity in the fat body as visualized with tGPH (green) (dissection at 74 hours AED). (**B**) Global levels of activated Akt in early L3 larvae of different genotypes, detected with antibodies to Ser$^{505}$-phosphorylated Akt. Relative chemiluminescence is indicated after normalization. *arm>PI3K* serves as a control for increased Akt activation. (**C**) Increased ecdysone signaling in *P0206>PI3K* or 20E-fed larvae causes nuclear localization of dFOXO in fat body cells (dissection at 74 hours AED; red, anti-dFOXO; blue, DAPI). (**D**) Inactivation of EcR signaling reduces nuclear localization of dFOXO. Clones of fat body cells expressing a dominant-negative form of EcR (EcR$^{F645A}$) labeled in green (GFP); red, anti-dFOXO; blue, DAPI (dissection at 90 hours AED).

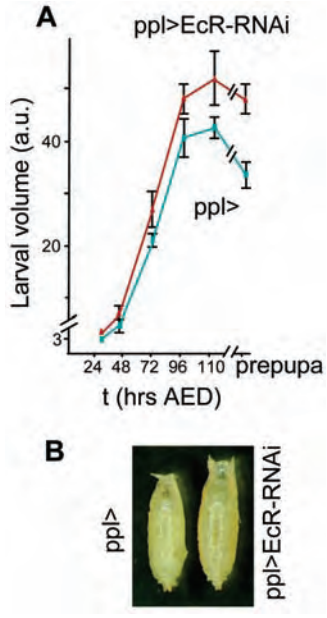


**Fig. 4.** The larval fat body relays the 20E-dependent growth inhibitory signal to larval tissues. The ppl-Gal4 driver (ppl>) allows specific expression of EcR-RNAi constructs in the larval fat body. (**A**) Measurement of larval volumes ($n$ = 10 per time point). (**B**) Size difference between control and *pplGal4>EcR-RNAi* prepupae (120 hours AED).

dominant-negative form of EcR ($EcR^{F645A}$) (*18*). In these conditions, we observed a reduced accumulation of dFOXO in the nuclei of $EcR^{F645A}$-expressing cells (Fig. 3D). As an expected consequence, global accumulation of *4E-BP* transcripts was consistently higher in *P0206>PI3K* as well as in 20E-fed early L3 larvae relative to control animals, and was reduced upon general EcR silencing (*arm>EcR-RNAi*) (Fig. 2E). Together, these results indicate that ecdysone-dependent inhibition of larval growth correlates with a general alteration of insulin/IGF signaling and a relocalization of dFOXO into the cell nuclei. To more directly test the role of dFOXO in the growth-inhibitory function of ecdysone signaling, we examined the effects of increasing ecdysone levels in a *dFOXO* mutant genetic background. Although homozygous $dFOXO^{21}$ animals do not display a detectable growth phenotype (Fig. 2F) (*16*), introducing the $dFOXO^{21}$ mutation was sufficient to totally reverse the growth defects of *P0206>PI3K* animals, either homozygous (Fig. 2F) or heterozygous (*9*). These data establish that dFOXO is required for 20E-mediated growth inhibition.

The endocrine activities of the brain and the fat body have previously been implicated in the humoral control of larval growth (*19*, *20*). To test for possible roles of these two organs in mediating the systemic growth effects of ecdysone, we silenced EcR expression specifically in the brain's insulin-producing cells (IPCs) or in the fat body. Whereas specific expression of *EcR* RNAi in the IPCs failed to reproduce the overgrowth observed in *armGal4>EcR-RNAi* animals (*9*), *EcR* silencing in the fat body elicited an acceleration of larval growth and a remarkable increase in pupal size (Fig. 4, A and B). Moreover, no detectable delay was observed in the larval timing of these animals (Fig. 1C). Thus, specifically reducing 20E signaling in the fat body is sufficient to recapitulate the systemic effects of global EcR silencing. Hence, the fat body is a major target for ecdysone, and this tissue can act to relay the 20E growth-inhibitory signal to all larval tissues.

Our results establish an additional role for 20E in modulating animal growth rates. This function is mediated by an antagonistic interaction with IIS that ultimately targets dFOXO function (fig. S2E). A similar antagonistic interaction between 20E and insulin signaling was recently shown to control developmentally regulated autophagy in *Drosophila* larva (*21*).

Although we do not rule out a direct effect of ecdysone on the cellular growth rate of all larval tissues, our experiments reveal a key role for the fat body in relaying ecdysone-dependent growth control signals. Together with previous work (*3*), these data suggest that various inputs such as nutrition and ecdysone converge on this important regulatory organ, which then controls the general IIS to modulate organismal growth (fig. S2E). How, then, is growth connected to developmental timing? Our finding that 20E can modulate growth rates in addition to developmental transitions places this hormone in a central position for coordinating these two key processes and controlling organismal size.

**References and Notes**

1. E. Hafen, *Curr. Top. Microbiol. Immunol.* **279**, 153 (2004).
2. J. S. Britton, W. K. Lockwood, L. Li, S. M. Cohen, B. A. Edgar, *Dev. Cell* **2**, 239 (2002).
3. J. Colombani *et al.*, *Cell* **114**, 739 (2003).
4. L. M. Riddiford, *Receptor* **3**, 203 (1993).
5. H. F. Nijhout, *Dev. Biol.* **261**, 1 (2003).
6. D. Stern, *Curr. Biol.* **13**, R267 (2003).
7. G. Adam, N. Perrimon, S. Noselli, *Development* **130**, 2397 (2003).
8. W. Janning, *Semin. Cell Dev. Biol.* **8**, 469 (1997).
9. J. Colombani *et al.*, data not shown.
10. J. P. Parvy *et al.*, *Dev. Biol.* **282**, 84 (2005).
11. F. D. Karim, C. S. Thummel, *Genes Dev.* **5**, 1067 (1991).
12. V. M. Chavez *et al.*, *Development* **127**, 4115 (2000).
13. J. T. Warren *et al.*, *Insect Biochem. Mol. Biol.* **34**, 991 (2004).
14. L. A. Johnston, D. A. Prober, B. A. Edgar, R. N. Eisenman, P. Gallant, *Cell* **98**, 779 (1999).
15. D. A. Prober, B. A. Edgar, *Cell* **100**, 435 (2000).
16. M. A. Junger *et al.*, *J. Biol.* **2**, 20 (2003).
17. O. Puig, M. T. Marr, M. L. Ruhf, R. Tjian, *Genes Dev.* **17**, 2006 (2003).
18. L. Cherbas, X. Hu, I. Zhimulev, E. Belyaeva, P. Cherbas, *Development* **130**, 271 (2003).
19. E. J. Rulifson, S. K. Kim, R. Nusse, *Science* **296**, 1118 (2002).
20. T. Ikeya, M. Galic, P. Belawat, K. Nairz, E. Hafen, *Curr. Biol.* **12**, 1293 (2002).
21. T. E. Rusten *et al.*, *Dev. Cell* **7**, 179 (2004).
22. We thank G. Jarretou for technical assistance; N. Tapon, J.-P. Vincent, M. Tatar, and P. Follette for comments on the manuscript; C. Mirth and P. Caldwell for communicating unpublished results; G. Adam for discussions; and L.-E. Zaragosi and J. Hopkins for assistance with quantitative real-time fluorescence polymerase chain reaction (QPCR). Supported by CNRS, INSERM, Association pour la Recherche contre le Cancer (grants 7696 and 3339), and Fondation de France.

**Supporting Online Material**
www.sciencemag.org/cgi/content/full/1119432/DC1
Materials and Methods
Figs. S1 and S2
References

29 August 2005; accepted 15 September 2005
Published online 22 September 2005;
10.1126/science.1119432
Include this information when citing this paper.

# Small-Molecule Inhibitor of *Vibrio cholerae* Virulence and Intestinal Colonization

**Deborah T. Hung,* Elizabeth A. Shakhnovich, Emily Pierson, John J. Mekalanos**

Increasing antibiotic resistance requires the development of new approaches to combating infection. Virulence gene expression in vivo represents a target for antibiotic discovery that has not yet been explored. A high-throughput, phenotypic screen was used to identify a small molecule 4-[*N*-(1,8-naphthalimide)]-*n*-butyric acid, virstatin, that inhibits virulence regulation in *Vibrio cholerae*. By inhibiting the transcriptional regulator ToxT, virstatin prevents expression of two critical *V. cholerae* virulence factors, cholera toxin and the toxin coregulated pilus. Orogastric administration of virstatin protects infant mice from intestinal colonization by *V. cholerae*.

We are entering a challenging era where microbial resistance to antibiotics will complicate the treatment of nearly all common bacterial infections. The development of antimicrobials has lagged behind the development of antibiotic resistance for many life-threatening bacterial species. Current antimicrobials, for the most part, target a relatively small number of essential gene functions, such as inhibition of cell wall synthesis, DNA replication, RNA

transcription, protein synthesis, and folate synthesis. What development there has been has been largely limited to improving existing antibiotics through chemical modification and developing synergistic drugs that augment the efficacy of existing antibiotics. Nevertheless, a recent report identifying a new antituberculosis drug suggests it is still possible to identify entirely new classes of antibiotics (*1*).

Targeting the regulation of virulence factors of specific pathogens represents one approach to identifying antibiotics. Here we report the identification of a small molecule inhibitor of *Vibrio cholerae* virulence regulation and demonstrate its ability to inhibit bacterial colonization in an animal model of cholera.

Cholera is caused by the Gram-negative bacterium *V. cholerae*, which elaborates two major virulence factors, cholera toxin (CT) and the toxin coregulated pilus (TCP) (*2*). CT is an adenosine diphosphate–ribosylating toxin encoded in the genome of the filamentous, lysogenic CTXΦ phage. Secretion of CT into the intestinal lumen results in elevated cyclic adenosine monophosphate levels in intestinal epithelial cells and the subsequent secretory diarrhea that is the hallmark of the disease. TCP is thought to play a role in early attachment to intestinal epithelium and is required for intestinal colonization in an infant mouse model of cholera (*2*). The regulation of CT and TCP expression has been studied extensively (*2*), but the mechanisms by which environmental signals stimulate virulence expression in vivo are not clear.

We performed a high-throughput screen of a 50,000-compound small molecule library from Chembridge Research Laboratories (Microformats) to identify inhibitors of *V. cholerae* virulence factor expression. We constructed a screening strain of the classical biotype strain O395 that carries a chromosomally integrated tetracycline resistance gene (*tetA*) controlled by the cholera toxin (*ctx*) promoter. In a 384-well format, the strain was treated with 10 μg/mL samples from the library to identify compounds that conferred tetracycline sensitivity when the strain was grown under in vitro conditions that would normally induce CT expression. We identified 109 compounds as inhibitors of *ctx* promoter activation by their ability to prevent *tetA* expression in the reporter strain. Fifteen of these compounds were notable for their inhibitory effects with minimal bacterial toxicity.

One of these 15 compounds, 4-[*N*-(1,8-naphthalimide)]-*n*-butyric acid (virstatin) (Fig. 1A) was selected for further study and was subsequently synthesized in gram quantities (*3*). We generated growth curves for two different *V. cholerae* biotype strains, O395 and C6706, and showed that virstatin did not inhibit growth (50 μM) (Fig. 1B). Minimal bactericidal concentrations (MBC) of 600 and 1200 μM were determined for the two strains, respectively. We confirmed that under in vitro virulence-inducing conditions for these strains, CT production was undetectable in the presence of virstatin (50 μM), as assayed by CT-enzyme-linked immunosorbent assay (CT-ELISA) (Fig. 1C). The minimal inhibitory concentrations for CT expression were 3 μM and 40 μM for O395 and C6706, respectively.

Because TCP is coregulated with CT, we examined virstatin's ability to inhibit the expression and function of TCP. Western blot analysis showed that the major subunit of TCP (TcpA) was not expressed under virulence-inducing conditions when either O395 or C6706 was treated with virstatin (Fig. 1C). Virstatin prevented the assembly of a functional pilus (TCP) in O395, as determined by its ability to prevent transduction of a bacteriophage (CTX-KmΦ) that uses TCP as its receptor (Fig. 1D) (*4*). CTX-KmΦ encodes kanamycin resistance and thus confers resistance when transduced into *V. cholerae*. Although $2.6 \times 10^6$ kanamycin-resistant colonies were obtained from phage transduction of O395 grown under virulence-inducing conditions, no kanamycin-resistant colonies were obtained when O395 was grown in the presence of virstatin, suggesting the absence of TCP on these cells.

We next examined whether virstatin affects known regulators of CT and TCP expression. In the canonical model for *V. cholerae* virulence regulation, environmental signals stimulate virulence by activating a cascading series of transcriptional regulators that ultimately induce transcription of the *ctx* and *tcp* genes (Fig. 2A) (*5*). The major role of regulators ToxRS and TcpPH is to activate transcription of *toxT*, which encodes an AraC-like transcriptional activator (*6*). ToxT activates multiple virulence genes (including *ctxAB*, *acfA*, and the *tcp* genes) and is autoregulated, presumably by self-inducing read-through transcription from the upstream *tcpA* promoter (*7*).

We investigated the effect of virstatin on these known virulence regulators by examining the transcription of *toxRS*, *tcpPH*, and *toxT* using transcriptional fusion reporters (Fig. 2B). In the presence of virstatin, the transcript levels of *toxRS*, *tcpPH*, and the most downstream gene, *toxT*, were all relatively unaffected, as determined by measuring β-galactosidase or β-glucuronidase activity. As expected, *ctx* transcription was notably decreased. Thus, virstatin blocks *ctx* transcription downstream of *toxT* transcription.

We also examined the effect of 50 μM virstatin on *V. cholerae* global transcription patterns by using a genomic microarray (*8*). Eleven of 15 genes in O395 and 21 out of 22 genes in C6706 significantly repressed by virstatin (to

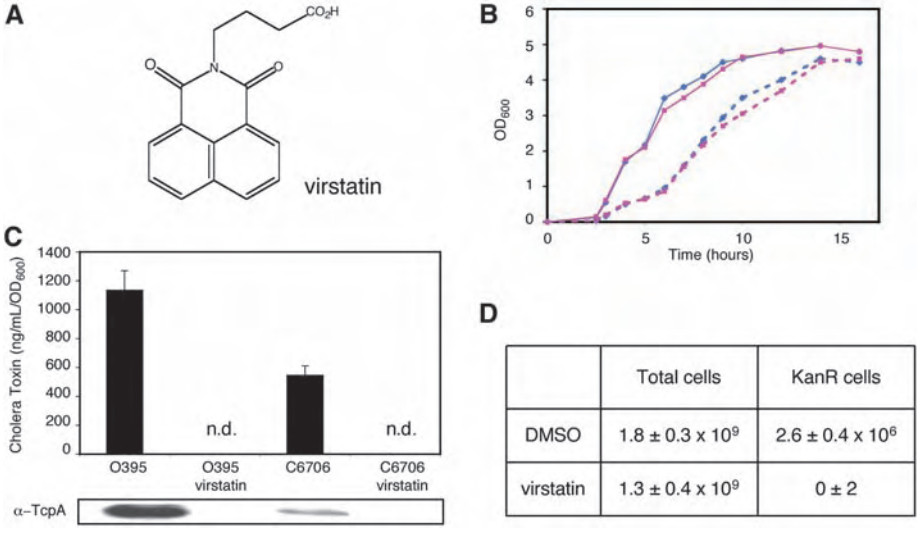


| | Total cells | KanR cells |
|---|---|---|
| DMSO | $1.8 \pm 0.3 \times 10^9$ | $2.6 \pm 0.4 \times 10^6$ |
| virstatin | $1.3 \pm 0.4 \times 10^9$ | $0 \pm 2$ |

**Fig. 1.** Virstatin inhibits virulence expression in *V. cholerae*. (**A**) Chemical structure of virstatin. (**B**) Growth curves in LB at 37°C for O395 (dotted line) and C6706 (solid line). Dimethyl sulfoxide (DMSO) control, blue; virstatin, pink; $OD_{600}$, optical density measured at 600 nm. (**C**) CT and TcpA expression in the presence or absence of virstatin. Top: CT expression was measured by ELISA from O395 and C6706 in the presence of DMSO control or virstatin (50 μM) after overnight growth under standard virulence-inducing conditions. Error bars represent the standard deviations from samples performed in triplicate. n.d., not detected. Bottom: TcpA expression was detected by Western blot with an α-TcpA antibody. (**D**) CTX-KmΦ transduction of O395 in the absence and presence of virstatin. Functional TCP was assayed by growing O395 to mid-log phase under virulence-inducing conditions (LB at pH 6.5 and 30°C) in the presence of DMSO control or virstatin (50 μM). After 30 min incubation with phage, cultures were plated on LB-Kanamycin plates to enumerate transduction events. Total cells and kanamycin-resistant (KanR) cells were counted to reflect transduction efficiency. In the presence of virstatin, no transduction events were measured, which is a 6-log reduction compared to DMSO control.

Department of Microbiology and Molecular Genetics, Harvard Medical School, 200 Longwood Avenue, Boston, MA 02115, USA.

*To whom correspondence should be addressed. E-mail: dhung@partners.org

levels less than one-third of control levels) are within the *tcp* or *ctx* loci (*3*). These findings are consistent with the results obtained with transcriptional reporters, with ToxT regulating most genes that are down-regulated by virstatin. Moreover, in accordance with the established model for CT and TCP regulation, virstatin appears to inhibit ToxT post-transcriptionally.

Virstatin inhibited ToxT activity when ToxT was expressed under the control of a heterologous pBAD promoter, induced by arabinose, in *V. cholerae* strain O395Δ*toxT* (Fig. 3A). To confirm that virstatin has no effect on ToxT expression, we constructed a *toxT* variant containing a C-terminal $Myc_5$ tag that both is active (albeit slightly less active than wild-type) and can be inhibited by virstatin (Fig. 3A) (*3*). Western blot analysis showed comparable levels of ToxT-$Myc_5$ expression in the presence and absence of virstatin, confirming that the inhibition is post-translational.

Virstatin also inhibited ToxT induction of *ctx-lacZ* in *Escherichia coli* reporter strain DTH3060 free of all other *V. cholerae* factors that might otherwise affect *ctx* induction (Fig. 3B) (*9*, *10*). When ToxT was expressed constitutively from plasmid pEP99.1 (*3*), β-galactosidase activity was induced 6 to 10 times more than in strain DTH3060 without and with control plasmid pJB658 (*11*). With virstatin present, this induction was suppressed to baseline levels. We obtained similar results using ToxT-$Myc_5$ (pEP99.2) and performed Western blot analysis to confirm that ToxT expression was not altered by virstatin.

A virstatin-resistant mutant of ToxT was isolated from a library of ToxT mutants by propagating pBAD*toxT* in the *E. coli* mutator strain XL1-Red (Stratagene), transforming the resulting plasmid library into the reporter strain DTH3060, and screening the resulting colonies on LB agar containing virstatin, arabinose, Xgal, ampicillin, tetracycline, and kanamycin. One intensely blue colony was isolated from ~20,000 colonies screened, indicating a clone that expressed a ToxT mutant capable of inducing *ctx-lacZ* in the presence of virstatin. Sequencing of the *toxT* gene revealed a single point mutation, L113P, that occurs in the N-terminal, putative dimerization domain based on its sequence homology to other AraC-like proteins.

$ToxT_{L113P}$ was resistant to virstatin when expressed in O395Δ*toxT* with equivalent amounts of CT produced in the absence or presence of virstatin (50 μM) (Fig. 3A). A similar phenomenon was observed in the heterologous *E. coli* strain DTH3060, with no inhibition of $ToxT_{L113P}$ by increasing concentrations of virstatin (until 60 μM), in stark contrast to the inhibition observed of wild-type ToxT (Fig. 3C). These data demonstrate that ToxT carrying a mutation in the N-terminal domain displays relative resistance to virstatin. Because the N-terminal domain of ToxT is its putative dimerization domain, virstatin may alter the dimerization state of ToxT, thus inactivating it.

In order to determine if the inhibition of virulence observed in vitro could affect in vivo infection, we tested the ability of virstatin to inhibit *V. cholerae* infection in an animal model. It has previously been shown that deletion of *toxT* attenuates TCP-dependent colonization of the small intestine of infant mice by *V. cholerae* (*12*).

We examined the effect of virstatin on the colonization of infant mice by *V. cholerae* strains that colonize in a TCP-dependent versus -independent manner. *V. cholerae* El Tor biotype strain C6706 was used as the TCP-dependent strain, because of its similar growth

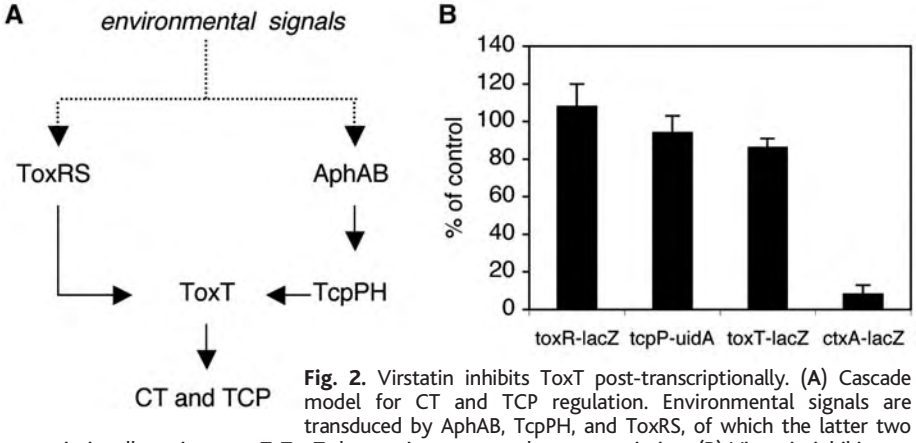


**Fig. 2.** Virstatin inhibits ToxT post-transcriptionally. (**A**) Cascade model for CT and TCP regulation. Environmental signals are transduced by AphAB, TcpPH, and ToxRS, of which the latter two transcriptionally activate *toxT*. ToxT then activates *ctx* and *tcp* transcription. (**B**) Virstatin inhibits *ctx* but not *toxR*, *tcpP*, or *toxT* transcription. Transcriptional reporter strains (O395) were grown overnight under virulence-inducing conditions (pH 6.5 and 30°C) in the presence of DMSO control or virstatin (50 μM). Transcriptional fusions of *toxR*, *toxT*, and *ctxA* with *lacZ* were assayed for β-galactosidase activity. A transcriptional fusion of *tcpP* with *uidA* was assayed for β-glucuronidase activity. Data are presented as the percentage of reporter activity in the presence of virstatin compared to the DMSO control. Error bars represent the standard deviation for samples performed in triplicate.

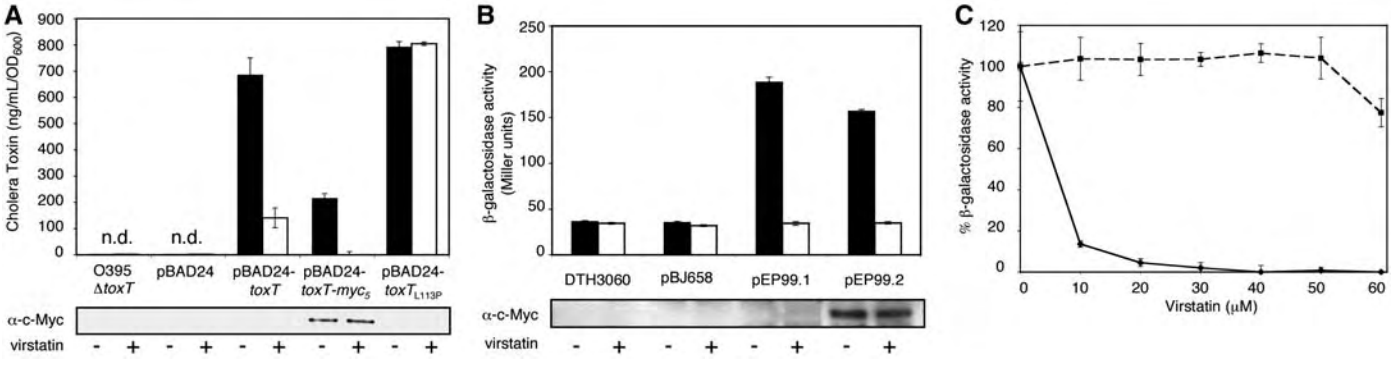


**Fig. 3.** Virstatin inhibits ToxT. (**A**) Top: Virstatin inhibits CT expression in O395 when ToxT is expressed under pBAD promoter control. O395Δ*toxT*, O395Δ*toxT* with pBAD24, pBAD24-*toxT*, pBAD24-*toxT-myc*$_5$, or pBAD24-*toxT*$_{L113P}$ were induced (with 0.001% arabinose) in the presence of DMSO or virstatin (50 μM). Virstatin inhibited CT expression in cells expressing wild-type and Myc-tagged ToxT but not $ToxT_{L113P}$. DMSO, black; virstatin, white. Bottom: Western blot with α-Myc demonstrates that virstatin does not alter ToxT-$Myc_5$ expression. (**B**) Top: Virstatin inhibits *ctx* transcription in *E. coli* reporter strain DTH3060 carrying *ctx-lacZ*, as measured by β-galactosidase activity. Constitutive ToxT (pEP99.1) and ToxT-$Myc_5$ (pEP99.2) expression under *tet* promoter control resulted in 6 to 10 times more than in induction over control strain DTH3060 without or with control plasmid (pJB658). Virstatin repressed induction to control levels. DMSO, black; virstatin, white. Bottom: Western blot with α-Myc demonstrates that virstatin does not alter ToxT-$Myc_5$ expression. (**C**) Virstatin, at increasing concentrations, inhibited β-galactosidase activity in DTH3060 when wild-type ToxT but not $ToxT_{L113P}$ was expressed (under pBAD promoter control; induced with 0.1% arabinose). Activity is presented as percentage of reporter activity in the presence of varying concentrations of virstatin compared to no virstatin. ToxT, solid line; $ToxT_{L113P}$, dotted line.

kinetics in the presence and absence of virstatin to TCP-independent *V. cholerae* strain S533. S533 is a non-O1 non-O139 clinical isolate that lacks the *toxT*, *tcp*, and *ctxAB* genes but is nevertheless able to colonize infant mice (*13*).

To validate comparison of the two strains, we examined their competitive capacity in vitro, in the presence and absence of virstatin, by growing S533 and C6706 together. The competitive index (CI) (*14*) of S533 versus C6706 was close to 1 in the presence and absence of virstatin (*3*).

Inoculation with single strains into the infant mouse in the presence of virstatin demonstrated a marked reduction in colonization of C6706 but not S533. Infant mice (5 to 6 days old) were orogastrically inoculated as previously described with *V. cholerae* strain C6706 or S533 (*15*) in the presence or absence of virstatin and killed at 18 to 24 hours (*3*). Small intestine homogenate from each mouse was plated on LB-agar containing streptomycin for enumeration of live bacterial counts. Under optimized conditions, S533 colonization was not affected by the presence of virstatin. However, C6706 colonization dropped by four logarithms in the presence of virstatin (Fig. 4A).

Competition experiments comparing the relative ratios of C6706 and S533 recovered after co-inoculation into the infant mouse showed the same selective effect of virstatin on C6706 but not S533 as the single-inoculation studies. A mixture of S533 and C6706 in the presence or absence of virstatin was orogastrically inoculated into infant mice. In the absence of virstatin, each mouse was colonized by both strains (CI 0.3 to 35). In contrast, in the presence of virstatin, very few C6706 colonies could be recovered. The CI of S533/C6706 increased over four logarithms (Fig. 4B). Thus, virstatin is able to significantly attenuate the TCP-dependent infection of C6706 relative to S533, a strain whose colonization is independent of ToxT and insensitive to the activity of virstatin.

Because virstatin's inhibition of ToxT and subsequent TCP expression is the likely cause of attenuation in C6706 colonization, we examined the ability of a C6706Δ*tcpA* strain to compete with the wild type in the presence of virstatin (Fig. 4C). Mice were orogastrically inoculated with or without virstatin and boosted again at 3 and 6.5 hours post-inoculation. Mice were killed at 2, 4.5, 7.5, and 24 hours post-inoculation. In the absence of virstatin, we observed the previously described, severely attenuated phenotype of the Δ*tcpA* strain (*16*) and were unable to recover any C6706Δ*tcpA* bacteria at 24 hours, whereas C6706 wild-type colonized efficiently (Fig. 4C). However, in the presence of virstatin, recovery of wild-type C6706 was significantly diminished, and nearly equivalent numbers of Δ*tcpA* and wild-type bacteria were recovered at all time points (Fig. 4D). Thus, virstatin is able to eliminate wild-type C6706's competitive advantage over C6706Δ*tcpA* during in vivo infection.

In vivo studies with C6706*toxT*$_{L113P}$, a mutant of wild-type C6706 carrying the mutation in the chromosome at the native *toxT* locus, confirmed that the differences in colonization are due to the effect of virstatin on ToxT. When inoculated alone, C6706*toxT*$_{L113P}$ colonization was unaffected by the presence of virstatin (Fig. 4A). When inoculated together in the presence of virstatin, C6706*toxT*$_{L113P}$ was able to colonize better than wild-type C6706 with a CI of 50 (Fig. 4B) [in vitro CI ~ 1, (*3*)]. Together, these data demonstrate that virstatin inhibits intestinal colonization specifically by blocking the activity of ToxT in vivo.

Finally, we examined whether virstatin could affect long-term infection if administered after colonization has already been established in the infant mouse model. This effect would be analogous to treatment of cholera patients with antibacterials such as tetracycline after the onset of diarrhea, which can reduce the duration of symptoms (*17*). We found that delayed administration of virstatin 12 hours after inoculation with C6706 still reduced the recovery of C6706 by over three logarithms relative to C6706 recovered from untreated infant mice (Fig. 4D). These data complement prior observations on the requirement of early in vivo virulence expression (*18*) and suggest that ongoing, late expression of ToxT-dependent genes is also necessary for optimal colonization in this animal model. This result also demonstrates that drugs such as virstatin, like conventional antibacterials, could have utility even after disease has been diagnosed.

Other small molecule inhibitors of virulence regulation have been reported, including inhibitors of a two-component regulator of alginate synthesis in *Pseudomonas aeruginosa* (*19*) and inhibitors of quorum sensing in *Staphylococcus aureus* (*20*) and *P. aeruginosa* (*21*). Inhibitors of virulence factors have also been explored, including compounds that block type III secretion in *Yersinia* (*22*) or anthrax toxin protease activity (*23*). Here we show that even in the absence of any chemical or target structural information, a high-throughput phenotypic screen can be used to identify small molecule virulence inhibitors that exhibit in vivo efficacy against bacterial infection after

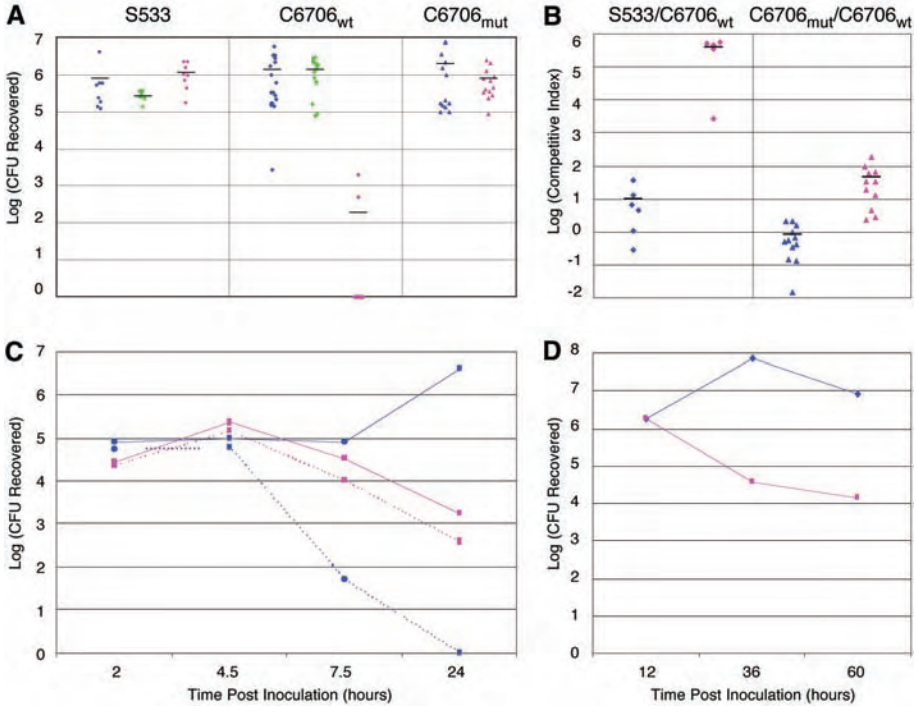


**Fig. 4.** Virstatin inhibits ToxT-dependent colonization of infant mice. (**A**) When inoculated alone, C6706 wildtype (C6706$_{wt}$) colonization was reduced 4 logs in the presence of virstatin under conditions that do not affect S533 or C6706*toxT*$_{L113P}$ (C6706$_{mut}$) colonization. Bacteria were recovered from mice 18 to 24 hours post-orogastric inoculation and plated for enumeration. Each data point represents the output from a single animal and the bar represents the log of the geometric mean of data obtained from individual mice. Control buffer inoculum, no boost, blue; control buffer inoculum, control buffer boost, green; virstatin in both inoculum and boost, pink. CFU, colony-forming units. (**B**) When strains were co-inoculated, virstatin increased the CI of S533 versus C6706$_{wt}$ by 4.5 logs, and the CI of C6706$_{mut}$ versus C6706$_{wt}$ by 1.5 logs. No virstatin, blue; virstatin, pink. (**C**) When C6706$_{wt}$ and C6706Δ*tcpA* were co-inoculated, virstatin decreased recovery of C6706$_{wt}$ by 3 logs, down to the levels of C6706Δ*tcpA*. Recovery of the two strains in the presence of virstatin at 24 hours was nearly 1:1, whereas no C6706Δ*tcpA* was recovered from a competition experiment in the absence of virstatin. C6706$_{wt}$, solid; C6706Δ*tcpA*, dotted; buffer, blue; virstatin, pink. (**D**) When C6706$_{wt}$ infection was allowed to establish for 12 hours and mice then were treated with virstatin, colonization was reduced 3 logs in comparison to control buffer–treated mice. Control boost, blue; virstatin, pink.

simple orogastric administration. Thus, identification of inhibitors of virulence represents a path to anti-infective discovery that is quite different from conventional approaches that target only bacterial processes that are essential both in vivo and in vitro. We further predict that drugs such as virstatin may act synergistically with conventional antibiotics, because they act through independent mechanisms to block in vivo bacterial replication or survival.

### References and Notes


1. K. Andries *et al.*, *Science* **307**, 223 (2005).
2. M. K. Waldor, J. J. Mekalanos, in *Enteric Infections and Immunity*, L. J. Paradise, Ed. (Plenum, New York, 1996), pp. 37–55.
3. Materials and methods are available as supporting material on *Science* Online.
4. M. K. Waldor, J. J. Mekalanos, *Science* **272**, 1910 (1996).
5. V. J. DiRita, *Mol. Microbiol.* **6**, 451 (1992).
6. D. E. Higgins, E. Nazareno, V. J. DiRita, *J. Bacteriol.* **174**, 6974 (1992).
7. R. C. Brown, R. K. Taylor, *Mol. Microbiol.* **16**, 425 (1995).
8. J. Bina *et al.*, *Proc. Natl. Acad. Sci. U.S.A.* **100**, 2801 (2003).
9. E. S. Krukonis, R. R. Yu, V. J. DiRita, *Mol. Microbiol.* **38**, 67 (2000).
10. DTH3060 is derived from *E. coli* strain VJ787 (*put::ctx-lacZ*) by deletion of *tolC*, an outer membrane porin, to confer greater sensitivity to virstatin.
11. J. M. Blatny, T. Brautaset, H. C. Winther-Larsen, P. Karunakaran, S. Valla, *Plasmid* **38**, 35 (1997).
12. G. A. Champion, M. N. Neely, M. A. Brennan, V. J. DiRita, *Mol. Microbiol.* **23**, 323 (1997).
13. Strain S533 was obtained from the Mekalanos lab collection of *V. cholerae* strain, originally isolated in 1981 from Soongnern Hospital in Thailand.
14. CI represents the ratio of test strain to wild type recovered from the intestine (or after overnight in vitro growth) divided by the ratio of input test strain to wild type. C6706 was marked with a *lacZ* mutation that does not affect colonization but allows it to be distinguished from S533 colonies by blue/white detection on LB-agar plates with Xgal. When the number of bacteria recovered were below the detection limit, 1 was chosen as the denominator to calculate the CI.
15. M. J. Angelichio, J. Spector, M. K. Waldor, A. Camilli, *Infect. Immun.* **67**, 3733 (1999).
16. R. K. Taylor, V. L. Miller, D. B. Furlong, J. J. Mekalanos, *Proc. Natl. Acad. Sci. U.S.A.* **84**, 2833 (1987).
17. G. H. Rabbani, M. R. Islam, T. Butler, M. Shahrier, K. Alam, *Antimicrob. Agents Chemother.* **33**, 1447 (1989).
18. S. H. Lee, D. L. Hava, M. K. Waldor, A. Camilli, *Cell* **99**, 625 (1999).
19. S. Roychoudhury *et al.*, *Proc. Natl. Acad. Sci. U.S.A.* **90**, 965 (1993).
20. J. S. Wright III, R. Jin, R. P. Novick, *Proc. Natl. Acad. Sci. U.S.A.* **102**, 1691 (2005).
21. M. Hentzer *et al.*, *EMBO J.* **22**, 3803 (2003).
22. A. M. Kauppi, R. Nordfelth, H. Uvell, H. Wolf-Watz, M. Elofsson, *Chem. Biol.* **10**, 241 (2003).
23. B. E. Turk *et al.*, *Nat. Struct. Mol. Biol.* **11**, 60 (2004).



24. We thank the National Cancer Institute's Initiative for Chemical Genetics (S. L. Schreiber, P.I.) and the Harvard Institute of Chemistry and Cell Biology for their support of and assistance with the high-throughput small molecule screen; the New England Regional Center of Excellence in Biodefense and Infectious Disease Research for its continued support of research activities involving the identification of small molecule inhibitors of bacterial virulence; and S. Chiang, J. Mougous, and J. Zhu for review of the manuscript. Supported by NIH grant nos. K08 AI060708-01 (D.T.H.) and AI26289 (J.J.M.) and by an NSF predoctoral fellowship (E.A.S.).


**Supporting Online Material**

www.sciencemag.org/cgi/content/full/1116739/DC1
Materials and Methods
SOM Text
Tables S1 to S3
References and Notes


29 June 2005; accepted 22 September 2005
Published online 13 October 2005;
10.1126/science.1116739
Include this information when citing this paper.


# The V-Antigen of *Yersinia* Forms a Distinct Structure at the Tip of Injectisome Needles


**Catherine A. Mueller,[1]* Petr Broz,[1]* Shirley A. Müller,[1,2] Philippe Ringler,[1,2] Françoise Erne-Brand,[1,2] Isabel Sorg,[1] Marina Kuhn,[1] Andreas Engel,[1,2] Guy R. Cornelis[1]†**



**Many pathogenic bacteria use injectisomes to deliver effector proteins into host cells through type III secretion. Injectisomes consist of a basal body embedded in the bacterial membranes and a needle. In *Yersinia*, translocation of effectors requires the YopB and YopD proteins, which form a pore in the target cell membrane, and the LcrV protein, which assists the assembly of the pore. Here we report that LcrV forms a distinct structure at the tip of the needle, the tip complex. This unique localization of LcrV may explain its crucial role in the translocation process and its efficacy as the main protective antigen against plague.**


Type III secretion (T3S) is commonly used by Gram-negative pathogenic bacteria to introduce effector proteins into target host cells (*1*). *Yersinia pestis* and *Y. enterocolitica*, causing bubonic plague and gastroenteritis respectively, share the same T3S system consisting of the Ysc (Yop secretion) injectisome, or "needle complex," and the secreted Yop (Yersinia outer protein) effector proteins. Three translocator proteins, YopB, YopD, and LcrV, are necessary to deliver the effectors across the target cell membrane (*2*–*5*). LcrV is required for the correct assembly of the translocation pore formed by YopB and YopD in the membrane of the target cell (*2*, *6*). LcrV (also known as V antigen) is a soluble protein important for virulence (*7*) and is a protective antigen against plague (*8*). Antibodies against LcrV prevent the formation of the translocation pore (*6*) and block the delivery of the effector Yops (*9*). The injectisome is composed of a basal body resembling that of the flagellum and a needle (*10*). The needle has a helical structure (*11*) and in *Yersinia* is formed by the 9.5-kD protein YscF (*12*, *13*).

Transmission electron micrographs of the surface of *Y. enterocolitica* E40 bacteria suggested that the injectisome needle ends with a well-defined structure (fig. S1). To characterize this structure, we purified needles from multi-effector knockout bacteria (strain ΔHOPEMT) that had been incubated under either secretion-permissive or -nonpermissive conditions (*14*), then analyzed them by scanning transmission electron microscopy (STEM). A distinct "tip complex" was observed for the wild-type needles, comprising a head, a neck, and a base (Fig. 1A, arrow, and fig. S2A). The tip structure was the same in both cases, but more needles were produced under secretion-permissive conditions (*15*). The purified needle fraction from secreting bacteria was analyzed to determine the components of the tip complex (fig. S3A). LcrV, YopD, and the needle subunit YscF were found. Other proteins included flagellins, which are usual contaminants of needle preparations (*13*). Upon cross-linking of purified needles, products formed between YscF and LcrV, suggesting that the latter is a structural component of the needle (fig. S3B).

The tip complex observed for wild-type needles was absent from needles prepared from bacteria deprived of LcrV (ΔHOPEMNVQ) (table S1) (*16*). Instead, this end of the needle was distinctly pointed (Fig. 1B, asterisk, and fig. S2B). The tip complex was restored after the mutation was complemented in trans with *lcrV*$^+$ (Fig. 1B, right, and fig. S2B). Needles from single *yopN* or *yopQ* knockout bacteria were analyzed as controls and displayed the same tip complex as the wild-type needles (fig. S4). Thus, the formation of the tip complex involved LcrV but not YopN or YopQ.

Needles from a *yopBD* double mutant (*15*) were analyzed to exclude the possibility that YopD and, although not detected on the gels, the third translocator protein YopB were tip complex components. The appearance of the tip complex was unchanged (fig. S4).

When wild-type needles were incubated with affinity-purified polyclonal antibodies to LcrV, the latter specifically bound to the tip


[1]Biozentrum der Universität Basel and [2]Maurice E. Müller Institute, Klingelbergstrasse 50-70, CH-4056, Basel, Switzerland.

*These authors contributed equally to this work.
†To whom correspondence should be addressed. E-mail: guy.cornelis@unibas.ch

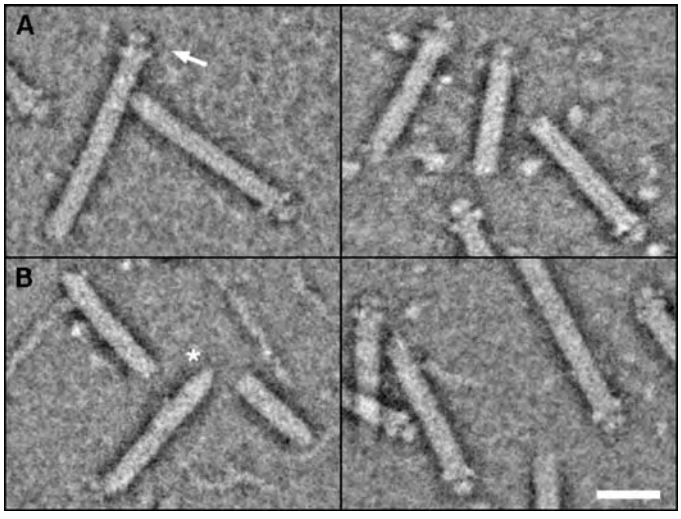


**Fig. 1.** STEM images of negatively stained wild-type needles. (**A**) Characteristic tip complexes (arrow), comprising a head, a neck, and a base, of wild-type needles isolated from ΔHOPEMT bacteria grown in secretion-permissive (left) and -nonpermissive (right) conditions. (**B**) Needles formed by *lcrV* mutant bacteria (ΔHOPEMNVQ, left) and by the complemented mutant (ΔHOPEMNVQ+LcrV, right). The needles of *lcrV* mutant bacteria are distinctly pointed at one end (asterisk). The tip complex was restored by complementation of the *lcrV* mutation in trans. Scale bar, 20 nm.

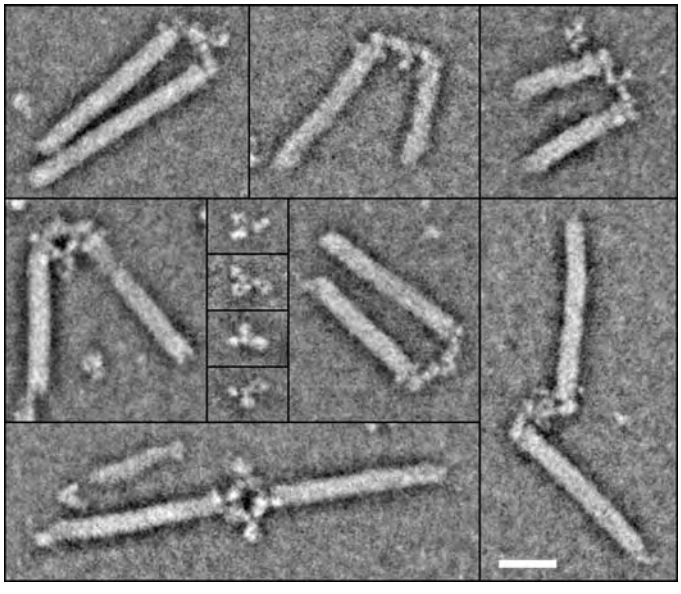

**Fig. 2.** STEM images of wild-type needles incubated with antibodies to LcrV and negatively stained. The antibodies generally attached to the head domain of the tip complex. The small central panels show individual antibodies. Scale bar, 20 nm.

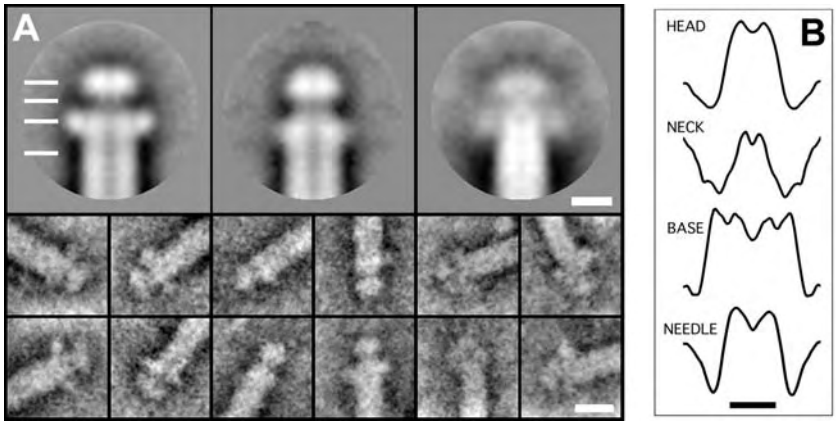


**Fig. 3.** The tip structures of ΔHOPENMVQ bacteria complemented with LcrV or its orthologs PcrV and AcrV, imaged by STEM. (**A**) Projection averages (top) and typical single images (bottom) of the tip complexes formed by LcrV (left; resolution 1.5 nm), PcrV (center; resolution 1.5 nm), and AcrV (right; resolution 2.5 nm). A central channel seems to permeate both the needle and the tip complex. The PcrV tip complex is similar to the LcrV tip complex but has a smaller base. Tip structures formed by AcrV (right) were more variable and larger than those made of LcrV. (**B**) Profiles from the LcrV tip complex average at the locations indicated by white lines in (A), suggesting a central channel. Scale bars, 5 nm in (A) and (B), 10 nm in galleries.

complex, and we observed many examples of two needles joined tip to tip by a single antibody (Fig. 2). No antibodies to LcrV attached to needles purified from the *lcrV* mutant strain (ΔHOPEMNVQ). Furthermore, antibodies directed against YopB or YopD did not bind to wild-type needles (*17*). In contrast, affinity-purified polyclonal antibodies against YscF bound to the needle end opposite the tip complex (fig. S5). Together, these results clearly indicate that LcrV forms the observed tip complex.

*Pseudomonas aeruginosa* and *Aeromonas salmonicida* possess an injectisome closely related to that of *Yersinia*. Their respective LcrV orthologs, PcrV (32.3 kD) and AcrV (40.2 kD), are different in size to LcrV (37.2 kD). The *pcrV*$^+$ and *acrV*$^+$ genes were used to complement the *lcrV* deletion in *Y. enterocolitica* E40 (ΔHOPEMNVQ). The recombinant bacteria could assemble translocation pores. Their needles contained proteins with the size of PcrV and AcrV (fig. S6) and exhibited distinct tip complexes (Fig. 3). The head and neck domains of the tip complex formed by PcrV (Fig. 3A, center) were similar to those formed by LcrV, but the base was narrower (fig. S7). The tip complex formed by AcrV was larger (Fig. 3A, right, and fig. S7), more variable in shape, and more fragile, being absent or altered for many needles. This is reflected by the lower resolution of the AcrV average. In all three cases, a central channel seemed to permeate both the needle and the tip complex (Fig. 3B and fig. S7).

That the needle has a defined tip structure at its distal end, comprising LcrV, is in agreement with previous reports showing that LcrV is surface-exposed (*3*, *4*) and essential for the assembly of a functional translocation pore (*6*). LcrV may act as an assembly platform for this pore (fig. S8) (*6*). The IpaD protein from *Shigella* may function in an analogous fashion (*18*), although it has no clear sequence homology to LcrV. LcrV can also be compared to the EspA filament of enteropathogenic *Escherichia coli*, which forms a physical bridge between the needle and the host cell (*19*). The EspA homolog, SseB of *Salmonella* SPI-2, forms an undefined sheathlike structure on the distal end of the T3S needle (*20*).

The localization of LcrV at the tip of the needle and its role in the assembly of the pore may explain the protective action of antibodies to LcrV. Possibly, the antibodies interfere with the function of the tip complex, impairing the translocation process.

### References and Notes

1. J. E. Galan, A. Collmer, *Science* **284**, 1322 (1999).
2. G. R. Cornelis, H. Wolf-Watz, *Mol. Microbiol.* **23**, 861 (1997).
3. J. Pettersson *et al.*, *Mol. Microbiol.* **32**, 961 (1999).
4. K. A. Fields, M. L. Nilles, C. Cowan, S. C. Straley, *Infect. Immun.* **67**, 5395 (1999).
5. M. N. Marenne, L. Journet, L. J. Mota, G. R. Cornelis, *Microb. Pathog.* **35**, 243 (2003).
6. J. Goure, P. Broz, O. Attree, G. R. Cornelis, I. Attree, *J. Infect. Dis.* **192**, 218 (2005).
7. T. W. Burrows, *Nature* **177**, 426 (1956).

8. W. D. Lawton, M. J. Surgalla, *J. Infect. Dis.* **113**, 39 (1963).
9. A. V. Philipovskiy *et al.*, *Infect. Immun.* **73**, 1532 (2005).
10. T. Kubori *et al.*, *Science* **280**, 602 (1998).
11. F. S. Cordes *et al.*, *J. Biol. Chem.* **278**, 17103 (2003).
12. E. Hoiczyk, G. Blobel, *Proc. Natl. Acad. Sci. U.S.A.* **98**, 4669 (2001).
13. L. Journet, C. Agrain, P. Broz, G. R. Cornelis, *Science* **302**, 1757 (2003).
14. *Yersinia* builds injectisomes when the temperature reaches 37°C, the host's body temperature. Yop secretion is triggered by contact with a target cell or artificially by chelation of $Ca^{2+}$ ions (*15*).
15. Materials and methods are available as supporting material on *Science* Online.
16. Removal of *lcrV* leads to reduced synthesis of YopB and YopD because of a regulatory effect of LcrV on their expression. This undesired effect can be compensated by deleting *yopQ* (*5*).
17. C. A. Mueller *et al.*, unpublished data.
18. W. L. Picking *et al.*, *Infect. Immun.* **73**, 1432 (2005).
19. S. J. Daniell *et al.*, *Cell. Microbiol.* **3**, 865 (2001).
20. D. Chakravortty, M. Rohde, L. Jager, J. Deiwick, M. Hensel, *EMBO J.* **24**, 2043 (2005).
21. We thank P. Jenö for mass spectrometry analyses, M. Duerrenberger for use of the TEM facility, and J. M. Meyer and J. Frey for supplying *P. aeruginosa* PAO1 and *A. salmonicida* JF2267. Supported by the Swiss National Science Foundation (grant nos. 32-65393.01 to G.C. and 3100-059415 to A.E.) and by the Maurice E. Müller Foundation of Switzerland.

**Supporting Online Material**
www.sciencemag.org/cgi/content/full/310/5748/674/DC1
Materials and Methods
Figs. S1 to S8
Tables S1 and S2
References and Notes

5 August 2005; accepted 4 October 2005
10.1126/science.1118476

# Bats Are Natural Reservoirs of SARS-Like Coronaviruses

**Wendong Li,[1,2] Zhengli Shi,[2]* Meng Yu,[3] Wuze Ren,[2] Craig Smith,[4] Jonathan H. Epstein,[5] Hanzhong Wang,[2] Gary Crameri,[3] Zhihong Hu,[2] Huajun Zhang,[2] Jianhong Zhang,[2] Jennifer McEachern,[3] Hume Field,[4] Peter Daszak,[5] Bryan T. Eaton,[3] Shuyi Zhang,[1,6]* Lin-Fa Wang[3]***

**Severe acute respiratory syndrome (SARS) emerged in 2002 to 2003 in southern China. The origin of its etiological agent, the SARS coronavirus (SARS-CoV), remains elusive. Here we report that species of bats are a natural host of coronaviruses closely related to those responsible for the SARS outbreak. These viruses, termed SARS-like coronaviruses (SL-CoVs), display greater genetic variation than SARS-CoV isolated from humans or from civets. The human and civet isolates of SARS-CoV nestle phylogenetically within the spectrum of SL-CoVs, indicating that the virus responsible for the SARS outbreak was a member of this coronavirus group.**

Severe acute respiratory syndrome (SARS) was caused by a newly emerged coronavirus, now known as SARS coronavirus (SARS-CoV) (*1*, *2*). In spite of the early success of etiological studies and molecular characterization of this virus (*3*, *4*), efforts to identify the origin of SARS-CoV have been less successful. Without knowledge of the reservoir host distribution and transmission routes of SARS-CoV, it will be difficult to prevent and control future outbreaks of SARS.

Studies conducted previously on animals sampled from live animal markets in Guangdong, China, indicated that masked palm civets (*Paguma larvata*) and two other species had been infected by SARS-CoV (*5*). This led to a large-scale culling of civets to prevent further SARS outbreaks. However, subsequent studies have revealed no widespread infection in wild or farmed civets (*6*, *7*). Experimental infection of civets with two different human isolates of SARS-CoV resulted in overt clinical symptoms, rendering them unlikely to be the natural reservoir hosts (*8*). These data suggest that although *P. larvata* may have been the source of the human infection that precipitated the SARS outbreak, infection in this and other common species in animal markets was more likely a reflection of an "artificial" market cycle in naïve species than an indication of the natural reservoir of the virus.

Bats are reservoir hosts of several zoonotic viruses, including the Hendra and Nipah viruses, which have recently emerged in Australia and East Asia, respectively (*9*–*11*). Bats may be persistently infected with many viruses but rarely display clinical symptoms (*12*). These characteristics and the increasing presence of bats and bat products in food and traditional medicine markets in southern China and elsewhere in Asia (*13*) led us to survey bats in the search for the natural reservoir of SARS-CoV.

In this study, conducted from March to December of 2004, we sampled 408 bats representing nine species, six genera, and three families from four locations in China (Guangdong, Guangxi, Hubei, and Tianjin) after trapping them in their native habitat (Table 1). Blood, fecal, and throat swabs were collected; serum samples and cDNA from fecal or throat samples were independently analyzed, double-blind, with different methods in our laboratories in Wuhan and Geelong (*14*).

Among six genera of bat species surveyed (*Rousettus*, *Cynopterus*, *Myotis*, *Rhinolophus*, *Nyctalus*, and *Miniopterus*), three communal, cave-dwelling species from the genus *Rhinolophus* (horseshoe bats) in the family *Rhinolophidae* demonstrated a high SARS-CoV antibody prevalence: 13 out of 46 bats (28%) in *R. pearsoni* from Guangxi, 2 out of 6 bats (33%) in *R. pussilus* from Guangxi, and 5 out of 7 bats (71%) in *R. macrotis* from Hubei. The high seroprevalence and wide distribution of seropositive bats is expected for a wildlife reservoir host for a pathogen (*15*).

The serological findings were corroborated by poylmerase chain reaction (PCR) analyses with primer pairs derived from the nucleocapsid (N) and polymerase (P) genes (table S1). Five fecal samples tested positive, all of them from the genus *Rhinolophus*: three in *R. pearsoni* from Guangxi and one each in *R. macrotis* and *R. ferrumequinum*, respectively, from Hubei. No virus was isolated from an inoculation of Vero E6 cells with fecal swabs of PCR-positive samples.

A complete genome sequence was determined directly from PCR products from one of the fecal samples (sample Rp3) that contained relatively high levels of genetic material. The genome organization of this virus (Fig. 1), tentatively named SARS-like coronavirus isolate Rp3 (SL-CoV Rp3), was essentially identical to that of SARS-CoV, with the exception of three regions (Fig. 1, shaded boxes). The overall nucleotide sequence identity between SL-CoV Rp3 and SARS-CoV Tor2 was 92% and increased to ~94% when the three variable regions were excluded. The variable regions are located at the 5′ end of the S gene (equivalent to the S1 coding region of coronavirus S protein) and the region immediately upstream of the N gene. These regions have been identified as "high mutation" regions among different SARS-CoVs (*5*, *16*, *17*). The region upstream of the N gene is known to be prone to deletions of various sizes (*5*, *16*, *18*).

Predicted protein products from each gene or putative open reading frame (ORF) of SL-CoV Rp3 and SARS-CoV Tor2 were com-

[1]Institute of Zoology, Chinese Academy of Sciences (CAS), Beijing, China. [2]State Key Laboratory of Virology, Wuhan Institute of Virology, CAS, Wuhan, China. [3]Commonwealth Scientific and Industrial Research Organization (CSIRO) Livestock Industries, Australian Animal Health Laboratory, Geelong, Australia. [4]Department of Primary Industries and Fisheries, Queensland, Australia. [5]The Consortium for Conservation Medicine, New York, USA. [6]Guangzhou Institute of Biomedicine and Health, Guangzhou, China.

*To whom correspondence should be addressed. E-mail: zlshi@wh.iov.cn (Z.S.); zhangsy@ioz.ac.cn (S.Z.); linfa.wang@csiro.au (L.-F.W.)

**Table 1.** Detection of antibodies to SARS-CoV and PCR amplification of N and P gene fragments with SARS-CoV–specific primers. ND, not determined because of poor sample quality or unavailability of specimens from individual animals.

| Sampling | | Bat species | Antibody test: positive/total (%) | PCR analysis: positive/total (%) | |
|---|---|---|---|---|---|
| Time | Location | | | Fecal swabs | Respiratory swabs |
| Mar 04 | Nanning, Guangxi | *Rousettus leschenaulti* | 1/84 (1.2%) | 0/110 | ND |
| | Maoming, Guangdong | *Rousettus leschenaulti* | 0/42 | 0/45 | ND |
| | | *Cynopterus sphinx* | 0/17 | 0/27 | ND |
| July 04 | Nanning, Guangxi | *Rousettus leschenaulti* | ND | 0/55 | 0/55 |
| | Tianjin | *Myotis ricketti* | ND | 0/21 | 0/21 |
| Nov 04 | Yichang, Hubei | *Rhinolophus pusillus* | ND | 0/15 | ND |
| | | *Rhinolophus ferrumequinum* | 0/4 | 1/8 (12.5%)* | ND |
| | | *Rhinolophus macrotis* | 5/7 (71%) | 1/8 (12.5%)† | 0/3 |
| | | *Nyctalus plancyi* | 0/1 | 0/1 | ND |
| | | *Miniopterus schreibersi* | 0/1 | 0/1 | ND |
| | | *Myotis altarium* | 0/1 | 0/1 | ND |
| Dec 04 | Nanning, Guangxi | *Rousettus leschenaulti* | 1/58 (1.8) | ND | ND |
| | | *Rhinolophus pearsoni* | 13/46 (28.3%) | 3/30 (10%)‡ | 0/11 |
| | | *Rhinolophus pussilus* | 2/6 (33.3%) | 0/6 | 0/2 |

*Positive fecal sample designated Rf1 †Positive fecal sample designated Rm1 ‡Positive fecal samples designated Rp1, Rp2, and Rp3, respectively.

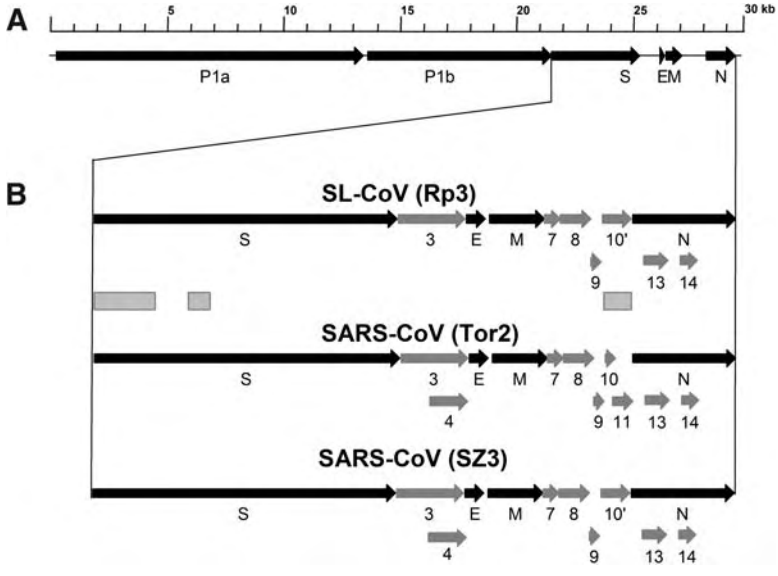


**Fig. 1.** Genome organization of, and comparison between, SL-CoV and SARS-CoV. (**A**) Overall genome organization of SL-CoV Rp3. (**B**) Expanded diagram of the 3′ region of the genome in comparison with SARS-CoV strains Tor2 and SZ3, following the same nomenclature used by Marra *et al*. (*4*). The genes (named by letters P, S, E, M, and N) present in all coronaviruses are shown in dark-colored arrows, whereas the SARS-CoV–specific ORFs are numbered and illustrated in light-colored arrows. ORF10′ follows the nomenclature by Guan *et al*. (*5*) to indicate that the single ORF present between ORF9 and N in SL-CoV is equivalent to the fusion of ORF10 and ORF11 in the same region in SARS-CoV Tor2. The shaded boxes mark the only three regions displaying significant sequence difference between the two viruses (table S2).

pared (table S2). The P, S, E, M, and N proteins, which are present in all coronaviruses, were similarly sized in the two viruses, with sequence identities ranging from 96% to 100%. The only exception was the S1 domain of the S protein, where sequence identity fell to 64%. The S1 domain is involved in receptor binding, whereas the S2 domain is responsible for the fusion of virus and host cell membranes (*19*). The sequence divergence in the S1 domain corroborated our serum neutralization studies, which indicated that although bat sera have a high level of cross-reactive antibodies (with enzyme-linked immunosorbent assay titers ranging from 1:100 to 1:6400), they failed to neutralize SARS-CoV when tested on Vero E6 cells. This finding suggests that S1 is the main target for antibody-mediated neutralization of this group of viruses, which is consistent with previous reports indicating that major SARS-CoV neutralization epitopes are located in the S1 region (*20*, *21*).

In addition to the five genes present in all coronavirus genomes, coronaviruses also have several ORFs between the P gene and the 3′ end of the genome that code for nonstructural proteins. The function of these nonstructural proteins is largely unknown. The location and sequence of ORFs are group- or virus-specific and hence can serve as important molecular markers for studying virus evolution and classification (*19*, *22*). SARS-CoV has a unique set of ORFs not shared by any of the known coronaviruses (*3*, *4*). Most of these ORFs were also present in SL-CoV, confirming the extremely close genetic relationship between SARS-CoV and SL-CoV (Fig. 1 and table S2).

Coronaviruses produce subgenomic mRNAs through a discontinuous transcription process not fully characterized (*19*). Conserved nucleotide sequences functioning as transcription regulatory sequences (TRSs) are required for the production of the subgenomic mRNAs. In SARS-CoV, such TRSs were identified at each of the predicted gene start sites (*3*, *4*). All of these TRSs were absolutely conserved between SARS-CoV Tor2 and SL-CoV Rp3 (table S3), further demonstrating that these two viruses are very closely related.

SL-CoV is completely different from a bat coronavirus (bat-CoV) recently identified by Poon *et al*. (*7*) from species of bats in the genus *Miniopterus* during a wildlife surveillance study in Hong Kong (Fig. 2). Because the complete genome sequence was not available for bat-CoV, only the trees covering the common sequences (i.e., parts of the P1b and S2 proteins) are shown. The phylogenetic analysis demonstrated that SL-CoV Rp3 and SARS-CoVs are clustered together but that bat-CoV is placed among the relatively distant group 1 viruses. Hereafter, SARS-CoVs and SL-CoVs will be collectively called the SARS cluster of coronaviruses.

In addition to the complete genome sequence of SL-CoV Rp3, partial genome sequences for the other four PCR-positive bat samples were also determined. Phylogenetic analysis based on the N protein sequences (Fig. 3A) revealed that the genetic variation among the SL-CoV sequences was much greater than that exhibited by SARS-CoVs (for simplicity, only three human and civet SARS-CoV isolates were used; the remainder are almost identical to those shown). This was especially obvious when SL-CoVs isolated from different bat species were compared. Moreover, the results suggested that SARS-CoVs nestle phylogenetically within the spectrum of SL-CoVs.

We also compared the "high mutation" regions in samples Rf1, Rm1, and Rp3. For the region upstream of the N gene, SL-CoVs from all three bat species contained a single ORF (ORF10′), similar to that found in SARS-CoV isolates from civets (*5*) and patients in the early phase of the outbreaks (*16*, *18*) but different from that in most human isolates, which

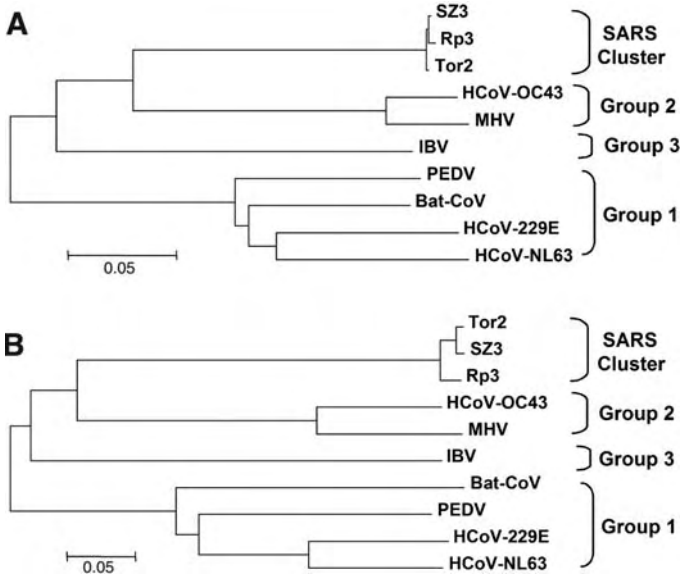


**Fig. 2.** Phylogenetic trees. (**A**) and (**B**) are trees based on deduced amino acid sequences of the same regions in P1b and S, respectively, as used by Poon *et al.* (*7*) for bat-CoV. Tor2 and SZ3, SARS-CoV strains Tor2 and SZ3; Rp3, SL-CoV Rp3; HCoV, human coronavirus; MHV, mouse hepatitis virus; PEDV, porcine epidemic diarrhea virus; IBV, avian infectious bronchitis virus.

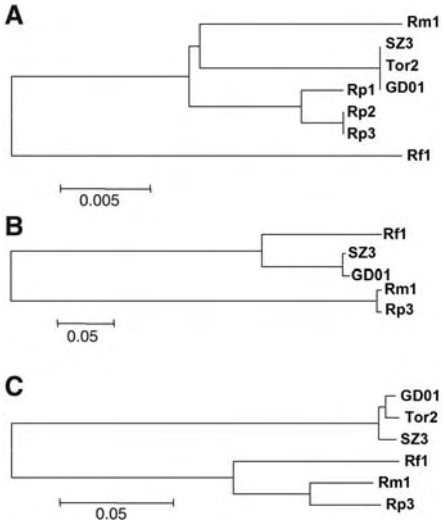


**Fig. 3.** Phylogenetic trees based on deduced amino acid sequences of (**A**) N, (**B**) ORF10′, and (**C**) S1 proteins. Tor2, SZ3, and GD01, different SARS-CoV strains; Rf1, Rm1, and Rp1-3, different SL-CoV sequences. The genetic distance scale shown for (A) is different from those for (B) and (C).

have a 29-nucleotide deletion in this region (*3*, *4*, *16*). ORF10′ in Rf1 codes for a protein having the same size (122 amino acids) as and more than 80% sequence identity to ORF10′ proteins of SARS-CoVs, but those in Rm1 and Rp3 code for a 121–amino acid protein with only 35% sequence identity (Fig. 3B and fig. S2). By contrast, analysis of the S1 protein regions (Fig. 3C and fig. S3) indicated that Rf1 was more closely related to SL-CoVs from two other bat species than to SARS-CoVs, suggesting that the SARS cluster of coronaviruses could recombine to increase genetic diversity and fitness, as is well documented for other coronaviruses (*19*). We were unable to sequence these regions for Rp1 or Rp2, owing to the poor quality of the fecal materials from these two animals. The limited amount of cDNA available was used up for N gene analysis and in initial sequencing trials with SARS-CoV–derived primers, which were largely unsuccessful. Judging from the close relationship of the N genes between Rp1, Rp2, and Rp3 (fig. S1), it is unlikely that Rp1 or Rp2 will have major sequence differences from Rp3 in the S1 or ORF10′ regions. This is not unexpected, considering that these three positive samples were obtained from the same bat species in the same location.

The genetic diversity of bat-derived sequences supports the notion that bats are a natural reservoir host of the SARS cluster of coronaviruses. A similar observation has been made for henipaviruses, another important group of emerging zoonotic viruses of bat origin, which show greater genetic diversity in bats than was observed among viruses isolated during the initial Nipah outbreaks in Malaysia (*23*–*26*). The overall nucleotide sequence identity of 92% between SL-CoVs and SARS-CoVs is very similar to that observed between Nipah viruses isolated from Malaysia and Bangladesh in 1999 and 2004, respectively (*25*) (fig. S4). SL-CoVs present a new challenge to the diagnosis and treatment of future disease outbreaks. The current tests and therapeutic strategies may not work effectively against all viruses in this group, owing to their great genetic variability in the S1 domain region of the S gene.

The genus *Rhinolophus* contains 69 species and has a wide distribution from Australia to Europe (*27*). They roost primarily in caves and feed mainly on moths and beetles. However, notwithstanding the predominant *Rhinolophus* findings in this study, it is highly likely that there are more SARS-related coronaviruses to be discovered in bats. Indeed, our positive serological findings in the cave-dwelling fruit bat *Rousettus leschenaulti* indicate that infection by a related virus could occur in fruit bats as well, albeit at a much lower frequency. A plausible mechanism for emergence from a natural bat reservoir can be readily envisaged. Fruit bats including *R. leschenaulti*, and less frequently insectivorous bats, are found in markets in southern China. An infectious consignment of bats serendipitously juxtaposed with a susceptible amplifying species, such as *P. larvata*, at some point in the wildlife supply chain could result in spillover and establishment of a market cycle while susceptible animals are available to maintain infection. Further studies in field epidemiology, laboratory infection, and receptor distribution and usage are being conducted to assess potential roles played by different bat species in SARS emergence.

These findings on coronaviruses, together with data on henipaviruses (*23*–*25*, *28*), suggest that genetic diversity exists among zoonotic viruses in bats, increasing the possibility of variants crossing the species barrier and causing outbreaks of disease in human populations. It is therefore essential that we enhance our knowledge and understanding of reservoir host distribution, animal-animal and human-animal interaction (particularly within the wet-market system), and the genetic diversity of bat-borne viruses to prevent future outbreaks.

### References and Notes

1. J. S. M. Peiris *et al.*, *Lancet* **361**, 1319 (2003).
2. T. G. Ksiazek *et al.*, *N. Engl. J. Med.* **348**, 1953 (2003).
3. P. A. Rota *et al.*, *Science* **300**, 1394 (2003).
4. M. A. Marra *et al.*, *Science* **300**, 1399 (2003).
5. Y. Guan *et al.*, *Science* **302**, 276 (2003).
6. C. Tu *et al.*, *Emerg. Infect. Dis.* **10**, 2244 (2004).
7. L. L. M. Poon *et al.*, *J. Virol.* **79**, 2110 (2005).
8. D. Wu *et al.*, *J. Virol.* **79**, 2620 (2005).
9. K. Murray *et al.*, *Science* **268**, 94 (1995).
10. K. B. Chua *et al.*, *Science* **288**, 1432 (2000).
11. L.-F. Wang, B. T. Eaton, *Infect. Dis. Rev.* **3**, 52 (2001).
12. S. E. Sulkin, R. Allen, *Monograph Virol.* **8**, 170 (1974).
13. S. P. Mickleburgh, A. M. Huston, P. A. Racey, *Oryx* **36**, 18 (2002).
14. Materials and methods are available as supporting material on *Science* Online.
15. P. J. Hudson, A. Rizzoli, B. T. Grenfell, H. Heesterbeek, A. P. Dobson, Eds., *The Ecology of Wildlife Diseases* (Oxford Univ. Press, Oxford, 2002).
16. Chinese SARS Molecular Epidemiology Consortium, *Science* **303**, 1666 (2004).
17. P. Liò, N. Goldman, *Trends Microbiol.* **12**, 106 (2004).
18. H.-D. Song *et al.*, *Proc. Natl. Acad. Sci. U.S.A.* **102**, 2430 (2005).
19. M. C. Lai, K. V. Holmes, in *Fields Virology*, D. M. Knipe *et al.*, Eds. (Lippincott, Williams & Wilkins, Philadelphia, 2001), vol. 2, chap. 35.
20. R. A. Tripp *et al.*, *J. Virol. Methods* **128**, 21 (2005).
21. Y. He, H. Lu, P. Siddiqui, Y. Zhou, S. Jiang, *J. Immunol.* **174**, 4908 (2005).
22. D. A. Brian, R. S. Baric, *Curr. Top. Microbiol. Immunol.* **287**, 1 (2005).
23. S. AbuBakar *et al.*, *Emerg. Infect. Dis.* **10**, 2228 (2004).
24. J.-M. Reynes *et al.*, *Emerg. Infect. Dis.* **11**, 1042 (2005).
25. B. H. Harcourt *et al.*, *Emerg. Infect. Dis.* **11**, 1594 (2005).
26. V. P. Hsu *et al.*, *Emerg. Infect. Dis.* **10**, 2082 (2004).
27. T. H. Kunz, M. B. Fenton, Eds., *Bat Ecology* (Univ. of Chicago Press, Chicago, 2003).
28. L.-F. Wang, K. B. Chua, M. Yu, B. T. Eaton, *Curr. Genomics* **4**, 263 (2003).
29. This work was jointly funded by a special grant for "Animal Reservoir of SARS-CoV," State Key Program for Basic Research Grant 2005CB523004, and State High Technology Development Program grant no.

2005AA219070 from the Ministry of Science and Technology, People's Republic of China; the Sixth Framework Program "EPISARS" from the European Commission (no. 51163); the Australian Biosecurity Cooperative Research Centre for Emerging Infectious Disease (Project 1.007R); and an NIH/NSF "Ecology of Infectious Diseases" award (no. R01-TW05869) from the John E. Fogarty International Center and the V. Kann Rasmussen Foundation. For the full-length genome sequence of SL-CoV Rp3, see GenBank accession no. DQ71615. Additional GenBank accession numbers are given in the supporting material.

**Supporting Online Material**
www.sciencemag.org/cgi/content/full/1118391/DC1
Materials and Methods
Figs. S1 to S4
Tables S1 to S3
References and Notes

4 August 2005; accepted 20 September 2005
Published online 29 September 2005;
10.1126/science.1118391
Include this information when citing this paper.

# Neurogenesis in the Hypothalamus of Adult Mice: Potential Role in Energy Balance

**Maia V. Kokoeva, Huali Yin, Jeffrey S. Flier***

**Ciliary neurotrophic factor (CNTF) induces weight loss in obese rodents and humans, and for reasons that are not understood, its effects persist after the cessation of treatment. Here we demonstrate that centrally administered CNTF induces cell proliferation in feeding centers of the murine hypothalamus. Many of the newborn cells express neuronal markers and show functional phenotypes relevant for energy-balance control, including a capacity for leptin-induced phosphorylation of signal transducer and activator of transcription 3 (STAT3). Co-administration of the mitotic blocker cytosine-β-D-arabinofuranoside (Ara-C) eliminates the proliferation of neural cells and abrogates the long-term, but not the short-term, effect of CNTF on body weight. These findings link the sustained effect of CNTF on energy balance to hypothalamic neurogenesis and suggest that regulated hypothalamic neurogenesis in adult mice may play a previously unappreciated role in physiology and disease.**

The obesity epidemic has prompted major efforts to develop safe and effective therapies (*1*, *2*). However, approved drugs for obesity have limited efficacy and act only acutely, with patients rapidly regaining weight after terminating treatment (*3*). Only the neurocytokine ciliary neurotrophic factor (CNTF) and Axokine, an analog of CNTF developed as a drug candidate for the treatment of obesity, appear to deviate from this paradigm. Rodents and patients treated with Axokine were reported to maintain lowered body weights weeks to months after the cessation of treatment (*4*, *5*). This feature of Axokine/CNTF action is unexplained and suggests that CNTF induces long-lasting changes in one or more elements of the energy-balance circuitry.

In rodents, CNTF is most potent when administered directly into the cerebrospinal fluid (*6*) and activates signaling cascades in hypothalamic nuclei involved in feeding control (*5*, *7*, *8*). For instance, CNTF activates phosphorylation of signal transducer and activator of transcription 3 (STAT3) in a population of hypothalamic neurons that substantially overlaps with those activated by leptin (*5*). However, in contrast to CNTF, leptin-treated animals do not maintain their lowered body weight after the cessation of treatment. We thus sought a CNTF-specific mechanism to explain this long-term effect.

CNTF supports the survival of neurons in vitro and in vivo (*9*) and has also been implicated in the maintenance of adult neural stem cells (*10*). Furthermore, other trophic factors, such as epidermal growth factor and fibroblast growth factor 2, are known to act as mitogens on adult neuronal progenitors (*11*, *12*), and they promote the functional regeneration of hippocampal pyramidal neurons (*13*). Neurogenesis in the adult brain is most clearly defined in the subventricular zone (SVZ) of the lateral ventricles and the subgranular zone (SGZ) of the hippocampal formation (*14*). However, recent reports indicate that the neuroproliferative potency in the adult extends to other brain structures, including the hypothalamus (*15*–*17*). On the basis of these findings, we hypothesized that the long-term effect of CNTF on body-weight regulation might involve neurogenesis in the hypothalamus, which is the brain region most relevant for energy-balance regulation.

To assess the mitogenic potency of CNTF in the adult nervous system in vivo, we delivered the cell-proliferation marker bromodeoxyuridine (BrdU) alone (vehicle treatment) or together with CNTF directly into the cerebrospinal fluid of mouse brains (*18*). CNTF and BrdU were continuously infused for 7 days into the right lateral ventricle using osmotic minipumps. Mice were switched to a high-fat diet two months before surgery and were kept on this diet throughout the experiments. In accordance with previous results (*5*), CNTF-treated mice showed a marked reduction in body weights (Fig. 1A), which persisted after termination of CNTF delivery. Mice were killed 22 days after surgery, and brain sections were immunostained with an antibody against BrdU. Because BrdU incorporates into DNA of dividing cells, BrdU-positive ($BrdU^+$) cells are thought to represent newborn cells. Figure 1B shows coronal sections of vehicle- and CNTF-infused animals at the level of the arcuate, ventromedial, and dorsomedial nuclei, well-known hypothalamic centers for energy-balance regulation (*19*). In vehicle-infused animals, few $BrdU^+$ cells were detected in the parenchyma surrounding the third ventricle (Fig. 1B, left). Administration with CNTF led to a dramatic increase of BrdU+ cells (Fig. 1B, right). Note the higher density of $BrdU^+$ cells at the base of the third ventricle, which is part of the arcuate nucleus/median eminence.

The pattern of CNTF receptor (CNTFR) mRNA expression is consistent with this observation. In situ hybridization using a riboprobe against CNTFR mRNA revealed strong staining in the walls of the basal third ventricle and surrounding arcuate nucleus parenchyma (Fig. 1C). Because this section originated from an animal treated with both CNTF and BrdU, we colabeled with antibodies to BrdU. Many $BrdU^+$ cells were positive for CNTFR expression, indicating that CNTF, at least in part, directly promotes cell division by binding to CNTFR on putative neural progenitor cells (Fig. 1D, inset). By counting all newly generated cells in the caudal hypothalamus, CNTF treatment led to a marked increase of $BrdU^+$ cells over vehicle-infused animals (Fig. 1E). The total number of $BrdU^+$ cells in CNTF-treated animals remained constant for at least 2 weeks after the infusion period. Subsequently, the numbers decreased but plateaued at a high level. Vehicle-infused animals showed a similar fractional decrease over time. Thus it appears that the majority of hypothalamic $BrdU^+$ cells do not die or migrate to distant areas as reported for newborn neurons of the SVZ, which follow the rostral migratory stream toward the olfactory bulb (*20*).

To investigate the origin of adult-born cells in the hypothalamus, we examined CNTF and vehicle-infused brains every 12 hours starting 48 hours after surgery, a time when the infused CNTF/BrdU should just reach the ventricular system (*18*). Hypothalamic BrdU incorporation was first detected 60 to 72 hours

Division of Endocrinology, Department of Medicine, Beth Israel Deaconess Medical Center and Harvard Medical School, 99 Brookline Avenue, Boston, MA 02215, USA.

*To whom correspondence should be addressed. E-mail: jflier@bidmc.harvard.edu

after surgery (fig. S1). Even at these early time points, BrdU$^+$ cells were found scattered within the parenchyma, suggesting that at least a fraction of the newly generated cells, endogenous and CNTF-induced, arise within hypothalamic parenchyma distant from the ependymal lining. Also at these early time points, BrdU$^+$ cells were often observed as close contacting pairs, suggestive of recently divided daughter cells (fig. S1B, insets).

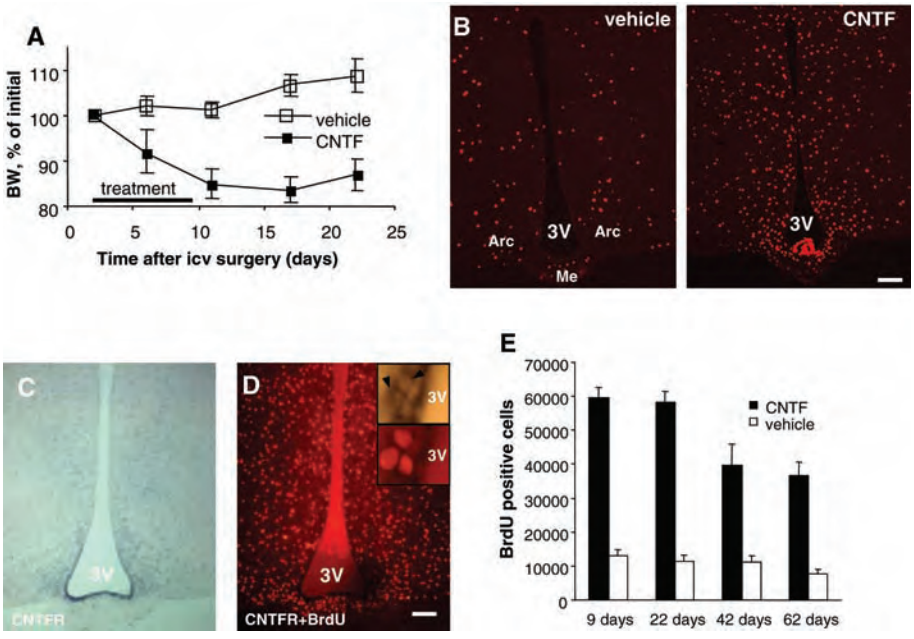


**Fig. 1.** CNTF reduces body weights long term and induces cell proliferation in the hypothalamus. (**A**) Mice were icv infused for 7 days with BrdU (12 μg/day) in artificial cerebrospinal fluid alone or together with CNTF (0.75 μg/day) at a flow rate of 12 μl/day. Body weight (BW) is shown as percentage difference from initial body weight. All data are mean ± SEM ($n$ = 5 animals per group). (**B**) BrdU-labeled cells in coronal sections of the hypothalamus on the level of the arcuate nucleus. (**C**) In situ hybridization with a digoxygenin-labeled probe directed against CNTFR mRNA. Blue precipitate indicates staining. (**D**) Fluorescence image of the same section reveals BrdU$^+$ cells (red). (Insets) High-power magnification of BrdU$^+$ cells that express CNTFR (arrowheads). (**E**) Total number of BrdU$^+$ cells detected in the caudal hypothalamus of vehicle- and CNTF-infused animals. Brains were inspected at the indicated times after surgery. Error bars represent mean ± SEM ($n$ = 3 animals per group). 3V, third ventricle; Arc, arcuate nucleus; Me, median eminence. Scale bars, 100 μm

We next explored the phenotype of hypothalamic BrdU$^+$ cells by using immunofluorescence double staining combined with confocal microscopy on hypothalamic sections of CNTF-infused animals. Double labeling with an antibody against Hu, which is a marker for immature and mature neurons that labels nuclei and perikarya (*21*), indicates that a substantial number of hypothalamic BrdU$^+$ cells take on a neuronal fate (Fig. 2A). Three-dimensional (3D) reconstruction using multiple confocal images clearly demonstrates that BrdU$^+$ cells express Hu (Fig. 2B). Based on confocal analysis of brain sections from CNTF-infused animals 42 days after surgery, 42.7% (±8.8) of the BrdU$^+$ cells in the caudal hypothalamus expressed Hu. Vehicle-infused animals had 20.7% (±9.6) co-labeled cells. Colabeling with an antibody against β-tubulin type III (TuJ1) (*22*), another marker for immature and mature neurons, confirmed these results (fig. S2, A and B). Another population of newborn cells could be assigned to a glial phenotype of the oligodendrocyte lineage (Fig. 2, C and D). Confocal analysis of CNTF-infused brains 42 days after surgery revealed that 22.9% (±6.0) of hypothalamic BrdU$^+$ cells expressed the oligodendrocyte marker adenomatosis polyposis coli (APC) (*23*). The percentage of colabeled cells was not substantially different in vehicle-infused animals (31.7 ± 12.1%). In contrast, we detected few if any BrdU$^+$ cells expressing the astrocytic marker glial fibrillary acidic protein (GFAP) (fig. S2C).

We also tested hypothalamic BrdU$^+$ cells for the expression of doublecortin (Dcx), a transient marker for early postmitotic neurons (*24*). In contrast to Hu and TuJ1, Dcx is expressed in migrating and differentiating neurons but not in mature neurons. Because Dcx is a microtubule-associated protein present in

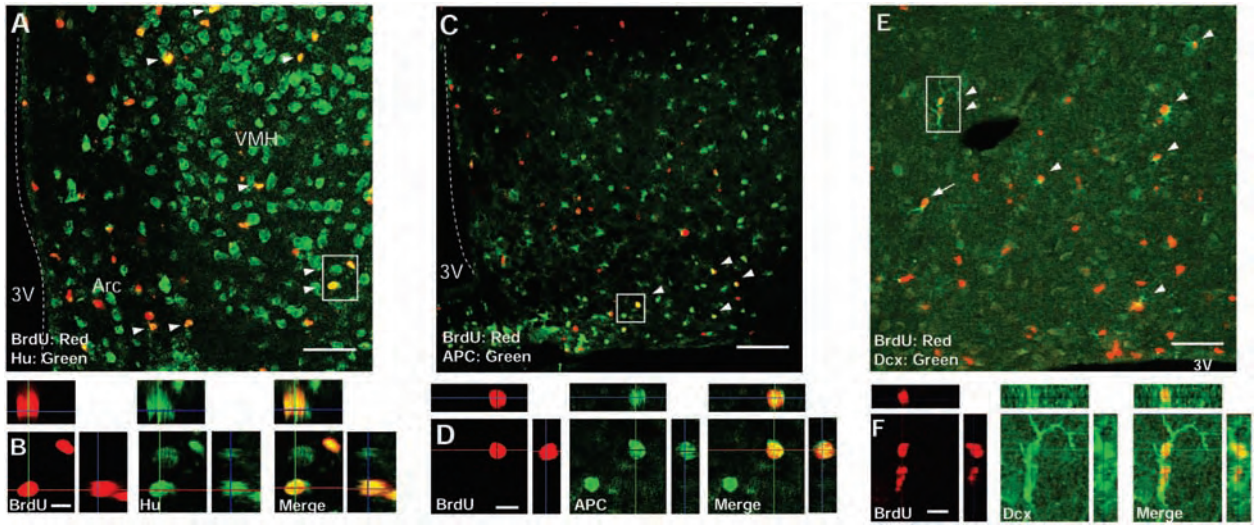


**Fig. 2.** Newborn hypothalamic cells exhibit neuronal and glial phenotypes. Brains were perfused 42 days (A to D) or 9 days (E and F) after icv surgery and immunolabeled sections of the caudal hypothalamus were inspected by laser-scanning confocal microscopy. (**A**) Numerous BrdU$^+$ cells (red) express the neuronal marker Hu (green, arrowheads). (**B**) Confocal 3D reconstruction of area boxed in (A). Top, $x$-$z$ plane; right, $y$-$z$ plane. (**C**) BrdU$^+$ cells expressing APC (arrowheads). (**D**) 3D reconstruction of area boxed in (C). (**E**) BrdU$^+$ (red) cells expressing the Dcx (green, arrowheads). (**F**) 3D reconstruction of the area boxed in (E). VMH, ventromedial hypothalamus. Scale bars in (A), (C), and (E), 50 μm; in (B), (D), and (F), 10 μm.

projections, antibodies to Dcx allow the visualization of dendritic arborization in immature neurons. Immunohistochemical inspection of hypothalamic brain sections from CNTF-treated animals revealed a large number of BrdU$^+$ cells expressing Dcx 9 days after surgery (Fig. 2E, arrowheads), estimated to match the number of BrdU$^+$/Hu$^+$ cells. Some BrdU$^+$/Dcx$^+$ cells exhibited fusiform shapes with a single process extending from their somata (Fig. 2E, arrow). Others displayed more complex morphologies with many often-arborized projections (Fig. 2F), which is a possible indication that these cells functionally integrate into the hypothalamic circuitry.

To determine whether newborn hypothalamic cells exhibit a critical functional phenotype relevant to energy-balance regulation, we used an antibody to phosphorylated (p) STAT3, a component of the leptin-activated signaling cascade in leptin receptor–containing cells of the hypothalamus (*25*). This cascade is a key signaling circuit for energy-balance regulation in hypothalamic feeding centers (*26*). Injection of leptin intraperitoneally (ip) induces STAT3 phosphorylation specifically in the arcuate, ventromedial, and dorsomedial nuclei of the hypothalamus (*27*, *28*). To induce STAT3 phosphorylation, we injected mice ip with leptin after overnight fasting, and 45 min later, we perfused them for immunohistochemical analysis. Labeling with antibody to pSTAT3 revealed strong nuclear staining throughout the arcuate, ventromedial, and dorsomedial nuclei in leptin-treated animals (fig. S3A). In contrast, the signal was virtually absent in saline-treated mice, confirming the specificity of the antibody to pSTAT3 (fig. S3B). We next applied this treatment to CNTF-infused mice 42 days after surgery. In these animals, many of the hypothalamic BrdU$^+$ cells were pSTAT3$^+$ after leptin treatment, indicating that these newborn cells acquired responsiveness to leptin (Fig. 3, A and B). 26.3% (±6.4) of all newly born cells confined to the arcuate, ventromedial, and dorsomedial nuclei were pSTAT3$^+$. A similar fraction of colabeled cells, 21.5% (±7.1), could be detected in vehicle-infused animals, indicating that CNTF-treatment substantially increases the absolute number of leptin-sensitive pSTAT3$^+$ cells.

If leptin-responsive STAT3 phosphorylation within newborn hypothalamic neurons is critical for the sustained weight-loss effect of CNTF, then mice lacking leptin signaling should show an altered CNTF response. To test this hypothesis, we intracerebroventricularly (icv) infused ob/ob mice, which lack endogenous leptin (*29*), with CNTF or leptin (Fig. 3C). CNTF enhanced cell proliferation in the hypothalami of ob/ob mice (fig. S4) similarly to mice with diet-induced obesity (DIO). However, in contrast to DIO mice, ob/ob mice did not maintain lowered body weights resulting from CNTF treatment. Instead, they regained weight shortly after drug cessation, similar to leptin-treated animals (Fig. 3C). For comparison, wild-type mice with DIO treated with an equal dose of CNTF displayed weight loss that was sustained well beyond treatment cessation (Fig. 3C). Consistent with our data, db/db mice lacking leptin receptors rapidly regained body weight after termination of peripheral CNTF treatment (*30*).

Neuropeptide Y (NPY) and pro-opiomelanocortin (POMC)–expressing neurons in the arcuate nucleus play crucial antagonistic roles in the regulation of energy balance (*19*). To assess whether BrdU$^+$ cells in the arcuate nucleus express either of these markers, we combined anti-BrdU immunolabeling and in situ hybridization using digoxigenin-labeled riboprobes against NPY or POMC mRNAs. In CNTF-infused animals 42 days after surgery, we identified several BrdU$^+$ cells per brain section expressing NPY or POMC (Fig. 4). Although the role of these specific neurons in the sustained CNTF effect is unknown, it is clear that CNTF can induce neurogenesis within neurocircuitry that is critical to energy balance in the adult mouse hypothalamus.

To investigate whether the stimulatory effect of CNTF on neurogenesis/cell proliferation underlies its ability to induce long-term weight loss, we used the antimitotic drug Ara-C (cytosine-β-D-arabinofuranoside), which prevents neural progenitor cells of the adult SVZ from dividing when centrally administered (*31*). Mice kept for 2 months on a high-fat diet were infused with Ara-C and/or CNTF into the lateral ventricle for 7 days. Inspection of brains 9 days after surgery revealed that, as before, CNTF treatment markedly increased the number of newborn cells (Fig. 5A). In contrast, we detected few if any BrdU$^+$ cells throughout the brain parenchyma of animals exposed to Ara-C (Fig. 5A). Thus, Ara-C efficiently blocks cell proliferation in the adult mouse brain, including the hypothalamus.

We next explored energy-balance regulation in the Ara-C–treated animals. As before, mice receiving CNTF alone had reduced body weights compared with animals infused with vehicle only or Ara-C only, and this was

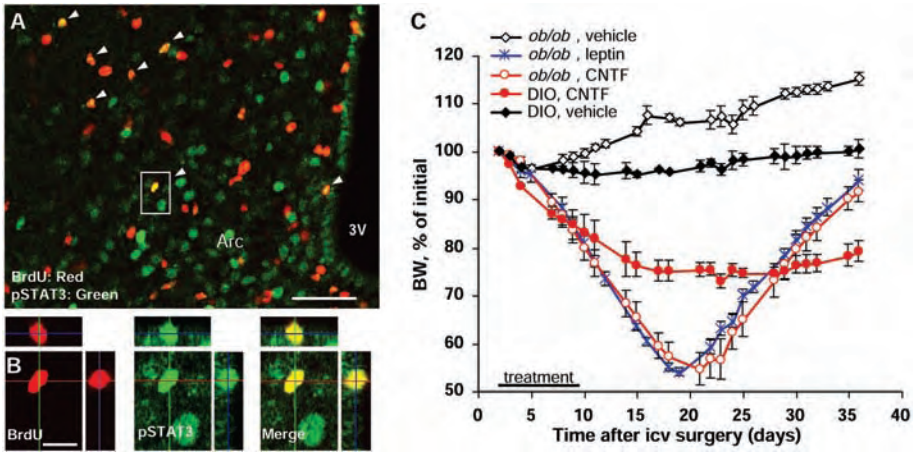


**Fig. 3.** (**A**) Newborn hypothalamic cells respond to leptin. Many BrdU$^+$ (red) cells of CNTF-treated mice were also positive for pSTAT3 (green) after ip leptin injection. (**B**) 3D confocal reconstruction of area boxed in (A). (**C**) Groups of DIO or ob/ob mice ($n$ = 5) were icv infused for 7 days with CNTF (0.75 μg/day) or leptin (0.60 μg/day). For all animals, BrdU (12 μg/day) was coadministered. To induce DIO, mice were placed on a high-fat diet for 5 months. Body weight is shown as percentage difference from initial body weight. All data are mean ± SEM. Scale bars in (A), 50 μm; in (B), 10 μm.

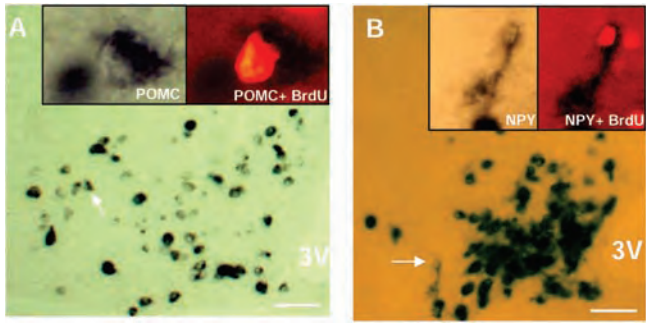


**Fig. 4.** In situ hybridization combined with anti-BrdU immunohistochemistry reveals newborn cells expressing NPY and POMC. Coronal sections at the level of the arcuate nucleus of a CNTF-treated mouse 42 days after surgery. (**A**) Brain section after hybridization to a digoxigenin-labeled probe for POMC. Inset left: High-power magnification of a POMC expressing cell (arrow). Inset right: Fluorescence image of the same cell demonstrating colocalization with BrdU. (**B**) Brain section hybridized to a NPY probe. The NPY-expressing cell marked by an arrow is also positive for BrdU (Insets). Scale bars: 100 μm.

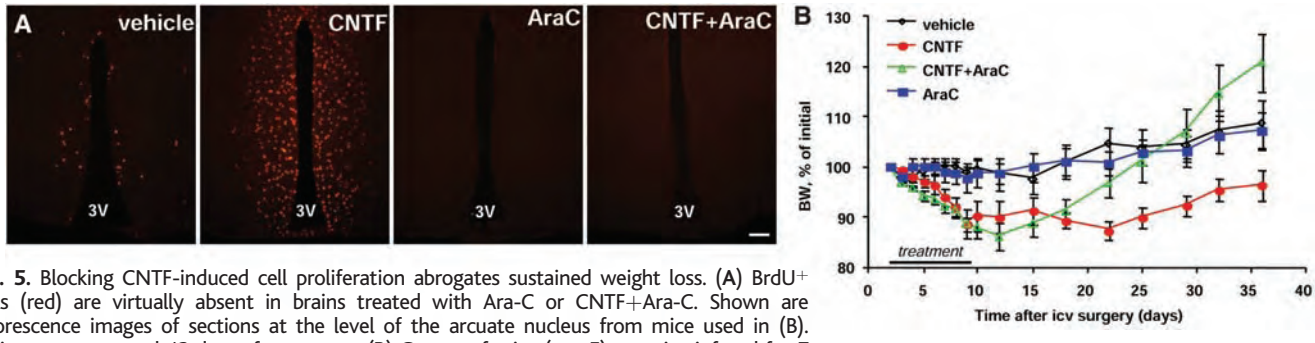


**Fig. 5.** Blocking CNTF-induced cell proliferation abrogates sustained weight loss. (**A**) BrdU+ cells (red) are virtually absent in brains treated with Ara-C or CNTF+Ara-C. Shown are fluorescence images of sections at the level of the arcuate nucleus from mice used in (**B**). Brains were removed 42 days after surgery. (**B**) Groups of mice ($n$ = 5) were icv infused for 7 days with CNTF (0.75 μg/day) and/or Ara-C (40 μg/day). For all animals, BrdU (12 μg/day) was coadministered. Body weight is shown as percentage difference from initial body weight. All data are mean ± SEM. Scale bar, 100 μm.

maintained beyond cessation of the drug (Fig. 5B). In contrast, the time course of body-weight changes of mice treated with both CNTF and Ara-C (CNTF+Ara-C) showed a distinct pattern. First, the acute CNTF-induced weight loss during the infusion period (days 0 to 9) was unaffected by Ara-C. However, after cessation of treatment, CNTF+Ara-C–infused animals rapidly regained weight, reaching body weights of vehicle-treated animals at about 20 days after treatment. In accordance with previous results (*5*, *30*), CNTF-induced weight loss was associated with reduced food intake, whereas Ara-C–dependent body-weight rebound after treatment cessation was paralleled by increased food intake (fig. S5).

Although Ara-C specifically inhibits mitosis, it has been reported that this mitotic blocker can also act as a cytotoxin, triggering apoptotic degradation of postmitotic neurons (*32*). To address this potential concern, we inspected Ara-C–treated brains using the sensitive cell-death marker Fluoro-Jade (*33*). We observed no signs of cell degeneration throughout the brain parenchyma after treatment (fig. S6A). As positive controls, we used mice treated with gold thioglucose, which induces cell death in the ventromedial hypothalamus (fig. S6B).

To determine whether Ara-C interferes with acute CNTF signaling and action, we examined the CNTF-dependent induction of hypothalamic STAT3 phosphorylation (*5*). STAT3 phosphorylation, which is acutely triggered during CNTF exposure, was unaffected by Ara-C (fig. S7A). Also, the CNTF-induced activation of astrocytes (*34*) appears unperturbed by Ara-C. The up-regulation of GFAP expression associated with glial activation is equally evident in mice treated with CNTF or CNTF+Ara-C, but not in vehicle-infused animals (fig. S7B). Thus, at the dose used in our experiments, Ara-C blocked the cell proliferation/neurogenesis effect of CNTF without detectable toxicity, or inhibition of its acute actions.

We show that CNTF robustly induces cell proliferation in the hypothalamus with many of the newborn cells taking on a neuronal fate. In the past, research on adult neurogenesis has mainly focused on the following two brain regions: the SVZ, which gives rise to neuronal precursors that migrate to the olfactory bulb, and the SGZ, which fuels the granular layer of the dentate gyrus with new neurons (*14*). In contrast, adult neurogenesis in the hypothalamus has received little attention (*17*, *35*). This may be attributable to the strong proliferative potency of the SVZ or the SGZ and the relative insensitivity of the methods used to reveal newborn cells in other brain regions (*36*). In our study, instead of injecting BrdU ip, the route commonly used to mark newborn cells, we administered BrdU centrally. This approach allowed the detection of newborn hypothalamic cells in response to CNTF and might be generally suitable to detect neurogenesis in brain regions with a proliferative potency lower than that in the SVZ or SGZ. The origin of newborn hypothalamic cells is presently unclear. It appears that rather than being exclusively restricted to the ependymal lining of the third ventricle, neural progenitors also reside within the hypothalamic parenchyma.

Many of the newborn hypothalamic cells induced by CNTF exhibit phenotypes important for energy-balance regulation, including neuropeptide expression and capacity for leptin-induced activation of STAT3. Mitotic blockade of CNTF-stimulated cell proliferation does not alter the acute CNTF-dependent weight loss but abrogates the long-term effect on body-weight regulation. These observations support a model in which the short-term effects of CNTF result from acute signaling in existing neurons, whereas the long-term effects on body weights of CNTF-treated animals require functional neurogenesis in hypothalamic structures that subserve energy homeostasis. Because CNTF stimulates hypothalamic cell proliferation yet does not cause a sustained weight loss in ob/ob mice, it is plausible that a leptin-sensitive component of the newborn cell population is central to the sustained antiobesity effect of CNTF, possibly by enhancing the satiety response of the leptin signaling circuitry. The precise identity and function of the responsive cells remain to be determined.

Because CNTF also induces cell proliferation/neurogenesis in the SVZ of the lateral ventricles (*37*) and because Ara-C blocks cell proliferation throughout the ventricular system, these studies cannot exclude a role for extra-hypothalamic neurogenesis in the long-term effect of CNTF on energy balance. This possibility seems unlikely, however, because CNTFR expression is exceptionally strong in the parenchyma surrounding the third ventricle at the level of the arcuate, ventromedial, and dorsomedial nuclei, all of which are key structures involved in energy homeostasis (Fig. 1C). We also observe a particularly dense population of newborn cells at the bottom of the third ventricle after CNTF administration (Fig. 1B). Furthermore, there are no structures adjacent to the walls of the lateral ventricles known to be involved in the control of energy balance. Thus, cell proliferation within the hypothalamus is likely to be responsible for the CNTF-induced sustained effects on energy balance.

Hypothalamic plasticity has recently been proposed to play a role in energy-balance regulation (*38*). It was shown that leptin can influence the number and types of synaptic inputs to POMC and NPY neurons in the adult arcuate nucleus (*39*) and that perinatal leptin adminstration to leptin-deficient mice increases the density of certain projections emanating from the arcuate nucleus (*40*). Our observation that CNTF-induced neurogenesis occurs within hypothalamic feeding centers represents another type of plastic change, with the capacity to reset the energy-balance set point.

Axokine appears capable of lowering body weights in obese humans, but the development of neutralizing antibodies has limited the development of this drug (*4*). Given that CNTF induces hypothalamic neurogenesis, which contributes to the sustained weight-loss effect of this neurocytokine, further investigation into the potential role of hypothalamic neurogenesis in the pathophysiology and treatment of obesity is warranted.

### References and Notes

1. R. S. Ahima, S. Y. Osei, *Trends Mol. Med.* **7**, 205 (2001).
2. D. S. Weigle, *J. Clin. Endocrinol. Metab.* **88**, 2462 (2003).
3. S. Z. Yanovski, J. A. Yanovski, *N. Engl. J. Med.* **346**, 591 (2002).
4. M. P. Ettinger *et al.*, *JAMA* **289**, 1826 (2003).
5. P. D. Lambert *et al.*, *Proc. Natl. Acad. Sci. U.S.A.* **98**, 4652 (2001).

6. K. D. Anderson *et al.*, *Soc. Neurosci. Abstract* **24**, 621 (1998).
7. C. Bjorbaek *et al.*, *Endocrinology* **140**, 2035 (1999).
8. J. F. Kelly *et al.*, *Diabetes* **53**, 911 (2004).
9. M. W. Sleeman, K. D. Anderson, P. D. Lambert, G. D. Yancopoulos, S. J. Wiegand, *Pharm. Acta Helv.* **74**, 265 (2000).
10. T. Shimazaki, T. Shingo, S. Weiss, *J. Neurosci.* **21**, 7642 (2001).
11. C. G. Craig *et al.*, *J. Neurosci.* **16**, 2649 (1996).
12. H. G. Kuhn, J. Winkler, G. Kempermann, L. J. Thal, F. H. Gage, *J. Neurosci.* **17**, 5820 (1997).
13. H. Nakatomi *et al.*, *Cell* **110**, 429 (2002).
14. F. H. Gage, *Science* **287**, 1433 (2000).
15. S. S. Magavi, B. R. Leavitt, J. D. Macklis, *Nature* **405**, 951 (2000).
16. E. A. Markakis, T. D. Palmer, L. Randolph-Moore, P. Rakic, F. H. Gage, *J. Neurosci.* **24**, 2886 (2004).
17. V. Pencea, K. D. Bingaman, S. J. Wiegand, M. B. Luskin, *J. Neurosci.* **21**, 6706 (2001).
18. Materials and methods are available as supporting material on *Science* Online.
19. J. K. Elmquist, C. F. Elias, C. B. Saper, *Neuron* **22**, 221 (1999).
20. C. Lois, A. Alvarez-Buylla, *Science* **264**, 1145 (1994).
21. M. F. Marusich, H. M. Furneaux, P. D. Henion, J. A. Weston, *J. Neurobiol.* **25**, 143 (1994).
22. M. K. Lee, L. I. Rebhun, A. Frankfurter, *Proc. Natl. Acad. Sci. U.S.A.* **87**, 7195 (1990).
23. R. V. Bhat *et al.*, *Glia* **17**, 169 (1996).
24. J. P. Brown *et al.*, *J. Comp. Neurol.* **467**, 1 (2003).
25. C. Vaisse *et al.*, *Nat. Genet.* **14**, 95 (1996).
26. S. H. Bates *et al.*, *Nature* **421**, 856 (2003).
27. T. Hubschle *et al.*, *J. Neurosci.* **21**, 2413 (2001).
28. H. Munzberg, L. Huo, E. A. Nillni, A. N. Hollenberg, C. Bjorbaek, *Endocrinology* **144**, 2121 (2003).
29. Y. Zhang *et al.*, *Nature* **372**, 425 (1994).
30. I. Gloaguen *et al.*, *Proc. Natl. Acad. Sci. U.S.A.* **94**, 6456 (1997).
31. F. Doetsch, J. M. Garcia-Verdugo, A. Alvarez-Buylla, *Proc. Natl. Acad. Sci. U.S.A.* **96**, 11619 (1999).
32. C. Sanz-Rodriguez, J. Boix, J. X. Comella, *Neurosci. Lett.* **223**, 141 (1997).
33. L. C. Schmued, K. J. Hopkins, *Brain Res.* **874**, 123 (2000).
34. S. W. Levison, M. H. Ducceschi, G. M. Young, T. L. Wood, *Exp. Neurol.* **141**, 256 (1996).
35. Y. Xu *et al.*, *Exp. Neurol.* **192**, 251 (2005).
36. E. Gould, C. G. Gross, *J. Neurosci.* **22**, 619 (2002).
37. J. G. Emsley, T. Hagg, *Exp. Neurol.* **183**, 298 (2003).
38. T. L. Horvath, S. Diano, *Nat. Rev. Neurosci.* **5**, 662 (2004).
39. S. Pinto *et al.*, *Science* **304**, 110 (2004).
40. S. G. Bouret, S. J. Draper, R. B. Simerly, *Science* **304**, 108 (2004).



41. We thank J. K. Elmquist, C. A. Walsh, V. L. Sheen and R. H. Friedel for critical reading of the manuscript and helpful comments; A. C. Budde for help with the gold thioglucose experiment; and K.-F. Storch for many valuable discussions during the course of this work. Confocal microscope analyses were carried out at the Harvard Center for Neurodegeneration and Repair. This work was supported by grant DKR3728082 from the NIH (J.S.F.).


**Supporting Online Material**

www.sciencemag.org/cgi/content/full/310/5748/679/DC1
Material and Methods
Figs. S1 to S7
References


26 May 2005; accepted 23 September 2005
10.1126/science.1115360


# NPY/AgRP Neurons Are Essential for Feeding in Adult Mice but Can Be Ablated in Neonates


**Serge Luquet, Francisco A. Perez, Thomas S. Hnasko, Richard D. Palmiter***



**Hypothalamic neurons that express neuropeptide Y (NPY) and agouti-related protein (AgRP) are thought to be critical regulators of feeding behavior and body weight. To determine whether NPY/AgRP neurons are essential in mice, we targeted the human diphtheria toxin receptor to the *Agrp* locus, which allows temporally controlled ablation of NPY/AgRP neurons to occur after an injection of diphtheria toxin. Neonatal ablation of NPY/AgRP neurons had minimal effects on feeding, whereas their ablation in adults caused rapid starvation. These results suggest that network-based compensatory mechanisms can develop after the ablation of NPY/AgRP neurons in neonates but do not readily occur when these neurons become essential in adults.**


The arcuate nucleus (ARC) of the hypothalamus is a site of convergence of central and peripheral signals of energy stores, and it contains at least two distinct populations of neurons that are critically involved in the regulation of body weight (*1*–*3*). Orexigenic neuropeptide Y/agouti-related protein (NPY/AgRP) neurons and anorexigenic pro-opiomelanocortin (POMC) neurons respond to circulating satiety and hunger signals, including glucose, leptin, insulin, ghrelin, and peptide YY (*4*, *5*). Both populations exert an inhibitory tone onto each other, and they also send dense projections to other hypothalamic areas, including the paraventricular nucleus (PVN), zona incerta, perifornical area, and lateral hypothalamic area (*6*, *7*). POMC neurons reduce food intake and increase energy expenditure by releasing α-melanocyte-stimulating hormone (αMSH), a product of POMC processing, which activates melanocortin-4 receptors (MC4R). NPY/AgRP neurons have the opposite effects, inhibiting POMC neurons and antagonizing the action of αMSH on MC4R-bearing cells via the release of AgRP (a natural antagonist of αMSH) (*8*). Despite the fact that intracranial injection of either NPY or AgRP stimulates robust feeding in rodents (*1*–*3*), mutations that prevent the expression of AgRP, NPY, or various receptors for NPY have little impact on feeding behavior (*3*, *9*–*11*). In contrast, mutations that prevent production of leptin, leptin receptor, POMC, or MC4R lead to obesity in mice and other species (*12*–*17*). These observations raise the question of whether signaling by NPY, AgRP, or any other transmitter made by these cells is important for the regulation of body weight.

To assess whether NPY/AgRP neurons are essential for feeding, we adopted a "toxin receptor–mediated cell knockout" strategy (*18*) to specifically ablate these neurons in a temporally controlled manner (*19*). Because *Agrp* gene expression is restricted to NPY/AgRP neurons in the brain (*20*, *21*), we targeted the expression of the human diphtheria toxin receptor cDNA (*DTR*) to the *Agrp* locus in embryonic stem cells and generated $Agrp^{DTR/+}$ mice that express the human *DTR* in NPY/AgRP neurons (fig. S1). In situ hybridization revealed that human *DTR* mRNA was expressed in the ARC of $Agrp^{DTR/+}$ mice but not in controls (fig. S2).

Neonatal ablation of NPY/AgRP neurons was performed by injecting 1-day-old $Agrp^{DTR/+}$ and control $Agrp^{+/+}$ pups (genotype unknown at time of injection) with diphtheria toxin (DT) at 50 μg of DT per kg mouse (μg/kg) (subcutaneous), a dose tolerated by controls (*18*, *21*). After 9 weeks, all mice were fasted for 2 days to increase NPY and AgRP expression before they were killed (*22*). Brains were fixed, sectioned, and analyzed for NPY expression by immunohistochemistry. DT injection reduced the number of NPY-positive cells in the ARC by ~85% ($Agrp^{DTR/+}$ mice had 9.7 ± 0.9 neurons per section, $n = 5$ mice; controls had 78 ± 2 neurons per section, $n = 3$, $P < 0.001$) (Fig. 1, A to D). There was a concomitant reduction of NPY fibers in the PVN (Fig. 1, E and F), but NPY-expressing cells outside the ARC were spared (fig. S3). AgRP staining in the ARC and PVN was also reduced after DT treatment in $Agrp^{DTR/+}$ mice (fig. S3). The integrity of POMC neurons was demonstrated by using antibodies to adrenocorticotropic hormone (ACTH), another peptide product of POMC (Fig. 1, G and H). The loss of NPY/AgRP cells and the retention of POMC cells in the ARC was also documented by semiquantitative reverse transcriptase polymerase chain reaction (RT-PCR) of *Agrp* and *Pomc* mRNA (Fig. 1I).

If NPY/AgRP neurons are critical regulators of energy balance, then their ablation should negatively affect food intake and body weight. However, when newborn pups generated from a cross of $Agrp^{DTR/+}$ and $Agrp^{+/+}$ mice were injected with DT and their body weights recorded starting at weaning, there


Howard Hughes Medical Institute and Department of Biochemistry, University of Washington, Box 357370, Seattle, WA 98195, USA.

*To whom correspondence should be addressed. E-mail: palmiter@u.washington.edu

was only a slight (~11%) reduction in the body weight of *Agrp*$^{DTR/+}$ mice compared with controls (fig. S4). Food consumption by 9-week-old littermates was monitored using "lickometer" cages that dispensed water and liquid food. The number of licks and total food consumption were the same for both groups of mice, either before or after a 12-hour fast (Fig. 2A). At the end of each experiment, the depletion of NPY immunoreactivity in the ARC was verified. Similar results were obtained when either *Agrp*$^{DTR/+}$ or *Agrp*$^{DTR/DTR}$ neonatal mice (up to 8 days old) were injected either once or twice with DT at 50 μg/kg (i.e., the survival of DT-injected mice to adulthood was independent of genotype, $n > 100$). These results indicate that the majority (approaching 100% in some cases) (fig. S3) of NPY/AgRP cells in the ARC can be ablated in neonatal mice with little impact on food consumption or body weight.

We also examined the effects of administering DT to adult *Agrp*$^{+/+}$, A*grp*$^{DTR/+}$, or *Agrp*$^{DTR/DTR}$ mice (table S1). Adult mice were allowed to acclimate to lickometer cages for several days and then two intraperitoneal (ip) injections of DT (50 μg/kg, 3 days apart) were administered. There was an irreversible arrest of feeding after the second injection of DT into *Agrp*$^{DTR/DTR}$ mice but not into controls (Fig. 2B). All *Agrp*$^{DTR/DTR}$ mice treated this way lost ~20% of their body weight within 2 days of the second injection and were killed for immunohistochemical detection of NPY/AgRP neurons, which were always depleted by >80%. Injection of adult heterozygous *Agrp*$^{DTR/+}$ mice with DT (either once or twice) also terminated feeding (table S1). The loss of AgRP-producing cells was also measured by semiquantitative RT-PCR in *Agrp*$^{DTR/+}$ mice, which revealed a comparable loss of AgRP transcripts in neonatal and adult mice treated with DT. Occasionally, control mice also succumbed from this treatment, probably because of nonspecific toxicity associated with ip administration of DT.

Intramuscular (im) injection of DT in adult mice produced more reliable responses compared with ip injection (*18*). Littermates (*Agrp*$^{+/+}$ or *Agrp*$^{DTR/DTR}$) received either one injection of DT (50 μg/kg, im), or two injections, 2 days apart. The consumption of liquid food by DT-treated *Agrp*$^{DTR/DTR}$ mice fell below 20% of normal 7 days after a single injection of DT or within 5 days with two injections (Fig. 3, A and C, and fig. S5). At these time points, all *Agrp*$^{DTR/DTR}$ mice lost ~20% of their body weight and had to be euthanized, whereas control mice maintained body weight and survived (Fig. 3, B and D, and table S1). Water consumption increased in *Agrp*$^{DTR/DTR}$ mice after DT injections, demonstrating that the reduction in food intake was not due to an inability to reach the feeding tubes or to lick. Hand feeding via oral gavage with liquid food could sustain DT-treated mice, confirming that the lack of feeding was responsible for their loss of body weight. NPY immunostaining of sections through the ARC confirmed that most NPY/AgRP cell bodies were ablated from the ARC of *Agrp*$^{DTR/DTR}$ mice (Fig. 3, E and F). The number of NPY fibers in the PVN was also reduced in *Agrp*$^{DTR/DTR}$ mice compared with controls (Fig. 3, I to L). The number of POMC neurons was normal, but the ACTH staining appeared to be more robust in the *Agrp*$^{DTR/DTR}$ mice treated with DT (Fig. 3, G and H), which is consistent with the loss of NPY/AgRP inhibitory input onto POMC cells.

To demonstrate that loss of feeding is the consequence of central action of DT, the toxin was delivered to the third ventricle of *Agrp*$^{DTR/DTR}$ mice. All injected *Agrp*$^{DTR/DTR}$ mice stopped eating, whereas controls were unaffected (table S1).

A*grp*$^{DTR/+}$ or *Agrp*$^{DTR/DTR}$ neonates survived all of the DT treatments that led to starvation in adults, despite comparable ablation of NPY/AgRP neurons, which suggests that some form of compensation occurs in neonates. Perhaps residual neonatal NPY/AgRP neurons can enhance their signaling better than can adult neurons, or DTR-expressing cells may continue to be born after neonatal DT injection, allowing survival. These explanations predict that mice treated neonatally with DT would be susceptible to DT exposure as adults. However, most (5 of 7) mice injected with DT as neonates survived when DT was injected in the third ventricle as adults (fig. S6). Ventricular injection of DT was used to minimize potential immune responses to prior DT exposure; however, in agreement with others (*23*), neonatal exposure to DT generates minimal neutralizing antibody (fig. S7). In another experiment, most (5 of 8) neonatally treated *Agrp*$^{DTR/DTR}$ mice survived im injection of DT (50 μg/kg) as adults. The fractional survival of doubly exposed *Agrp*$^{DTR/DTR}$ mice suggests alternate modes of compensation (*24*).

The ablation of NPY/AgRP neurons in neonates is not only tolerated but produces compensatory changes that allow almost normal growth and feeding in the adult. Nevertheless, we predict that hormonal or metabolic signals that depend on NPY/AgRP neurons, e.g., ghrelin (*25*), may be compromised. The melanocortin signaling pathway, which is important for body-weight regulation in adults, may not be critical for feeding by neonates. Thus, ablating NPY/AgRP neurons before the POMC cells become critical may allow development of a network-based compensatory mechanism. Changes in synapses within the ARC after restoration of leptin to young *Lep*$^{ob/ob}$ mice illustrate one form of plasticity that can occur in the hypothalamus (*26*, *27*). Presumably, the loss of signaling molecules made by NPY/AgRP neurons initiates the compensatory adaptations in neonates, but the nature of those signals and the identity of the cells that respond remain to be discovered. This adaptation could explain why conventional inactivation of *Npy* and/or *Agrp* genes has little effect on body-weight regulation (*10*, *11*).

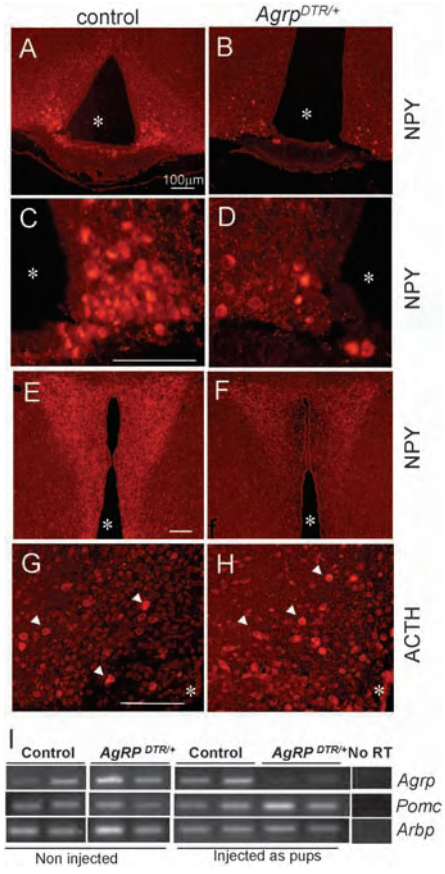


**Fig. 1.** DT injection in neonates ablates NPY neurons in the arcuate nucleus. Both control and *Agrp*$^{DTR/+}$ mice were injected as pups with DT (50 μg/kg). After 9 weeks, animals were fasted for 2 days to increase NPY signal and killed for brain immunohistochemistry. (**A** and **B**) Representative NPY immunostaining of ARC neurons of control (A) and *Agrp*$^{DTR/+}$ mice (B). (**C** and **D**) Higher magnifications of ARC region. (**E** and **F**) NPY immunostaining of PVN from control (E) and *Agrp*$^{DTR/+}$ mice (F). (**G** and **H**) ACTH immunostaining of the ARC from controls (G) and *Agrp*$^{DTR/+}$ mice (H). White arrowheads point to POMC cell bodies. The asterisks indicate third ventricle. Scale bar, 100 μm. (**I**) Semi-quantitative RT-PCR for *Agrp*, *Pomc* mRNA, and *Arbp* mRNA, as control.

The NPY/AgRP neurons in the ARC become a critical component of the feeding neurocircuitry sometime between 8 and 45 days after birth. By this time, the melanocortin signaling pathway is established; hence, ablation of NPY/AgRP neurons may remove a critical inhibitory tone, leading to excessive melanocortin signaling and starvation. However, NPY/AgRP neurons project widely (*19*), so their ablation in the adult may perturb other critical signaling pathways, resulting in starvation.

*Note added in proof*: Two related papers (*28*, *29*) were published online while this Report

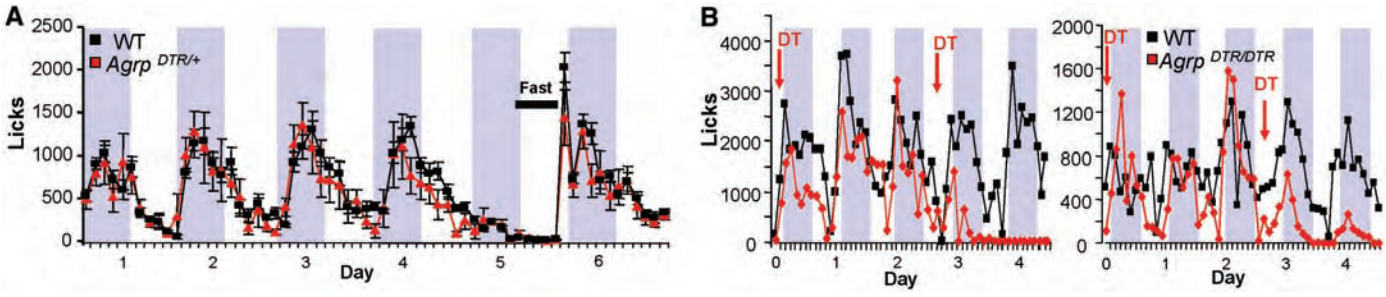


**Fig. 2.** Ablation of NPY/AgRP neurons in neonatal or adult mice differentially alters feeding behavior. (**A**) Licking pattern of control (wild type, WT) (black, $n = 4$) and $Agrp^{DTR/+}$ mice (red, $n = 4$) that were injected with DT (50 μg/kg) as neonates and tested at 9 weeks. The graph illustrates 3 days of baseline feeding, followed by a 12-hour fast, and refeeding response. The total number of licks in 2-hour bins is plotted. (**B**) Representative licking pattern of an individual control and $Agrp^{DTR/+}$ mouse (left panel, 12 weeks old; right panel, 7 weeks old) in response to two injections (arrows) of DT (50 μg/kg, ip). Shaded areas represent the dark phase. Error bars represent SEM.

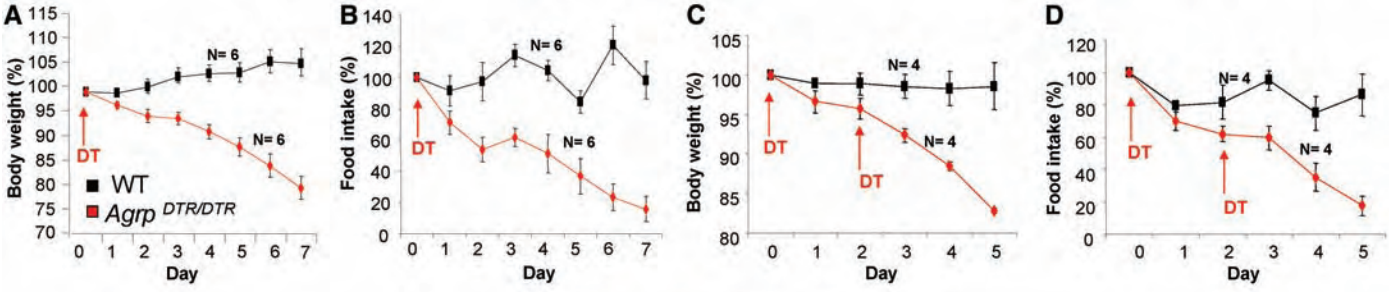


**Fig. 3.** DT injection induces a dose-dependent arrest of feeding in adult $Agrp^{DTR/DTR}$ mice. (**A** and **B**) Body weight (A) and food intake (B) of adult control (black, $n = 6$) and $Agrp^{DTR/DTR}$ mice (red, $n = 6$) injected once (arrow) with DT (50 μg/kg, im). (**C** and **D**) Body weight (C) and food intake (D) of adult control (black, $n = 4$) and $Agrp^{DTR/DTR}$ mice (red, $n = 4$) injected twice (arrows) with DT (50 μg/kg, im). Error bars represent SEM. (**E** and **F**) Representative NPY immunostaining of control (E) and $Agrp^{DTR/DTR}$ (F) mouse. (**G** and **H**) ACTH immunostaining of ARC neurons in control (G) and $Agrp^{DTR/DTR}$ mouse (H) that were injected as adults with DT. Brains were collected for histology when the mice had lost ~20% of body weight; controls were fasted to comparable weight loss. Arrowheads, POMC cell bodies; asterisk, third ventricle. (**I** and **J**) NPY-fiber immunostaining in the PVN of the same control (I) and $Agrp^{DTR/DTR}$ mice (J) as above. (**K** and **L**) Higher magnification of boxed areas in (I) and (J), respectively. Scale bar, 100 μm.

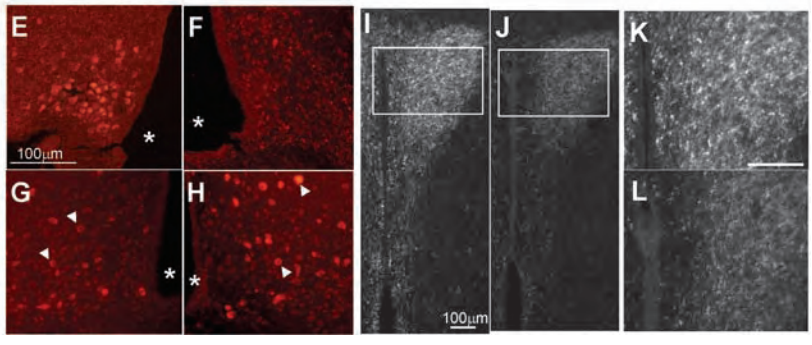


was under review. In both cases, the authors report that partial ablation of NPY/AgRP neurons results in smaller mice that eat less than controls do. The partial ablation is probably the consequence of gradual ablation or partial penetrance of transgene expression. Neither paper describes the starvation phenotype nor the neonatal compensation reported here.

### References and Notes


1. J. T. Clark, P. S. Kalra, W. R. Crowley, S. P. Kalra, *Endocrinology* **115**, 427 (1984).
2. S. C. Woods, R. J. Seeley, D. Porte Jr., M. W. Schwartz, *Science* **280**, 1378 (1998).
3. D. J. Marsh, G. Hollopeter, K. E. Kafer, R. D. Palmiter, *Nat. Med.* **4**, 718 (1998).
4. M. W. Schwartz, S. C. Woods, D. Porte Jr., R. J. Seeley, D. G. Baskin, *Nature* **404**, 661 (2000).
5. M. W. Schwartz, D. Porte Jr., *Science* **307**, 375 (2005).
6. J. K. Elmquist, C. Bjorbaek, R. S. Ahima, J. S. Flier, C. B. Saper, *J. Comp. Neurol.* **395**, 535 (1998).
7. J. K. Elmquist, C. F. Elias, C. B. Saper, *Neuron* **22**, 221 (1999).
8. R. D. Cone *et al.*, *Recent Prog. Horm. Res.* **51**, 287 (1996).
9. R. D. Palmiter, J. C. Erickson, G. Hollopeter, S. C. Baraban, M. W. Schwartz, *Recent Prog. Horm. Res.* **53**, 163 (1998).
10. S. Qian *et al.*, *Mol. Cell. Biol.* **22**, 5027 (2002).
11. J. C. Erickson, K. E. Clegg, R. D. Palmiter, *Nature* **381**, 415 (1996).
12. Y. Zhang *et al.*, *Nature* **372**, 425 (1994).
13. J. M. Friedman, J. L. Halaas, *Nature* **395**, 763 (1998).
14. D. Huszar *et al.*, *Cell* **88**, 131 (1997).
15. H. Krude, D. Schnabel, W. Luck, A. Gruters, *Ann. N. Y. Acad. Sci.* **885**, 419 (1999).
16. A. Hinney *et al.*, *J. Clin. Endocrinol. Metab.* **84**, 1483 (1999).
17. L. Yaswen, N. Diehl, M. B. Brennan, U. Hochgeschwender, *Nat. Med.* **5**, 1066 (1999).
18. M. Saito *et al.*, *Nat. Biotechnol.* **19**, 746 (2001).
19. Materials and methods are available as supporting material on *Science* Online.
20. C. Broberger, J. Johansen, C. Johansson, M. Schalling, T. Hökfelt, *Proc. Natl. Acad. Sci. U.S.A.* **95**, 15043 (1998).
21. T. M. Hahn, J. F. Breininger, D. G. Baskin, M. W. Schwartz, *Nat. Neurosci.* **1**, 271 (1998).
22. D. J. Marsh *et al.*, *Brain Res.* **848**, 66 (1999).
23. T. Buch *et al.*, *Nat. Methods* **2**, 419 (2005).
24. There may be two different modes of compensation. In one mode, a critical number of NPY/AgRP neurons survive neonatal exposure to DT and continue to function in the adult; their subsequent ablation results in loss of appetite and rapid loss of weight. In the other mode, most NPY/AgRP neurons are ablated in the neonates, and compensatory mechanisms develop; these mice are unaffected by adult exposure to DT.
25. H. Y. Chen *et al.*, *Endocrinology* **145**, 2607 (2004).
26. S. G. Bouret, S. J. Draper, R. B. Simerly, *Science* **304**, 108 (2004).
27. S. Pinto *et al.*, *Science* **304**, 110 (2004).
28. G. A. Bewick *et al.*, *FASEB J.* **19**, 1680 (2005).
29. E. Gropp *et al.*, *Nat. Neurosci.* **8**, 1289 (2005).


30. We thank K. Kohno for the *hDTR* cDNA clone, P. Soriano for AK18.1 embryonic stem cells, G. Froelick for help with histology, and our colleagues for their input during the course of these studies.


**Supporting Online Material**

www.sciencemag.org/cgi/content/full/310/5748/683/DC1
Materials and Methods
Figs. S1 to S7
Table S1


31 May 2005; accepted 19 September 2005
10.1126/science.1115524

## Digital Inverted Research Microscopes

Two new digital inverted research microscopes, DMI3000 B and DMI4000 B, join the well-received DMI6000 B to provide solutions ranging from simple micromanipulation to advanced live cell fluorescence imaging. The fully manual DMI3000 B is tailored for micromanipulation. The DMI4000 B provides a flexible, modular platform for adding automation based on experimental needs. Even manually operated components are encoded so that the microscope can guide the user to proper operation. Through improved optics and reduced stray light, these units achieve especially brilliant fluorescence. The fluorescence turret is equipped with up to six filter cubes that can be moved into position quickly, without vibration, at the touch of a button. The fluorescence axis also features a fast internal filter wheel that supports changing the excitation of fluorochromes in less than 20 ms. The Fluorescence Intensity Manager reduces light stress for living cells and the bleaching of fluorochromes—the intensity of the excitation light can be reduced in a reproducible manner while the quality of the fluorescence is improved. The motorized Excitation Manager balances a variety of emission intensities when simultaneously observing multiple fluorochromes.

**Leica** For information 800-248-0123 www.leica-microsystems.com

## Low Cell Binding Plates

The Nunc low cell binding (LCB) surface presents a phosphorylcholine moiety to cells, mimicking the surface of a cell membrane. This plate surface is biologically inert, biocompatible, and can be used even with implants. Typical applications for these LCB plates are cultures of cells in suspension or non-adherent cell clusters (spheroids) and measurements of soluble cell products, such as proteins. For embryoid body formation, it is necessary that the plate surface not induce monolayer formation. Nunc LCB surface plates eliminate using the laborious hanging drop method, and permit easy microscopy and transfer.

**Nunc** For information 800-446-2543 www.nuncbrand.com



## Spectroscopy Platform

SpectraSuite is modular, Java-based spectroscopy software that operates on Windows, Macintosh, and Linux operating systems. The software can be used to control any Ocean Optics USB spectrometer and device as well as any other manufacturer's USB instrumentation using the appropriate drivers. With SpectraSuite, a user can combine data from multiple USB spectrometers in applications that include upwelling/downwelling measurements, dual-beam referencing, and process monitoring. Original equipment manufacturers will find SpectraSuite's modularity beneficial as all visual and computational aspects of the program's interface can be changed to create a fully branded application. Every function in the software can be altered or replaced. For example, the data acquisition functions, the scheduling functions, the data processing functions, and the rendering functions are all separate modules. A user can add or delete modules to create a proprietary user interface or functionality, create modules to perform calculations, automate experiment routines, and more.

**Ocean Optics** For information 727-733-2447 www.OceanOptics.com

## Automated Cell Culture System

The CompacT SelecT automated laboratory cell culture system is designed for reproducible generation of assay-ready plates. With a footprint slightly larger than a standard Class II safety cabinet, it automates manual cell culture processes via a small six-axis anthropomorphic robotic arm that automatically manipulates standard T-175 flasks under negative pressure laminar airflow, thereby preventing any contamination. The system also operates with full bar code tracking to ensure a complete audit trail. The CompacT SelecT has 10 separate pumps dispensing a range of media for simultaneous culture of multiple cell lines. The cells produced can be either harvested or automatically plated into 96- and 384-well plates ready for use in cellular assays.

**The Automation Partnership** For information +44 (0) 11763 227200 www.automationpartnership.com

## Proteomics Software

DeCyder Extended Data Analysis (EDA) version 1.0 is advanced software for the proteomics research market that enables combined analysis of different data sets and facilitates interpretation of results through public and local database retrieval. EDA v1.0 is two-dimensional (2D) difference gel electrophoresis (DIGE) software that offers advanced statistical analysis in an easy-to-use format. It is expected to contribute to a better understanding of regulatory pathways and help proteomics researchers more rapidly and accurately identify proteins to discriminate between healthy and diseased tissue samples and different disease states and tumor types. DeCyder EDA features multivariate analysis and sophisticated clustering methods to uncover patterns in protein expression data derived from 2D DIGE. The software makes use of a data set as the basis for 2-D gel analysis. Defined as a group of spots with matched protein spots, each data set can be displayed in different ways depending on the goals of the experiment.

**GE Healthcare** For information 732-457-8149 www.gehealthcare.com

Newly offered instrumentation, apparatus, and laboratory materials of interest to researchers in all disciplines in academic, industrial, and government organizations are featured in this space. Emphasis is given to purpose, chief characteristics, and availability of products and materials. Endorsement by *Science* or AAAS of any products or materials mentioned is not implied. Additional information may be obtained from the manufacturer or supplier by visiting www.science.labvelocity.com on the Web, where you can request that the information be sent to you by e-mail, fax, mail, or telephone.




*Published by AAAS*